FEASIBILITY OF A SOLAR-POWERED LIQUID DESICCANT COOLING SYSTEM FOR GREENHOUSES

GEORGIOS LYCHNOS

Doctor of Philosophy

ASTON UNIVERSITY

JUNE 2010

ASTON UNIVERSITY

FEASIBILITY OF A SOLAR-POWERED LIQUID DESICCANT COOLING SYSTEM FOR GREENHOUSES

GEORGIOS LYCHNOS

2010

SUMMARY

To investigate the technical feasibility of a novel cooling system for commercial greenhouses, knowledge of the state of the art in greenhouse cooling is required. An extensive literature review was carried out that highlighted the physical processes of greenhouse cooling and showed the limitations of the conventional technology. The proposed cooling system utilises liquid desiccant technology; hence knowledge of liquid desiccant cooling is also a prerequisite before designing such a system. Extensive literature reviews on solar liquid desiccant regenerators and desiccators, which are essential parts of liquid desiccant cooling systems, were carried out to identify their advantages and disadvantages. In response to the findings, a regenerator and a desiccator were designed and constructed in lab.

An important factor of liquid desiccant cooling is the choice of liquid desiccant itself. The hygroscopicity of the liquid desiccant affects the performance of the system. Bitterns, which are magnesium-rich brines derived from seawater, are proposed as an alternative liquid desiccant for cooling greenhouses. A thorough experimental and theoretical study was carried out in order to determine the properties of concentrated bitterns. It was concluded that their properties resemble pure magnesium chloride solutions. Therefore, magnesium chloride solution was used in laboratory experiments to assess the performance of the regenerator and the desiccator.

To predict the whole system performance, the physical processes of heat and mass transfer were modelled using gPROMS® advanced process modelling software. The model was validated against the experimental results. Consequently it was used to model a commercials-scale greenhouse in several hot coastal areas in the tropics and sub-tropics. These case studies show that the system, when compared to evaporative cooling, achieves $3^{o}C-5.6^{o}C$ temperature drop inside the greenhouse in hot and humid places (RH>70%) and $2^{o}C-4^{o}C$ temperature drop in hot and dry places (50%<RH< 65%).

KEYWORDS

Bitterns, solar liquid desiccant regenerator, desiccator, hot coastal areas, evaporative cooling

This thesis is dedicated to my loving parents, Ροδόπη and Διονύση. Thank you for your unconditional support with my studies. Most of all, thank you for giving me the chance to reach my dreams.

ACKNOWLEGMENTS

Firstly I would like to express my sincerest gratitude to my supervisor, Dr Philip Davies, who has supported me with patience and knowledge. His technical expertise and guidance on areas I had little or no experience helped a lot to overcome obstacles and achieve my goals. Above all I would like to thank him for giving me the opportunity to work on this project. I would also like to thank Dr John Fletcher for his valuable advice during the 1st year of my research.

Secondly I would like to thank all the technicians who were involved in my project. I especially would like to thank Mr Paul Pizer who greatly helped with the construction of the desiccator rig.

This project would have not been viable without the financial support of Aston University and the Greek State Scholarship Foundation.

I would also like to thank all my friends, colleagues (Alister, Adam) and family who supported me throughout this thesis; especially my brother Spyros and my officemate and friend Paul Knowles with whom I enjoyed having inspiring conversations on scientific subject matters. Thanks for the support Paul.

Lastly, I owe my deepest gratitude to Prof. Gregory Lambrinos (Agricultural University of Athens) for enlightening me the first glance of research.

CONTENTS

CONTENTS continued **Page No.**

CONTENTS continued **Page No.**

CONTENTS continued **Page No.**

LIST OF TABLES

LIST OF TABLES continued **Page No**

LIST OF TABLES continued **Page No**

LIST OF FIGURES

LIST OF FIGURES continued **Page No**

LIST OF FIGURES continued **Page No**

LIST OF FIGURES continued **Page No**

LIST OF FIGURES continued **Page No**

LIST OF FIGURES continued **Page No**

NOTATION

List of symbols	Units	Definition
a	-	chemical activity
A	-	coefficient
a_{abs}	$m^2\ m^{-3}$	wetted surface per volume ratio
C_p	$J\ kg^{-1}\ K^{-1}$	specific heat
C	-	concentration factor
c	-	mass fraction
$D_{w\text{-}a}$	$m^2\ s^{-1}$	binary diffusion coefficient of water vapour in air
D	m	external diameter
d	m	internal diameter
ERH	-	equilibrium relative humidity
E	J	energy
e	-	mass fraction per total dry mass of solute
F	-	coefficient
Gr	-	Grasshoff number
g	$m\ s^{-2}$	gravitational acceleration
H	J	enthalpy
h	$J\ kg^{-2}$	specific enthalpy
h_c	$W\ m^{-2}\ K^{-1}$	convective heat transfer coefficient
h_D	$kg\ m^{-2}\ s^{-1}$	mass transfer coefficient based on concentration gradient
h_m	$s\ m^{-1}$	mass transfer coefficient based on pressure gradient
$\dot{H}$	$J\ s^{-1}$	enthalpy rate
I_α	$W\ m^{-2}$	solar irradiance incident

NOTATION continued

I'	mol kg^{-1}	ionic strength
J	-	cationic strength fraction
k	W m^{-1} K^{-1}	thermal conductivity
Le	-	Lewis number
L_c	m	characteristic length
m	mol kg^{-1}	molality
$\dot{M}$, $\dot{m}$	kg s^{-1}	mass flow rate
N	-	cationic strength fraction
NTU	-	number of transfer units
Nu	-	Nusselt number
P	Pa	pressure
$\dot{Q}$	J s^{-1}	sensible heat rate
R	kJ $kmole^{-1}$ k^{-1}	air gas constant
S	m^2	surface
Sc	-	Schmidt number
Sh	-	Sherwood number
T	^oC	temperature
U	W m^{-2} K^{-1}	overall heat transfer coefficient
u	m s^{-1}	velocity
V	m^3	volume
$\dot{V}$	m^3 s^{-1}	ventilation rate
w	m	width
X	kg kg^{-1}	mass concentration
Y	-	anionic strength fraction

NOTATION continued

Greek variables

δ	m	film thickness
ε	-	residue term
η_h	%	enthalpy effectiveness
η_w	%	moisture effectiveness
μ	Pa.s	dynamic viscosity
ν	-	number of ions released
ρ	kg m^{-3}	absolute density
ϕ	-	osmotic coefficient
$\omega_a \rho$	kg kg^{-1}	absolute humidity of the air
$\omega_{Ts,sat}$	kg kg^{-1}	absolute humidity of the air in equilibrium with the desiccant solution

Superscripts

M	in a multi-electrolyte solution
s	in a single-salt solution

Subscripts

a	air
amb	ambient
at	atmospheric
con	convective
fg	latent
i	single salt

NOTATION continued

in	inlet
j	anion
k	cation
Li	lithium
M	of a multi-electrolyte solution
out	outlet
s	solution
T	total
w	water
0	pure water

CHAPTER 1. INTRODUCTION

This thesis investigates the feasibility of a solar powered liquid desiccant cooling system for greenhouses. In this chapter background information is provided regarding the needs and problems that are ultimately motivating this study, thus showing the potential impact of the proposed cooling system when applied to greenhouses in hot and humid places. A review of the growth of greenhouse technology worldwide is presented. The reasons for this growth are discussed and the broad trends in this area are analysed. Consequently the origins of this thesis are explained in terms of the particular technology studied. Lastly the aims and objectives are stated and the methodology and structure of the thesis is outlined.

1.1 The need - motivation

According to the U.N.O and FAO (Food and Agricultural Organization, 2009, United Nations, 2009) the world population stood at 6.8 billion in 2009 but it is projected to reach 9.1 billion in 2050. Figure 1.1 illustrates the projected world population change between 1990 and 2035. Noticeably most of the population growth takes place in the developing and least developed countries the majority of which lie in low latitudes and therefore have hot climates (see Fig. 1.2). It is estimated that almost one billion people are undernourished. Figure 1.3 shows the prevalence of undernourished people in the world. It is worth noticing that nearly all the countries who will experience high population growth are also the ones where hunger is a major problem at present.

The essential prerequisites of food security are: food availability, food accessibility, food utilization and food system stability (Food and Agricultural Organization, 2002). Amongst them food availability is the one that focuses on food production. Thus, increasing agricultural production is a key element in improving food availability. This increase can be achieved by using more land for agricultural production, by increasing the intensity of cultivated crops and by boosting yields. The implementation of the pre mentioned strategies depend on local economical, political, ecological and technological conditions. It is estimated that agricultural output will have to increase by 70% between now and 2035 in order to match the demand for food. In addition, it is fair to say that this increase would take place mainly in the developing and least developed countries since only 16% of the

world food production is traded internationally at present (Food and Agricultural Organization, 2009).

There are different levels of food insecurity in the world. Howe and Devereux (2004) presented an intensity scale for food security where level 0 is for countries with food security conditions and level 5 is for countries with extreme famine conditions. According to this scale, countries that face seasonal shortage of food, resulting in price instability, are placed in level 1. In hot countries, like the ones in the Persian Gulf, this problem is common during summertime and is usually addressed by increasing food imports. It is worth mentioning though that these countries already import more than 60% of their food raising serious concerns about food security.

Fig. 1.1: Projected population change in 1990-2035. (source: Population Action International)

The developing and least developing world have always been vulnerable to climate extremes i.e. extreme high temperatures and prolonged draughts which resulted in chronic famine occurred in the past in Sahel and most likely will happen again with higher frequency due to climate change (Battisti and Naylor, 2009, IPCC, 2007).

Figure 1.4 illustrates the surface and ocean mean temperature differences in the world over the period of 1990-2009 relative to the base period of 1952-1980. It is seen that in the last

twenty years there is a departure of the mean temperature in most of the earth's land surface ranging from 0.5-2^{o}C.

Fig. 1.2: Global observed mean surface temperatures of January during 1960-1990 (obtained from www.ipcc-data.org).

Climate change may have direct and indirect impacts on the abiotic (temperature, relative humidity, atmosphere composition, soil) and biotic (fungi, bacteria, viruses and insects) environment that affects agriculture, resulting in reduced yields, crop damage and increase of crop diseases (Food and Agricultural Organization, 2008). Figure 1.5 illustrates the projected temperature change in the world. It is seen that the highest temperature rise will occur in the pole regions (higher than 2^{o}C). A 1-2^{o}C rise will take place in most of the world. Most of the developing countries will experience a 0.5-1^{o}C rise but they are also more likely to experience heat waves and extreme high temperatures with higher frequency than before.

Fig. 1.3: Prevalence of undernourished people in total population at present (source: (FAOSTAT, 2010).

Fig. 1.4: Surface and ocean mean temperature anomalies (source: (NASA, 2010)).

Battisti and Naylor (2009) showed with a greater than 90% chance to happen that growing season temperatures by the end of the 21st century will exceed even the most extreme seasonal temperatures from 1900 to 2006 for most of the tropics and subtropics. They also reported that a 1°C increase in seasonal temperature can cause direct crop yield losses of 2.5-16%.

Fig. 1.5: The projected temperature change from 1990 to 2035 (source: (Population.Action.International, 2007).

FAO (2009) has proposed various methods for improving agricultural production and thus addressing the problem of food security. These methods are categorised in cropland management, water management, pasture and grazing management and restoration of degraded lands. However, climatic conditions affect all these methods, especially the ones who are related to the open field agriculture. Protected cultivation can reduce the adverse impacts of extreme weather conditions and thus improve crop quality and yields.

1.2 Protected Cultivation

In response to the threats posed by climate change on food security, this thesis puts forward an improved means of protected cultivation that can cope with elevated temperatures. Before the proposed technology is introduced, it is worth reviewing briefly the history of protected cultivation and its recent growth in the form of greenhouse technology.

Irrigation could be considered the oldest means of protected cultivation (Wittwer and Castilla, 1995). Since antiquity (the irrigation system of the river Nile in ancient Egypt, the irrigation system of Mesopotamia etc.) men have developed various irrigation methods in order to protect their crops from droughts. Irrigation systems extended crop production to semi-arid lands and even partially addressed the problem of seasonal droughts. However, droughts have not been the only problem of crop losses. Flooding, extreme cold and hot temperatures, hail and strong winds can damage plants and cause serious losses in crop yields and crop quality depending on the plant growth stage they occur. All the pre mentioned conditions are related to climate. In order to lessen the effects of extreme climatic conditions on crop production various methods of protected cultivation have been developed over time such as windbreaks, soil mulches and plant covers including direct covers, low and high tunnels and greenhouses. Here we briefly review each type and point out its use emphasising greenhouses since they are advantageous to the rest. For comprehensive studies of protected cultivation and specifically greenhouses the reader is referred to the studies of Wittwer and Castilla (1995) and Von Zabeltitz (1999).

Windbreaks provide mechanical protection from strong winds and can be natural (trees, bushes, tall crops) or artificial (polyethylene and polypropylene nets and screens). They are placed vertically at the side of the field, where strong winds blow, and must have permeability of 40-50%.

Soil mulches are soil covers made from natural (straw, crop and plant dried residues, sand, gravel, rocks) and artificial (paper, aluminium foil, plastic films) materials. The benefits of mulching are the minimisation of water evaporation from the soil and the elimination of weed growth.

Low tunnels are inexpensive structures of 1m height or less, too low for workers to walk in. Plastic films such as infrared PE, PVC and simple PE are used as covering materials. They provide protection from low temperatures (frost), wind, rain, hail, birds and insects. Walk-in or high tunnels are similar structures of 1.8-2.0 m height which the farmer can enter and perform agricultural practices from inside.

The protected cultivation methods mentioned above provide only partial control over some extreme climatic conditions. The need for a better environmental control drove engineers to develop more sophisticated structures called greenhouses. They are high and large enough buildings where the grower can perform all the necessary cultural practices and are especially designed in order to protect the plants from extreme ambient conditions, pests and diseases.

1.2.1 Greenhouse Technology

Greenhouses were first developed in regions were there was a need for protected cultivation during winters, specifically in Northern Europe at the beginning of the previous century. These early structures used glass as cladding material. Later, the need for a cheaper cladding material than glass led to the use of polyethylene (1948, University of Kentucky, USA). This was the beginning of plasticulture, the use of plastic films in greenhouses (Jensen, 2010). In recent decades greenhouses have spread rapidly in Europe because of the demand for out of season crops and high quality and exotic products (Pardossi et al., 2004). According to Hickman (2010) there are 1,166,154 hectares (~10 000 km^2) worldwide covered by greenhouses and high tunnels used for vegetable production, with China leading the way having a total covered area of 753,000 hectares.

Figure 1.6 illustrates the greenhouse vegetable production area of several countries as a percentage of the total worldwide covered area. The low cost plastic films produced in China pushed the Chinese greenhouse industry to a remarkable growth making China the leading country in greenhouse vegetable production today (Jiang *et al.*, 2003).

At present, glass, rigid plastic and plastic films are used as cladding materials. Plastic films, however, dominate over the other cladding materials. In northern climates such as those of Northern Europe glass greenhouses are used to a much greater extent than plastic

film greenhouses because glass has better light transmissivity, durability and chemical stability. Despite the fact that plastic films' transmissivity reduces with time as a result of polymerization caused by the global radiation, at southern climates, such as those of Southern Europe plastic film greenhouses dominate because of lower costs. Plastic films used as cladding materials are made of polyethylene (PE), ultraviolet stabilised PE, PE infrared, PE anti-drop, EVA, PVC, PVF, FEP.

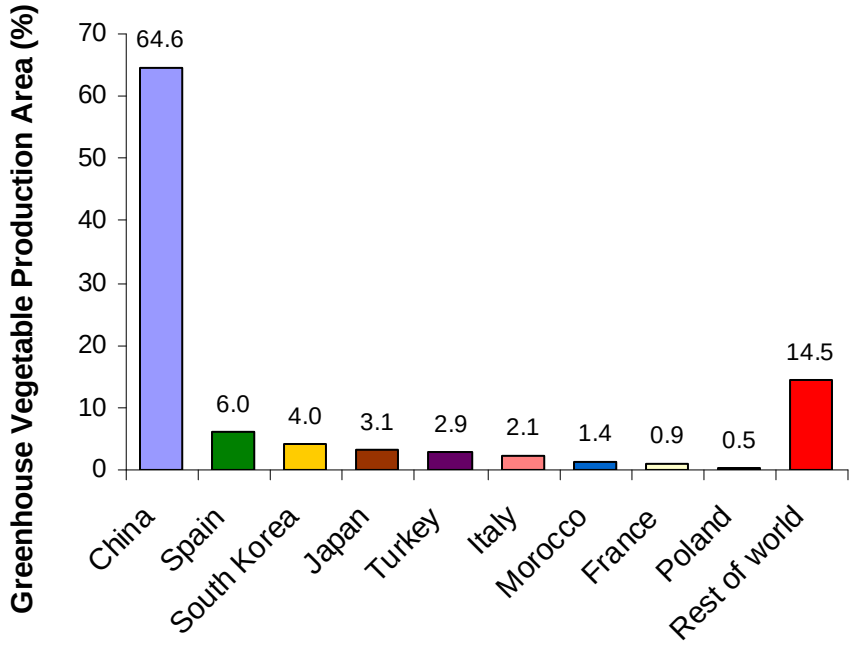

Fig 1.6: Greenhouse vegetable production area of various countries as a percentage of total worldwide greenhouse vegetable production area based on Hickman's report (2010).

After the Second World War greenhouses evolved from simple structures that protect the plants from extreme weather conditions into environmentally controlled units where the air temperature, humidity, solar radiation, nutrition and carbon dioxide can be regulated in order to achieve the optimum crop growth conditions. Based on the investment cost, which reflects the level of technology, Pardossi *et al.* (2004) reported that greenhouses can be of low-technology (25-30$/m^2), medium-technology (30-100$/m^2) and high-technology (100-200$/m^2). The low-tech greenhouses are very simple structures with plastic film as cover and their environmental control is not satisfactory. The medium-tech greenhouses' structure is made of metal and the cladding material can either be glass or plastic. The environmental conditions can be controlled during the cultivation period most of the time. Hydroponics are also used and the production is almost entirely under automated control. In high-tech greenhouses the structure is made of galvanised iron and the cladding material used is glass. They have total environmental control using sophisticated computer systems.

In order to control the environmental conditions inside the greenhouses various technologies are implemented that provide heating, cooling, humidity and carbon dioxide control. Briefly, the main heating systems used for addressing the problem of low temperatures utilise steam, hot water, hot air and infrared radiation (Hanan, 1998). Alternative sources of heat such us geothermal, solar energy and waste heat have also been used. High heat losses from cladding are reduced with the implementation of thermal screens (widely known and preferred by growers).

The problem of high temperatures is addressed using various cooling methods depending on the climate zone. For example, in Northern climates passive ventilation is adequate. On the other hand in Southern climates additional cooling is required. Therefore, forced ventilation, shading and evaporative cooling are used. Evaporative cooling, especially the fan-pad system, has proved to be very efficient in dry and hot climates. Figure 1.7 illustrates fan-pad systems implemented to greenhouses and Figure 1.8 shows the process. However, the amount of cooling that can be achieved from evaporative cooling depends on how much water can be evaporated. Consequently, in hot and humid climates (RH>60%), i.e. coastal areas in the tropics and the subtropics, this method is not effective and fails to produce adequate cooling. Further details on greenhouse cooling can be found in Chapter 2 where the state of the art in greenhouse cooling is reviewed in detail.

Fig. 1.7: Greenhouse vertical fan-pad systems (source: anonymous).

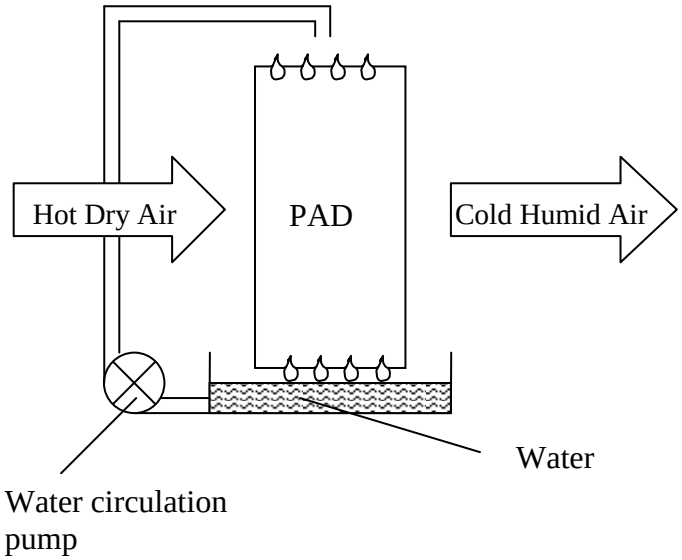

Fig. 1.8: The process of evaporative cooling through a vertical pad.

In conclusion, the above discussion confirms that protected cultivation and particularly greenhouses can increase agricultural production by boosting yields on existing farmland, producing high quality and out of season crops. Since large scale control over climate is not yet an option the only way to prevent damage to crops caused by extreme weather conditions is protected cultivation. Protected cultivation can be beneficial to poor countries in the world by providing new jobs for the local population. In places where there is seasonal food insecurity low-tech and medium-tech greenhouses can be used and decrease food imports. However, in hot climates, crop cultivation in greenhouses during summertime is almost impossible because the high temperatures induced inside cause plant stress and death. This problem limits the growing season for crop cultivation and thus drives countries to increase food imports. The growing season can be extended if the greenhouse air temperature is reduced to the desired optimum value for crop cultivation. The conventional greenhouse cooling systems, i.e. evaporative cooling and fan ventilation fail to produce adequate cooling in hot and humid places and this shortcoming will in future be aggravated by climate change.

1.3 Origins of the project

The thesis came about as a result of Davies' (2005) study where it was shown the potential of using a liquid desiccant cooling system for greenhouses when compared to conventional cooling systems and also Davies and Knowles inspiring study (2006) on the use of concentrated seawater brines as liquid desiccant to drive such a system.

Evaporative cooling can be considered as the state-of-the-art in greenhouse cooling. These systems are effective in hot and dry climates but perform poorly in hot and humid conditions. The conventional refrigeration methods (various vapour-compression systems) which are widely used for air-conditioning of human dwellings are too expensive (high installation and operational cost) to find application in cooling greenhouses. Here we set out to develop a more effective cooling system that retains the relatively low energy consumption of the evaporative cooling systems.

The particular approach pursued is solar-powered liquid desiccant cooling technology. Whereas Chapter 2 gives an in-depth review of the various cooling technologies that are applicable to greenhouses, including desiccant cooling, this section aims only to introduce the reader to the concepts that form the basis of this thesis thus providing the immediate background to the statement of the aims and objectives.

In addition to proposing the use of liquid desiccant cooling, a second innovation put forward here is the use of seawater-derived salts to provide the desiccant. Therefore the technology could be used in sunny locations near the sea, taking advantage of seawater in raw and concentrated forms to drive the cycle.

The immediate background to this thesis is provided by the theoretical study of Davies (2005) which, based on preliminary calculations, suggested a solar powered liquid desiccant cooling system for greenhouses that lowers maximum summer temperatures by 5^{o}C. Figure 1.9 shows the flow process diagram of a simplified system. The essential parts of the system are the regenerator, the desiccator and the evaporative pad. There are three process fluids in this system, the air, the liquid desiccant and the water. The illustrated system uses a liquid desiccant pad (a highly porous medium with large surface area per volume) and an evaporative cooling pad (same medium as the desiccant pad) in line. The air is dehumidified as it comes in contact with the liquid desiccant before passing through the evaporative pad. The liquid desiccant becomes less concentrated as it absorbs the water

vapour from the air and has to be regenerated in order to maintain its ability to absorb water. Therefore, it is collected in a tank and pumped to the solar regenerator where becomes more concentrated. The solar regenerator provides the necessary latent heat to drive off water from the desiccant solution and it can be placed on the greenhouse roof or on the ground. The concentrated solution is collected in a tank and then is pumped back to the desiccant pad. The desiccant pad has also embedded cooling pipes (the cooling fluid is water) for the dissipation of the latent heat of condensation and heat of dilution of the liquid desiccant. The air which is drawn out of the greenhouse with exhaust fans leaves the evaporative pad cooler and humid before entering the greenhouse.

Whereas the study cited above did not favour any specific desiccant compound, the idea of using concentrated seawater brines (known as bitterns) was developed later and described by Davies and Knowles (2006). The proposed solar-cooling system using bitterns was compared with two other cooling systems, direct evaporative and indirect evaporative. Figure 1.11 illustrates the processes in a psychrometric chart. It is seen that the liquid desiccant cooling process (ideal or not) achieves better cooling than the others. Figure 1.12 shows the results that Davies and Knowles predicted for the three cooling methods when applied to the climate of Abu Dhabi.

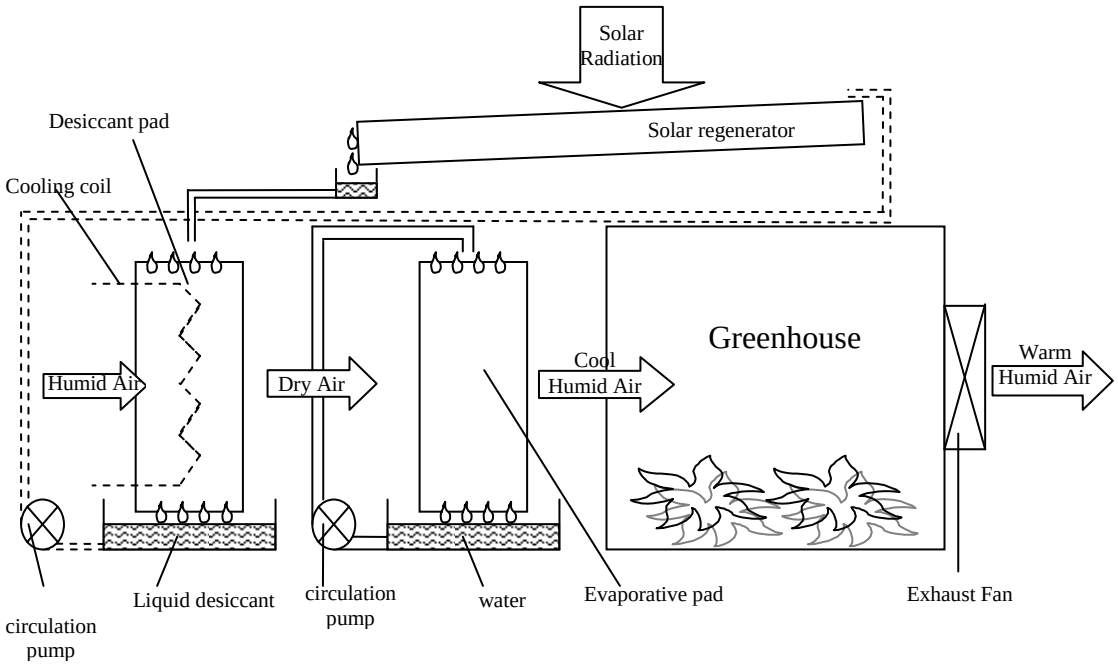

Fig. 1.9: Flow process diagram of the proposed system.

The possibility of using seawater bitterns as liquid desiccants arises from the composition of the seawater, in particular from the minor constituents besides sodium chloride. The most common of these are: Mg^{+2}, $S0_4^{-2}$, Ca^{+2}, K^+, Br^-, $C0_3^{-2}$ ions. During the process of evaporation they form compounds and precipitate according to their solubility.

This process occurs naturally in saline lakes and solar salts works to be found at various coastal locations around world. In a solar salt works (see Fig. 1.10), seawater is passed through a series of ponds with increasing concentration. Eventually crystallisation takes place as the brine becomes saturated. Calcium, sodium, and potassium salts precipitate before magnesium salts which relatively have higher solubility than the others. This results in concentrated brines rich in magnesium whose concentration can be 69 times higher of that in raw seawater (Amdouni, 2000). The high concentration of Mg^{+2} ions give a bitter taste to the brines and for that reason they are called bitterns.

Fig. 1.10: Solar salt works in Mesolongi, Greece.

Not only the commercial production of salt produces bitterns and concentrated brines but so do desalination plants. These brines are considered by-products and they are usually disposed of to the sea. Ahmed and co-authors investigated the possibility of using these brines in other applications such us aquaculture, solar ponds and also as a source of highly concentrated $MgCl_2$ (Ahmed *et al.*, 2001, Ahmed *et al.*, 2003). Bitterns can be considered liquid desiccants since $MgCl_2$, the main constituent, is a hygroscopic salt (it has the ability to absorb water). Although it is not as strong a desiccant as the lithium salts, it is not expensive, it is abundant and it has low toxicity, according to Davies and Knowles (2006).

Pressure: 101325 Pa

Fig. 1.11: Psychrometric chart of direct evaporative cooling AB, indirect evaporative cooling AC and desiccant cooling AD (with internal cooling) processes. Ideal processes are shown by red lines and non-ideal by black lines. All processes include an evaporative cooling stage (reproduced from the study of Davies and Knowles (2006)).

Fig. 1.12: Cooling results achieved in Abu Dhabi (as presented by Davies and Knowles (2006)).

The preliminary work of Davies and Knowles on the feasibility of solar desiccant cooling and use of bitterns as a desiccant was mostly based on theory and made a number of assumptions about the effectiveness of the components of the system and the properties of the bitterns solution; it was assumed to have the same properties with pure $MgCl_2$ solutions. Furthermore, their work did not look into design parameters of the system such as the thickness of the desiccator or the size of the regenerator that affect the performance of the system.

1.4 Aim and Objectives

The aim of the current work is to investigate, at the laboratory scale, the feasibility of a solar-powered liquid desiccant cooling system for greenhouses, using desiccants obtained from concentrated seawater brines. This aim will be met through the following specific objectives:

i) To determine the properties of concentrated salt solutions obtainable from seawater, consisting of magnesium chloride and impurities including calcium, sodium and sulphate ions. Properties to be measured include vapour pressure, density and viscosity.

ii) To review the state of the art in greenhouse cooling technology. This will set a benchmark against which any new system must be judged and will define the original contribution of this thesis.

iii) To develop the solar regenerator and characterise its performance under a range of conditions.

iv) Similarly, To design and build the desiccator and characterise its performance through experiments.

v) Alongside the above, to develop appropriate mathematical models for scaling, thus providing predictions of performance for the full size system, and to apply these in specific case studies to arrive at overall conclusions about the system compared to alternative approaches.

This feasibility study is technical and not commercial. It investigates if and how well the proposed solar liquid desiccant cooling system will work under various climatic conditions. A commercial feasibility study would require good knowledge of local markets in order to estimate capital costs, running costs, revenues etc. Therefore any such study

will only be valid within a context and for a limited time. On the other hand, the results of the present study should inform any specific commercial feasibility study that may follow from it.

1.5 Structure of the thesis

The remaining chapters of this thesis are organized as follows:

In Chapter 2, a review is given of the state of the art in greenhouse cooling systems. This sets the scene for the new technology that is proposed and studied in the rest of the thesis.

Chapter 3 reviews the theories of electrolyte solutions, focusing on finding suitable mathematical models that can be applied to concentrated seawater brines and bitterns in order to predict vapour pressure, viscosity and density. The experimental method and results for the properties of various brines are presented along with the theoretical models and comparisons are made in order to draw general conclusions about the usefulness of these desiccant solutions.

Next, in Chapter 4, a theoretical and experimental study of the open type flat plate regenerator is carried out. There is also a review of previous work on solar liquid desiccant regenerators. Based on this, a suitable mathematical model is chosen that can predict the water evaporation rate. The validation of the experimental measurements was made against the theoretical model and vice versa. Then in Chapter 5, following the same methodology as in Chapter 4 the desiccator is studied. Based on a literature review, a mathematical model is developed that can predict the water vapour absorption rate under various ambient conditions. Once again, the experimental results are presented in comparison to the model.

The whole system modelling and design are described in Chapter 6. The desiccator model and the regenerator model (presented in Chapters 5 and 4 respectively) are combined with a greenhouse model reported and validated in the literature. Based on the whole system model, case studies are carried out for various locations in Chapter 7.

Finally, conclusions are drawn about the feasibility of the proposed cooling system in Chapter 8.

CHAPTER 2. BACKGROUND LITERATURE REVIEW

2.1 The State of the Art in Greenhouse Cooling

One of the main objectives of growing crops in a greenhouse is to extend the productive life of plants and to produce yields when this is not feasible in open field agriculture due to extreme ambient conditions. These extreme environmental conditions depend on the location. For example, in north Western Europe the basic problem is the low temperatures and frost during winter and spring which can be addressed by heating the greenhouse. However in lower latitudes (the subtropics and tropics) the main problem is the high temperatures induced in greenhouses during summer because of the excessive ambient temperature. Engineers have tried to reduce the greenhouse temperature using various methods of cooling. Here, we present the main cooling methods that have been under research for many years and have become commercial such as ventilation, shading and reflection, and evaporative cooling. We also look into alternative methods of cooling which could be the future trends in greenhouse cooling. For more detailed literature reviews in greenhouse cooling the reader is referred to the studies of Sethi and Sharma (2007) and Kumar *et al.* (2009).

2.2 Ventilation

2.2.1 Passive Ventilation

Passive ventilation (often referred to as natural ventilation in literature) is the simplest, cheapest and historically the first method applied for cooling greenhouses. Natural ventilation cooling systems utilise roof openings only (most common practice), side openings or both. It has been found that cooling with roof and side vents is more efficient than cooling with roof vents only or side vents only (Papadakis *et al.*, 1996).

There are mainly two driving forces that define the phenomenon of passive ventilation:

a) The wind which creates pressure differences around the vents and hence causes air movement (forced convection).
b) Vertical thermal gradients which create air density differences and thus buoyancy forces that cause air circulation (natural convection).

Kozai *et al.* (1980), who used the energy balance method, and Sase *et al.* (1984) who used wind tunnel experiments, were amongst the pioneers who investigated the effects of these two driving forces on the air exchange in small-scale greenhouses with roof and side openings.

Several studies have showed that the wind is the most important driving force for ventilation in greenhouses with roof vents only (Boulard and Draoui, 1995, Fernández and Bailey, 1992, Kittas *et al.*, 1995) and also with both roof and side vents (Papadakis et al., 1996). The buoyancy effect is considered to be insignificant comparatively to the wind effect for wind velocities greater than 1.8 m/s. Although for wind velocities lower than 1.8 m/s the buoyancy effect is still small, it cannot be neglected (Papadakis *et al.*, 1996).

Various studies in literature investigate the passive ventilation in different types of greenhouses using tracer gas techniques to measure the air exchange rate. Boulard and Draoui (1995) investigated the passive ventilation of a greenhouse equipped with continuous roof vents using the N_2O, CO_2 and H_2O vapour constant enrichment technique. They found that the wind is the main factor in passive ventilation and that there is a linear dependence of the air exchange rate on the wind speed and the effective opening of the vent. Boulard *et al.* (1996) performed a theoretical analysis of the physical mechanisms that influence passive ventilation of a greenhouse with continuous side vents. Their estimations of the mean flow of sensible heat and of the turbulent flow (caused by wind speed fluctuations) showed that the latter does not exceed 45% of the total heat flux. Papadakis *et al.* (1996), following the approach of Boulard *et al.*, split the wind effect into a steady and a turbulent component, investigated the air exchange rate in a plastic greenhouse with continuous roof and side vents. It was found that the side vent configuration performs less efficiently than roof only and roof and side configurations. Further more, Boulard *et al.* (1997) analysed the natural ventilation performance in six greenhouses and tunnel types that had either roof or side vents or roof and side vents. It was found that the presence of crops has a negative effect on the ventilation efficiency and that the continuous vents are more efficient than the discontinuous ones. Teitel *et al.*'s (2006) experimental study on the natural ventilation of a greenhouse with continuous roof and side vents confirmed earlier findings by other researchers. It concluded that roof and side vents provide more efficient cooling than roof vents only, depending on the type of insect screen installed. Coelho *et al.* (2006) compared four different natural ventilation

configurations and developed a semi-empirical simplified climatic model. The best performance was achieved by the combination of roof and side vents. Similarly, Perez Parra *et al.* (2004) investigated the natural ventilation of a greenhouse (parral type) under different vent configurations. It was found that the flap vent facing the wind achieved the highest ventilation rate per unit ventilation area. Nielsen (2002) carried out experiments in a greenhouse with roof vents only. The natural ventilation performance was improved (the air exchange was improved by 50% in the canopy) by placing a 1m high vertical screen placed at the top of the greenhouse in parallel to the ridge.

Several researchers investigated the effects of insect screens in roof openings on greenhouse air exchange rate. Soni *et al.* (2005) analysed the effect of various types of insect screens on natural ventilation of tropical greenhouses. It was shown that insect screens with high porosity affect adversely the vertical thermal gradients (5–10% increase). Romero *et al.* (2006) performed an experimental and numerical study on the natural ventilation of a greenhouse located in central Mexico equipped with an insect screen. It was found that an enlargement of roof-vent area equivalent to 15% of the greenhouse floor area results in a 25% increase of ventilation rate. The removal of the insect screen could increase ventilation rate by 25–30%.

Also worth mention is the study of Demrati *et al.* (2001) who investigated the performance of natural ventilation in a large-scale banana greenhouse located in Morocco. They developed a dimensionless ventilation function that can be also applied to plastic film roll up vent systems. It was found that the wind related efficiency of the large greenhouse was higher by 20% than for smaller greenhouses.

2.2.2 Forced Ventilation

Since passive ventilation is mainly wind driven, this can be a major disadvantage at low or zero wind speeds. Therefore, the need for a ventilation system that overcomes this problem led engineers to employ new methods in greenhouse cooling. One of these methods was the use of exhaust fans and blowers which increase the air circulation and air exchange rate of the greenhouse. The cooling of greenhouses with the aid of mechanical means such us exhaust fans, blowers, etc. is called forced ventilation (sometimes found as ‘fan ventilation’ in literature).

Here, we selectively review studies carried out by researchers since the 90's. Amongst the studies on forced ventilation found in literature, of particular interest is the work of Papadakis *et al.* (1992) in which the forced, mixed and free convection heat transfer mechanisms occurring inside greenhouses were investigated. In another study, Fuchs *et al.* (1997) investigated the effect of four different ventilation configurations (passive and forced) on the energy balance of a greenhouse with dry sandy soil. It was found that the passive configuration was the most effective in the presence of regular winds. The forced ventilation configuration had low efficiency and the fans operated far below their nominal speed because of the pressure drop across the insect nets. Willits (2003) presented a model for a fan ventilated greenhouse where a fan-pad system was also used for comparison. It was concluded that the forced ventilation system performed well when used for flow rates lower than 0.05 m^3/m^2 s. Higher flow rates did not provide better cooling; in fact there was an adverse effect when RH was low. When the fan-pad system was used substantial cooling was predicted for air flow rates higher than 0.05m^3/m^2 s. Kittas *et al.* (2005) investigated the forced ventilation of a greenhouse with rose crop located in Greece. The experimental findings showed that the temperature difference between the inside and outside was significantly affected by the ventilation rate and the incoming solar radiation. Based on this, a simplified climatic model for fan-ventilated greenhouses was presented.

In literature there are few studies which compare different methods applied for greenhouse cooling (Castilla and Montero, 2008). An exception is the study by Kittas *et al.* (2001) where the performances of a forced ventilation configuration (fans and roof openings) and a passive ventilation one (roof vents only) were compared to find that the former system achieves a more homogeneous temperature and RH field vertically than the latter one does. It was also found that a high rate of ventilation does not necessarily cause better cooling because there is an optimal air exchange rate which depends on the ambient air temperature, ambient relative humidity, the internal airflow patterns and the species of the crop (different response of stomata in humidity). The response of a sweet pepper crop to different cooling methods (natural ventilation and whitening, fogging, forced ventilation) was investigated by Gazquez *et al.* (2006). It was shown that the forced ventilation system did not control the greenhouse maximum temperature and vapour pressure deficit as effectively as the other methods.

2.3 Shading and Reflection

Passive ventilation is generally not enough to cool the greenhouse air temperature down to a desirable temperature (ie. optimum temperature for crop cultivation) during the hot season. Thus, shading or reflection, a supplementary low cost method, is usually employed by farmers. This method is cheaper than forced ventilation and is widely used commercially but has the disadvantage of reducing PAR (photosynthetically active radiation). It can be done by the use of external shade clothes, paints, slatted blinds, nets, reflective shade screens. Other ways of shading/reflection include the use of liquid foams between the greenhouse walls (Shamim and McDonald, 1995).

Baille *et al.* (2001) investigated the influence of whitening on greenhouse microclimate and the behaviour of a rose crop grown in Greece. It was found that the greenhouse air temperature, vapour pressure deficit and canopy to air temperature difference decreased drastically. Whitening reduced significantly the crop's water stress. It was concluded that this technique can be used in reducing the summer heat load in warm countries. However, a disadvantage of whitening is that once applied the intensity of the paint cannot be changed.

Reflective shade nets or screens are extensively used in greenhouses for reducing the solar heat load during the hot season of the year. Cohen and Fuchs (1999) measured the radiometric properties of reflective shade nets and thermal screens found in market. All five screens studied contained highly reflective aluminized materials. The measured properties can be used to predict radiant fluxes above and below screens of different compositions. Kittas *et al.* (1999) investigated the effect of blanking (roof whitening providing 35% shading), the use of an aluminized shade screen (70% shading) and an external shade net (30% shading) on the spectral distribution of light in greenhouses. It was found that whitening enhances slightly the PAR enrichment effect of the glass material. This can be advantageous to the other tested shading treatments in warm countries with high radiation load during summer. In addition, whitening does not interfere with the greenhouse ventilation as the shading nets do adversely.

Sethi *et al.* (2004) carried out an experimental study on a greenhouse located in Northern India. The cooling effect of an aluminized polyester sheet, used inside the greenhouse for shading, was investigated. It was found that the total solar radiation entering the

greenhouse was reduced by 43% and the greenhouse air temperature was decreased by 3 – 4 ^{o}C when compared to the greenhouse without shading. However shading by its own was not enough to reduce the greenhouse air temperature down to the required optimum temperature for crop growth.

2.4 Evaporative Cooling

Ventilation (passive and/or forced) with or without shading proved to be inadequate for cooling greenhouses located in the subtropical and tropical zones during the hot season of the year at the desired temperature for optimum crop growth. Therefore, water evaporation, well-known since antiquity from other applications, was applied to greenhouses. The evaporative cooling systems are based on a simple thermodynamic principle: when water is evaporated in air, sensible heat is removed from the air and is converted into latent heat of vaporisation. The evaporative cooling systems used in greenhouses are the fan-pad, fog-mist system and roof evaporative cooling.

2.4.1 Fan-Pad System

The best known fan-pad system consists of exhaust fans located at one end of the greenhouse and wet pads at the opposite end. The fans draw air through the wet pads; the air is cooled and humidified up to saturation (ideally). A pump is used to supply the pads with water. Based on the simple psychrometric principle that the lower the RH of the incoming air the higher the air temperature drop (for constant water temperature) we can infer that wet pads perform better in dry climates. The same principle applies to fog-mist systems hence they are also more suitable for hot and dry climates (Montero et al., 1990).

Fuchs *et al.* (2006) investigated a fan-pad cooling system. A theoretical numerical model was developed and validated against experimental data. The experimental findings showed that, in a greenhouse with a fan ventilation system (set at 30 volume changes per hour) and cover materials that reduce solar radiation transmission by 30%, transpiration can cool foliage and air below outside air temperature. The simulations showed that this can take place for RH lower than 50% and for an outside air temperature of 35 ^{o}C. However, when the fan-pad system is used it lowers the greenhouse air temperature and decreases the water vapour pressure deficit. It was also shown that for RH higher than 60% the fan-pad system fails to maintain temperature below 30 ^{o}C when the irradiance is 1000 Wm^{-2}. Kittas *et al.*

(2003) developed a climate model for greenhouses that combines the effects of ventilation rate, roof shading and crop transpiration. The simulations showed that high ventilation rates and shading improve the cooling effect of the fan-pad cooling system by lowering the temperature gradients. This, however, enhances plant transpiration and results in water stress. Shading reduces plant transpiration but also reduces photosynthetic rate which results in lower yields. It was also shown that at hot and dry conditions (35^{o}C and RH<50%) the temperature can be 5^{o}C less than the ambient at 30 m distance from the inlet, but at hot and humid conditions (35^{o}C and RH>65%) it is almost the same as the ambient if not increased. Ganguly and Ghosh (2007) presented a thermal model of a greenhouse equipped with a fan-pad system. Based on the simulations it was found that during summer the use of a fan-pad system satisfactorily improves the inside climatic conditions of a greenhouse 12m long located in Kolkata, India. During the monsoon period, however, the fan-pad system was not effective because of the high ambient RH; the greenhouse air temperature was 2^{o}C less than ambient.

Worth mentioning is Sabeh *et al.*'s experimental study (Sabeh *et al.*, 2006). The water consumption of a fan-pad system, used for cooling a greenhouse in Arizona, was investigated. It was found that at higher ventilation rates the fan-pad system achieves lower cooling efficiencies and also water consumption increases. High ventilation rates did not necessarily provide better cooling. A ventilation rate limit was observed and beyond this the climate conditions of the greenhouse did not improve.

Arbel *et al.* (1999) carried out a comparative study of a fog/mist system and a fan-pad system. It was found that the fog system provides uniform distribution of temperature and humidity in the greenhouse while the fan-pad system causes horizontal temperature gradients along the greenhouse. It was recommended to use a combination of on/off at low pressure, when the heat load is small and continuous operation at high pressure when the heat load is high.

2.4.2 Fog-Mist System

The fog or mist system (also found as fogging system in literature) produces a fine mist which is created by the spraying of water in small drops (2-60 μm in diameter) with high pressure into the air above the canopy of the plants. Spraying of water in small droplets increases the water surface in contact with air and therefore evaporation takes place almost instantaneously. The water droplets are carried by the air streams inside the greenhouse and do not wet the foliage, thus leaving it dry.

Two fogging systems have been mainly studied by researchers:

a) Giacomelli *et al.* (1989) used high pressure nozzles (0.1-0.3mm diameter) to generate mist. Pretreatment of water is required to avoid blocking of nozzles.
b) The twin fluid nozzles system was used by Montero *et al.* (1990). It combines compressed air and water by varying pressure and flow rates in order to generate water droplets of the desired size. Therefore, this system requires a compressor which consumes a lot of electrical energy. Thus it is more expensive (higher operation and installation cost) than the pre mentioned system.

The performance of a fog system was investigated and compared to that of a fan-pad system by Arbel *et al.* (1999). The fog system performed better than the fan-pad achieving unvarying air temperature and RH inside the greenhouse. On the contrary, the fan-pad system created temperature and RH gradients. In another study Arbel *et al.* (2003) investigated how the level and uniformity of the climatic conditions are affected in a greenhouse that uses a combined forced ventilation system and fogging system for cooling. It was concluded that this system achieves high uniformity level of air temperature and RH. It also maintained the greenhouse air temperature at 28^{o}C and RH at 80% during the summer at noon in the Arava valley of Israel. The disadvantage of this system is the high inclusive cost per unit area of the structure.

Öztürk (2003) investigated the efficiency of a fogging system for multi-span plastic greenhouses. Uniform relative humidity and temperature levels were observed. The temperature difference between the outside and inside was 6.6^{o}C and the RH was increased by approximately 25%. A fogging system efficiency of 50.5% was achieved.

An improvement of the fog system was presented by Toida *et al.* (2006). They investigated the effect on cooling performance of a fog system when using an upward air stream with the aim of two small fans. It was found that this system improved the greenhouse cooling efficiency when compared to the conventional fog systems.

2.4.3 Roof Evaporative Cooling

Roof evaporative cooling refers to the sprinkling of water on the surface of the roof so as to form a thin layer, hence increasing the free water surface area and resulting in an increased water evaporation rate. Consequently, the water temperature falls to the wet bulb temperature of the closely surrounded air.

Cohen *et al.* (1983) carried out an experimental study in order to compare the cooling effect of roof evaporative cooling and wetting the top of the canopy and soil surfaces in a glasshouse. It was found that wetting the roof was less efficient than wetting the foliage. When the two treatments were combined the greenhouse air temperature was decreased by 5^{o}C and foliage temperature by 7^{o}C below the ambient temperature. Sutar and Tiwari (1995) conducted an analytical and numerical study of a plastic greenhouse equipped with a roof evaporative cooling system located in India. It was found that this treatment could lower the greenhouse air temperature by 4-5^{o}C. A shade cloth on the roof with water film could lower the greenhouse air temperature by 10^{o}C. In another study, Ghosal *et al.* (2003) developed a model for flowing water film on shade cloth, stretched over the roof and south wall of an even span greenhouse. The model was validated against experimental data and the simulations showed that the air temperature can be reduced by 6^{o}C when using the shade cloth with water flow while shading only reduces the temperature by 2^{o}C. Also worth mentioning is the study of Garzoli (1989) who also investigated roof evaporative cooling but used a dye dissolved in water in order to absorb more radiation. The dye can however be the downfall of this system due to its toxicity to plants.

2.5 Future Trends

Substantial effort has been given to improve the greenhouse cladding materials in order to become photo selective and thus limit the solar energy load (also referred to as Near Infrared Radiation [NIR] blocking). These plastic films are most promising as they manage to decrease the greenhouse temperature by 4^{o}C (Montero *et al.*, 2009). NIR selective filters can be applied as:

a) Permanent additives or coatings to the cover
b) Seasonal "whitewash"
c) Movable flexible film screens

According to Castilla and Montero (2009) a permanent filter can be applied successfully in tropical environments. Hemming *et al.* (2006) investigated the potential of using NIR-filtering methods in greenhouse cooling. It was concluded that NIR-filtering multilayer coatings perform effectively and NIR-filtering reflecting materials achieve better results NIR-absorbing materials. Simulations showed that during summer time the greenhouse air temperature can be reduced by 1^{o}C approximately. Sonneveld *et al.* (2006) investigated the use of a NIR-reflective cover material with the use of a PV solar driven cooling system. It was found that absorption or compression coolers are not a feasible alternative for greenhouse cooling since their cooling capacities would be too large. In contrast the combination of NIR–reflective material and fan–pad system was found to be feasible reducing the electrical energy consumption by a factor of ten. The simulations showed that the heat load can be reduced by 50%. Garcia-Alonso *et al.* (2006) tested various "cool" plastic films (meaning films that block NIR) for covering greenhouses in tropical and subtropical areas. It was found that the new plastic films reduced the maximum greenhouse air temperature by approximately 0.5-4.2^{o}C depending on season. The yield increased by 26% and the quality was significantly improved.

The potential of using Fresnel Lenses instead of typical glass covering material for cooling greenhouses has been investigated in the past by several researchers (Jirka *et al.*, Tripanagnostopoulos *et al.*, 2005). Souliotis *et al.* (2006) estimated that a Fresnel Lenses system with thermal absorbers can reduce greenhouse ventilation and cooling by 50%.

Santamouris *et al.* (1995) proposed the use of buried pipes to conserve energy in greenhouse cooling. It was concluded that underground earth-air heat exchangers can reduce the cooling requirements. Their parametric analysis showed that the indoor air

temperature decreases with increasing pipe length, decreasing pipe diameter, increasing depth up to 4 m and increasing air velocity inside the pipes. Ghosal *et al.* (2004) presented a simplified analytical model to study the year round effectiveness of an earth–air heat exchanger which was used with a greenhouse in Delhi, India. It was found that the system can reduce greenhouse temperature by 3–4 ^{o}C in summer compared to a greenhouse without earth-air heat exchanger. Ghosal and Tiwari (2006) developed a thermal model which was used to investigate the cooling potential of an earth-air heat exchanger for greenhouses. It was found that the greenhouse air temperature during summertime was 5–6 ^{o}C lower than the one in the same greenhouse without earth-air heat exchanger. It is to be noted though that most of the year the air temperature remained high and above the plant comfort zone.

Other attempts at enhanced greenhouse cooling include the work of Yildiz and Stombaugh (2006). They investigated the potential of using a heat pump system for energy and water conservation in open and confined greenhouses. It was concluded that the heat pump system can achieve energy and water savings, cooling and dehumidification. The cooling system COP ranged between 0.93–1.03. However the initial investment unit can restrain the commercial feasibility of the system. The main energy savings are basically achieved in heating. There is no energy saving in cooling when compared to a conventional fan-pad system. The heat pump system is much more expensive. Hamer *et al.* (2006) investigated alternative methods of cooling and heating greenhouses. It was found that evaporative cooling is the lowest investment cost option for cooling when compared to vapour compression heat pump and absorption heat pump systems. However, a CHP system that utilises an absorption heat pump can give an annual margin increase of £9.8 m^{-2}.

2.6 Liquid Desiccant Cooling

Liquid desiccant cooling has been developed as an alternative and complementary method of cooling focusing on applications such as cooling of human dwellings, commercial buildings, hospitals (Dai *et al.*, 2001, Gommed and Grossman, 2004, Jain *et al.*, 2000, Mei and Dai, 2008, Oliveira *et al.*, 2000). It is a solar thermal sorption refrigeration method. Sorption refrigeration can be divided into three main categories (see Fig. 2.1):

a) Desiccant cooling or open sorption cooling. The hygroscopic substance (or desiccant) in this process is used to dehumidify the air. The desiccant can be liquid (liquid desiccant cooling) or solid (solid desiccant cooling). The liquid desiccants utilised are aqueous solutions of lithium salts (LiCl, LiBr), aqueous solutions of calcium chloride (or mixtures of LiCl and $CaCl_2$) and tri-ethylene glycol. The solid desiccants used are silica gel, activated alumina and zeolite.

b) Absorption. It is a closed cycle process using liquid desiccants such as LiBr-H_20, NH_3-H_20.

c) Adsorption. Closed cycle process that can be subcategorised based on the nature of the process in:

   i. Physical adsorption. High porosity substances such as zeolite, silica gel, activated carbon and alumina are used as adsorbents.

   ii. Chemical adsorption. In this process the strength of the chemical bond between the adsorbent and the adsorbate drives the phenomenon. Usually $CaCl_2$ is utilised with ammonia.

For comprehensive literature reviews in solar refrigeration the reader is referred to the studies of Kim and Infante Ferreira (2008) and Grossman (2002).

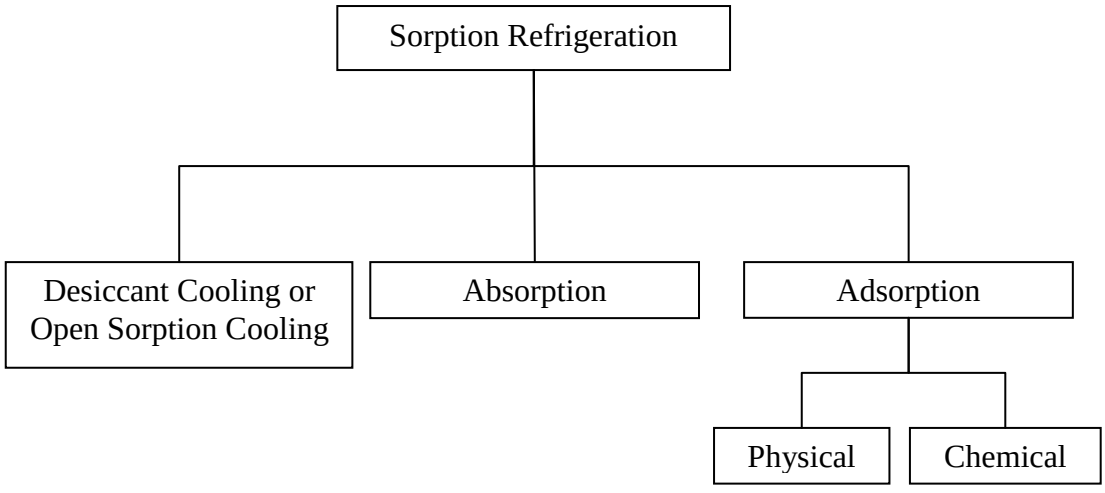

Fig. 2.1: Tree diagram showing the different types of sorption refrigeration.

As mentioned in Chapter 1, the use of liquid desiccants with solar regeneration in a fan-pad system coupled to a greenhouse was investigated theoretically by Davies (2005). The model presented used climatic data of Abu Dhabi and it was found that this system could lower summer maximum temperatures by 5^{o}C when compared to conventional evaporative cooling.

2.7 Discussion

This review has differentiated among the various physical processes of greenhouse cooling and identified the technologies used to implement them. Ventilation (passive/forced) provides adequate cooling for greenhouses located in the temperate zone, especially in high latitudes. The need for cooling increases with decreasing latitudes, hence in lower latitudes only ventilation is not enough. In the subtropics, complementary methods to ventilation are used for cooling e.g. shading-reflection which adversely affects photosynthesis as it reduces PAR. However, even the combination of ventilation and shading-reflection is not enough in warmer climates. Evaporative cooling has proved to achieve better cooling than all the other mentioned methods in hot and dry climates. But even the latter method, as already shown by Ganguly and Ghosh (2007) and Kittas *et al*. (2003), fails to generate enough cooling when applied to hot and humid climates such as the tropics and the coastal area of the subtropics as also pointed by Kumar *at al.* (2009). In fact these studies concluded that a fan-pad evaporative cooling system can marginally decrease greenhouse air temperature by 2^{o}C during 12-14hrs (high irradiance, high ambient relative humidity ~ 75%) or sustain temperatures at the ambient level if not increased (depending on the greenhouse length). Nevertheless, a solar liquid desiccant cooling system could address this problem as already discussed in Chapter 1, section 1.3. by lowering maximum summer temperatures by 5^{o}C at least on the basis of theoretical predictions. This is the option explored further in this thesis.

Table 2.1 summarises studies published since the 80's focusing on the type of cooling system, the geographical zone and whether the method is commercial or experimental.

Table 2.1: Brief summary of studies on greenhouse cooling published since 1980's.

Year	Authors	Type of Cooling System	Geographical Zone	Experimental / Commercial
1980	Kozai *et al.*	Passive Ventilation	subtropics	commercial
1983	Cohen *et al.*	Roof evaporative cooling	subtropics	experimental
1984	Sase *et al.*	Passive Ventilation	subtropics	commercial
1989	Giacomelli *et al.*	Fog-mist	subtropics	experimental
1989	Garzoli	Roof evaporative cooling	tropics/subtropics	experimental
1990	Montero *et al.*	Fog-Mist	subtropics	commercial
1992	Fernandez and Bailey	Passive Ventilation	temperate	commercial
1992	Papadakis *et al.*	Forced Ventilation	subtropics	commercial
1995	Boulard and Draoui	Passive Ventilation	subtropics	commercial
1995	Kittas *et al.*	Passive Ventilation	subtropics	commercial
1995	Shamim and McDonald	Shading/Reflection	temperate	experimental
1995	Sutar and Tiwari	Roof evaporative cooling	tropics	experimental
1995	Santamouris *et al.*	Earth-Air Heat Exchanger	subtropics	experimental
1996	Papadakis *et al.*	Passive Ventilation	subtropics	commercial
1996	Boulard *et al.*	Passive Ventilation	subtropics	commercial
1997	Boulard *et al.*	Passive Ventilation	subtropics	commercial
1997	Fuchs *et al*	Passive/Forced Ventilation	subtropics	commercial
1999	Cohen and Fuchs	Shading/Reflection	subtropics	commercial
1999	Kittas *et al.*	Shading/Reflection	subtropics	commercial
1999	Arbel *et al.*	Fan-Pad, Fog-Mist	subtropics	commercial
1999	Jirka *et al.*	Fresnel Lenses covering material	temperate	experimental
2001	Demrati *et al.*	Passive Ventilation	subtropics	commercial
2001	Kittas *et al.*	Passive and Forced Ventilation	subtropics	experimental
2001	Baille *et al.*	Shading/Reflection	subtropics	commercial
2002	Nielsen	Passive Ventilation	temperate	commercial
2003	Willits	Forced Ventilation, Fan-Pad	subtropics	commercial
2003	Kittas *et al.*	Fan-Pad, Shading	subtropics	commercial
2003	Ozturk	Fog-Mist	subtropics	Commercial
2003	Arbel *et al.*	Forced Ventilation, Fog-Mist	subtropics	Commercial
2003	Ghosal *et al.*	Roof evaporative cooling	tropics	Experimental
2004	Parra *et al.*	Passive Ventilation	subtropics	commercial
2004	Sethi *et al.*	Shading/Reflection	tropics	commercial

(Table 2.1 continued)

2004	Tripanagnostopoulos *et al.*	Fresnel Lenses covering material	subtropics	experimental
2004	Ghosal *et al.*	Earth-Air Heat Exchanger	tropics	experimental
2005	Soni *et al.*	Passive Ventilation	tropics	commercial
2005	Kittas *et al*	Forced Ventilation	subtropics	commercial
2005	Davies	solar liquid desiccant cooling	subtropics	experimental
2006	Teitel *et al.*	Passive Ventilation	subtropics	commercial
2006	Coelho *et al.*	Passive Ventilation	subtropics	commercial
2006	Romero *et al.*	Passive Ventilation	temperate	commercial
2006	Gazquez *et al.*	Passive/Forced Ventilation, Fogging, Shading	subtropics	commercial
2006	Fuchs *et al.*	Fan-Pad	subtropics	commercial
2006	Sabeh *et al.*	Fan-Pad	subtropics	commercial
2006	Toida *et al.*	Fog-Mist	subtropics	experimental
2006	Hemming *et al.*	NIR filtering methods	temperate	experimental
2006	Sonneveld *et al.*	NIR reflective covering material	temperate	experimental
2006	Garcia-Alonso *et al.*	cool plastic films	subtropics	experimental
2006	Souliotis *et al.*	Fresnel Lenses covering material	subtropics	experimental
2006	Ghosal and Tiwari	earth-air heat exchanger	tropics	experimental
2006	Yildiz and Stombaugh	heat pump	temperate	experimental
2006	Hamer *et al.*	various heat pump based systems	temperate	experimental
2007	Ganguly and Ghosh	Fan-Pad	tropics	commercial
2009	Montero *et al.*	NIR blocking plastic films	subtropics	commercial

2.8 The Contribution of this thesis

This research contributes to the resolution of the problem of high temperatures induced in greenhouses during summer in hot and humid places. As discussed in Chapter 1, this problem is expected to increase due to climate change. We propose the use of a solar powered liquid cooling system that utilises bitterns as liquid desiccants. As described in earlier sections of this chapter current cooling technologies fail to address this problem in hot and humid places such as the ones located in the tropical and subtropical zones.

This study builds on previous work published by Davies (2005), Davies and Knowles (2006) and Davies *et al.* (2006). But, in contrast to those earlier theoretical studies which made a number of simplifying assumptions regarding the performance of essential parts of the system such us the regenerator and the desiccator, this work looks critically at those assumptions. In particular it includes a number of experiments, detailed theoretical analyses and models aimed at answering the question about what cooling performance can be achieved with the system.

For example, in previous studies it was also assumed that bitterns have the same properties as pure $MgCl_2$ solutions due to the lack of information on the physical properties of concentrated brines. Therefore, here we investigate further the concept of using bitterns as liquid desiccants for cooling greenhouses in order to assess their suitability for driving the desiccant cooling cycle. We particularly emphasize measuring the properties of vapour pressure, density and dynamic viscosity.

Consequently to test our hypothesis we develop a computer model of the proposed system to evaluate its performance when applied to a greenhouse under different climatic conditions.

CHAPTER 3. PROPERTIES OF SEAWATER BITTERNS

3.1 Introduction

Since antiquity men have used salt as a food supplement and as preservative. Various methods of salt production were developed in the world. In hot climate coastal areas the most common method of salt production has been the evaporation of seawater in shallow basins using solar heat. In these solar salt works, Seawater is passed through a series of shallow lagoons with increasing concentration. Ultimately sodium chloride is crystallized and precipitated as the brine becomes saturated in sodium chloride. Besides Na^{+} and Cl^{-} ions, seawater and natural brines contain other constituents in minor concentrations e.g. Mg^{+2}, $S0_4^{-2}$, Ca^{+2}, K^{+}, Br^{-}, $C0_3^{-2}$. During the process of evaporation they form compounds and precipitate according to their solubility. Calcium, sodium, and potassium salts precipitate before magnesium salts which relatively have higher solubility than the others. This results in concentrated brines rich in magnesium whose concentration can be 69 times higher of that in raw seawater (Amdouni, 2000) called bitterns.

Bitterns can be considered liquid desiccants since $MgCl_2$, the main constituent, is a hygroscopic salt. Although it is not as strong desiccant such as lithium chloride, lithium bromide or calcium chloride it is not expensive, it is abundant and it has low toxicity - properties which would be useful in applications requiring large volumes of low-grade cooling (Davies and Knowles, 2006).

However, besides magnesium and chloride ions bitterns contain impurities including sulphate, sodium, potassium and calcium ions. The studies of Davies and Knowles (2006) and Davies *et al.* (2006) concluded that bitterns can be used as liquid desiccants but their analysis was based on the published properties of pure magnesium chloride solutions; the effects of the impurities were not taken into account. The objective of the work reported here was to determine more accurately the properties of concentrated seawater bitterns, specifically their vapour pressure (and therefore equilibrium relative humidity, ERH), density and viscosity, as these are the properties of greatest interest in the design of the proposed cooling system. Therefore, another objective was to obtain theoretical models that predict these properties as a function of the composition, concentration and temperature. Such models would be needed as a tool in the design of the proposed cooling system.

For reasons of convenience when conducting experiments with a prototype refrigeration system in the laboratory, it was more convenient to obtain and use pure a magnesium chloride reagent rather than a multicomponent bitterns mixture. Hence we had to quantify the difference between the properties of seawater bitterns and those of pure magnesium chloride solution in order to evaluate the validity of this experimental approach.

Bitterns are a complex mixture of electrolytes in high concentrations. Thus published data were not readily available and a number of competing theoretical data were identified, the accuracies of which were guaranteed only for dilute solutions. Therefore experiments with highly concentrated brines were carried out focusing on finding and validating the best model. In accordance it was used to generate a number of useful results and conclusions.

3.2 Theories of electrolytes solutions

The desired characteristics of the theoretical model are that it should be sufficiently accurate for engineering purposes and lead to concise and usable mathematical formulations. Further, an established theory is preferable to one that is entirely novel. Historically, research on modelling thermodynamic properties of electrolyte solutions has developed along two main lines as follows.

1) Fundamental electrolyte solution theories, as discussed thoroughly by Loehe and Donohue (Loehe and Donohue, 1997). Generally these are too complex and do not lead to formulations that are convenient for the current purpose.

2) Engineering models of the empirical and semi-empirical kind. These can be sub-divided in different categories according to the underlying physical concepts: (i) local composition based models (Abrams and Prausnitz, 1975, Chen *et al.*, 1982, Chen and Evans, 1986, Renon and Prausnitz, 1968), (ii) adsorption-theory models (Abraham and Abraham, 2000, Ally and Braunstein, 1998), (iii) speciation-based models for mixed-solvent electrolyte systems (Wang *et al.*, 2002, Wang *et al.*, 2004) and (iv) empirical and semi-empirical models based on variable theories including the Debye Hückel (Pitzer, 1973, Pitzer, 1981, Pitzer, 1991, Pitzer and Guillermo, 1974, Pitzer *et al.*, 1985, Pitzer *et al.*, 1999, Reilly *et al.*, 1971, Robinson and Stokes, 1959, Stokes and Robinson, 1966, Pitzer and Kim, 1974).

In this study we focussed on the fourth of these options, as already adopted in references (El Guendouzi *et al.*, 2005, El Guendouzi *et al.*, 2004) and by Ha and Chan (1999) to predict water activity in electrolyte mixture solutions similar to seawater.

3.2.1 Local composition based models

Initially the local composition models, proposed by Wilson, Renon and Prausnitz (NRTL), Abrams and Prausnitz (UNIQUAC) (Wilson, 1964, Abrams and Prausnitz, 1975, Renon and Prausnitz, 1968) were developed for non-electrolyte systems because the short range forces between molecules, i.e. molecule-molecule interactions, are only significant at close range and their effects drop rapidly as the separation distance increases. In dilute electrolyte solutions the long range forces are dominant but at high concentrations the importance of the short range effects increases.

The non random two liquid model (NRTL) was firstly modified by Chen and his associates in order to be applied in single solvent and single completely dissociated systems (Chen *et al.*, 1982) and later was generalised to represent aqueous multicomponent electrolyte systems (Chen and Evans, 1986). It is known as Electrolyte-NRTL and can be considered as an extension to the Pitzer's model since it takes into account not only the long range forces, but also the short range ones. The model uses the following excess Gibbs energy expression:

$$\frac{G^{ex}}{RT} = \frac{G^{ex,PDH}}{RT} + \frac{G^{ex,LC}}{RT}, \tag{3.1}$$

which yields $\ln\gamma_i = \ln\gamma_i^{PDH} + \ln\gamma_i^{LC}$. The first and the second terms on the right hand side of the equations are respectively the long and the short range contribution. It has been through modifications for improving the activity coefficient of aqueous electrolytes by adding empirical parameters (Jaretun and Aly, 2000) and for simplifying the model by replacing the elec-NRTL binary parameters with ion-specific parameters (Kuramochi *et al.*, 2005). Now it is applied successfully to multicomponent electrolyte solutions over the entire range of concentrations and is included in commercial process simulators like Aspen Plus® (Aspen Technology Inc, Massachusetts USA).

The modified NRTL model by Kolker and de Pablo neglects the long range interaction contribution and uses constant mixture parameters (Kolker and de Pablo, 1995, Kolker and de Pablo, 1996). The advantage of this method is that only pure component data and infinite dilution data are necessary. The practical difficulty of the model is the determination of the excess Gibbs energy for a hypothetical mixture of pure electrolytes.

3.2.2 Adsorption theory models

Ally and Braunstein extended the adsorption theory of electrolytes to predict water and electrolyte activities in multicomponent electrolyte solutions (Ally and Braunstein, 1998). The equations presented by them were quite complicated. Abraham and Abraham published a model which is simpler than the one previously mentioned (Abraham and Abraham, 2000). This model is based on the Stokes and Robinson modified BET (Brunauer, Emmet and Teller) model and uses additivity rules for its parameters. The equations for calculating water activity are:

$$\frac{a_w(1-x_w)}{x_w(1-a_w)} = \frac{1}{cr} + \frac{(c-1)}{cr}a_w \tag{3.2}$$

$$r = \sum_i X_{ei} r_i \quad (3.3), \qquad r\varepsilon = \sum_i X_{ei} r_i \varepsilon_i \quad (3.4), \qquad c = \exp\left(\frac{\varepsilon}{RT}\right) \quad (3.5), \qquad \varepsilon = E_L - E \quad (3.6),$$

$$r = \frac{N_s}{N_A} \tag{3.7}$$

where x_w is the water mole fraction, a_w is the water activity, c is a constant related to the heat of adsorption E, E_L is the molar binding energy of water in pure water, r is a structural parameter, X_{ei} is the mole fraction of an electrolyte i in the anhydrous mixture of electrolytes, N_A is the Avogadro constant and N_s is the number of available sites of water molecules with the molar binding energy E per mole of electrolyte.

A constraint of this model is that r and ε parameters are required for each electrolyte in an anhydrous mixed electrolyte system and these data are not readily available.

3.2.3 Speciation based models for mixed-solvent electrolyte systems

The MSE (mixed solvent electrolyte model) is a recent advancement in modelling thermodynamic properties of multicomponent solutions that contain salts, acids and bases

(Wang *et al.*, 2002, Wang *et al.*, 2004). In this model the excess Gibbs energy is expressed as:

$$\frac{G^{ex}}{RT} = \frac{G^{ex}_{LR}}{RT} + \frac{G^{ex}_{MR}}{RT} + \frac{G^{ex}_{SR}}{RT} \tag{3.8}$$

On the right hand side of the equation the first, the second and the third term are the long, the medium and short range interactions contribution correspondingly. The first term is calculated from the Pitzer-Debye-Hückel equation, the third term is calculated from the UNIQUAC equation and second term by a second virial coefficient type equation. The model is applicable to aqueous multicomponent systems from infinite dilution to molten salts to a wide range of temperatures. It has been used in commercial process simulators under OLI Systems®.

3.2.4 Empirical or semi empirical models for predicting water activity - ERH

In a desiccant cooling system, a property of prime importance is the Equilibrium Relative Humidity (ERH) which compares the humidity of air in contact with the desiccant, to that of air in contact with pure water. By definition ERH must be in the range $0<ERH\leq100\%$. The ERH depends directly on the solution vapour pressure and in turn on the chemical activity of the water, which is a fundamental thermodynamic property appearing in many of the standard theories available. In so far as the water vapour can be treated as an ideal gas, these quantities are related by the following expression.

$$a_w = P^* / P_o = ERH \times 100\% \tag{3.9}$$

where a_w is the water activity of the liquid desiccant, P_o is the vapour pressure of pure water and P^* is the vapour pressure of the liquid desiccant at the same temperature.

Empirical or semi empirical models have been used by researchers to predict water activity in electrolyte mixture solutions. The most commonly used are the following: Pitzer model, Zdanovskii–Stokes–Robinson (ZSR), the Kusik and Meissner (KM), Robinson and Stokes (RS), Lietzke and Stoughton (LSII) and Reilly, Wood and Robinson (RWR) models.

In all six models were considered, the principal features of which are outlined below.

a) Pitzer's model (Pitzer, 1973, Pitzer, 1991) which is an extension to the Debye-Hückel theory. Based on Bronsted's work (Bronsted, 1922) and improvements by Guggenheim (Guggenheim, 1935) describing the properties of non-ideal gasses, Pitzer extended the theory to electrolyte solutions while including the Debye-Hückel term to describe the long range forces (ie. the electrostatic effects) in addition to the short-range forces of the earlier models. He refined this ion-interaction approach extending its applicability to mixed electrolyte solutions with ionic strength up to 6 molal (Pitzer, 1973).

Pitzer and his associates in a series of papers (Pitzer, 1975, Pitzer and Guillermo, 1974, Pitzer and Mayorga, 1973, Pitzer and Kim, 1974) applied this model successfully to a large number of pure aqueous electrolytes from strong electrolytes with univalent anions to strong electrolytes with bivalent and higher valence type, including saturated mixtures of them (Lima and Pitzer, 1983a, Lima and Pitzer, 1983b, Pitzer *et al.*, 1985).

This model requires five empirical parameters when applied to single electrolyte solutions and its basic disadvantage is that the concentration range cannot exceed 6 molal. Modifications of the model were made by Pitzer to extend its applicability to higher concentrations regarding electrolytes with large solubility such as $CaCl_2$ and $MgCl_2$ up to 11 and 5.9mol-kg^{-1} (Pitzer *et al.*, 1999). Pitzer summarises his work and provides an excellent source of data for his model parameters with a wide list of tables and references in his book (Pitzer, 1991).

Perez-Villasenor modified the model to a three parameter form and to concentrations up to 25molal (Perez-Villasenor *et al.*, 2002), but their work was limited to 1:1 and 1:2 single strong electrolytes, not dealing with mixtures or higher valence type strong electrolytes.

However, any modification of the model that has been made to date concerns specific electrolyte systems and there is no generalised form applicable to the majority of strong electrolytes and their mixtures for concentrations higher than 6 molal. The mathematical formulation of the Pitzer model is complex and the reader is referred to references (Pitzer, 1973) and (Pitzer, 1991). The equations of Pitzer's model used in this work are found in the appendix A1.

b) The model of Zdanovskii–Stokes–Robinson (ZSR) (Stokes and Robinson, 1966, Ha and Chan, 1999, Clegg and Seinfeld, 2004, Clegg *et al.*, 2003). ZSR is a simple empirical equation, first discovered by Zdanovskii empirically and later by Stokes and Robinson mathematically. The ZSR method can be described briefly by the following relationship:

$$\sum_{\mathrm{i}} \frac{m_{\mathrm{i}}}{m_{0,\mathrm{i}}(a_{\mathrm{w}})} = 1 \tag{3.10}$$

where m_{i} is the molality of species in a multicomponent solution with a water activity of a_{w} and $m_{0,\mathrm{i}}(a_{\mathrm{w}})$ is the molality of the single-component solution of which the water activity a_w equals that of the solution mixture.

This model requires the expression of the molality of any single electrolyte in the solution as a function of water activity. Ha and Chan (Ha and Chan, 1999) reported the coefficients of the polynomial fits used to express $m_{0,\mathrm{i}}$ as a function of a_{w} for binary solutions of $MgCl_2$-H_2O and $MgSO_4$-H_2O. In this study we additionally report the coefficients of the polynomial fits to published experimental data (Robinson and Stokes, 1959) for KCl-H_2O, $CaCl_2$-H_2O, NaCl-H_2O, LiCl-H_2O in Table 3.1.

c) The Kusik and Meissner (KM) model (Kusik and Meissner, 1978) was suggested by Bronsted's principle of specific ion interaction. According to it the interactions between ion pairs dominate and hence determine the physical properties of the solution. The model of Kusik and Meissner (KM) proposes the following equation for a mixed-electrolyte solution containing cations i= 1, 3, 5, … and anions j = 2, 4, 6,…

$$\log_{10}(a_{\mathrm{w}})_{\mathrm{mix}} = \sum_{\mathrm{j}} \sum_{\mathrm{i}} W_{\mathrm{ij}} \log_{10}\left(a_{\mathrm{w}}^{\mathrm{o}}\right)_{\mathrm{ij}} + r \tag{3.11}$$

in which $W_{\mathrm{ij}} = X_{\mathrm{i}} \cdot Y_{\mathrm{j}}$ (3.12)

where $(a_{\mathrm{w}})_{\mathrm{mix}}$ is the water activity of mixed-electrolyte solution, X_{i} and Y_{j} are the cationic and anionic strength fractions, respectively and $a_{\mathrm{w}}^{\mathrm{o}}$'s are the activity of water in various single-electrolyte solutions, and *r* is the residue term which is generally small and can be neglected.

The model requires the expression of the water activity a_w^o of any single electrolyte in the solution as a function of the total ionic strength of the mixed-electrolyte solution. Polynomial fits were used to express a_w^o as a function of the ionic strength I. The coefficients of the polynomial fits to published experimental data are presented in Table 3.2.

Simplified versions of KM equation were presented by El Guendouzi and co authors (El Guendouzi *et al.*, 2005, El Guendouzi *et al.*, 2004) and were used in this work for predicting the water activity of the $MgCl_2.MgSO_4.H_2O$ solutions. These are:

for two unsymmetrical mixed electrolytes

$$\ln a_w = \frac{y(2+y)}{3}\ln a_{wMX}^0 + \frac{(2+y)(1-y)}{2}\ln a_{wNX}^0 - 0.003y(1-y)I \quad (3.13)$$

for two symmetrical mixed electrolytes

$$\ln a_w = y\ln a_{wMX}^0 + (1-y)\ln a_{wNX}^0 \quad (3.14)$$

where y is the ionic strength function of the solution.

d) The Robinson and Stokes (RS) (also known as the Robinson and Bower) relation (Robinson and Stokes, 1970, Sangster and Lenzi, 1974) ,

$$(1 - a_{w(m)}) = \sum \left(1 - a_{w(i,m)}\right)\left(\frac{m_i}{m}\right) \quad (3.15)$$

where $a_{w(m)}$, $a_{w(i,m)}$ and m_i are respectively the water activity of the multicomponent solution, the water activities of the single electrolyte solutions at the total molality m of the multicomponent solution and the molality of the single electrolyte. The concept of this relation is that the vapour pressure of the mixture is lowered down additively by the lowering vapour pressures of the solutes. This model requires the water activities of binary solutions, determined experimentally, to be expressed as a function of molality. The coefficients of the polynomial fits to published experimental data are presented in Table 3.3.

e) The model of Lietzke and Stoughton (LS) (Lietzke and Stoughton, 1972, Lietzke and Stoughton, 1975)

$$\phi \sum \nu_{\mathrm{i}} m_{\mathrm{i}} = \sum \nu_{\mathrm{i}} m_{\mathrm{i}} \phi_{\mathrm{i}} \tag{3.16}$$

where $\nu_i, m_{\mathrm{i}}, \phi_i$ and ϕ are respectively the number of ions released by the complete dissociation of an electrolyte i, the molality of electrolyte i , the osmotic coefficient of electrolyte i at the total ionic strength of the mixture and the total osmotic coefficient of the multicomponent solution. LS requires expressing the osmotic coefficients of binary solutions, using experimental published data, as a function of ionic strength. Hence for a mixture of two electrolytes MX and NX the LSII relation becomes

$$(\nu_{MX} m_{MX} + \nu_{NX} m_{NX}) \cdot \phi = \nu_{MX} m_{MX} \phi_{MX} + \nu_{NX} m_{NX} \phi_{NX} \tag{3.17}$$

The coefficients of the polynomial fits to experimental data are shown in Table 3.4.

f) The Reilly, Wood and Robinson (RWR) (Reilly *et al.*, 1971) model:

$\phi_{mix} = f(\phi_i) + g(\textit{interaction term})$

where ϕ_{mix} is the osmotic coefficient of the mixture and ϕ_i the osmotic coefficient of i electrolyte at the ionic strength of the mixture.

Simplifying the model by neglecting the solute-solute interactions (which require experimental data from ternary solutions that are not readily available) leads to the following relation:

$$\phi = 1 - \frac{\sum [m_{\mathrm{i}} (1 - \phi_{\mathrm{i}})]}{\sum m_{\mathrm{i}}} \tag{3.18}$$

Like the previous model, this model requires the osmotic coefficients of binary solutions to be expressed as a function of ionic strength. The polynomial fits used in e) were used in this model too. The expression that relates water activity to osmotic coefficient is the following:

$$\phi = \frac{-55.1 \cdot \ln(a_w)}{\sum_i \nu_i \cdot m_i} \tag{3.19}$$

The polynomials fits used in this study are valid for concentrated solutions with ionic strength as high as 18molal.

3.2.5 Viscosity and density models

These properties are of secondary but significant importance in a liquid desiccant refrigeration system. For example, they will influence how much power is needed to pump the liquid and how the liquid will behave in a device such as a heat or mass exchanger. Hefter *et al.* (2003) have reviewed the viscosity theories and models used for predicting viscosity in electrolyte mixtures. According to their study, Young's Rule is suitable for predicting viscosities in concentrated electrolyte solutions i.e.

$$\mu = \sum \left[\left(\frac{I_i}{I_T} \right) \cdot \mu_i \right] \tag{3.20}$$

where μ, μ_i and I_i are respectively the viscosity of the multicomponent solution, the viscosity of the binary solution of electrolyte i at the total ionic strength I_T of the mixture and the ionic strength of the binary solution of electrolyte i. Hefter *et al.* claim that this expression can predict viscosity within 8% error. The coefficients of $\eta(I)$ from the polynomial fits for binary solutions required by Young's rule are given in Table 3.5.

Based on the linear isopiestic relation for multicomponent solutions density can be calculated by the following equation as presented by Hu (Hu, 2000),

$$\rho = \sum_j Y_j \Big/ \sum_j \left(Y_j / \rho_j^o \right) \tag{3.21}$$

where $Y_j = m_i / m_j^o + m_j M_j$, ρ is the multicomponent solution density at total molality m of the solution, m_j^o is the molality of the binary solution of solute j at the water activity of the multicomponent solution (calculated by the polynomial fits mentioned before), M_j is

the molar mass of solute j, ρ_j^o is the density of binary solution of solute j at m total molality of the solution. ρ_j^o is calculated using polynomial fits to binary density data (Lobo, 1989). The coefficients of the polynomial fits are seen in Table 3.6.

Tang *et al.* (Tang, 1997, Ha and Chan, 1999) used the following additive rule for predicting the density of multicomponent solutions:

$$\frac{1}{\rho} = \sum_i \frac{x_i}{\rho_{oi}} \tag{3.22}$$

where ρ is the multicomponent solution density at the total mass fraction of the solution, ρ_{oi} is the density of binary solution at the total mass fraction of solution, and x_i is the mass fraction of solute i. ρ_{oi} is calculated using polynomial fits to binary density data. The coefficients of the polynomial fits are seen in Table 3.7.

Zaytsev and Aseyev (Ivan Dmitrievich Aseyev and Georgievich, 1992) reported modified Ezrokhi equations for calculating density and viscosity in multicomponent electrolyte solutions based on data from binary solutions:

$$\log_{10}\rho = \log_{10}\rho_o + \sum_i (A_i c_i) \tag{3.23}$$

where ρ is the density of the multicomponent solution in $kg \cdot m^{-3}$, ρ_o is the water density in $kg \cdot m^{-3}$ and A_i are coefficients functions of temperature. The A_i values used at 25 ^oC are given in Table 3.8.

$$\log_{10}\mu_t = \log_{10}\mu_o + \sum_i (D_i c_i) \tag{3.24}$$

where μ_t is the viscosity of the multicomponent solution in Pa.s, μ_o is the water viscosity in Pa.s, D_i are coefficients functions of temperature and c_i is the mass content of the component in kilograms of the substance per 1kg of the solution. The D_i values used at 25

^{o}C are given in Table 3.8. In this work equation (3.23) was further modified as follows to extend its applicability to concentrated brines:

$$\log_{10}\mu_{t} = \log_{10}(\mu_{o}) + \sum_{i}(D_{i}c_{i}) + A_{1}\cdot c_{t} + A_{2}\cdot c_{t}^{2} + A_{3}\cdot c_{t}^{3} \qquad (3.25)$$

where c_t is the total mass content of solute per mass of solution. The coefficients A_1, A_2, A_3 are given in Table 3.9.

3.3 Experimental equipment and methods

3.3.1 Brine samples

Concentrated salt solutions were made up from Analar reagents and deionised water, based on the compositions reported from Mediterranean salt works (Amdouni, 2000). The salts were weighed and mixed with deionised water in the sequence $MgCl_2$, $MgSO_4$, NaCl, KCl, $CaCl_2$ and LiCl. Further solutions were made based on the phase diagram for $MgCl_2.MgSO_4.H_2O$, these being the salts most abundant in bitterns. Sometimes when making up concentrated solutions, some solute remained undissolved and was removed by filtration. The final composition of the filtrate was then determined by accredited laboratory (Stansted Laboratories, Essex, UK) using inductively coupled plasma mass spectrometry and photometry based on turbidimetric and colorimetric principles.

The vapour pressure (needed to determine the ERH) was measured using an isoteniscope arrangement (see Fig. 3.1 and 3.2) following reference (ASTM, 1997 (Reapproved 2002)) and a manometer filled with dibutyl phthalate, which is a fluid having low surface tension and extremely low vapour pressure as explained in reference (McAllan, 1965). The brines were filtered and degassed before introducing them into the isoteniscope. The ERH was determined with an accuracy of ± 1.5 percent points, based on the random error of reading the manometer scale (±1 mm) and the systematic error of the isoteniscope arrangement. The latter was estimated to be ±0.05 kPa from comparison of the measured vapour pressure of pure water at 25^{o}C with published data (Rogers and Mayhew, 1995).

3.3.2 Experimental Procedure

To carry out the experimental procedure using the equipment shown in Figure 3.1, the following steps were followed:

1. Filter the salt solution using Whatman number 3 filter paper
2. Introduce the solution inside the isoteniscope, taking care that the flask is almost filled up and that there is enough solution at the bottom U shaped part.
3. Place the isoteniscope inside the constant temperature bath.
4. Open valves 1 and 2 and close valve 3.
5. Switch on the vacuum pump.
6. Let the sample de-gas for a 5 seconds (it is important to do so because a significant amount of air is dissolved in concentrated solutions).
7. Close valve 1. This causes a pressure difference to build up inside the apparatus, registered in the manometer)
8. Watch the height difference between the levels of the free surfaces of the salt solution inside the U-shaped part of the isoteniscope. When there is equilibrium (zero height difference) record the manometer measurement.
9. Repeat the measurement by opening valve 1 for a second and then close it. Follow the previous step and record the measurement. Repeat as many times as to obtain the same measured vapour pressure value. Usually no more than 5 repetitions with 2 min intervals are needed for stabilisation.
10. Open the air bleeding valve 3 (for a few seconds) only when vacuum is very high and no movement of the salt solution is observed within the isoteniscope. In the case of salt precipitating inside the isoteniscope the process should be stopped because otherwise the instrument will be blocked and hence, no accurate measurements can be taken. In such a case the sample should be discarded and the isoteniscope should be thoroughly cleaned with pure water before taking a new measurement.
11. Open valve 1.
12. Switch off the vacuum pump.
13. Open valve 3 slowly.

Steps 12, 13, 14 regard the turning off.

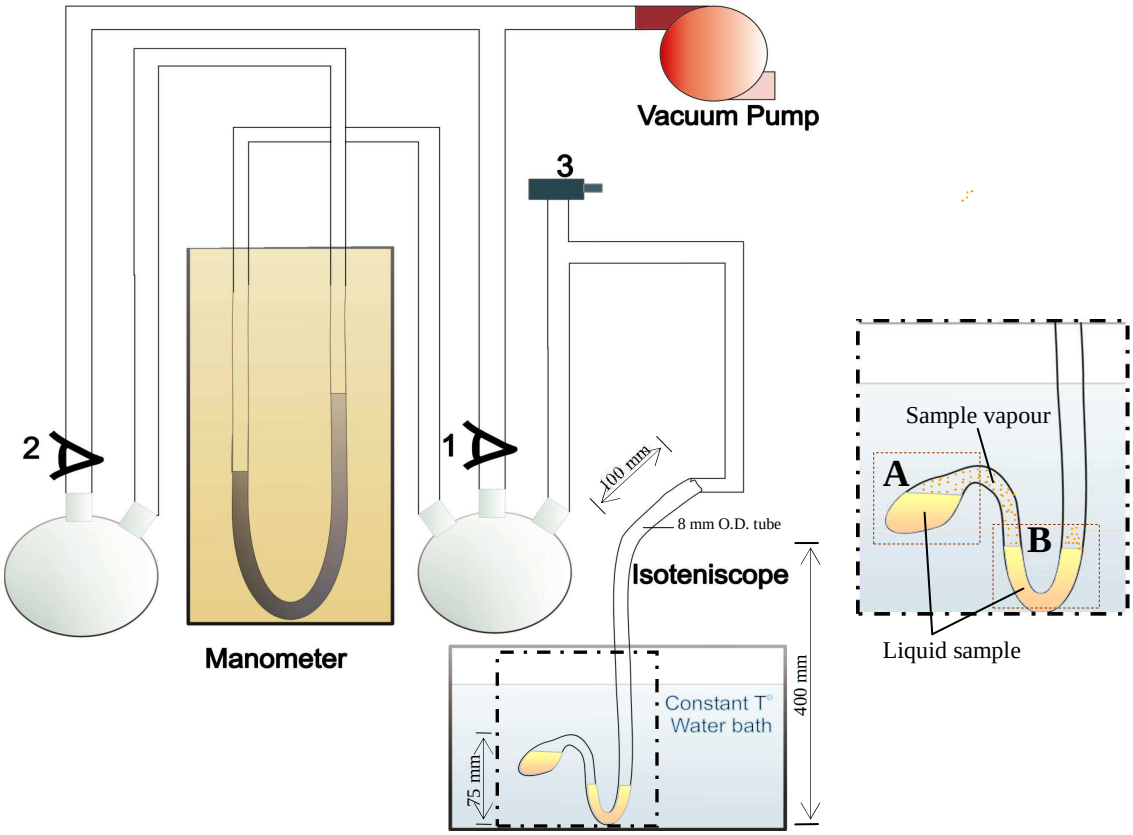

Fig. 3.1: A schematic of the vapour pressure rig.

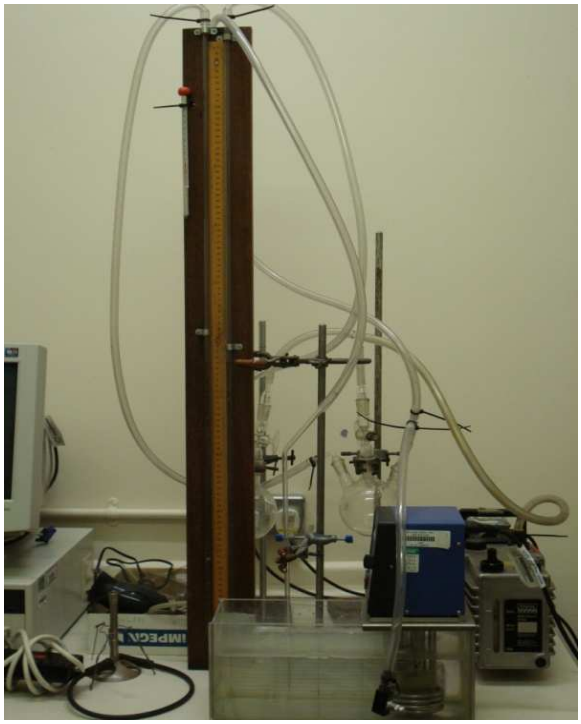

Fig. 3.2: Photo of the vapour pressure rig.

The isoteniscope is a closed borosilicate glass vessel and is designed to minimize composition changes which may occur during the course of measurement. For a more detailed description of the isoteniscope the reader is referred to the relevant American National Standard (ASTM, 1997 (Reapproved 2002)).

When valve 1 closes a pressure difference is built up inside the isoteniscope which can be recorded in the manometer. The vapour pressure of the sample contained in part A of the isoteniscope (see detail in Fig. 3.1) is transferred through part B (U shape tube of the isoteniscope) in the manometer. Equilibrium is reached when the height difference between the free surfaces of the solution inside the two branches of part B is zeroed. At that moment the recorded pressure difference in the manometer is the vapour pressure of the sample solution.

The determination of density was made according to reference (BS4522:1988) using a 50 ml pyknometer flask and a constant temperature water bath with an accuracy of ± 0.1^{o}C. The viscosity measurements were made based on reference (BS188:1977) following the detailed procedure for U-tube viscometers for direct flow, by using a BS/U viscometer and a constant temperature bath of ± 0.1^{o}C accuracy. All experiments were carried out at 25^{o}C.

3.4 Results

Table 3.10 summarises the compositions of the brines tested and Table 3.11 compares the measured ERH to the values predicted by the six different models. For those brines containing only $MgCl_2$ and $MgSO_4$, the compositions are indicated on the phase diagram of Figure 3.3. All models except that of Pitzer give an average relative error in ERH of less than 5.4%. Furthermore a statistical analysis was carried out using the package StatGraphics®. The predicted values were plotted against the measured and straight lines were fitted to each model. It was concluded that there are no significant differences among the models with the exception of Pitzer model. The LS was the most accurate for all the investigated brines. However, the ZSR model is the most accurate for the more concentrated brines (3 and 5), for which it gives an average error of 3.7%, and this model is therefore preferred. It also has the advantage of a simple mathematical formulation.

Table 14 shows the linear regression results for ZSR. It is seen that there is a strong linear relationship between the predicted and the measured values (r^2 = 0.985).

Tables 3.12 and 3.13 summarise the results for viscosity and density respectively. The most accurate models prove to be those based on Ezrokhi for density and viscosity which gave errors of 0.41% and 1.47% correspondingly. The same statistical analysis as for ERH was carried out for density and viscosity. Table 3.14 shows the linear regression results for Ezrokhi predicted values of density and viscosity against the measured. Again it is seen that there is a strong linear relationship between the predicted and the measured values.

In a practical desiccant cooling system, water would be continually added to and removed from the solution as it is used to carry out operations of humidification and dehumidification in contact with air. To replicate this situation, solutions were made up with the same relative salt concentrations as concentrated bitterns but with varying amounts of water added. The equilibrium relative humidity was measured and also predicted using the ZSR model. The results are plotted against mass fraction in Figure 3.4 along with the corresponding curve for pure $MgCl_2$ solution. It can be seen that the difference between these two curves is small. The average relative error between the interpolated values of ERH of pure $MgCl_2$ (by a quadratic polynomial, r^2=0.98) and the experimental values for brine 5 is just 5.1%.

Having validated the ZSR model for a range of solutions, we are able to present further results on the seawater salt system. In particular Figures 3.5, 3.6 and 3.7 show respectively the effect on ERH, density and dynamic viscosity of adding progressively minor ions to the $MgCl_2$ solution, following the compositions of two brines measured in salt works (Amdouni, 2000). The addition of these minor ions depressed ERH by 7–11%. Density and dynamic viscosity were respectively increased by 3.5–4.8% and 20.5–26.2%. These percentages indicate the degree of similarity between pure magnesium chloride solution and bitterns.

In salt works it is conventional and convenient to measure the concentration of bitterns according to the highly soluble lithium ions which remain in the solvent even at high concentrations. The lithium concentration factor c_{Li} refers to the final concentration of lithium divided by that in raw seawater. In Figures 3.8, 3.9 and 3.10 we show how the

ERH, density and viscosity vary with this concentration factor, on the basis of the preferred models and the compositions reported in reference (Amdouni, 2000). It is useful to fit empirical equations to these relations as shown below with the corresponding correlation coefficients for the fit against the point data:

$$\mathrm{ERH\%} = 97.75 - 66.88 \cdot [1 - e^{-0.0715 \cdot (C_{\mathrm{Li}} - 1)}] \qquad (r^2 = 0.98) \qquad (3.26)$$

$$\rho = 1020 + 390 \cdot [1 - e^{-0.129 \cdot (C_{\mathrm{Li}} - 1)}] \qquad (r^2 = 0.99) \qquad (3.27)$$

$$\mu = 0.88 + 19.56 \cdot [1 - e^{0.0254 \cdot (C_{\mathrm{Li}} - 1)}] \qquad (r^2 = 0.96) \qquad (3.28)$$

3.5 Discussion and conclusion

In this study the properties of seawater brines and bitterns were compared to those of pure $MgCl_2$ solutions. The lowest reported ERH value of a pure saturated $MgCl_2$ solution is 32.8% at 25^{o}C (OIML, 1996) while the lowest measured ERH in the brines investigated here was 34%. The maximum density measured here was 1339 kg/m^3 while the reported density from the literature of a saturated $MgCl_2$ solution is 1330 kg/m^3 (Lobo, 1989). Regarding dynamic viscosity, the maximum reported value of a saturated $MgCl_2$ solution is 12.8 mPa.s at 25^{o}C (Lobo, 1989) while the dynamic viscosity of the most concentrated brine measured here was 13.2 mPa.s.

The cooling performance of a liquid desiccant refrigeration system is strongly affected by ERH. Desiccants with low ERH achieve better lowering of the wet bulb temperature and hence a better cooling performance. Here we have shown that bitterns occurring in salt works can be as hygroscopic as pure concentrated $MgCl_2$ solutions. It is to be noted though that the data and experimental verification reported here are for 25ºC only. However, substantial data for the properties of $MgCl_2$ solution up to 100ºC are also available (Lobo, 1989, Zaytsev and Aseyev, 1992).

Density and to a lesser extent viscosity affect the energy consumption of the system because electrical energy is needed to drive the pumps required to circulate the liquid desiccant. A more viscous solution needs more energy to pump it. Therefore, we compared

the shaft pump power required to circulate brine 5 and pure $MgCl_2$ of the same ERH from the ground (where the desiccator is placed) to the roof (where the solar regenerator is placed) in a greenhouse of 5 m height with PVC pipes of 0.025 m internal diameter, and a volumetric flow of 2.7 m^3/h. The results are seen in Table 15. It is seen that there are no significant differences between brine 5 and pure $MgCl_2$ solution. Thus pure concentrated $MgCl_2$ solutions will perform in a similar way to bitterns when used for assessing the performance of the proposed cooling system.

This work showed that the conclusions of Davies and Knowles study (2006) are still valid. In principle, liquid desiccant cooling systems using bitterns could be employed for the cooling of greenhouses in hot, humid climates. Bitterns are less hygroscopic but also less toxic and more readily available than more commonly used desiccants such as LiCl or LiBr. To know the properties of bitterns is prerequisite when designing a solar refrigeration system, but there are also practical characteristics of the solar regenerator and the dehumidifier that need to be considered. These will be explored in chapters 4 and 5. The properties and relations discovered here will be valuable in completing this feasibility study.

Table 3.1: Coefficients in the polynomial $m = A + B \cdot a_w + C \cdot a_w^2 + D \cdot a_w^3 + E \cdot a_w^4 + F \cdot a_w^5$ for binary solutions as required by the ZSR model. Obtained by fitting to data in reference (Robinson and Stokes, 1959) , except in the case of $MgCl_2$ and $MgSO_4$ where the coefficients are those provided in reference (Ha and Chan, 1999).

salt	*A*	*B*	*C*	*D*	*E*	*F*
$MgCl_2$	11.505	-26.518	34.937	-19.829	0	0
$MgSO_4$	-0.7776	177.74	-719.79	1174.6	-863.44	232.31
KCl	10.694	24.693	-49.35	13.95	0	0
$CaCl_2$	15.132	-38.522	49.159	-25.676	0	0
NaCl	55.076	-148.5	163.4	-69.984	0	0
LiCl	24.411	-58.791	72.612	-38.219	0	0

Table 3.2: Coefficients in the polynomial fit $a_w = A + B \cdot I_T + C \cdot I_T^2 + D \cdot I_T^3 + E \cdot I_T^4$ to data in reference (Robinson and Stokes, 1959) for the activity of binary solutions as required by the KM model.

salt	*A*	*B*	*C*	*D*	*E*
KCl	0.9996	-0.0311	-0.0002	-0.00002	0
$CaCl_2$	0.9953	-0.0086	-0.0028	0.00008	0
NaCl	0.9995	-0.0308	-0.0021	0.00006	0
LiCl	0.9949	-0.0212	-0.0084	0.0006	-0.00001
K_2SO_4	0.9998	-0.0136	0.0012	-0.0002	0
Li_2SO_4	0.9993	-0.0129	-0.0002	-0.0002	0
Na_2SO_4	0.9987	-0.0119	0.0004	-0.00004	0
$MgCl_2$	0.9964	-0.0094	-0.0031	0.00008	0
$MgSO_4$	0.9993	-0.0042	0.00002	-0.00003	0

Table 3.3: Coefficients in the polynomial fit $a_w = A + B \cdot m + C \cdot m^2 + D \cdot m^3 + E \cdot m^4 + F \cdot m^5 + G \cdot m^6$ to data in reference (Robinson and Stokes, 1959) for the activity of binary solutions as required by the RS relation.

salt	*A*	*B*	*C*	*D*	*E*	*F*	*G*
$MgCl_2$	0.9964	-0.0282	-0.0277	0.0022	0	0	0
$MgSO_4$	0.9996	-0.0184	0.0029	-0.0031	0.0002	0	0
KCl	0.9998	-0.0318	0.0004	-0.0002	0.00002	0	0
$CaCl_2$	1.0001	-0.0456	-0.0046	-0.0062	0.0016	-0.0001	0.000004
NaCl	0.9995	-0.0308	-0.0021	0.00006	0	0	0
LiCl	0.9949	-0.0212	-0.0084	0.0006	-0.00001	0	0

Table 3.4: Coefficients in the polynomial fit $\phi_i = \mathrm{A} + \mathrm{B} \cdot I + \mathrm{C} \cdot I^2 + \mathrm{D} \cdot I^3 + \mathrm{E} \cdot I^4 + \mathrm{F} \cdot I^5$ to data in reference (Robinson and Stokes, 1959) for the osmotic coefficient of binary solutions as required by the LS model.

salt	*A*	*B*	*C*	*D*	*E*	*F*
$MgCl_2$	0.7892	0.1025	0.0034	0	0	0
$MgSO_4$	0.629	-0.0924	0.0229	-0.0018	0.00006	0
KCl	0.906	-0.0079	0.0055	0	0	0
$CaCl_2$	0.827	0.0496	0.0087	-0.0003	0	0
NaCl	0.9055	0.0386	0.0054	0	0	0
LiCl	0.9206	0.0834	0.0153	-0.0008	-0.000009	0.0000007

Table 3.5: Coefficients in the polynomial fit $\mu = A + B \cdot I + C \cdot I^2 + D \cdot I^3$ to the data in reference (Lobo, 1989) for binary solutions as required by the Young's rule for viscosity.

salt	*A*	*B*	*C*	*D*
$MgCl_2$	0.7905	0.2868	-0.0381	0.0036
$MgSO_4$	0.9077	0.1288	0.0485	0
KCl	0.8897	-0.0075	0.0047	0
$CaCl_2$	1.0393	-0.0786	0.0237	0
NaCl	0.897	0.0589	0.0133	0
LiCl	0.6806	0.3003	-0.0303	0.0026

Table 3.6: Coefficients in the polynomial fit $\rho = \mathrm{A} + \mathrm{B} \cdot m + \mathrm{C} \cdot m^2 + \mathrm{D} \cdot m^3$ to the data in reference (Lobo, 1989) for the density of binary solutions as required by Hu's density model.

salt	*A*	*B*	*C*	*D*
$MgCl_2$	0.9976	0.0759	-0.0015	-0.0003
$MgSO_4$	0.9974	0.1191	-0.0069	0.0003
KCl	0.9972	0.0465	-0.0023	0.0001
$CaCl_2$	0.9976	0.0885	-0.0045	0.0001
NaCl	0.9972	0.0406	-0.0016	0.00006
LiCl	0.9984	0.0226	-0.0006	0.00001

Table 3.7: Coefficients in the polynomial fit $\rho = A + B \cdot x + C \cdot x^2$ to the data in reference (Lobo, 1989) for the density of binary solutions as required by the density model of Tang *et al*.

salt	*A*	*B*	*C*
$MgCl_2$	0.9955	0.0089	0.00002
$MgSO_4$	0.9978	0.0097	0.00006
KCl	0.9974	0.0062	0.00003
NaCl	0.9974	0.0069	0.00003
LiCl	0.9994	0.0051	0.00003
$CaCl_2$	0.9978	0.0079	0.00005

Table 3.8: Coefficients in equations (3.23) and (3.24).

model	Coefficients of Ezrokhi models at 25°C					
Density	A_{MgCl_2}	A_{MgSO_4}	A_{KCl}	A_{NaCl}	A_{CaCl_2}	A_{LiCl}
	0.3515	0.4464	0.2744	0.3112	0.2452	0.3628
Viscosity	D_{MgCl_2}	D_{MgSO_4}	D_{KCl}	D_{NaCl}	D_{CaCl_2}	D_{LiCl}
	2.0127	2.5952	-0.003	0.8077	1.744	1.444

Table 3.9: Coefficients in equation (3.25), the modified Ezrokhi model for viscosity.

A_1	A_2	A_3
-0.4838	3.5017	2.6730

Table 3.10: The chemical composition of the brines made up in the lab from Analar reagents and deionised water, based on the compositions reported from Mediterranean salt works and on the phase diagram for $MgCl_2.MgSO_4.H_2O$

Brine	Composition (mol kg^{-1})						
	Na^+	K^+	Mg^{2+}	Ca^{2+}	Cl^-	SO_4^{2-}	Li^+
1	0.548	0.012	0.072	0.0118	0.656	0.0273	0.00003
2	1.740	0.324	1.444	0.00474	4.373	0.406	0.000594
3	0.160	0.082	3.281	0.0014	6.346	0.298	0.00188
4	1.976	0.308	1.373	0.00555	4.212	0.531	0.000565
5	0.072	0.021	3.733	0.00153	7.790	0.247	0.00250
6			3.342		6.328	0.178	
7			3.493		6.895	0.046	
8			3.545		6.837	0.126	
9			3.399		6.404	0.197	
10			3.266		5.832	0.350	

Table 3.11: Measured values of water activity of the brine samples of Table 4, compared to the predictions of six models. The calculation of average relative error for each model shows that the ZSR model is the most accurate for the two most concentrated brines of those based on reported natural compositions, i.e. samples 3 and 5.

Sample number	**Measured** a_w	**Model**											
		Pitzer		ZSR		KM		RS		LS		RWR	
		Pred.	Rel. Error %	Pred.	Rel. Error %	Pred.	Rel. Error %	Pred.	Rel. Error %	Pred.	Rel. Error %	Pred.	Rel. Error %
1	0.981	0.978	0.4	0.977	0.4	0.977	0.4	0.977	0.4	0.977	0.4	0.973	0.8
2	0.668	0.696	4.1	0.729	9.1	0.719	7.6	0.700	4.7	0.707	5.8	0.714	6.8
3	0.424	0.420	1	0.448	5.7	0.435	2.6	0.447	5.6	0.432	2.0	0.439	3.7
4	0.658	0.704	7	0.729	10.8	0.718	9.2	0.699	6.3	0.703	6.8	0.709	7.8
5	0.346	0.299	13.6	0.340	1.6	0.306	11.5	0.328	5.2	0.309	10.5	0.314	9.2
6	0.458	0.482	5.1	0.455	0.8	0.445	2.8	0.462	0.8	0.451	1.6	0.461	0.7
7	0.399	0.413	3.5	0.401	0.6	0.395	1.1	0.408	2.2	0.401	0.4	0.404	1.2
8	0.406	0.411	1.1	0.393	3.4	0.379	6.8	0.396	2.6	0.385	5.3	0.393	3.4
9	0.445	0.468	5	0.439	1.4	0.427	4	0.446	0.1	0.433	2.8	0.444	0.2
10	0.479	0.534	11.5	0.490	2.3	0.473	1.2	0.495	3.4	0.478	0.2	0.496	3.5
	Average error %		5		4		5		3		4		4

Table 3.12: Comparison of experimental measurements of absolute density (kg/m^3x10^3) with model predictions for three models: Hu, Ezrokhi and Tang's rule. The calculation of average error in each case shows that the Ezrokhi is the most accurate for all the brines.

Brine	Measured	**Density Model**					
		Hu		**Ezrokhi**		**Tang's rule**	
		Pred.	Relative Error %	Pred.	Relative Error %	Pred.	Relative Error %
1	1.025	1.031	0.57	1.028	0.28	1.030	0.46
2	1.255	1.255	0.03	1.240	1.18	1.345	7.14
3	1.317	1.323	0.43	1.315	0.15	1.506	14.4
4	1.264	1.268	0.30	1.252	0.95	1.365	8.01
5	1.339	1.347	0.59	1.349	0.75	1.593	18.9
6	1.301	1.309	0.63	1.300	0.07	1.309	0.63
7	1.307	1.313	0.52	1.307	0.01	1.313	0.52
8	1.315	1.322	0.57	1.317	0.15	1.322	0.57
9	1.308	1.315	0.51	1.306	0.12	1.315	0.51
10	1.296	1.312	1.21	1.302	0.47	1.312	1.21
	Average error % (all brines)		0.5		0.4		5

Table 3.13: Comparison of experimental measurements of dynamic viscosity (mPa.s) with model predictions for two models: Young's rule and Ezrokhi. The calculation of the average relative error in each case shows that the modified Ezrokhi model is the most accurate for all the brines.

Brine	Measured	Model			
		Young's rule		Ezrokhi	
		Prediction	Rel. Error %	Prediction	Rel. Error %
1	1.00	0.98	2.38	0.95	5.11
2	3.49	3.68	5.49	3.49	0.00
3	8.99	10.2	13.16	9.00	0.02
4	3.69	4.08	10.50	3.75	1.61
5	13.21	15.5	17.63	13.36	1.13
6	8.37	8.89	6.22	8.10	3.17
7	8.95	10.0	12.04	8.94	0.15
8	9.93	11.0	10.96	9.78	1.56
9	8.99	9.56	6.35	8.66	3.74
10	7.93	8.78	10.63	8.08	1.83
	Average error %		9.5		1.5

Table 3.14: Results of the linear regression of the predicted against the measured values for the preferred models.

		predicted vs. measured		
Property	**Preferred model**	Slope	Intercept	r^2
ERH	ZSR	1.021	1.231	0.985
Density	Ezrokhi	1.0044	-0.0067	0.993
Viscosity	Ezrokhi	0.999	-0.0382	0.998

Table 3.15: Comparison of pumping power between bitterns and pure $MgCl_2$ solution, each with concentration chosen to give ERH=34%, assuming a pump efficiency of 75%, a volumetric flow of 2.7 $m^3.h^{-1}$, gravity head of 5m and a pipe length of 7 m and roughness 15 μm as in reference (Perry *et al.*, 1984). The Colebrook formula was used to calculate the friction factors.

Variable	**Unit**	**Bitterns (Brine 5)**	**$MgCl_2$**
Concentration (mass solute/mass solution)		0.367	0.350
Density	kg m^{-3}	1339	1332
Dynamic Viscosity	mPa.s	13.21	12.27
Friction factor		0.0403	0.0395
Friction head	m	1.35	1.32
Shaft Pump Power	W	83	83

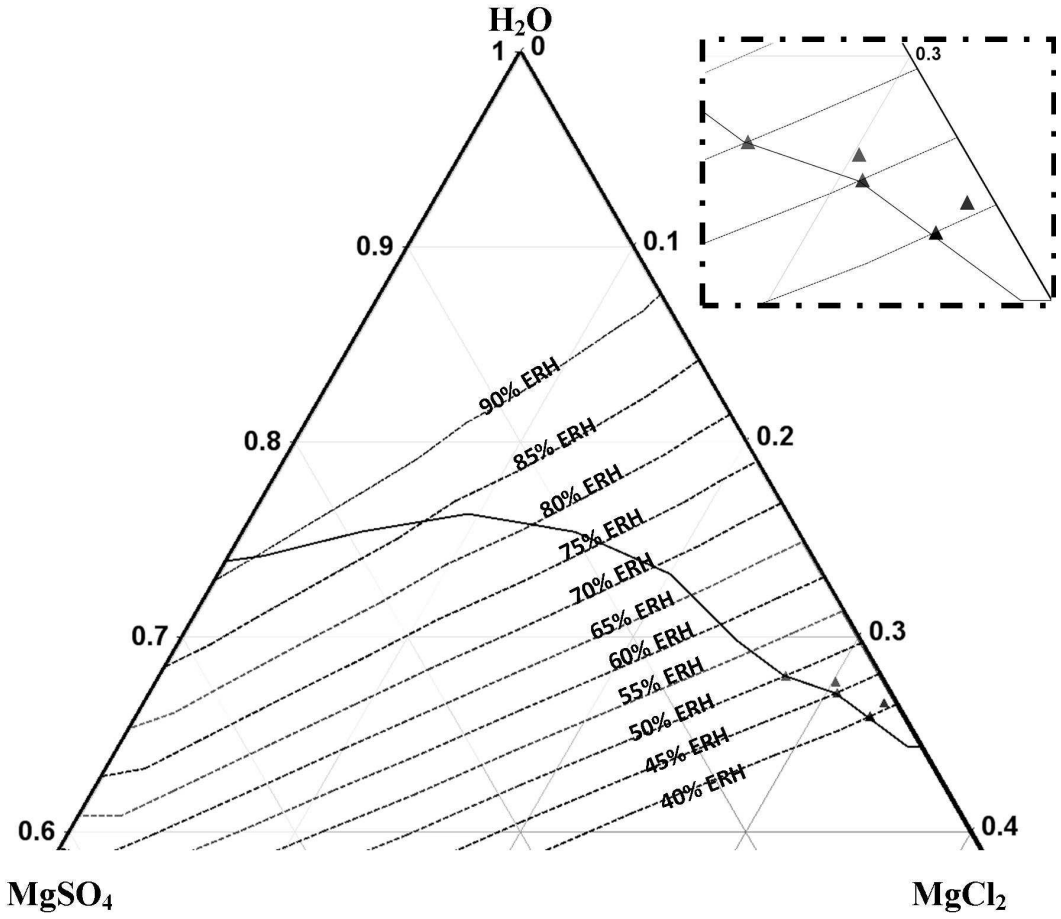

Fig. 3.3: Phase diagram for $MgCl_2.MgSO_4.H_2O$ systems indicating brines 6-10 used for the property-measurement experiments.

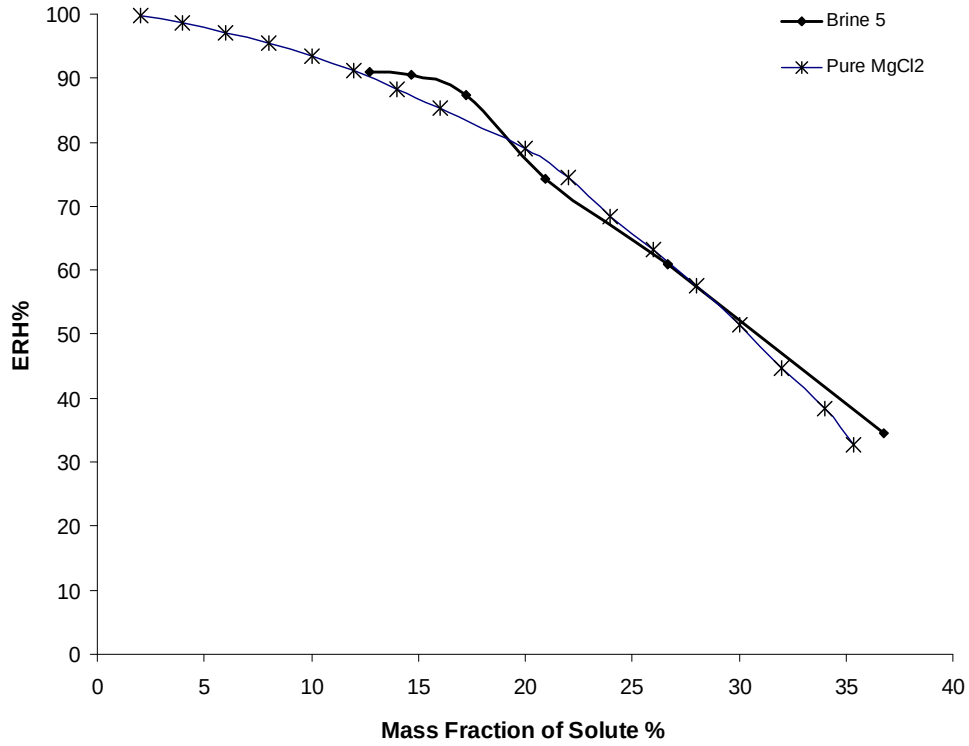

Fig. 3.4: ERH% vs. mass fraction for solutions with the same relative salt concentrations as concentrated bitterns (brine 5) but with varying amounts of water added; along with the corresponding curve for pure magnesium chloride solution.

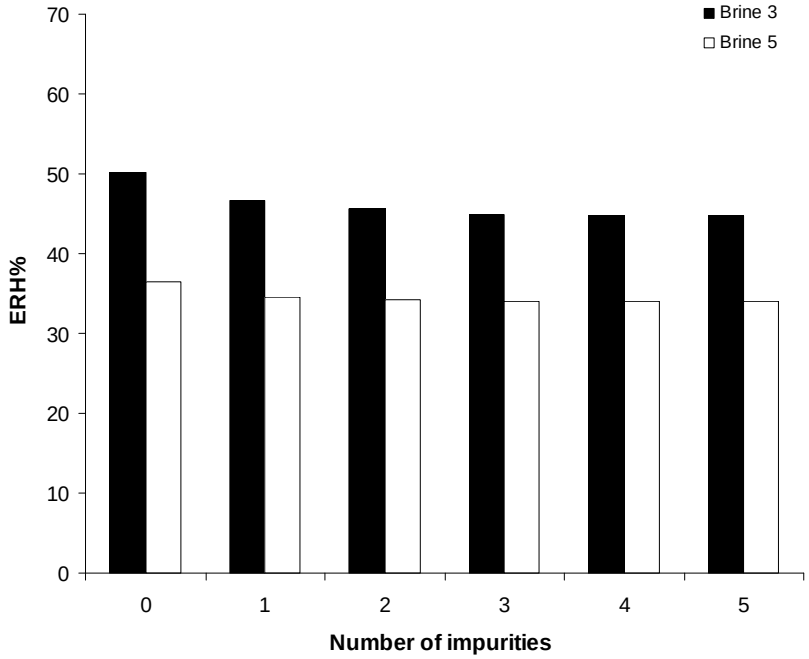

Fig. 3.5: Histogram showing the effect on ERH of adding 1, 2, 3, 4 and 5 impurities to the $MgCl_2$ solution, based on the ZSR model. For brine 3 the compositions used are: 0 is pure $MgCl_2$, 1 is 0+ $MgSO_4$, 2 is 1+NaCl, 3 is 2+KCl, 4 is 3+LiCl, 5 is 4+$CaCl_2$

For brine5: 0 is pure $MgCl_2$, 1 is 0+ $MgSO_4$, 2 is 1+NaCl, 3 is 2+KCl, 4 is 3+$CaCl_2$, 5 is 4+LiCl

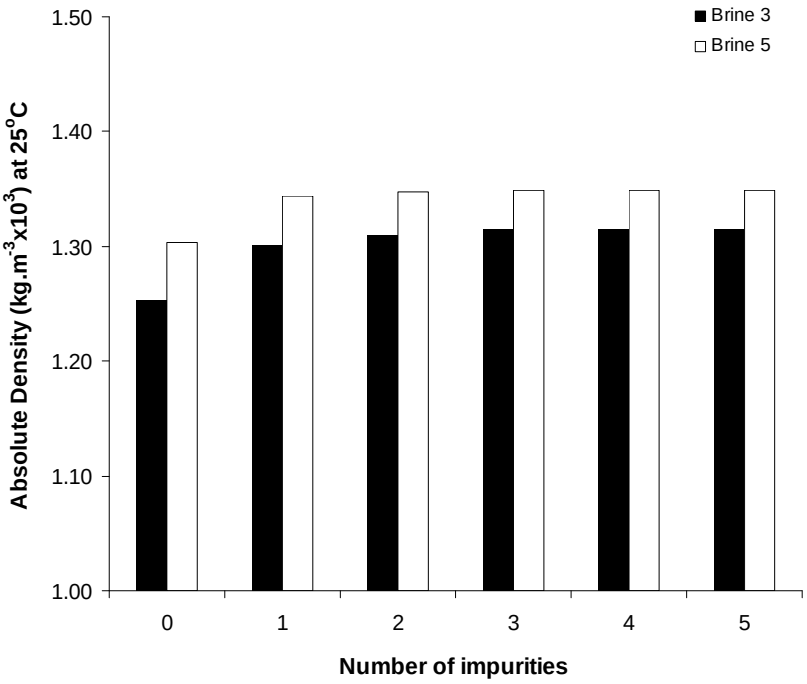

Fig. 3.6: Histogram showing the effect on density of adding 1, 2, 3, 4 and 5 impurities to the $MgCl_2$ solution, based on the ZSR model. For brine 5 the compositions used are: 0 is pure $MgCl_2$, 1 is 0+ $MgSO_4$, 2 is 1+NaCl, 3 is 2+KCl, 4 is 3+LiCl, 5 is 4+$CaCl_2$

For brine3: 0 is pure $MgCl_2$, 1 is 0+ $MgSO_4$, 2 is 1+NaCl, 3 is 2+KCl, 4 is 3+$CaCl_2$, 5 is 4+LiCl

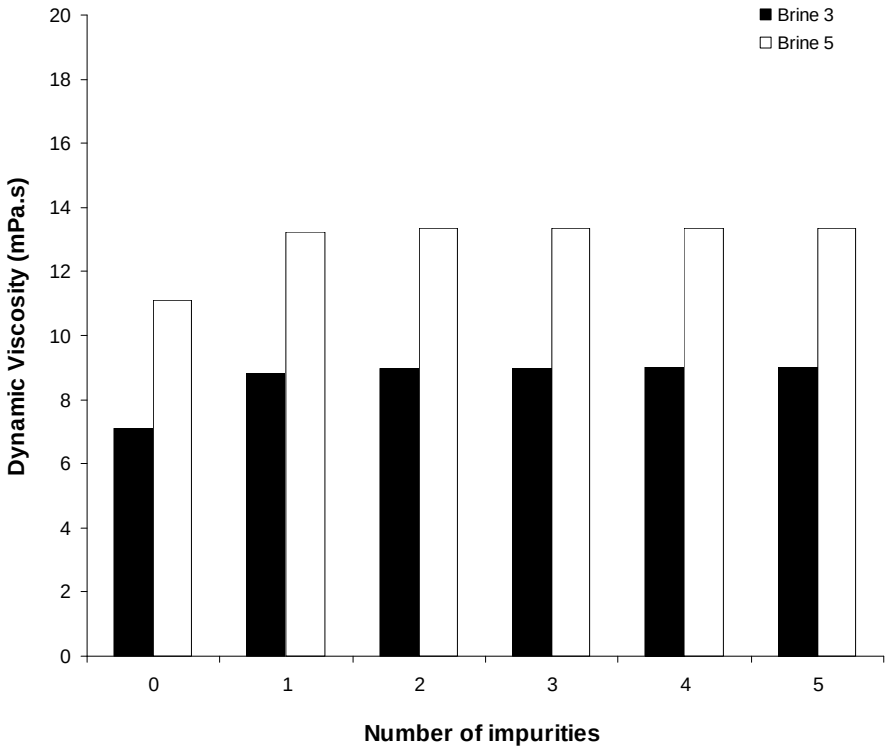

Fig. 3.7: Histogram showing the effect on viscosity of adding 1, 2, 3, 4 and 5 impurities to pure $MgCl_2$ solution, based on the modified Ezrokhi model. The composition used for both brines is: 0 is pure $MgCl_2$, 1 is 0+ $MgSO_4$, 2 is 1+NaCl, 3 is 2+KCl, 4 is 3+$CaCl_2$, 5 is 4+LiCl.

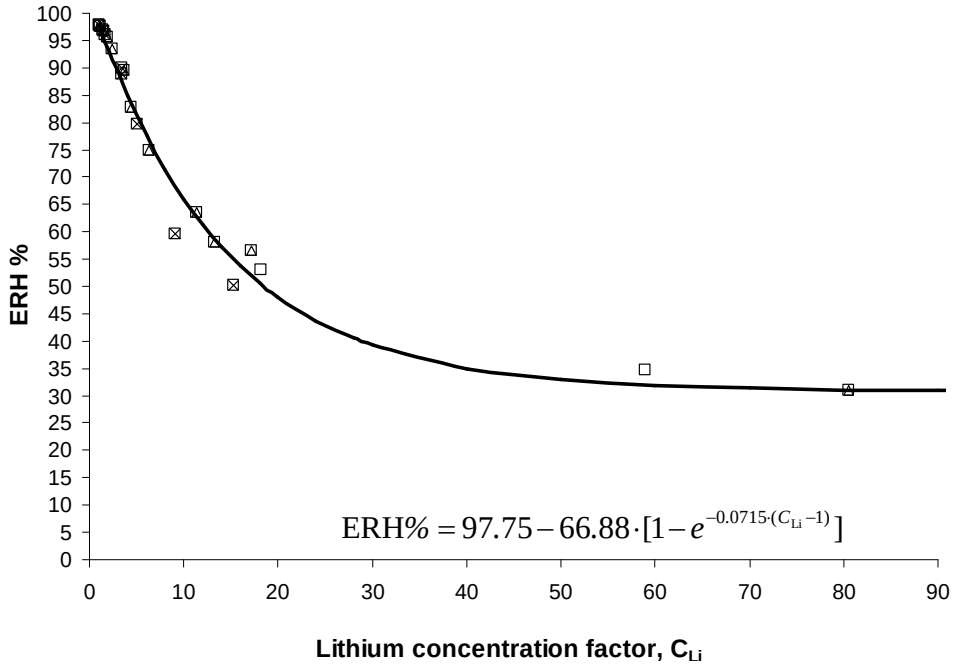

Fig. 3.8: ERH as a function of the concentration factor c_{Li}, on the basis of the ZSR model and the compositions reported in reference (Amdouni, 2000). The correlation coefficient was $r^2 = 0.98$.

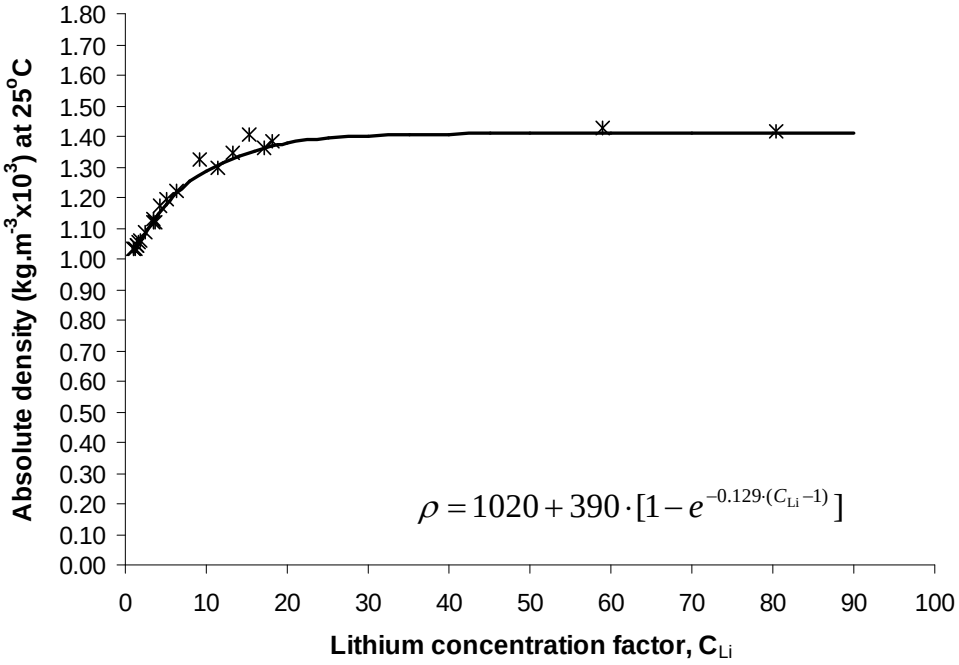

Fig. 3.9: Density as a function of the concentration factor c_{Li}, on the basis of the Ezrokhi model and the compositions reported in reference (Amdouni, 2000). The correlation coefficient was $r^2 = 0.99$.

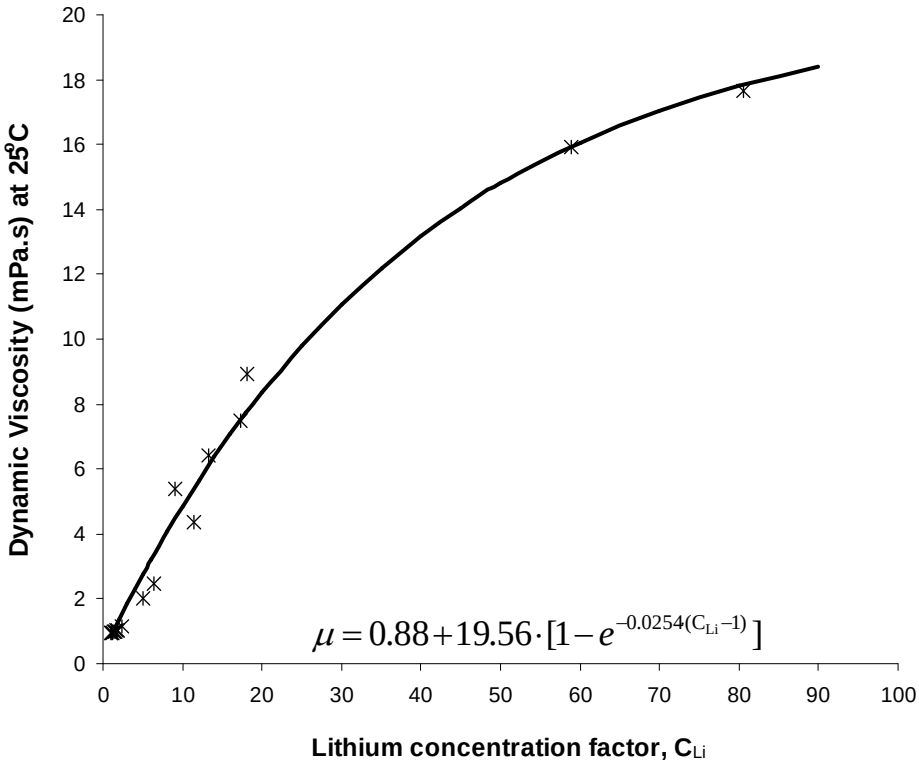

Fig. 3.10: Viscosity as a function of the concentration factor c_{Li}, on the basis of the Ezrokhi model and the compositions reported in reference (Amdouni, 2000). The correlation coefficient was $r^2 = 0.96$

CHAPTER 4. REGENERATOR

4.1 Introduction

In the past, the technology of liquid desiccant cooling systems has been extensively studied and applied to the cooling of human dwellings using sorption materials such as lithium salts, calcium chloride and tri-ethylene glycol (Dai *et al.*, 2001, Gommed and Grossman, 2004, Jain *et al.*, 2000, Mei and Dai, 2008, Oliveira *et al.*, 2000). However, the potential of using this technology as a means of cooling greenhouses to temperatures below those achieved by conventional means has been shown only recently (Davies, 2005). Researchers have proposed the use of brines rich in $MgCl_2$ (bitterns) as low cost and non toxic alternative liquid desiccants for low grade cooling (Davies and Knowles, 2006). Magnesium chloride solution can be a reasonable model for bitterns for the purpose of developing a greenhouse cooling system as shown in Chapter 2, see also (Lychnos *et al.*, 2010a).

The open-cycle solar liquid desiccant cooling system utilises solar energy to increase the chemical potential of the absorbent solution so as to be used in driving the desiccation process. The regenerator is the part of the system where the weak desiccant solution becomes more concentrated by evaporating water and therefore is a key component of such a system. Its performance affects the overall system performance significantly. Therefore, when designing the system it is essential to be able to predict the rate of evaporation of water from the weak solution under the climate conditions of interest.

The aim of the present work is to arrive at conclusions that would be useful for engineering purposes in order to design a solar cooling system. In order to achieve this, an experimental and theoretical study was carried out. The performance of an open-type flat plate regenerator using $MgCl_2$ as liquid desiccant was investigated under four different irradiance levels ($400Wm^{-2}$, $600Wm^{-2}$, $760Wm^{-2}$, $970Wm^{-2}$) and three initial solution mass flows ($0.0020kg\ s^{-1}$, $0.0040kg\ s^{-1}$, $0.0060kg\ s^{-1}$). The solution concentration effect on the performance of the regenerator was also investigated by using more dilute desiccant solutions. The experimental results were compared with predicted ones obtained from an analytical model which was based on Collier's approach (Collier, 1979).

4.2 Previous work on Solar Liquid Desiccant Regenerators

There are mainly two categories of regenerators that have been intensively investigated in the literature (Fig. 4.1) :

a) the open surface flat plate regenerator and
b) the closed-type which can be subcategorised in i) glazed flat plate, ii) solar still type and iii) packed beds.

Here we focus on previous work done in a), b)i, b) ii as these are simpler to design, easiest to operate and cheaper than option iii).

Historically, research on solar liquid desiccant regenerators has developed through the modelling of the heat and mass transfer phenomena taking place on the surface of the regenerators leading to analytical expressions of the water evaporation rate or to more sophisticated numerical ones. Additionally, experimental studies have been undertaken by researchers in order to assess the performance of the different types of regenerators operating under various climatic conditions and eventually to find the optimum solution. Various liquid desiccants i.e. LiCl, LiBr, $CaCl_2$ and triethylene glycol, have been used in these experimental or theoretical studies.

Among the pioneers of this research area are Kakabaev and Khandurdyev (1969) who carried out heat and mass transfer analysis on a flat plate open regenerator. They found an analytical solution that relates the amount of water evaporated per unit area of the surface to the climatic conditions, the heat transfer coefficient and the initial solution parameters. Their solution is based on expressing the vapour pressure of the solution as a linear function of temperature and concentration.

Several studies have used Kakabaev and Khandurdyev's approach in the past. Collier extended Kakabaev and Khandurdyev's early work on flat plate open regenerators and presented simulations of the performance of an open cycle absorption refrigeration system, under different climatic conditions using real weather data. He also suggested the use of established correlations of Nu and Sh numbers for free and forced convection that can be used to evaluate the heat and mass transfer coefficients in order to evaluate the heat losses and the mass transport in an open flat regenerator (Collier, 1979).

Following Kakabaev and Khandurdyev's approach on the approximation for vapour pressure, Baum *et al.* (1972) arrived at an analytical solution for predicting the mass flux of evaporated water in an open-type solar regenerator. This model used a new

approximation for the average solution concentration expressing it as a function of the initial concentration, the evaporated water and solution mass flow. The comparison of the experimental values with those predicted showed good agreement despite the approximations used in the model. Fagbenle and Karayiannis (1998) used Baum's analytical solution with empirical relations for heat and mass transfer already known from the literature in order to carry out a first- and second-law analysis of an open-type solar regenerator. Their analysis led to simple expressions of efficiency that characterise the performance of such systems.

Based on Kakabaev's and Collier's studies Kumar and Devotta (1989) modelled the heat and mass transfer taking place in an open type regenerator using correlations of heat and mass transfer coefficients for forced convection found experimentally in an earlier study published by Kumar *et al.* (1985). The predicted water evaporation rate values had a 9.3 average percent error.

Extending Kakabaev and Khandurdyev's approach by using the same linear approximation of solution vapour pressure, Alizadeh and Saman (2002) modelled the heat and mass transfer processes taking place in a closed-type forced flow solar regenerator and evaluated the performance of the system under different conditions. The differential equations of the model were solved by the finite difference method. They arrived at the conclusion that the water evaporation rate depends on the regenerator length, solution mass flow rate, the air Reynolds number, the climatic conditions (wind excluded) and the ratio of the solution to air mass flow rate.

Researchers started to investigate more systematically closed type regenerators in the early 1980's. Gandhidasan and his co-workers performed a theoretical study that focused on heat and mass transfer taking place in a closed –type flat plate regenerator (Gandhidasan *et al.*, 1981). Differential equations were used to model the processes taking into account the effect of the normal convective diffusive velocity and the buoyancy effect. Later, in another paper the same author came up with an analytical solution of the heat and mass transfer equations that describe the physical processes occurring in a closed-type solar regenerator. It was concluded that this type of regenerator can be used in hot and humid climates rather than hot and dry (Gandhidasan, 1982). Theoretical comparative studies on open flat plate, forced parallel flow and tilted solar still type solar regenerators were also performed by Gandhidasan (Gandhidasan, 1983a, Gandhidasan, 1983b, Gandhidasan,

1983c). All studies used the same linear approximation of solution vapour pressure as the one presented by Kakabaev and Khandurdyev (1969) and also the average solution concentration approximation as presented by Baum *et al.* (1972). Regarding the open flat plate regenerator and the solar still type, the analysis showed that the derived analytical models can be used for preliminary design calculations to predict the water evaporated from the weak solution to the air. A numerical model was developed for the forced parallel flow regenerator and it was found that the climatic conditions and the ratio of flow rate of solution to flow rate of air affect the performance of the regenerator. In another study by Gandhidasan (1984) the performance of a closed type and an open type regenerator under optimum operating conditions was investigated using analytical models. The closed type performed better in both climatic scenarios; hot-dry and hot-humid.

The possible inadequacies of analytical solutions caused by simplifying assumptions drove Peng and Howell (1982) to develop a numerical model for predicting the mass rate of evaporated water in an open-type solar regenerator using non dimensional parameters taking into account the fact that the heat capacity of the solution is a function of temperature and solution concentration. Their model was more accurate and representative of the physical non-linear problem than the analytical one presented by Collier (1979). However, their analysis also showed that the analytical model was able to give results close to the ones obtained by the more sophisticated numerical model. This numerical model was used by the same authors to predict the performance of various regenerator designs using tri-ethylene glycol as desiccant. By comparing an open type solar regenerator to a glazed and a packed bed it was concluded that the open type did not perform well under hot and humid climatic conditions (Peng and Howell, 1984).

Noteworthy is Novak and Wood's experimental work on open type regenerators. They experimentally investigated the performance of an open-type solar regenerator and simulated its performance under a range of climatic conditions (Novak and Wood, 1985, Novak *et al.*, 1985). Based on the experimental data local correlations of heat and mass transfer were derived and used in a numerical model to predict the performance of the system. This model differed from previous models because it considered the change in solution enthalpy as a function of temperature and concentration change. The simulations showed that the open type solar regenerator would work effectively under hot, arid climate with high solar irradiance and low to moderate wind speeds. Additionally, they concluded

that the optimum length of the regenerator would be 10.5 m because further increase in length did not affect the evaporation rate significantly.

Similarly a numerical two dimensional model for a natural convection glazed regenerator was developed by Nelson and Wood (1990). Comparison of the performance of the glazed regenerator with an unglazed showed that the glazed one performed better under various climatic conditions. Their analysis showed the sensitivity of the open type regenerator to changes of the ambient conditions and that in windy and humid climate the only regenerator to perform effectively is the closed type. However this study was theoretical and did not experimentally validate the accuracy of the predicted performance.

Later, Hawlander *et al.* (1992) evaluated the performance of a glazed (closed-type, natural convection) and an unglazed (open-type) regenerator using LiCl as liquid desiccant using the same model as the one presented by Novak *et al.* (1985) but using their own empirical non dimensional correlations of heat and mass transfer. It was experimentally found that the unglazed performed better at the climatic conditions of Tempe, Arizona. It was also shown that the glazed one was less sensitive to changes of climatic conditions.

Worth mention are the works of Mullick and Gupta (1974) who experimentally and theoretically investigated the performance of a closed-type natural convection regenerator using $CaCl_2$ as desiccant. It was found that this type of regenerator performs better than the solar still type. Kaudinya and Kaushik (1986) compared the performance of an open type regenerator with a closed one using LiBr and LiCl as desiccants in order to validate earlier theoretical studies. The analysis showed that the regenerators performed better when using LiBr and that the closed type forced flow regenerator performed better than the open type in hot and dry climatic conditions. Kushik *et al.* (1992) summarised heat and mass transfer analytical models already known from the literature for three types of regenerators (open, closed/glazed, closed/solar still) and compared them with the numerical model of Peng and Howell. It was concluded that the analytical models are able to predict the performance under a wide range of solution mass flow, concentration and ambient conditions almost as accurate as the numerical one. The open and closed/glazed regenerators proved to be more efficient than the closed/solar still type. Haim *et al.* (1992) simulated and analysed an open cycle absorption system for solar cooling. The system's performance was evaluated using two different forced flow closed-type solar regenerators (direct and indirect). It was concluded that the cooling system performs better when using the direct type solar

regenerator because the direct solar heating of the solution minimises heat losses that cannot be avoided by the indirect type. Kabeel (2005) carried out an experimental study that investigated the performance of a forced cross flow solar regenerator using $CaCl_2$ as desiccant under real conditions. By comparison with an open-type regenerator it was demonstrated that the forced cross flow regenerator performs better than the open type because of the higher mass transfer coefficient.

A brief summary of the studies published since late 1960's can be seen in table 4.1.

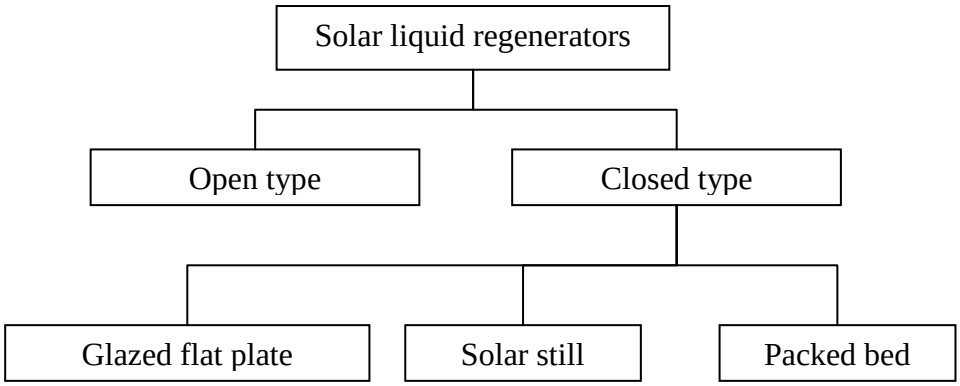

Fig. 4.1: Tree diagram showing the different types of solar liquid regenerators as categorised in literature.

In conclusion, research has shown that the open type regenerator would perform effectively under hot and dry climatic conditions while the closed type glazed regenerator would perform better than the open under hot and humid conditions. It is worth noting that the closed type is not affected by windy conditions and thus the desiccant is not contaminated with dust which can cause clogging of the distribution pipes and therefore degradation of the whole cooling system. Solar stills proved to perform less effectively than all the other types of regenerators. The analytical models developed can actually predict the performance of the regenerators with good accuracy and thus can be used for designing purposes. The numerical models provided a closer approach to the physical problem, making fewer assumptions and therefore achieve higher accuracy in predicting the performance. However they are more difficult to use than the analytical ones. No author has yet investigated the use of $MgCl_2$ as a liquid desiccant.

Table 4.1: Summary of published work on solar liquid regenerators

Year	Authors	Type of Regenerator	Desiccant	Experimental/ Theoretical
1969	Kakabaev and Khandurdyev	open	LiCl	Theory
1972	Baum *et al*	open	LiCl	Theory and Experiment
1974	Mullick and Gupta	closed-glazed, solar still	$CaCl_2$	Theory and Experiment
1979	Collier	open	LiCl	Theory
1981	Gandhidasan *et al*	closed-glazed	any	Theory
1982	Peng and Howell	open	LiCl	Theory
1982	Gandhidasan	closed-glazed	$CaCl_2$	Theory
1983	Gandhidasan[a]	open	$CaCl_2$	Theory
1983	Gandhidasan[b]	closed-glazed	$CaCl_2$	Theory
1983	Gandhidasan[c]	closed-tilted solar still	$CaCl_2$	Theory
1984	Peng and Howell	open and closed	Triethylene glycol	Theory
1984	Gandhidasan	open and closed-glazed	$CaCl_2$	Theory
1985	Novak *et al.*	open	LiCl	Theory and Experiment
1985	Novak and Wood	open	LiCl	Theory
1986	Kaudinya and Kaushik	open and closed-glazed	LiCl, LiBr	Theory and Experiment
1989	Kumar and Devotta	open	LiCl	Theory and Experiment
1990	Nelson and Wood	closed-glazed	LiCl	Theory
1992	Kushik *et al*	open, closed-glazed, solar still	LiCl	Theory
1992	Haim *et al*	closed-glazed	LiCl	Theory
1992	Hawlander *et al*	open and closed-glazed	LiCl	Theory and Experiment
1998	Fagbenle and Karayiannis	open	$CaCl_2$, LiCl	Theory
2002	Alizadeh and Saman	closed-glazed	$CaCl_2$	Theory
2005	Kabeel	open and closed-glazed	$CaCl_2$	Experiment

4.3 Theoretical model

The open surface flat plate regenerator is basically a modified solar collector. The conventional solar collector extracts energy from the sun and stores it as thermal energy while the solar regenerator stores it as chemical energy in the desiccant solution. As the liquid desiccant flows freely on the surface of the solar regenerator water is evaporated leaving the liquid desiccant more concentrated. The surface of the regenerator absorbs a fraction of the solar energy incident (I_α). Then a fraction of the absorbed energy is transferred to the solution thus resulting in increasing its temperature (sensible heat, $\Delta H_s=H_{out}-H_{in}$) and evaporating water (latent heat of vaporisation, H_{fg}). The rest of the absorbed energy is rejected to the environment as heat transferred by radiation (Q_{rad}), convection (Q_{conv}) and conduction (Q_{back}). However, the heat loss from the backing of the regenerator is considered negligible since there is good insulation. Hence if we consider an overall heat loss coefficient U_L then we can express the heat losses as

$$\dot{Q}_{loss} = \dot{Q}_{rad} + \dot{Q}_{conv} = U_L \cdot (T_s - T_{amb}) \cdot A \tag{4.1}$$

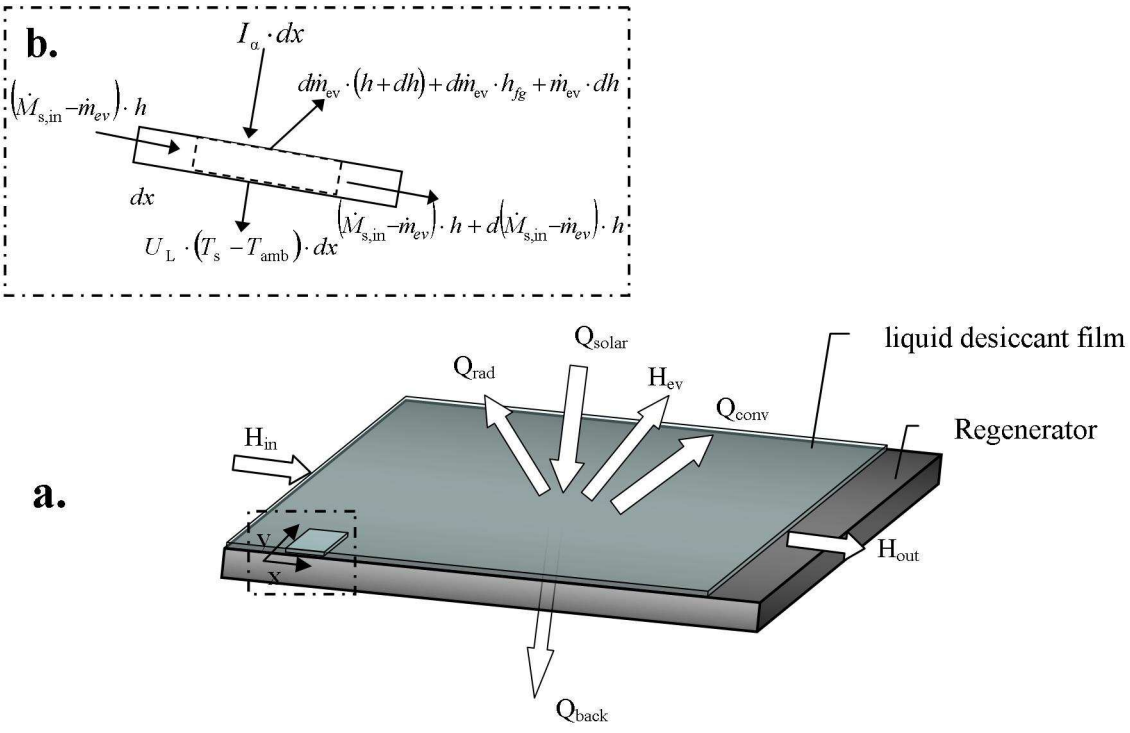

Fig. 4.2: **a)** Energy Balance on the surface of the regenerator and **b)** Energy Balance in a Differential control volume of the solution.

The energy balance on the surface of the regenerator can be expressed mathematically as:

$\sum E_{in} = \sum E_{out} \Rightarrow Q_{solar} + H_{in} = H_{out} + Q_{loss} + H_{ev}$ which becomes for a differential element

$$dQ_{solar} = \Delta H_s + dQ_{loss} + dH_{ev} \tag{4.2}$$

The following analysis follows that of Kakabaev and Khandurdyev (1969), Collier (1979) and Kumar and Devotta (1989).

Considering an energy balance in a differential control volume of the solution film with length dx, unit width w and negligible film thickness (Fig. 4.2) and assuming that :

a) heat and mass transfer take place under steady state
b) the temperature gradient and the diffusion in the solution film are negligible because of its small thickness
c) the mean values of h_m , the mass transfer coefficient based on pressure gradient, and U_L , the overall heat loss coefficient, are considered constant local values
d) h_{fg} , the latent heat of vaporisation, is constant
e) analysis is one dimensional (no variation with *y*)

the following equations can be derived

$$d\dot{Q}_{solar} = I_\alpha \cdot w \cdot dx \tag{4.3}$$

where dQ_{solar} is the solar heat transfer rate at the differential element, I_α is the solar irradiance absorbed by the surface of the regenerator in dimension *x* and *w* is the width perpendicular to direction of flow and equals 1 in this analysis thus

$$d\dot{Q}_{solar} = I_\alpha \cdot dx \tag{4.4}$$

$$\dot{H}_{in} = \left(\dot{M}_{s,in} - \dot{m}_{ev}\right) \cdot h \tag{4.5}$$

where $\dot{H}_{in}$ is the total enthalpy rate of the solution flowing in the differential element, $\dot{M}_s^o$ is the solution mass flow rate per unit width at the inlet, $\dot{m}_{ev}$ is the water evaporation rate per unit width and *h* is the specific enthalpy rate of the solution

$$\dot{H}_{\text{out}} = \left(\dot{M}_{\text{s,in}} - \dot{m}_{\text{ev}}\right)\cdot h + d.\left(\dot{M}_{\text{s,in}} - \dot{m}_{\text{ev}}\right)\cdot h \tag{4.6}$$

$\dot{H}_{\text{out}}$ is the total enthalpy rate of the solution flowing out of the differential element hence

$$\Delta\dot{H}_{\text{s}} = \dot{H}_{\text{out}} - \dot{H}_{\text{in}} = d.\left(\dot{M}_{\text{s,in}} - \dot{m}_{\text{ev}}\right)\cdot h \tag{4.7}$$

$d\dot{Q}_{\text{loss}} = U_{\text{L}}\cdot\left(T_{\text{s}} - T_{\text{amb}}\right)\cdot w\cdot dx$, where w = 1 hence

$$d\dot{Q}_{\text{loss}} = U_{\text{L}}\cdot\left(T_{\text{s}} - T_{\text{amb}}\right)\cdot dx \tag{4.8}$$

where $d\dot{Q}_{\text{loss}}$ is the heat loss transfer rate of the differential element, T_{s} and T_{amb} are the average solution temperature and the ambient air temperature respectively

The total enthalpy rate of the evaporating water $\dot{H}_{\text{ev}}$ can be expressed as the sum of the sensible heat rate and the latent heat rate as follows

$$\dot{H}_{\text{ev}} = \dot{m}_{\text{ev}}\cdot h + \dot{m}_{\text{ev}}\cdot h_{fg} \tag{4.9}$$

by differentiating (7) we arrive at the following

$$d\dot{H}_{\text{ev}} = d\dot{m}_{\text{ev}}\cdot\left(h + dh\right) + d\dot{m}_{\text{ev}}\cdot h_{fg} + \dot{m}_{\text{ev}}\cdot dh \tag{4.10}$$

The specific enthalpy of the solution can be expressed as

$$h = C_{\text{p}}\cdot T_{\text{s}} \tag{4.11}$$

where C_{p} is the specific heat of the solution, considered constant in this analysis, and by differentiating equation (9) yields:

$$dh = C_{\text{p}}\cdot dT_{\text{s}} \tag{4.12}$$

By substituting (4.4), (4.7), (4.10), (4.12) in (4.2) we arrive at the following equation

$$I_{\alpha} \cdot dx - U_{\mathrm{L}} \cdot \left(T_{\mathrm{s}} - T_{\mathrm{amb}}\right) \cdot dx - \dot{M}_{\mathrm{s,in}} \cdot C_{\mathrm{p}} \cdot dT_{\mathrm{s}} - d\dot{m}_{\mathrm{ev}} \cdot h_{fg} = 0 \tag{4.13}$$

$$\Rightarrow I_{\alpha} - U_{\mathrm{L}} \cdot \left(T_{\mathrm{s}} - T_{\mathrm{amb}}\right) - \dot{M}_{\mathrm{s,in}} \cdot C_{\mathrm{p}} \cdot \frac{dT_{\mathrm{s}}}{dx} - \frac{d\dot{m}_{\mathrm{ev}}}{dx} \cdot h_{fg} = 0 \tag{4.14}$$

The mass flux of evaporated water from a differential volume can be expressed based on the vapour pressure gradient as:

$$\frac{d\dot{m}_{\mathrm{ev}}}{dx} = h_{\mathrm{m}} \cdot \left(P_{\mathrm{s}} - P_{amb}\right) \tag{4.15}$$

where P_{s} and P_{amb} are the vapour pressure of the solution and the ambient pressure respectively.

The weight concentration of the desiccant in the solution is given by

$$X_{\mathrm{s}} = \frac{\dot{m}_{\mathrm{des}}}{\dot{M}_{\mathrm{s,in}} - \dot{m}_{\mathrm{ev}}} \tag{4.16}$$

where $\dot{m}_{\mathrm{des}}$ is the salt mass flow rate per unit width.

The vapour pressure of the solution can be approximated by a linear function of temperature and concentration:

$$P_{\mathrm{s}} = a \cdot T_{\mathrm{s}} + \frac{b}{X_{\mathrm{s}}} + c \tag{4.17}$$

where a, b, c are constants calculated empirically (from experimental values of vapour pressure reported in the literature) for a small range of temperatures and concentrations in order to maintain the accuracy of the linear equation (within 5% error).

From (4.15), (4.16) and (4.17) by eliminating P_{s} we arrive at the following equation

$$T_{\mathrm{s}} = \left(\frac{1}{a \cdot h_{\mathrm{m}}}\right) \cdot \frac{d\dot{m}_{\mathrm{ev}}}{dx} + \frac{P_{\mathrm{amb}}}{a} - \frac{b \cdot \dot{M}_{\mathrm{s,in}}}{a \cdot \dot{m}_{\mathrm{des}}} - \left(\frac{b}{a \cdot \dot{m}_{\mathrm{des}}}\right) \cdot \dot{m}_{\mathrm{ev}} - \frac{c}{a} \tag{4.18}$$

now taking the derivative of T_s with respect to x yields:

$$\frac{dT_s}{dx} = \left(\frac{1}{a \cdot h_m}\right) \cdot \frac{d^2 \dot{m}_{ev}}{dx^2} + \left(\frac{b}{a \cdot \dot{m}_{des}}\right) \cdot \frac{d\dot{m}_{ev}}{dx} \tag{4.19}$$

If we substitute (16) and (17) in (12) we arrive at:

$$\frac{d^2 \dot{m}_{ev}}{dx^2} + \frac{\mathrm{A}}{\dot{M}_{s,in}} \cdot \frac{d\dot{m}_{ev}}{dx} + \frac{\mathrm{B}}{\left(\dot{M}_{s,in}\right)^2} \cdot \dot{m}_{ev} - \frac{\Gamma}{\dot{M}_{s,in}} = 0 \tag{4.20}$$

where:

$$\mathrm{A} = \frac{U_L}{C_p} + \frac{h_m \cdot b}{X_{s,in}} + \frac{h_{fg} \cdot a \cdot k_p}{C_p} \tag{4.21}$$

$$\mathrm{B} = \frac{U_L \cdot b \cdot h_m}{X_{s,in} \cdot C_p} \tag{4.22}$$

$$\Gamma = \frac{h_m}{C_p} \cdot \left[a \cdot \left(I_\alpha + U_L \cdot T_{amb}\right) + U_L \cdot \left(\frac{b}{X_{s,in}} - P_{amb} + c\right)\right] \tag{4.23}$$

$$X_s^{\,o} = \frac{\dot{m}_{des}}{\dot{M}_{s,in}} \tag{4.24}$$

Equation (4.20) is a second order linear inhomogeneous equation whose general solution is:

$$\begin{aligned} &\dot{m}_{ev} = L_1 \cdot e^{\frac{K_1 \cdot x}{\dot{M}_{s,in}}} + L_2 \cdot e^{\frac{K_2 \cdot x}{\dot{M}_{s,in}}} + \frac{\Gamma}{\mathrm{B}} \cdot \dot{M}_{s,in} \\ &K_1 = \frac{-\mathrm{A} + \sqrt{\mathrm{A}^2 - 4\mathrm{B}}}{2}, \quad K_1 = \frac{-\mathrm{A} - \sqrt{\mathrm{A}^2 - 4\mathrm{B}}}{2} \end{aligned} \tag{4.25}$$

The constants L_1 and L_2 are found from the boundary conditions

$$\left\{ \begin{aligned} &\dot{m}_{ev} = 0, \quad x = 0 \\ &\frac{d\dot{m}_{ev}}{dx} = h_m \cdot \left(P_0 - P_{amb}\right), \quad x = 0 \end{aligned} \right\} \Rightarrow \left\{ \begin{aligned} &L_1 + L_2 + \frac{\Gamma}{\mathrm{B}} \cdot \dot{M}_{s,in} = 0 \\ &L_1 \cdot \frac{K_1}{\dot{M}_{s,in}} + L_2 \cdot \frac{K_2}{\dot{M}_{s,in}} = h_m \cdot \left(P_0 - P_{amb}\right) \end{aligned} \right\}$$

Solving the system for L_1 and L_2 and then substituting to equation (4.25) yields:

$$\dot{m}_{ev} = \frac{\dot{M}_{s,in} \cdot \left[\frac{\Gamma}{B} \cdot K_2 + h_m \cdot (P_0 - P_{amb}) \right]}{K_1 - K_2} \cdot e^{\frac{K_1 \cdot x}{\dot{M}_{s,in}}} - \frac{\dot{M}_{s,in} \cdot \left[\frac{\Gamma}{B} \cdot K_1 + h_m \cdot (P_0 - P_{amb}) \right]}{K_1 - K_2} \cdot e^{\frac{K_2 \cdot x}{\dot{M}_{s,in}}} + \frac{\Gamma}{B} \cdot \dot{M}_{s,in} \quad (4.26)$$

The empirical values of equation (4.17) regarding $MgCl_2$ used in this study are presented on the following table:

Table 4.2: The empirical values used in equation (4.17)

Temperature range (^oC)	Concentration range (kg/kg %)	Average percent error	*a*	*b*	*c*
20-25	28-34	2	76	793	-23710
25-30	28-36	4	99	1084	-31600
30-35	28-36	4	135	1493	-43760
35-40	28-36	5	136	1494	-43920

a , *b*, *c*, were derived from experimental data (Zaytsev and Aseyev, 1992).

4.3.1 Derivation of Nusselt and Sherwood numbers

From the analysis above is apparent that the only unknown variables in equation (4.20) are the heat loss coefficient U_L and the mass transfer coefficient h_m. Therefore, it would be convenient for modelling purposes to be able to predict them.

Regarding h_m the following equations can be applied:

$$h_m = \frac{h_D}{R \cdot T} \quad \text{see ref (Kumar, 2003)} \quad (4.27)$$

where R is the air gas constant and h_D is the mass transfer coefficient based on concentration gradient.

$$h_D = \frac{\overline{Sh} \cdot D_{w\text{-}a}}{L_c} \text{ (Incropera } et\ al.\text{, 2007)} \quad (4.28)$$

where $\overline{Sh}$ is the average Sherwood number, $D_{w\text{-}a}$ is the binary diffusion coefficient of water vapour in air and L_c is the characteristic length

$$\overline{Sh} = f(Gr, Sc) \tag{4.29}$$

where *Gr* snd *Sc* are the Grashoff and Schmidt numbers respectively.
U_L can be expressed as the sum of the radiant heat transfer coefficient and the convective heat transfer coefficient:

$$U_L = h_{rad} + h_{conv} \tag{4.30}$$

Based on the Stefan-Boltzmann law the radiation heat transfer coefficient can be expressed as

$$h_{rad} = \frac{\sigma \cdot \varepsilon \cdot \left(T^4 - T_{sky}^4\right)}{\left(T - T_{amb}\right)} \text{ (Kumar and Devotta, 1989)} \tag{4.31}$$

where σ is the Stefan-Boltzmann constant, ε is the emissivity, T_{sky} is the effective sky radiation (in this analysis we used T_{amb} instead because all the experiments were conducted inside the laboratory).

$$h_{conv} = \frac{\overline{Nu} \cdot k}{L_c} \tag{4.32}$$

where $\overline{Nu}$ is the average Nusselt number, *k* is the themal conductivity of air.

$$\overline{Nu} = f(Gr, \mathrm{Pr}) \tag{4.33}$$

where Pr is the Prandtl number

Thus by knowing correlations of the average Nusselt number $\overline{Nu}$ and the average Sherwood number $\overline{Sh}$ we can predict h_{conv} and h_m. According to the literature simple empirical correlations for $\overline{Nu}$ and $\overline{Sh}$ in natural convection are of the form:

$$\left.\begin{aligned}\overline{Nu} &= C\cdot(Gr\cdot Pr)^n\\ \overline{Sh} &= C\cdot(Gr\cdot Sc)^n\end{aligned}\right\} \tag{4.34}$$

C and n are constants that depend on the geometry of the surface and the flow regime (Cengel, 2006). In addition the natural convection heat transfer on a surface depends on its orientation, the temperature variation of the surface and the thermo physical properties of the fluid.

The general empirical correlations of heat and mass transfer as published in the literature find application to problems of simple geometry such as of a flat plate, a cylinder etc. (Incropera *et al.*, 2007). Such correlations for a flat plate were also proposed by Collier for a regenerator model. However his study was theoretical and did not compare the correlations to any experimental data.
In practice, differences are likely to arise due to factors such as:

a) surface roughness
b) non uniform surface wetting
c) solution flow patterns
d) laboratory environment not fully controlled (varying ambient RH and temperature)

In this work we derived new correlations of heat and mass transfer based on our experimental data since there was a significant departure from the general correlations.

In order to derive new correlations of heat and mass transfer an energy balance was considered (equation (4.2)) for each experiment. All the variables were determined experimentally except Q_{loss}.

$$Q_{\text{solar}} = I_{\text{tot}}\cdot\alpha\cdot A - I_{\text{ref}}\cdot A \tag{4.35}$$

$$H_{\text{in}} = \dot{M}_{\text{s,in}}\cdot C_{\text{p,s}}\cdot T_{\text{in}} \tag{4.36}$$

$$H_{\text{out}} = \dot{M}_{\text{s,in}}\cdot C_{\text{p,s}}\cdot T_{\text{out}} \tag{4.37}$$

$$H_{\text{ev}} = M_{\text{ev}} \cdot h_{\text{fg}} \tag{4.38}$$

I_{ref} is the reflected light on the surface of the regenerator. It is assumed that the reflection is mainly specular hence the angle of reflection equals the angle of incidence of the radiation beam. The angle of incidence was taken to be 15^{o} and then the well established Fresnel equations were used to calculate the reflectance. It was found that only 3.3% of the irradiance was reflected.

By substituting (4.35), (4.36), (4.37), (4.38) in (4.2) Q_{loss} was calculated as the only remaining unknown variable. Q_{loss} can be expressed as

$$Q_{\text{loss}} = U_{\text{L}} \cdot \left(T_{\text{s}} - T_{\text{amb}}\right) \tag{4.39}$$

Hence for each experiment a total heat loss coefficient U_{L} was calculated and then the average Nusselt number was calculated from equations (4.30), (4.31) and (4.32). The Rayleigh number was in the range of 10^4-10^7, hence the flow of air was in the laminar region in all the experiments carried out.

Based on the general empirical correlation for natural convection over a horizontal flat plate and using solver function in Excel (setting the percent error of the predicted average Nusselt number to be 0) the following Nusselt number correlation was derived

$$\overline{Nu} = 0.54 \cdot Pr^{0.25} \cdot Gr_{\text{tot}}^{0.421} \tag{4.40}$$

The majority of the experimental *Nu* values were close to the predicted ones, but in some cases they were greater, even 1.94 times higher than the predicted. This indicates that there was some enhancement of the heat convective process that was not accounted for by the developed correlation.

The experimental $\dot{m}_{\text{ev}}$ was measured based on the method described in section 4.5.1 of this chapter. The mass rate of evaporation can be expressed as:

$$h_{\text{D}} = \frac{M_{ev}}{\rho_a \cdot \left(\omega_{\text{int}} - \omega_{amb}\right) \cdot A} \tag{4.41}$$

where ρ_a is the density of the air, ω_{int} and ω_{amb} are the moisture content at the interface of the solution-air and the moisture content of the ambient air respectively, *A* is the total area of the regenerator.

Substituting (4.41) in (4.28) and solving for $\overline{Sh}$ yields:

$$\overline{Sh} = \frac{M_{ev} \cdot L_{\text{c}}}{\rho_a \cdot D_{\text{w-a}} \cdot \left(\omega_{\text{int}} - \omega_{amb}\right) \cdot A} \tag{4.42}$$

which gives the experimental Sherwood number.

Since there is an analogy between heat and mass transfer, the Sherwood number correlation was derived following the same method as with Nusselt number above

$$\overline{Sh} = 0.54 \cdot Sc^{0.25} \cdot Gr_{\text{tot}}^{0.427} \tag{4.43}$$

The majority of the experimental *Sh* values were close or greater than the predicted ones, in some cases 1.75 times higher than the predicted. This also indicates that there was some enhancement of the mass convective process that was not accounted for by the developed correlation. The experimental Lewis number varied from 0.85 to 0.87 (less than 1 in all cases) showing that the mass diffusion in the concentration boundary layer was greater than the heat diffusion in the thermal boundary layer.

All the physical properties of air and water used in this model were calculated based on well known formulae published in literature or were calculated using polynomial regression based on experimental data (Cengel, 2006, Incropera *et al.*, 2007).

4.4 Experimental equipment and methods

The performance of an open regenerator is affected by:

a) Ambient conditions such as solar irradiance, air temperature and humidity, and wind speed, and
b) Design parameters such as the mass flow rate and concentration of the desiccant solution, how it is distributed, the length and width of the regenerator, its orientation, and the materials from which the regenerator is made.

The aim here is to establish how these design parameters should be chosen so as to optimise the performance under the ambient conditions according to the local climate. Further, these ambient conditions will vary with the time of day and year and it may be desirable to control some design parameters, such a solution flow rate, in response to this variation. In this case the optimum control strategy also needs to be established.

In this work we have investigated the performance of the regenerator under lab conditions. The experimental set up enabled us to control the irradiance, the solution mass flow and the solution concentration. However, ambient humidity could not easily be controlled and wind speed was effectively zero. Although not as efficient as the closed type, an open type flat plat regenerator was preferred as it is the simplest and cheapest and therefore most likely to be suited to the application in greenhouses where large areas will be required.

Table 4.3: The experimental equipment

Material	Manufacturer / spec	Supplier
6mm black neoprene foam sheet	part No 303-2246	RS Components Ltd, UK
Black mulch sheet, 50gsm polypropylene	Weed control fabric/mulch	R&H Garden Supplies, Lincolnshire, UK
Distributor pipe, polyethylene	25 mm internal diameter	Screwfix, UK
$MgCl_2$ $6H_20$	Fisher Scientific Brand, Analytical Grade Reagent MW 203.31,	Fisher Scientific, Loughborough, UK
Transparent plastic tank	Savic 0130 Fauna Box, 10L	Aquatics Online Ltd, UK
Peristaltic pump	Watson Marlow sci-Q 323 series	Fisher Scientific, Loughborough, UK
Bulbs	Halogen EIKO Q50MR16 Solux bulb, 50W, 4700 K (daylight simulation bulb), 36 deg. Dichroic spot	–
Pyranometer	CMP 11, ISO-9060	Kipp & Zonen Ltd, Lincolnshire, UK
Platinum resistance detectors	PT100, SE012 PT104 Pico Technology	Pico Technology, Cambridgeshire, UK

(Table 4.3 continued)

Infrared digital thermometer	Raytek MiniTemp Series MT4	-
Refractometer	Abbe 60 series, No 530406	Bellingham + Stanley Ltd, Kent, UK
Silica test plate	Bellingham and Stanley Ltd	Bellingham and Stanley Ltd, Tunbridge Wells, UK
Testo 400 RH probe	-	-
Silicone tubing	Fisher Scientific Brand, FB56478	Fisher Scientific, Loughborough, UK
Diffusion paper	tracing paper	Paperway Ltd, Birmingham, UK
Half round gutter	Kitemarked / KM501316	Screwfix, UK

4.4.1 Set up

The experimental regenerator, shown in Fig 4.3 and 4.6, was inclined at 2.5 degrees to the horizontal and measured 0.73 m long, in the direction of flow, by 0.84 m wide, giving an active area of 0.61 m^2. Its surface consisted of a 6mm black neoprene foam sheet and a woven black mulch sheet on the top for better dispersion of the solution on the surface. These were supported by a steel backing. The weak magnesium chloride solution was pumped to a distributor at the top of the regenerator surface. This distributor consisted of a polyethylene pipe extended over the width of the regenerator with 21 holes of 2mm diameter spaced at 30 mm intervals.

The concentrated solution was collected in a rectangular transparent plastic tank, which had been calibrated so as to monitor the volume change by measuring the change in height of the free surface of the solution and hence the volume of water evaporated from the regenerator. In order to accurately calculate the volume, taking into account any variations in width and length, we calibrated the height gauge against known volumes of water. Figure 4.4 shows the calibration graph. The error in measuring the evaporated water was ±14 g, based on the random error of reading the scale of the height gauge (±0.5 mm). A peristaltic pump was used to return the solution to the top of the regenerator. The solution was concentrated by passing multiple times over the regenerator surface. Figure 4.3 shows a photograph of the experimental rig.

Under real conditions the sun will provide the necessary heat to drive off water from the weak solution. To simulate this, an array of 90 daylight simulation bulbs, arranged in a triangular pattern with pitch 109 mm (see Fig. A2.1 in appendix 2), was constructed on an aluminium frame and fed from a 4.5 kW power supply. A diffusion paper was used to diffuse the light of the lamps and hence achieve better distribution of light at the surface of the regenerator. The diffusion paper improved the uniformity (ratio of standard deviation divided by the average multiplied by 100) by lowering the coefficient of variation from 15% down to 9%.

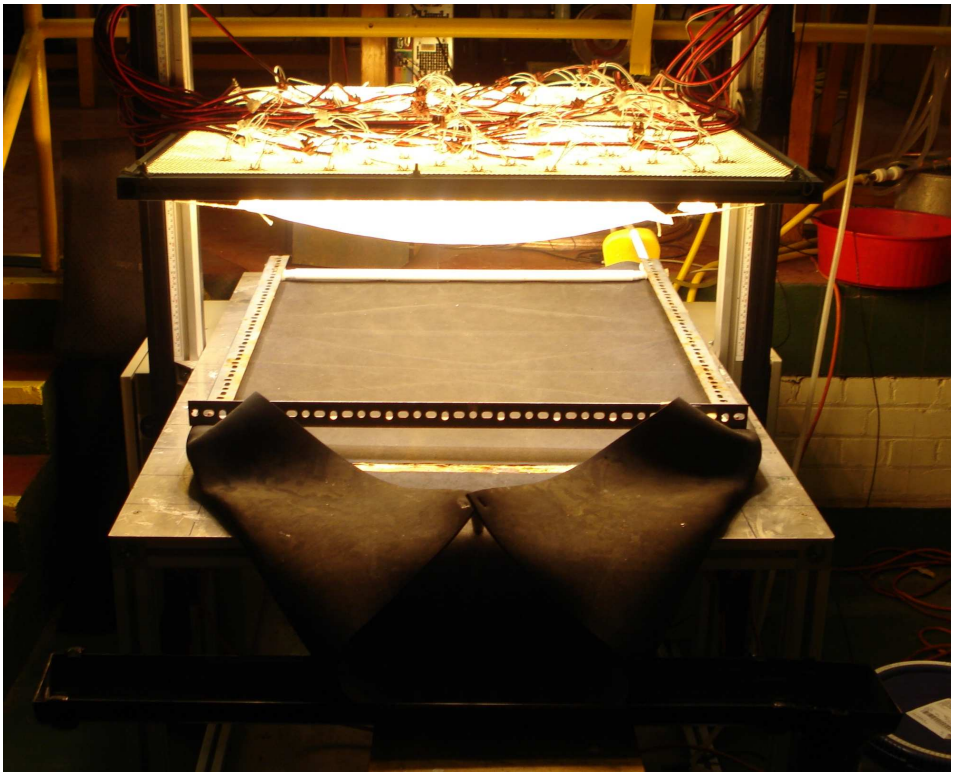

Fig. 4.3: Photo of the experimental regenerator rig.

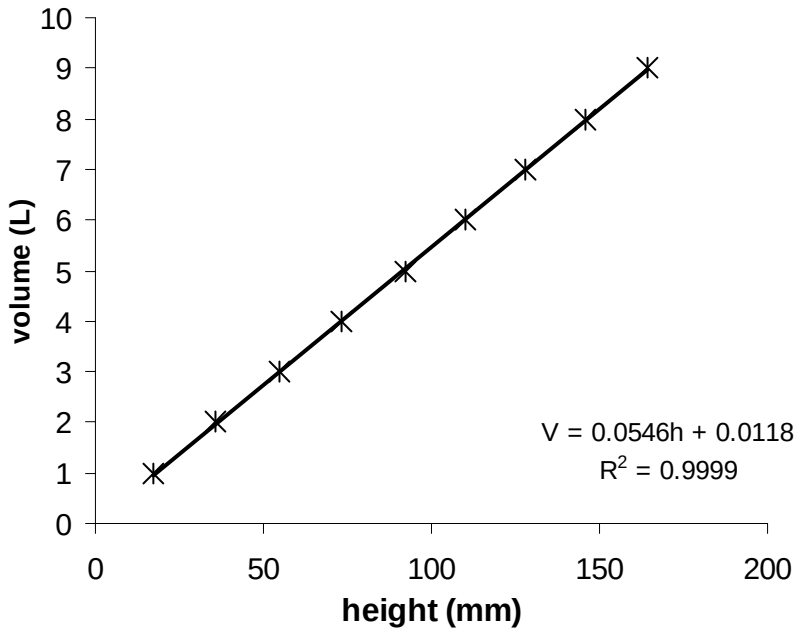

Fig. 4.4: Calibration graph of the rectangular tank used to collect the concentrated $MgCl_2$ solution.

The array of lamps was set horizontally. A pyranometer was used to measure the irradiance at the regenerator surface. Irradiance was varied by changing the height of the lamp array. A calibration was carried out of irradiance with respect to height, enabling irradiances of 418, 454, 498, 544, 763 and 974 Wm^{-2} to be achieved. See appendix 2 for more details of the solar simulator calibration. The results can be seen in Table 4.4 and in Fig 4.4. The E values represent averages of 15 pyranometer readings for each height. The obtained graph was used as a calibration graph and the detailed measurements can be found in the appendix.

Table 4.4: The results from the calibration of the solar simulator

height (cm)	Average E(Wm^{-2})	Standard Dev	CV%
23	974	98	10.1
33	763	65	8.5
52.5	544	46	8.5
61.5	498	46	9.3
67.5	454	43	9.6
73.5	418	35	8.4

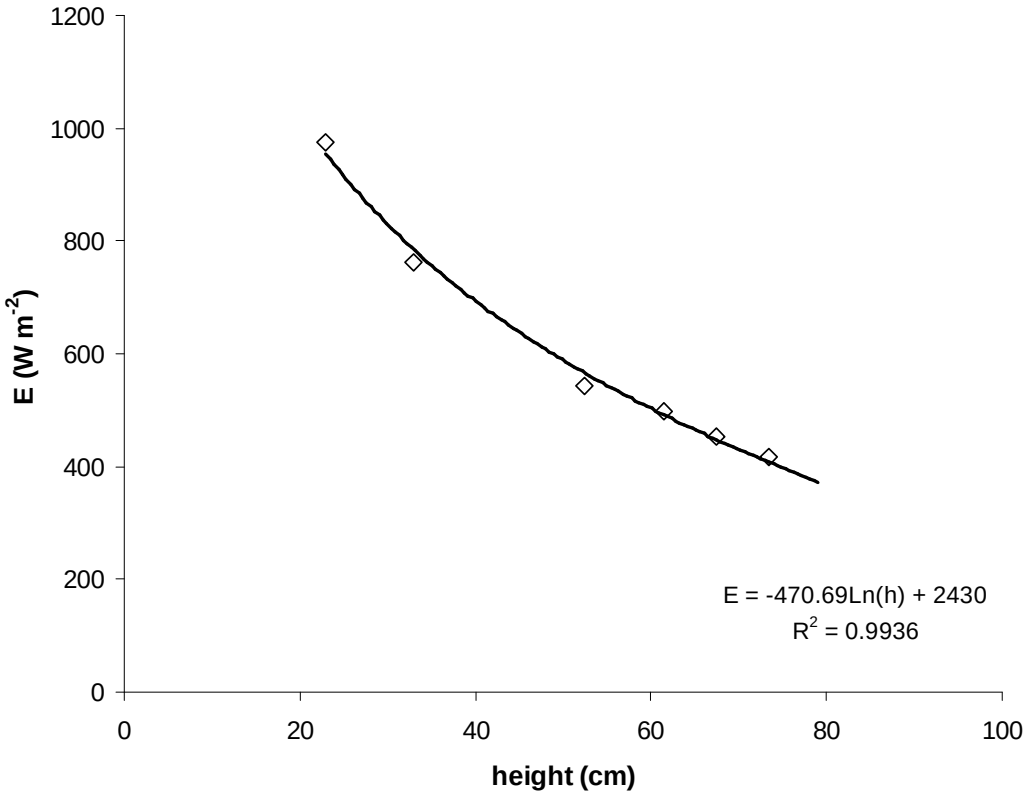

Fig. 4.5: Solar simulator calibration graph.

The solution and ambient air temperatures were measured using platinum resistance detectors (PT100 ±0.03 °C @ 0 °C) connected to a PC and the readings were recorded by the PicoLog data logging software. The data logger was set to record every 1 sec. The regenerator surface temperature was measured in 9 positions using an infrared digital thermometer with an accuracy of ±2%. Measurements were taken every 15 min. The positions of the temperature measurements can be seen in Figure 4.7

A refractometer of high accuracy ± 0.00004 RI was used to measure the refractive index (RI) of the $MgCl_2$ solution. This method was chosen as the most accurate for measuring indirectly the concentration of the solution (expressed as the ratio of the mass of the desiccant divided by the mass of the solution). The solution concentration was calculated from published data of concentration and RI of pure aqueous $MgCl_2$ solutions (Perry *et al.*, 1984) by linear interpolation. The refractometer was calibrated using a certified silica test plate (percent error = -0.06%). Volume samples of the $MgCl_2$ solution were taken from the tank at predefined time intervals so as to monitor the concentration throughout the regeneration process by measuring the refractive index. The volume of solution removed each time was no more than 3 ml.

The relative humidity was measured with a Testo 400 (Testo Ltd, Alton, Hampshire UK) probe of ± 1% RH accuracy. The relative humidity and ambient temperature in the laboratory were not controlled but they varied within a range of 27-38.5%RH and 19-26 ^{o}C respectively.

The solution volumetric flow was measured at the outlet by timing known volumes of solution using a volumetric cylinder and a stop watch. The error in measuring the volumetric flow was ± 1.3% based on the random error of reading the volumetric cylinder scale ± 2.5 ml and random error of stop watch ± 1 s. There was no significant recorded change in the solution volumetric flow at the regenerator outlet in any of the experiments.

Each experiment was continued until the system reached steady state condition, i.e. when a constant evaporation rate was achieved, or until crystallisation started to occur. Thus the experiments lasted for between 180 and 525 minutes. It is worth noting that beyond the crystallisation point flow measurements were not reliable at the outlet of the regenerator because the increasing salt deposition and crystal formation on the surface of the regenerator caused large and small fragments of salts to be washed up and carried over in the tank. Nevertheless as stated earlier the volumetric flow remained almost constant at the outlet until crystallisation.

Fig. 4.6: Photo of the experimental regenerator rig.

4.4.2 Experimental procedure

1. Mix up the $MgCl_2$ solution by stirring known masses of water with known masses of $MgCl_2$.
2. Decant approximately 8L of the solution in the rectangular plastic tank (see bubble No7 in Fig. 4.7).
3. Put all the temperature probes for measuring solution and ambient air temperature in place (see Fig. 4.7)
4. Start the pump at the desired speed.
5. Wait until the surface of the regenerator is wet and flow at the outlet is balanced.
6. Set the computer to log readings.
7. Take a reading at the height gauge of the rectangular plastic tank (repeat every 15 or 30 min).
8. Take a reading of the solution flow at the outlet of the regenerator (repeat every 15 or 30 min).
9. Take solution sample from the rectangular plastic tank after good stirring (repeat every 15 or 30 min).
10. Take surface temperature readings in positions showed in Figure 4.7 (repeat every 15 or 30 min).
11. Measure RI of samples after the end of the experiment.
12. Remove the temperature probes and wash them with water.

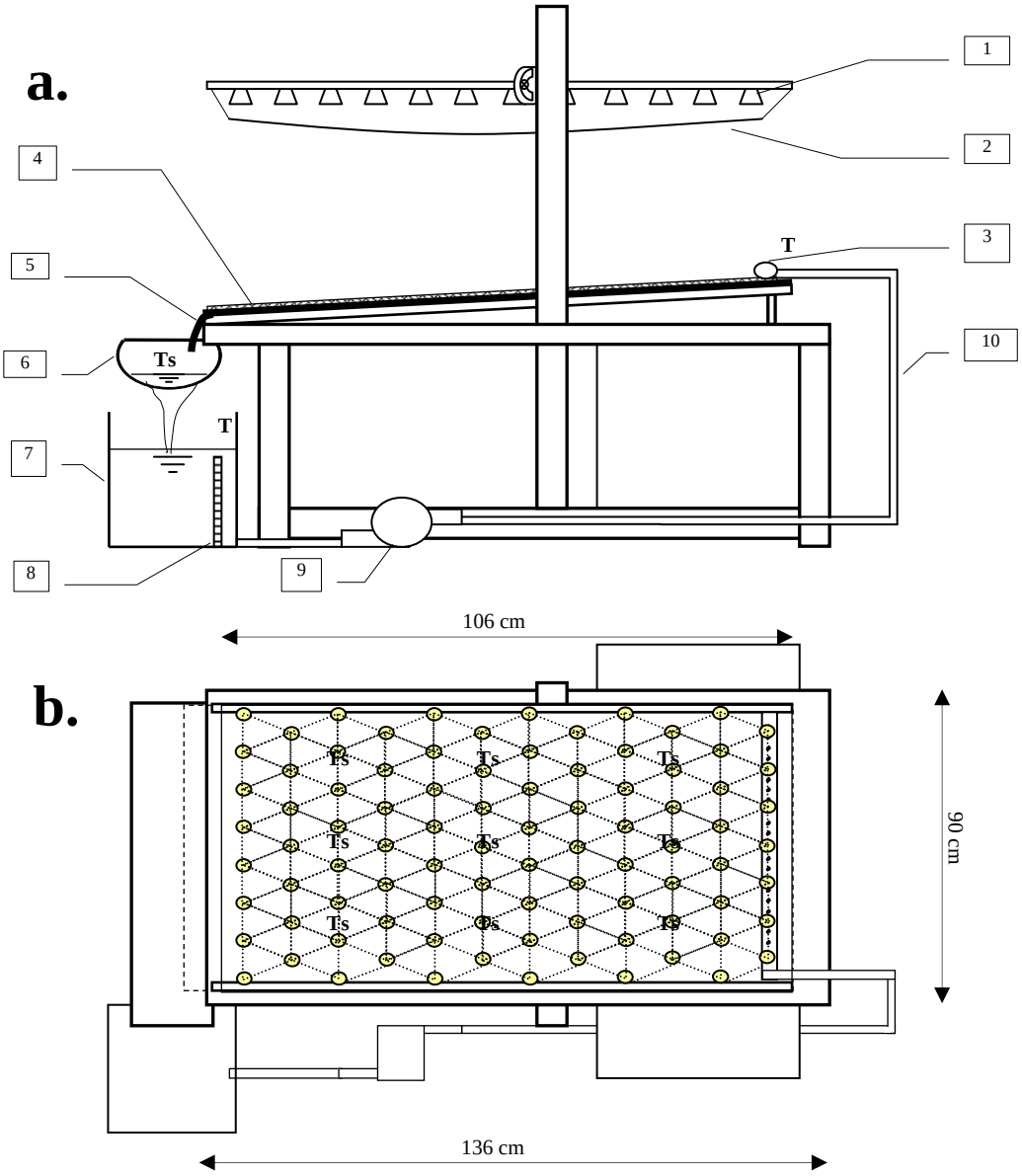

T : PT100 positions
Ts : Surface temperature and outlet reading positions

	Material	Manufacturer / series	Supplier
1	bulb	EIKO / Q50MR16	–
2	diffusion paper	tracing paper	Paperway Ltd
3	distribution pipe	polyethylene (25 mm ID)	Screwfix
4	mulch sheet	50gsm polypropylene	R&H Garden Supplies
5	neoprene foam sheet	part No 303-2246	RS Components Ltd
6	half round gutter	Kitemarked / KM501316	Screwfix
7	plastic tank	Savic 0130 Fauna Box	Aquatics Online Ltd
8	height gauge		WHSmith
9	peristaltic pump	Watson Marlow /sci-Q 323	Fisher Scientific
10	silicone tubing	Fisher Brand / FB56478	Fisher Scientific

Fig. 4.7: a) side view and b) plan view of the regenerator rig.

4.5 Results and Discussion

4.5.1 Experimental Design and Method

Four different series of experiments were carried out at irradiance levels of 400, 600, 760 and 970 Wm^{-2}. Each series consisted of three experiments at three solution mass flows; 0.0020±0.0001 kg s^{-1}, 0.0039±0.0002 kg s^{-1}, 0.0064±0.0001 kg s^{-1}. The initial concentration of the solution varied in a small range 0.293-0.334kg of solute / kg of solution. We chose to conduct the most of the experiments with high initial concentrations which correspond to 40.8-53.4% ERH. If the desiccator is to work under dry and hot conditions (below 50%RH) efficiently then this would be achieved with a solution of lower than 40%ERH. Hence the ERH of the solution at the inlet of the regenerator/outlet of desiccator should be no higher of 55% under the current set up. However, in order to explore the effect of concentration on the performance of the regenerator two supplementary experiments were conducted in lower initial concentrations keeping the irradiance and the solution mass flow constants.

The solution becomes more concentrated as it runs on the regenerator surface and water is evaporated resulting in a total volume decrease of the solution when circulating in a closed loop. This volume decrease was recorded by the tank method which was described before. We calculated the solution volume from the following equation, derived from the calibration graph (see Fig. A4.2 appendix 4),

$$V = 0.0546 \cdot h + 0.0118 \tag{4.44}$$

V is the solution volume (L) and h is the height(mm).

Thus by taking the difference of the reading of the height gauge at the start (t_o) and the reading at the end of a period (t_i) we obtain the volume (or mass since $\rho_{H20} = 1$ kg/L) of evaporated water. Readings were taken every 15 or 30 min (depending on the irradiance level). The mass flux of evaporated water in g/h m^2 was calculated by the following formula:

$$\dot{m}_{ev} = \frac{\Delta V \cdot 60 \cdot 1000}{\Delta t \cdot A} \tag{4.45}$$

where ΔV is the volume change and is equal to the mass of evaporated water (kg), and Δt is the total time (min).

The effectiveness of the regenerator was calculated as the ratio of the energy spent to evaporate water from the solution to the absorbed solar energy.

$$\eta_{\text{eff}} = \frac{M_{\text{ev}} \cdot h_{\text{fg}}}{I_{\text{tot}} \cdot \alpha \cdot A} \cdot 100\% \tag{4.46}$$

The analytical measurements of water evaporation and solution concentration can be found in Tables A3.1 – A3.12 in appendix 3. Here we present these results in graphs. Fig 4.9 – Fig 4.20 show the calculated mass flux of evaporated water and the concentration change during the experiments carried out at 400, 600, 760 and 970 W m^{-2} irradiance and at three different solution flow rates. Here in Figure 4.8 we present the average values of the effectiveness at various irradiance levels and concentration ranges.

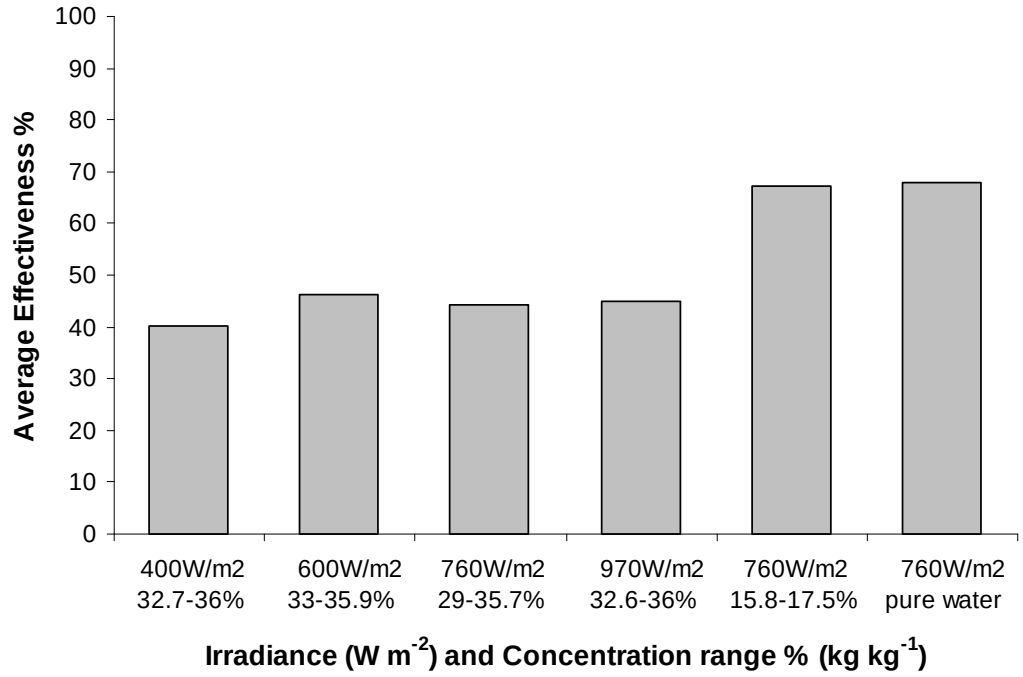

Fig. 4.8: Average measured effectiveness at different values of Irradiance and Concentration range.

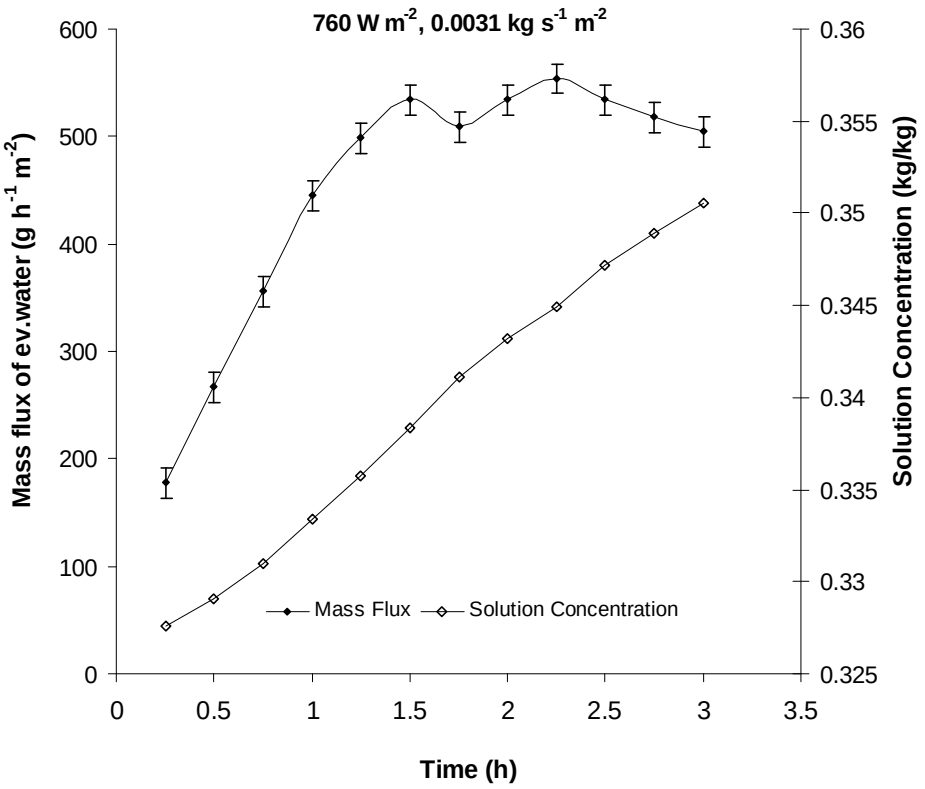

Fig. 4.9: Mass flux of water evaporation and solution concentration against time at 760 W m^{-2} irradiance and 0.0031kg s^{-1} m^{-2} solution mass flux.

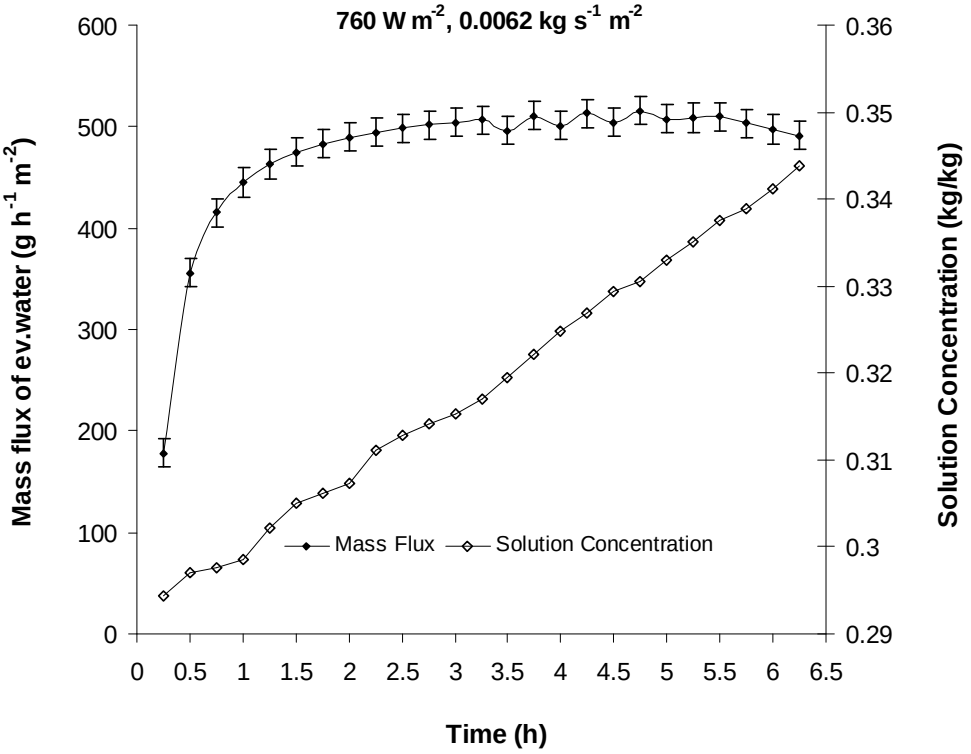

Fig. 4.10: Mass flux of water evaporation and solution concentration against time at 760 W m^{-2} irradiance and 0.0062 kg s^{-1} m^{-2} solution mass flux.

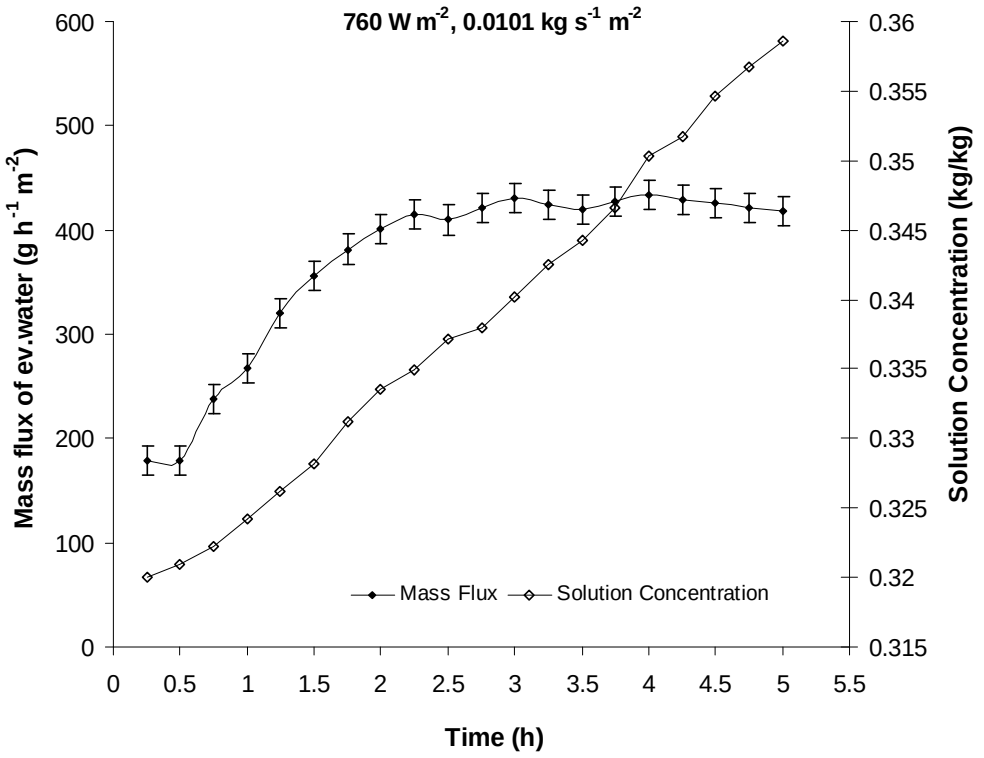

Fig. 4.11: Mass flux of water evaporation and solution concentration against time at 760 W m^{-2} irradiance and 0.0101 kg s^{-1} m^{-2} solution mass flux.

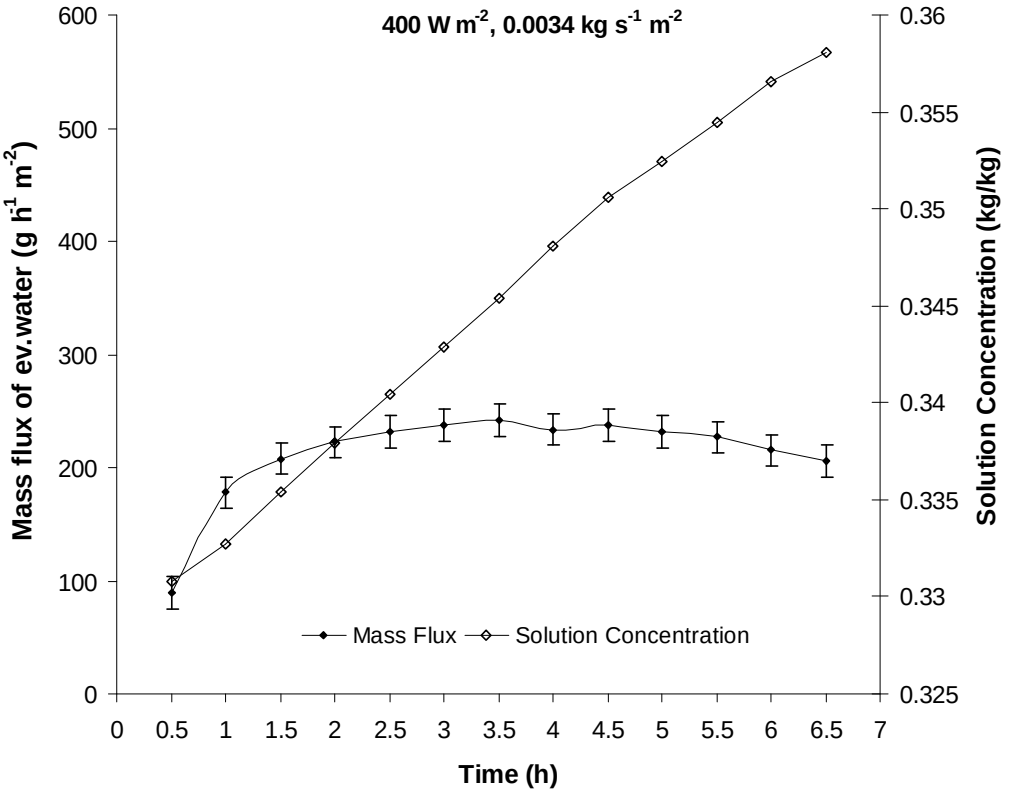

Fig. 4.12: Mass flux of water evaporation and solution concentration against time at 400 W m^{-2} irradiance and 0.0034 kg s^{-1} m^{-2} solution mass flux.

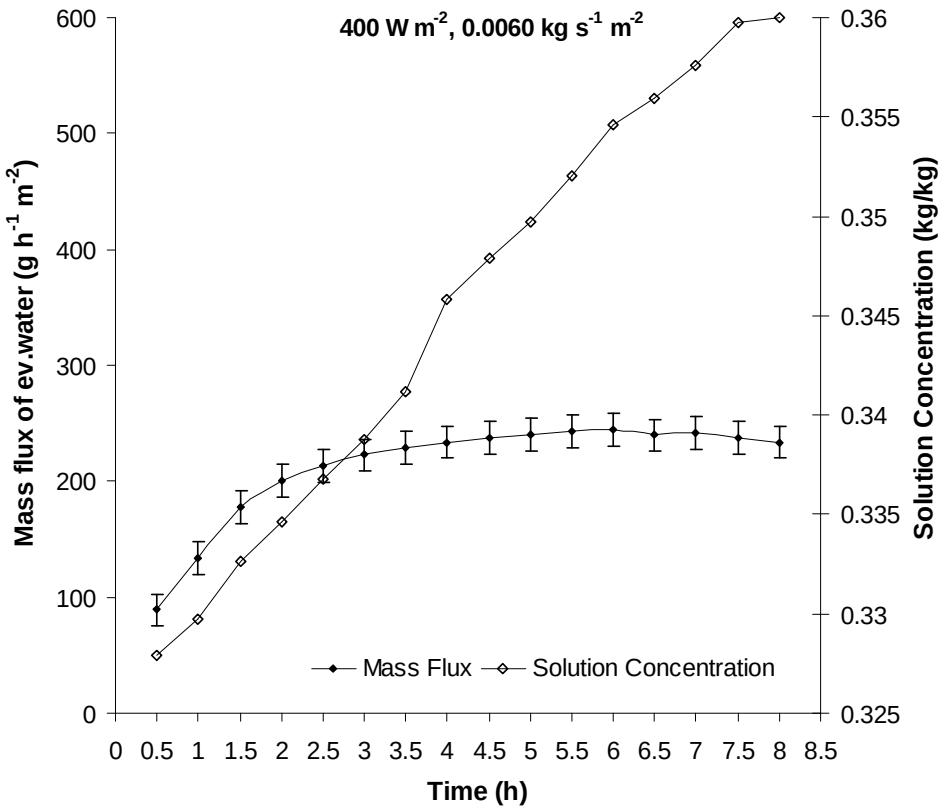

Fig. 4.13: Mass flux of water evaporation and solution concentration against time at 400 W m^{-2} irradiance and 0.0060 kg s^{-1} m^{-2} solution mass flux.

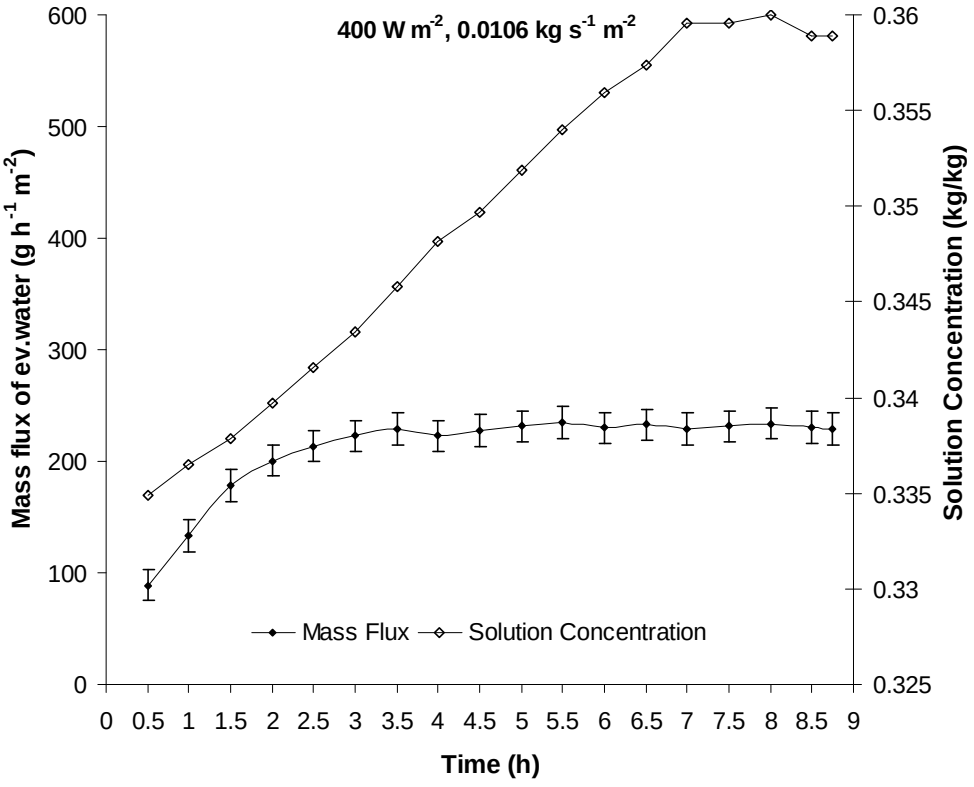

Fig. 4.14: Mass flux of water evaporation and solution concentration against time at 400 W m^{-2} irradiance and 0.0106 kg s^{-1} m^{-2} solution mass flux.

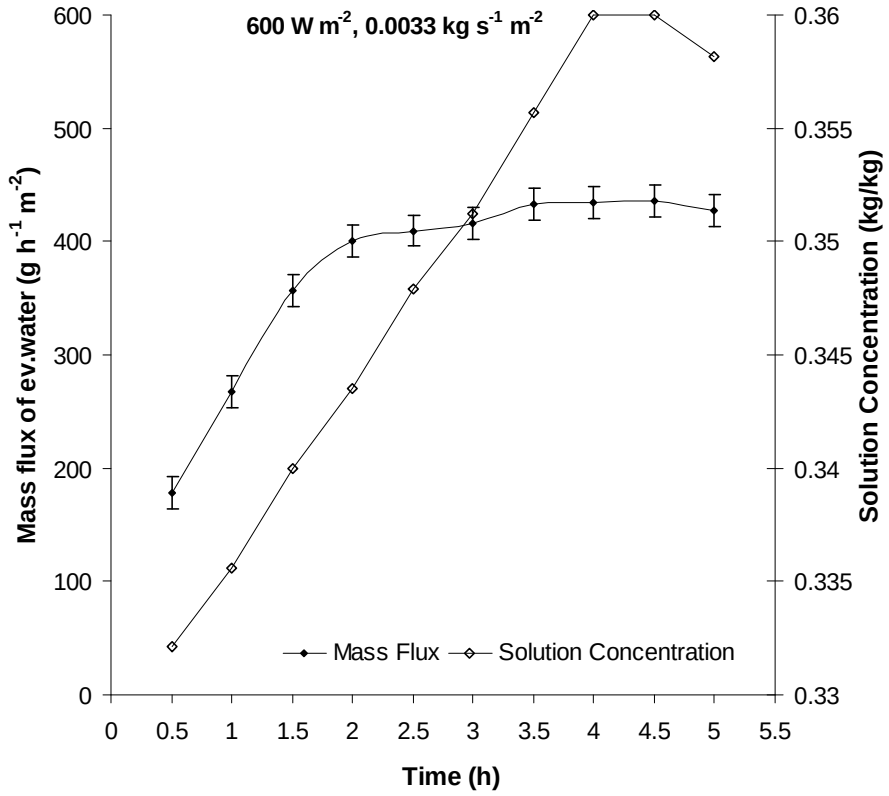

Fig. 4.15: Mass flux of water evaporation and solution concentration against time at 600 W m^{-2} irradiance and 0.0033 kg s^{-1} m^{-2} solution mass flux.

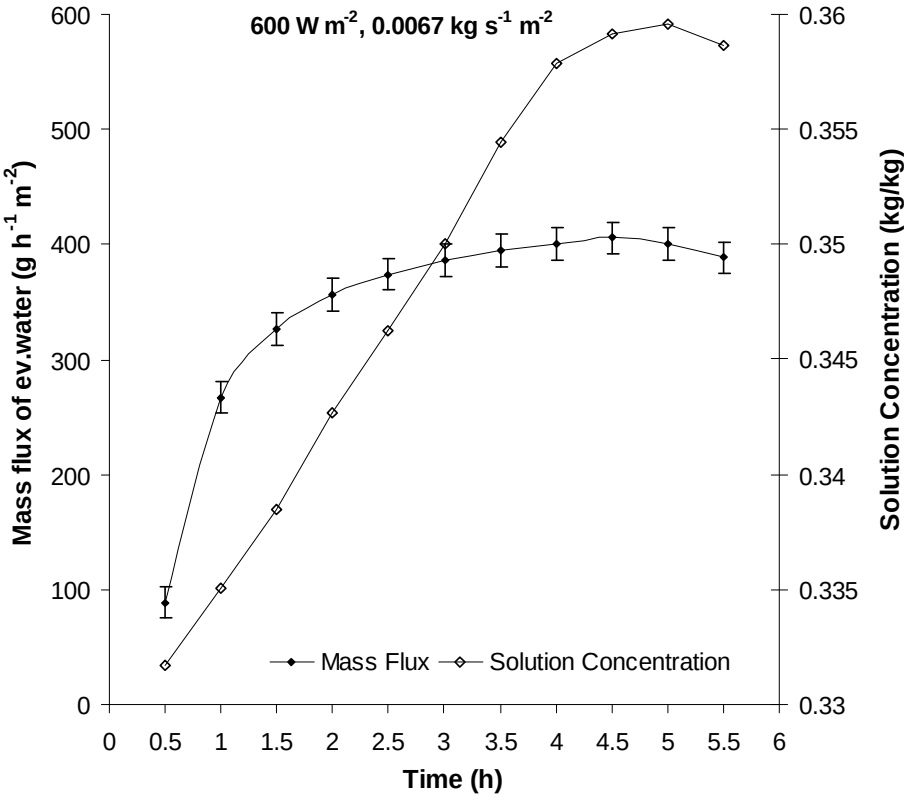

Fig. 4.16: Mass flux of water evaporation and solution concentration against time at 600 W m^{-2} irradiance and 0.0067 kg s^{-1} m^{-2} solution mass flux.

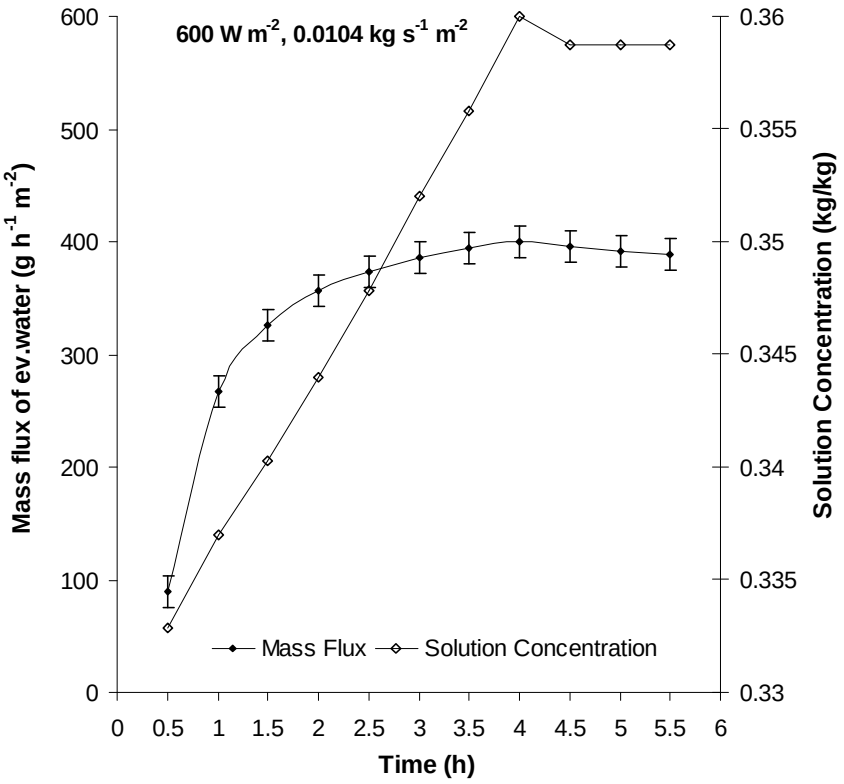

Fig. 4.17: Mass flux of water evaporation and solution concentration against time at 600 W m^{-2} irradiance and 0.0104 kg s^{-1} m^{-2} solution mass flux.

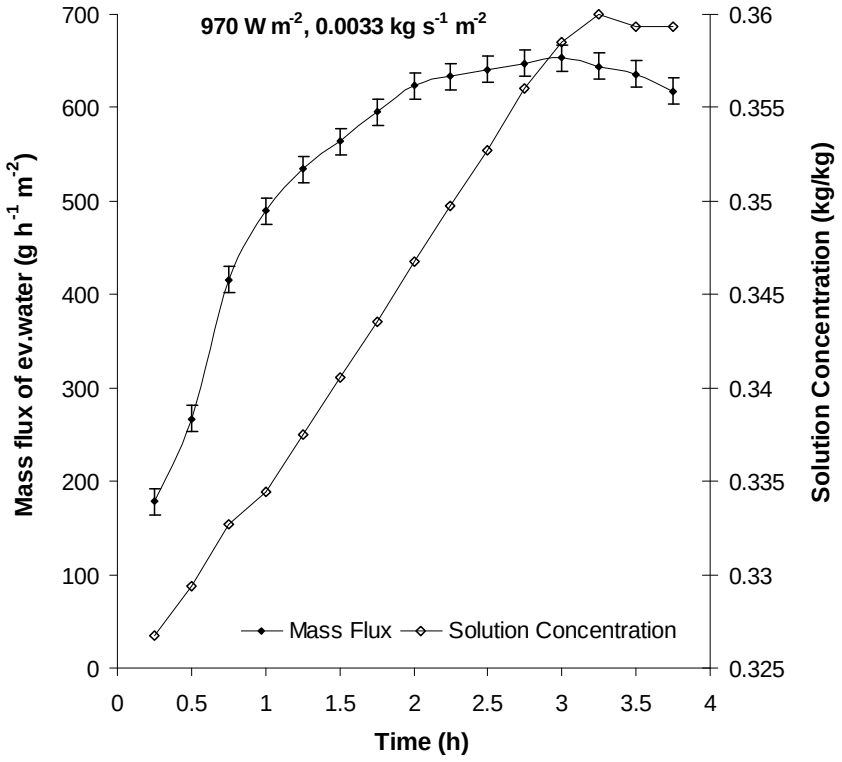

Fig. 4.18: Mass flux of water evaporation and solution concentration against time at 970 W m^{-2} irradiance and 0.0033 kg s^{-1} m^{-2} solution mass flux.

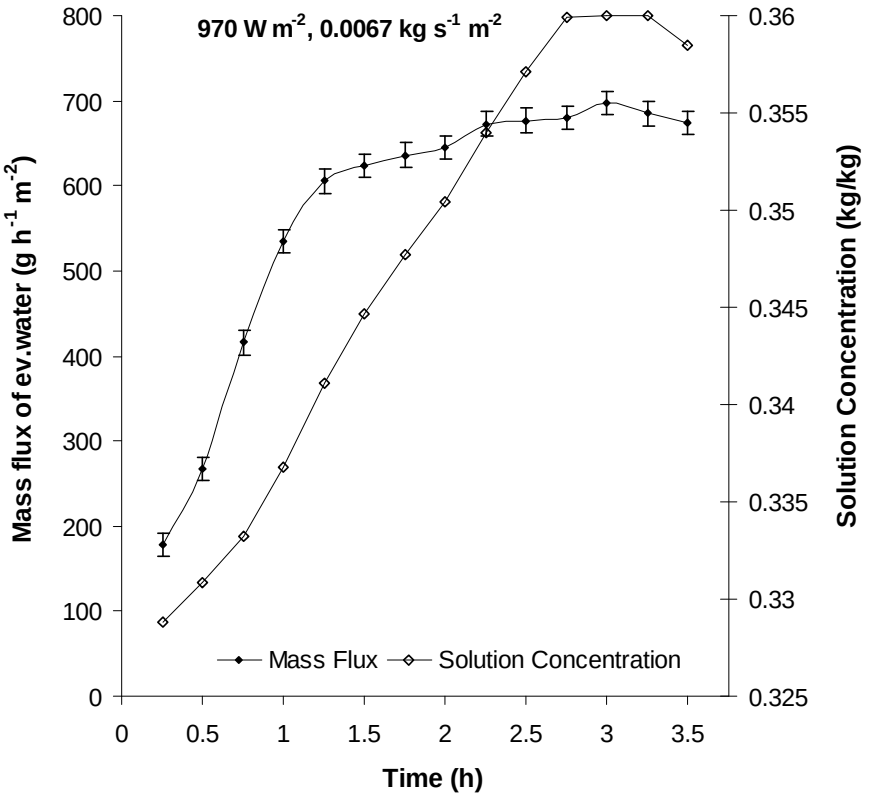

Fig. 4.19: Mass flux of water evaporation and solution concentration against time at 970 W m^{-2} irradiance and 0.0067 kg s^{-1} m^{-2} solution mass flux.

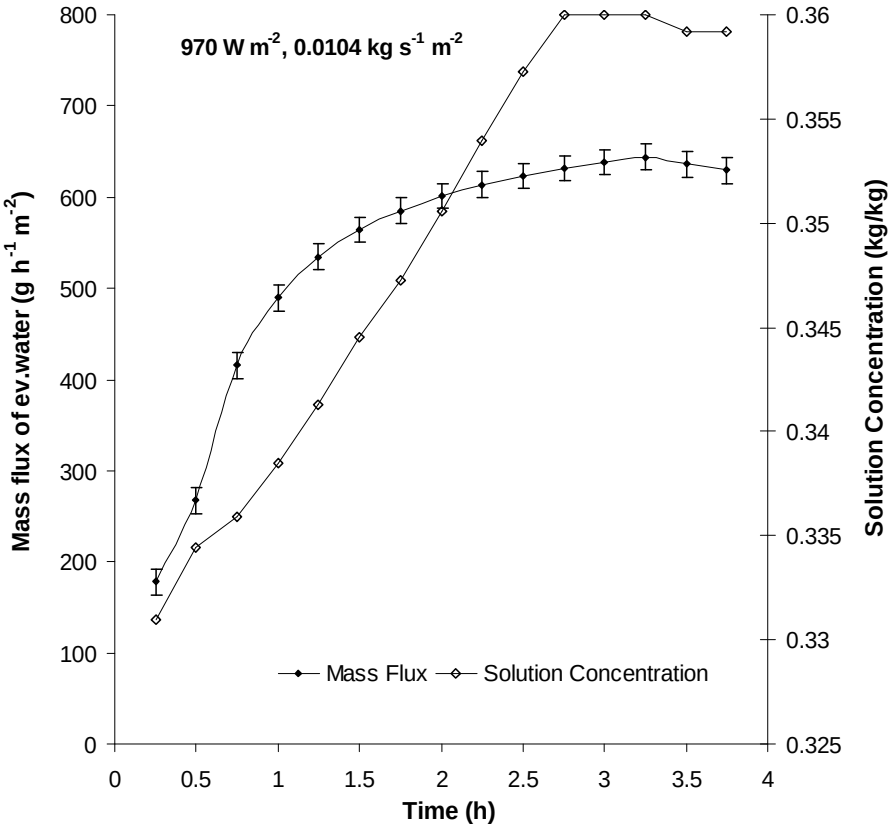

Fig. 4.20: Mass flux of water evaporation and solution concentration against time at 970 W m^{-2} irradiance and 0.0104 kg s^{-1} m^{-2} solution mass flux.

4.5.2 Comparison with model

The developed model with the new heat and mass transfer correlations managed to predict the mass flux of evaporation with a 37 percent average error when compared to the experimental values. However the model predicts the mass flux of water evaporation occurring at the regenerator considering that the whole surface area of the regenerator is wetted and thus effective. That was not the case with all the experiments. The effective area of evaporation was smaller due to bad wetting, salt deposition and solution flow patterns. To account for these uncertainties, the model deviations were calculated and then the average deviation for given irradiance and solution mass flow was used as a constant to correct the predicted values resulting in decreasing the average percent error down to 5 (see Table 4.5). The corrected predicted values of the mass flux of water evaporation along with the experimental values against time are illustrated in Figures 4.21 – 4.24. It is to be noted that the predicted values of total mass flux of water evaporation were calculated based on the average mass flow of water evaporation at the inlet and at the outlet of the regenerator.

Table 4.5: Average model deviation for the mass flux of evaporated water.

Constants				
M_s^o \ I_{tot}	400	600	970	760
0.0021	0.94	0.82	0.79	0.83
0.0041	0.63	0.76	0.72	0.75
0.0065	0.67	0.7	0.68	0.66

4.6 Conclusion

The experimental findings showed that the highest evaporation rate was observed at the highest irradiance level (970W/m^2) regardless the solution mass flow (see Fig 4.25). Increasing solution mass flow did not necessarily cause increasing mass flux of water evaporation. This may be attributed to the fact that flow patterns were observed on the surface of the regenerator which resulted in smaller residence times and hence smaller evaporation rates. The average maximum effectiveness achieved by the regenerator, when conducting experiments with concentrated solutions of $MgCl_2$ (29-36% kg of solute / kg of solution), was 46% while for more dilute solutions (15.8- 17.5% kg of solute / kg of solution) and pure water it was 68%. The presented analytical model with the new heat and mass transfer correlations will be used to predict the mass flux of water evaporation, as part of the whole system model developed in Chapter 6.

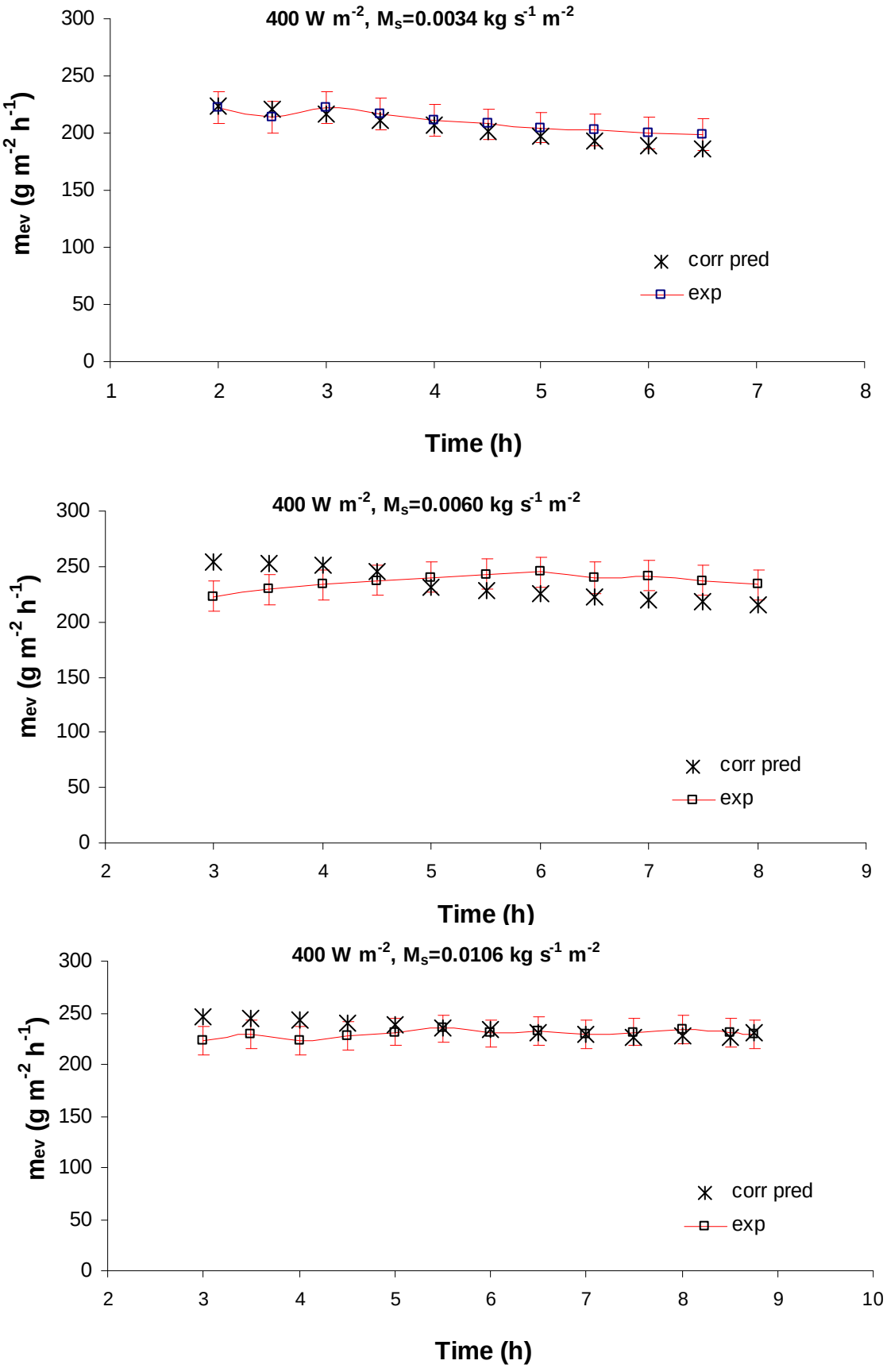

Fig. 4.21: Experimental vs. predicted mass flux of water evaporation against time at 400 W m^{-2} irradiance and 0.0034, 0.0060, 0.0106 kg s^{-1} m^{-2} solution mass flow.

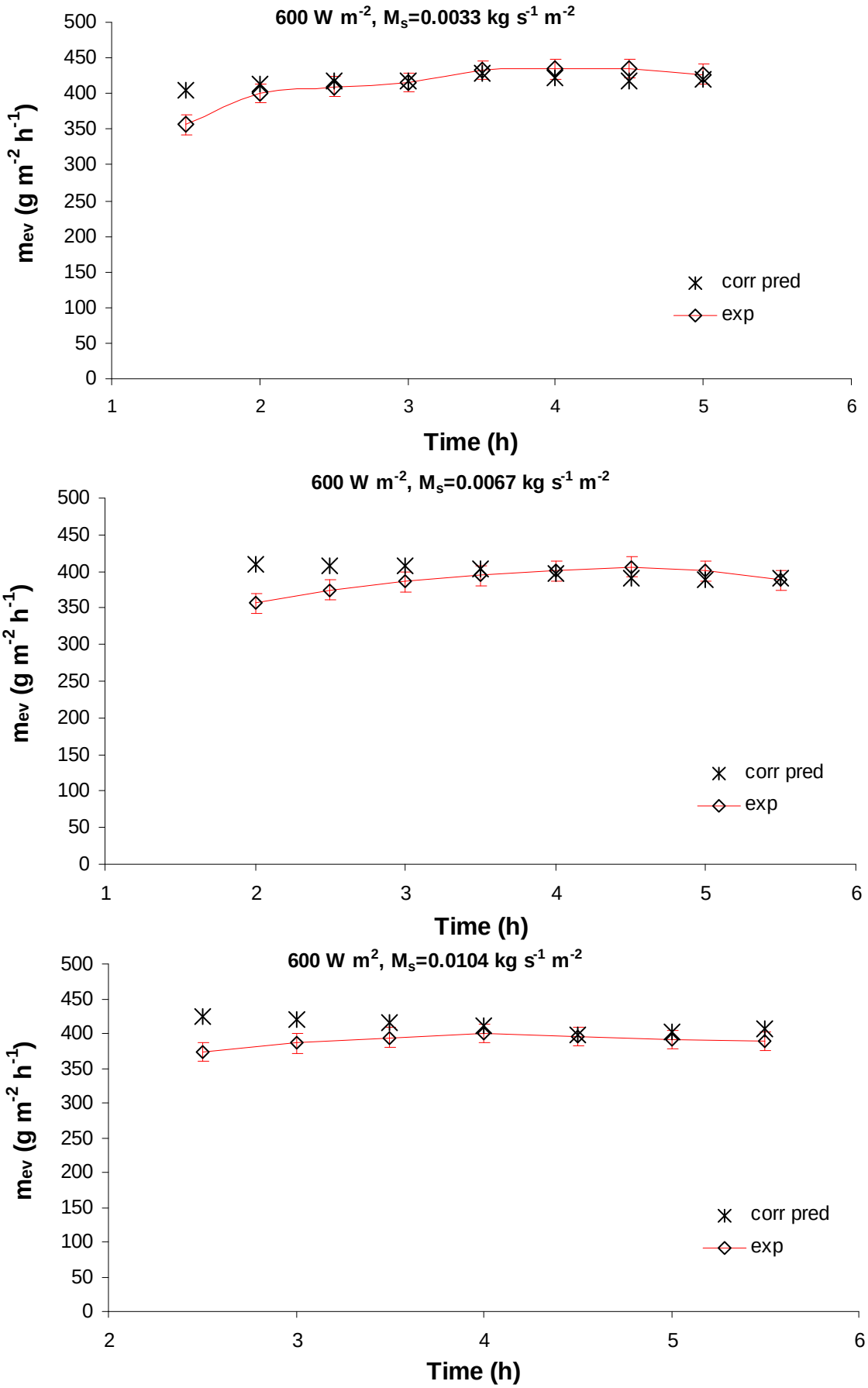

Fig. 4.22: Experimental vs. predicted mass flux of water evaporation against time at 600 W m^{-2} irradiance and 0.0033, 0.0067, 0.0104 kg s^{-1} m^{-2} solution mass flow.

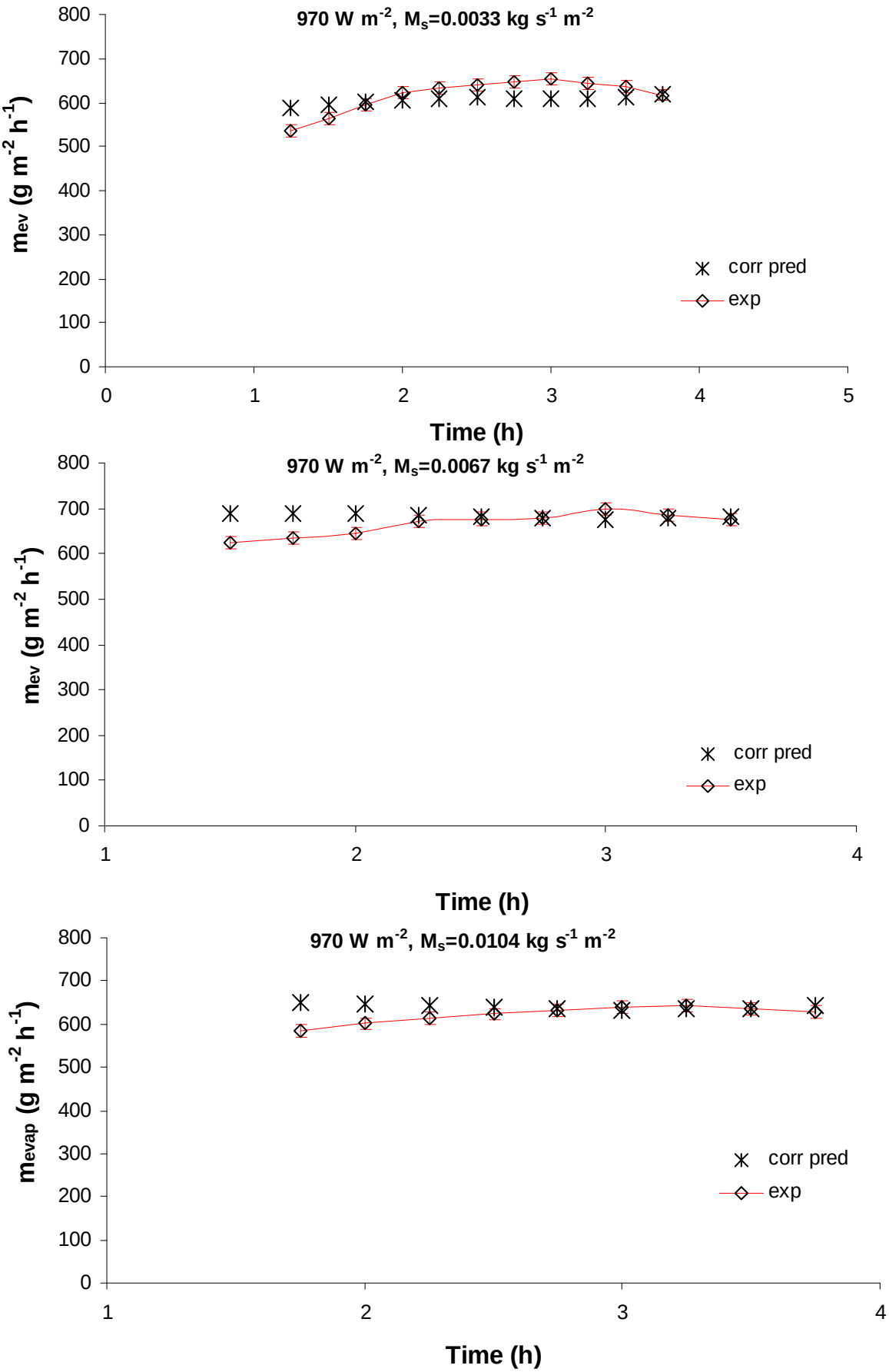

Fig. 4.23: Experimental vs. predicted mass flux of water evaporation against time at 970 W m^{-2} irradiance and 0.0033, 0.0067, 0.0104 kg s^{-1} m^{-2} solution mass flow.

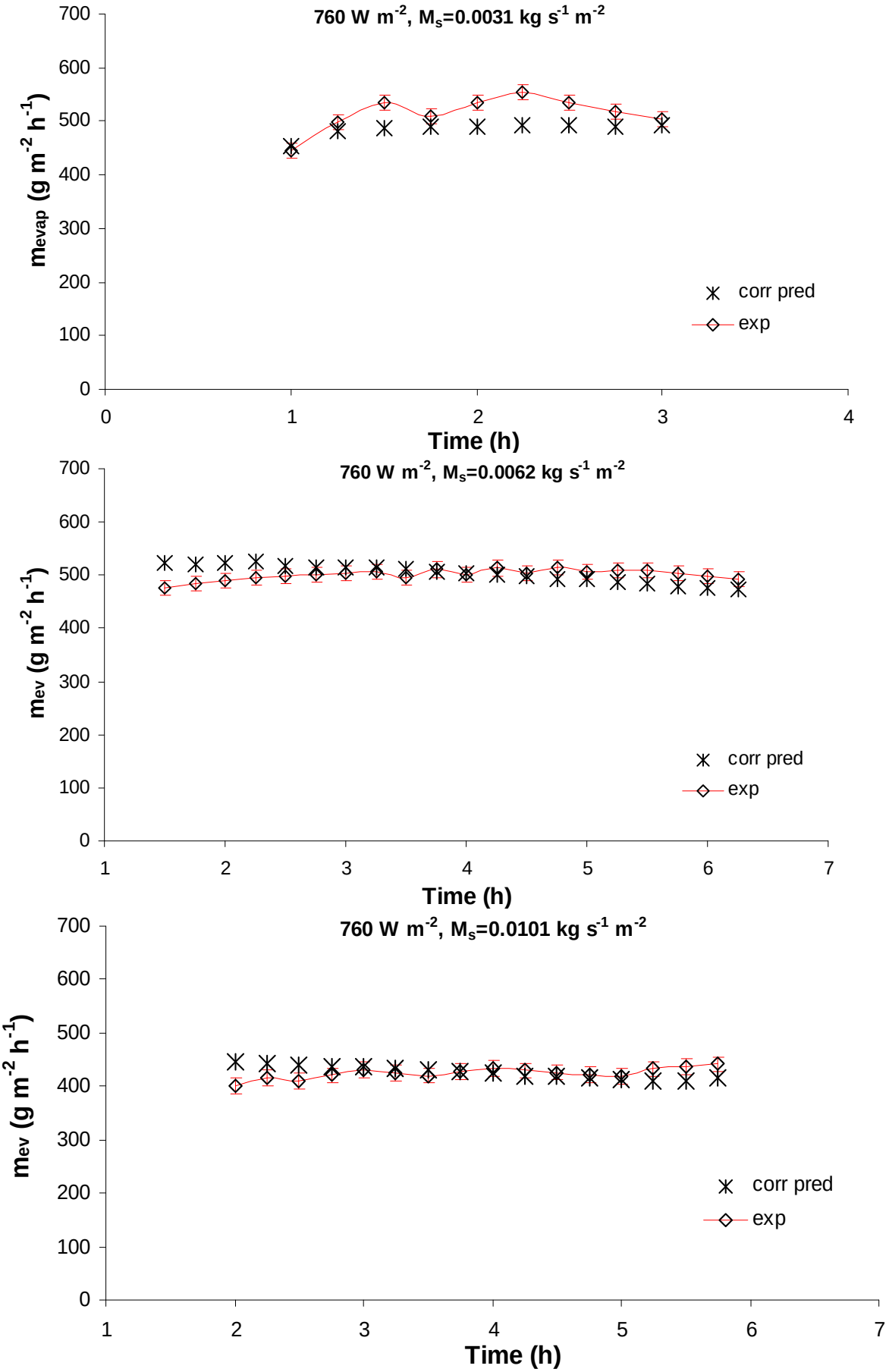

Fig. 4.24: Experimental vs. predicted mass flux of water evaporation against time at 760 W m^{-2} irradiance and 0.0031, 0.0062, 0.0101 kg s^{-1} m^{-2} solution mass flow.

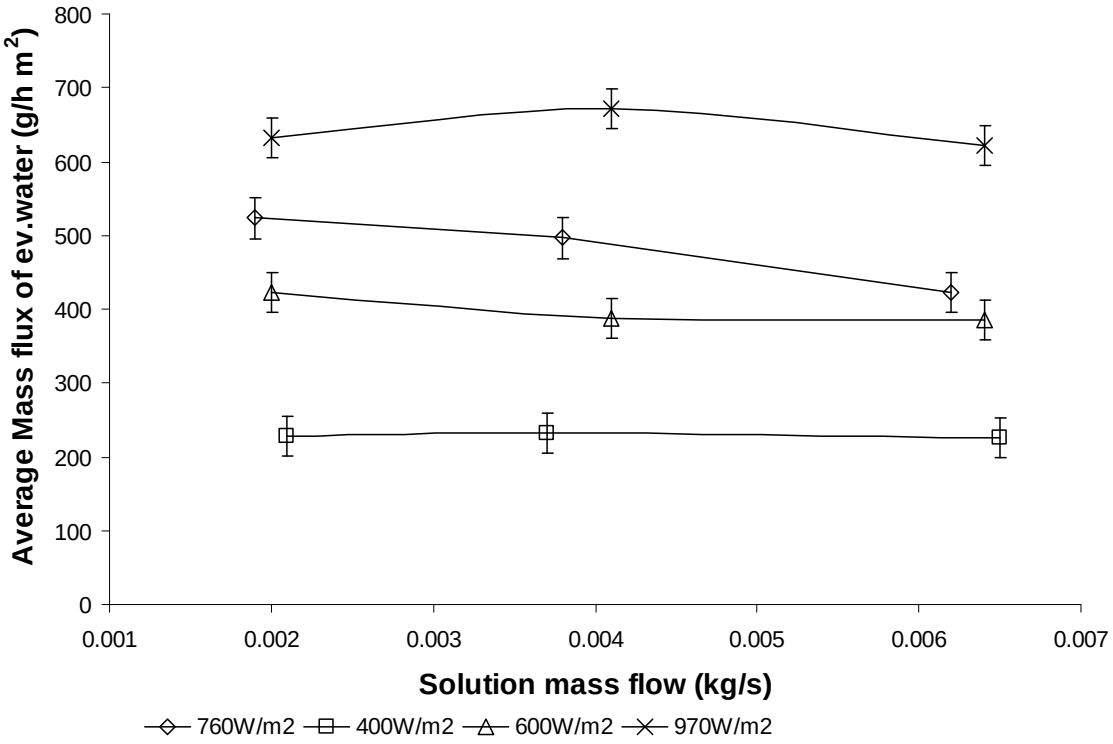

Fig. 4.25: Average Mass flux of water evaporation against solution mass flow at four irradiance levels: 400, 600, 760 and 970 W/m^2.

CHAPTER 5. DESICCATOR

5.1 Introduction

This Chapter is about the development of the desiccator which, like the regenerator and the evaporator, is one of the main components of the liquid desiccant cooling system. It is used to reduce the humidity of the atmospheric air and thus boost the cooling effect of the evaporator at the inlet to the greenhouse. In the desiccator, moisture is removed from the air while heat is removed from the liquid by means of an embedded heat exchanger. This is essentially the opposite of the regeneration process described in the last chapter, in which heat is added to the liquid causing it to release moisture to the air.

The driving force for desiccation is the vapour pressure gradient at the surface of the solution. Here, the partial vapour pressure of the air is higher than the partial vapour pressure of the strong liquid desiccant solution at equilibrium. Consequently, this results in the absorption of water vapour by the solution. The liquid desiccant cooling systems utilise porous structures where the desiccation process takes place when the air comes in contact with the liquid sorbent solution. The main objective in the design of these structures, known as desiccators or dehumidifiers, is to achieve high wetted surface area per volume and thus enhance water vapour absorption rate. It is essential to achieve high water vapour absorption rates because this corresponds to lower air wet bulb temperatures at the outlet and thus better cooling.

The performance of the desiccators limits the whole system's performance; hence predicting the water vapour absorption rate under different conditions (air and solution mass flows, air and solution temperatures, solution concentrations) is imperative when designing such a system. In this study, an extensive literature review of desiccator technology was carried out focusing on cross flow desiccators with structured packing. Based on the findings, a cross-flow desiccator with internal cooling was designed and constructed in lab. Its performance was investigated under various inlet conditions and the experimental results were compared to predicted ones obtained from a finite element model developed here.

5.2 Previous work on Liquid Desiccant Heat and Mass Exchangers (desiccators)

The devices used as heat and mass exchangers in liquid desiccant cooling systems do not differ fundamentally from those used by chemical engineers for gas-liquid operations. Heat and mass transfer take place simultaneously in such operations. For example, wetted-wall towers have been used industrially as absorbers for hydrochloric acid. In this case absorption is accompanied by a large production of heat (Treybal, 1980). Ideally, the liquid desiccant heat and mass exchanger (also known from literature as absorber or dehumidifier or desiccator) used for cooling should be able to dehumidify the ambient air to a desirable point without increasing the temperature of the air, with zero pressure drop through the desiccator and zero carryover of the liquid desiccant in the process air stream. Engineers have put effort in designing a desiccator that could meet these standards. Thus far, various designs have been presented and tested by researchers. These can be mainly categorised into three groups that have been widely investigated in the literature (Fig. 5.1) :

a) spray towers and spray chambers where the liquid desiccant is sprayed on coils or in a cross flow plate heat exchanger or in heat pipes.
b) packed towers or columns subdivided based on the packing material in:
    i) random packing (Berl and Intalox saddles, Lessing rings, Raschig rings, etc.)
    ii) regular or structured packing (cross corrugated cellulose sheets, cross corrugated PVC sheets, wood grids, double spiral rings, etc.)
c) wetted–wall towers or columns where the liquid flows over vertical surfaces(tubes or plates)

Further, the desiccators can be categorised in adiabatic and non adiabatic (internally cooled desiccators).

Historically, research on desiccators has focused on modelling the heat and mass transfer processes taking place inside the desiccators leading to various theoretical representations e.g. complicated finite difference models, effectiveness-NTU models, complicated analytical expressions and simplified models. Additionally, experimental studies have been undertaken by researchers in order to assess the performance of the different types of desiccators operating under various conditions and eventually to find the optimum operation. These studies also lead to empirical expressions of the dehumidification effectiveness. Various liquid desiccants i.e. LiCl, LiBr, $CaCl_2$, CELD (50% $CaCl_2$, 50% LiCl), monoethylene and triethylene glycol, have been used in these experimental or theoretical studies.

Among the first few researchers who investigated the heat and mass transfer phenomena taking place in a direct contact absorber with a counter flow configuration was Olander (1960). He presented a finite difference model applicable to systems other than air-water which was solved numerically.

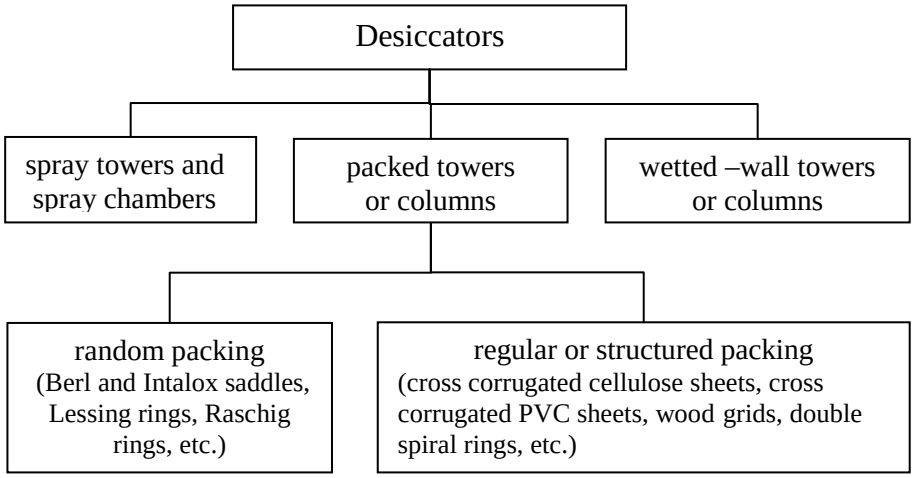

Fig. 5.1: Tree diagram showing the different types of desiccators as categorised in the literature.

Later, Factor and Grossman (1980) carried out experiments with a packed column desiccator filled with Intalox saddles using monoethylene glycol and lithium bromide as liquid desiccants. They validated their experimental results against predicted ones obtained by a theoretical numerical model (counter flow configuration) which was based on Olander's early work (1961). The LiBr results had very good agreement with the experimental ones; the average percent error was less than 8%. Longo and Gasparella (2005) investigated the performance of a packed column with random packing working as dehumidifier/regenerator using LiCl, LiBr and potassium formate. The differential model presented regarded counter flow configuration too and it was solved by an iterative procedure. The experimental dehumidification efficiency reported ranged between 30-90% approximately and the predicted values of efficiency had 8.8% mean absolute deviation when compared to the experimental results. The studies of Chengqin and his associates (Chengqin *et al.*, 2005, Chengqin *et al.*, 2006) also dealt with counter flow configurations. In the first study, Chengqin *et al.* developed a numerical model which was used to create characteristic process curves and numerical simulations were carried out under practical conditions using $CaCl_2$ as the liquid desiccant. In the second study, a one-dimensional

differential model was presented which was solved numerically. By assuming that the equilibrium humidity ratio is a linear function of solution temperature an analytical solution was obtained. The comparison between the two models, numerical and analytical, showed good agreement. LiCl, LiBr and $CaCl_2$ were used as desiccants in this analysis.

Rahamah *et al.* (1998) presented a numerical solution of a finite difference theoretical model for parallel flow configurations. The predicted results were compared with experimental ones found in the literature and they showed good agreement. The effect of various operating conditions on the performance of the desiccator was also investigated and found that low flow rates produced better dehumidification, increasing the channel height resulted in better cooling and increasing the liquid desiccant's concentration enhanced the dehumidification process. Chen *et al*. (2006) found an analytical solution of a finite difference model for parallel and counter flow configurations suitable for packed columns. There was good accuracy between the analytical solution and the experimental data. Ren (2008) developed an effectiveness-NTU double film model for parallel and counter-flow configurations applicable to packed column desiccators. He found an analytical solution by rearranging the original differential equations and making the coupled equations linear. LiCl, LiBr and $CaCl_2$ were used as liquid desiccants in the analysis so as to compare analytical and numerical results. The comparison showed good agreement.

A new approach in heat and mass transfer analysis of desiccators was given by Khan and co authors (Khan, 1998, Khan and Ball, 1992). He first used the effectiveness-NTU method to develop a differential model, applicable to internally cooled desiccators, that was solved numerically. A performance model was derived based on this method and a parametric analysis was carried out to show that the performance of the desiccator was strongly affected by the water-air mass flow rate ratio, the water inlet temperature and the desiccant solution operating concentration. Saman and Alizadeh (2001) extended Khan's model to cross flow type plate heat exchangers used as desiccators. The differential element model was solved numerically. Calcium chloride was used as liquid desiccant in this analysis and the performance of the desiccator was predicted under various inlet conditions. It was concluded that its performance strongly depends on the size of the desiccator, the liquid desiccant's concentration and the air flow ratio. Furthermore, the theoretical model was validated by comparison with experimental results (Saman and Alizadeh, 2002). Liu *et al.* (2007b) based on Khan's approach developed a two

dimensional simplified model called Le-NTU model for cross flow configurations. A packed column with structured packing, CELDEK®, and LiBr as liquid desiccant were used to carry out experiments in order to validate the model. Lewis number (Le) and NTU were input values, usually Le=1 and NTU is determined experimentally. The predicted and experimental values of enthalpy and dehumidification effectiveness agreed well. Liu and his associates presented analytical solutions for parallel, counter and cross flow configurations (Liu *et al.*, 2007a). The analytical solutions compared well with the experimental results found in literature. Yin and Zhang (2008), building on the work of Liu *et al*, developed a new method called h_D-Le separative evaluation method that uses experimental data to calculate heat and mass transfer coefficients and mass transfer correlations in a packed structured column with CELDEK®. LiCl was used as liquid desiccant in this analysis. The comparison of the experimental and calculated values of RH, air temperature and solution temperature change showed less than 12% difference.

The study of Ali *et al.* (2004) is worth noting. They investigated theoretically the heat and mass transfer enhancement in a cross flow configuration when ultrafine Cu particles are added to the liquid desiccant. It was predicted that an increase of Cu volume fraction would result in higher dehumidification rate and cooling.

Also noteworthy is the numerical study by Yoon *et al.* (2005) who developed a numerical model of a water-cooled vertical plate absorber using LiBr (cross flow configuration). The model can predict temperature and concentration profiles, local and total heat and mass fluxes, heat and mass transfer coefficients.

These complicated numerical models and their analytical solutions drove Gandhidasan (2004) to develop a simplified analytical model for predicting the mass rate of absorbed water, solution temperature and air temperature at the outlet. The comparison of the predicted values with published data showed good agreement with less than 10.5% error.

Several researchers (Chung *et al.*, 1993, Gommed and Grossman, 2007) have carried out experimental studies investigating the performance of packed columns, or the performance of a complete liquid desiccant cooling system whose performance is evaluated based on the dehumidification and enthalpy effectiveness of the desiccator. Chung *et al.* (1993) investigated the performance of a packed column filled with polypropylene flexi rings, using LiCl as the liquid desiccant, under various operating conditions. The measured

efficiency ranged between 50-71.6%. The efficiency increased with decreasing air flow rate or with lowering the solution temperature. It was also concluded that flexi rings, are better contacting equipment compared to Raschig rings, Pall rings and Berl saddles. Gommed and Grosman (2007) investigated the seasonal performance of solar liquid desiccant cooling system for the purpose of cooling a group of offices.

Several experimental studies are found in literature where empirical correlations of heat and mass transfer coefficients and of dehumidification effectiveness were derived based on the experimental data. Ullah *et al.* (1988) performed a theoretical study that provides the theoretical background for deriving empirical correlations of the dehumidification effectiveness that depend on the desiccator geometry and the liquid desiccant. Based on the work of Ullah *et al.*, Chung (1994) developed a correlation of dehumidification effectiveness for different random packings and desiccant solutions. The average error between predicted and experimental values was 7%. Chung *et al.* (1995) carried out an experimental study on packed columns filled with polypropylene Flexi rings and ceramic Intalox saddles. Correlations of heat and mass transfer coefficients were derived based on the experimental data. Potnis and Lenz (1996) investigated experimentally packed columns with random and structured packings (CELdek®) and developed mass transfer correlations. Chung and Ghosh (1996) compared the efficiency of random with structured packings (cross corrugated cellulose sheets and cross corrugated PVC sheets) and presented correlations of heat and mass transfer based on dimensionless groups with an accuracy of ±10%. Based on the dehumidification effectiveness approach of Ullah *et al.* (1988) and Chung (1994), Liu *et al.* (2006a) proposed a new correlation for structured packings (CELdek®) which agreed well with the experimental results. Liu *et al.* (2006b) also proposed new forms of empirical correlations of enthalpy and dehumidification effectiveness. An excellent source that compiles experimental data and empirical correlations of mass transfer coefficients and dehumidification effectiveness is Jain and Bansal's (2007) work. Moon *et al.* (2009) developed a new correlation of dehumidification effectiveness applicable to packed columns with cross corrugated cellulose sheets. The accuracy of the new correlation is ±10%. A brief summary of the studies published since early 1960's can be seen in Table 5.1.

It can be concluded that, among the various theoretical heat and mass transfer models, the finite difference model gives more accurate performance predictions based on fundamental

equations. However, these models usually need an iterative procedure to solve them or a numerical solution if the analysis becomes too complex. The analytical solutions that researchers have recently developed are still quite complex. The effectiveness-NTU methodology is less complicated, but a short iteration procedure is required in order to find the solution. The empirical correlations of the dehumidification effectiveness, the mass transfer and the heat transfer coefficient derived from experimental data have only restricted validity to the type of desiccator, liquid desiccant and operating conditions. From Table 5.1 it is seen that $MgCl_2$ has never been used as a liquid desiccant in either theoretical or experimental studies; the use of this desiccant is one of the novel aspects of this thesis.

Based on the published literature reviewed before, packed columns dominate over the other configurations since they provide high surface-volume ratio and thus achieve better dehumidification effectiveness. Internally cooled desiccators remove the heat of absorption and hence the process air temperature is not increased. That makes them comparatively advantageous to desiccators without internal cooling. In this work the desiccator was designed as an internally cooled cross flow configuration.

Table 5.1: Summary of published work on desiccators

Year	**Authors**	**Type of Desiccator**	**Desiccant**	**Experimental/ Theoretical**
1961	Olander	any	any	Theory
1980	Factor and Grossman	packed column/ random packing	Monoethylene Glycol, LiBr	Theory and Experiment
1988	Ullah *et al*	packed column/ random packing	$CaCl_2$	Theory
1993	Chung *et al*	packed column/ random packing	LiCl	Experiment
1994	Chung	packed column/ random packing	LiCl, Triethylene Glycol	Theory and Experiment
1995	Chung *et al*	packed column/ random and structured packing	Triethylene Glycol	Theory and Experiment

(Table 5.1 continued)

1996	Potnis and Lenz	packed column/ random and structured packing	LiBr	Theory and Experiment
1996	Chung and Ghosh	packed column/ random and structured packing	LiCl	Theory and Experiment
1998	Rahamah *et al*	wetted–wall column	any	Theory
1998	Khan	spray tower	any	Theory
2000	Jain *et al*	wetted–wall column	LiBr	Theory and Experiment
2001	Saman and Alizadeh	spray chamber	$CaCl_2$	Theory
2002	Saman and Alizadeh	spray chamber	$CaCl_2$	Experiment and Theory
2002	Al-Farayedhi *et al*	packed column/ structured packing	$CaCl_2$, LiCl, CELD (50% $CaCl_2$, 50% LiCl)	Theory
2004	Gandhidasan	packed column/any type of packing	LiCl	Theory
2004	Ali *et al*	any (with a cross flow configuration)	any	Theory
2005	Chengqin *et al*	packed column/ any type (with a counter flow configuration)	$CaCl_2$	Theory
2005	Yoon *et al*	wetted–wall column	LiBr	Theory
2005	Longo and Gasparella	packed column/ random packing	LiCl, LiBr, KCOOH	Theory and Experiment
2006	Chengqin *et al*	packed column/ structured packing	LiCl, LiBr, $CaCl_2$	Theory
2006	Liu *et al*[a]	packed column/ structured packing	LiBr	Experiment
2006	Liu *et al*[b]	packed column/ structured packing	LiBr	Theory and Experiment
2006	Chen *et al*	packed column	LiCl	Theory
2007	Gommed and Grossman	packed column	LiCl	Experiment

(Table 5.1 continued)

2007	Jain and Bansal	packed column	LiCl, CaCl2, Triethylene Glycol	Theory
2007	Liu *et al*[a]	packed column/ structured packing	LiBr	Theory and Experiment
2007	Liu *et al*[b]	any	LiBr	Theory
2008	Ren	packed column	LiCl, LiBr, $CaCl_2$	Theory
2008	Yin and Zhang	packed column/ structured packing	LiCl	Theory and Experiment
2009	Moon *et al*	packed column/ structured packing	$CaCl_2$	Theory and Experiment

5.3 Theoretical Model

The model developed here is based on the works of Liu and his associates (Liu *et al.*, 2007a, Liu *et al.*, 2007b, Liu *et al.*, 2006a, Liu *et al.*, 2006b) and Khan (1998, , 1992). However, the present author has simplified the differential equations by making a number of assumptions and thus reduced them to algebraic form wherever this was possible. The model also uses predictive formulas of Nusselt and Sherwood numbers developed specifically for CELdek® packing material for calculating the heat and mass transfer coefficients h_c and h_D respectively. Based on the relevant inputs (temperature and relative humidity of the process air, the air mass flow rate and the solution mass flow rate, the solution concentration and temperature, the temperature and mass flow rate of cooling water at the inlet) the model predicts the mass flux of water absorption along with the properties of air, solution and water at the outlet.

5.3.1 Finite Volume Model for CELdek® packing

The CELdek® pad is divided into a finite number of control volumes called elements (see Fig 5.2). The set of governing equations presented below are applied for each element. For each element one-dimensional analysis was carried out, thus enabling us to simplify the governing differential equations and integrate. Specifically, the assumptions used in this model are the following:

1. The desiccator operates under steady state conditions and heat losses to the surroundings are negligible.
2. The properties of air change only in the *y* direction (see Fig 5.2).
3. The properties of the desiccant solution change only in the *x* direction (see Fig 5.2).
4. The specific heat of air and desiccant solution are considered constant inside the control volume.
5. The solution is perfectly mixed and uniformly distributed to each element. The same applies to the process air.

The partial vapour pressure of the air is higher than the partial vapour pressure of the liquid desiccant at its surface, thus mass transfer occurs. If we define as the wetted area of packing per volume ($m^2\ m^{-3}$) to be

$$\alpha_w = \frac{\alpha}{V} \tag{5.1}$$

where α is the wetted surface area and V is the volume

Then if we take a control volume (see Fig 5.2) the mass transfer equation can be defined as

$$\dot{m}_a \cdot d\omega_a = h_D \cdot \left(\omega_{Ts,sat} - \omega_a\right) \cdot \alpha_w \cdot \delta x \cdot \delta z \cdot dy \tag{5.2}$$

where h_D is the mass transfer coefficient, $\omega_{Ts,sat}$ is the absolute humidity of the air in equilibrium with the desiccant solution, ω_a is the absolute humidity of the air, δx and δz are the height and length of the control volume respectively.

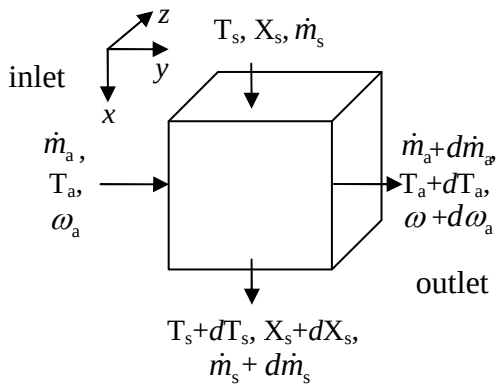

Fig. 5.2: Differential control volume.

if we integrate from state 1 (inlet) to state 2 (outlet) we arrive at

$$\dot{m}_a \cdot \int_1^2 d\omega_a = h_D \cdot \left(\omega_{Ts,sat} - \omega_a\right) \cdot \alpha_w \cdot \delta x \cdot \delta z \cdot \int_1^2 dy$$

or $\dot{m}_a \cdot \omega_a \Big|_1^2 = h_D \cdot \left(\omega_{Ts,sat} - \omega_a\right) \cdot \alpha_w \cdot \delta x \cdot \delta z \cdot \delta y$

or $\dot{m}_a \cdot \Delta\omega_{a,1\text{-}2} = h_D \cdot \left(\omega_{Ts,sat} - \omega_a\right) \cdot \alpha_w \cdot \delta x \cdot \delta z \cdot \delta y$ (5.3)

where δy is the width of the control volume

Heat transfer takes place between the air and the liquid desiccant surface. This can be mathematically expressed as

$$\dot{m}_a \cdot Cp_a \cdot dT_a = h_c \cdot \left(T_s - T_a\right) \cdot \alpha_w \cdot \delta x \cdot \delta z \cdot dy \quad (5.4)$$

where h_c is the heat transfer coefficient

In a similar way as before if we integrate we arrive at the following

$$\dot{m}_a \cdot \Delta T_{a,1\text{-}2} = h_c \cdot \left(T_s - T_a\right) \cdot \alpha_w \cdot \delta x \cdot \delta z \cdot \delta y \quad (5.5)$$

The enthalpy change of air can be defined from the enthalpy equation of moist air as

$$dh_a = Cp_a \cdot dT_a + h_{fg} \cdot d\omega_a \quad (5.6)$$

if we integrate it yields

$$\Delta h_{a,1\text{-}2} = Cp_a \cdot \Delta T_{a,1\text{-}2} + h_{fg} \cdot \Delta\omega_{a,1\text{-}2} \quad (5.7)$$

By substituting (5.3) and (5.5) in (5.7) we arrive at

$$\dot{m}_a \cdot \Delta h_{a,1\text{-}2} = h_c \cdot \left(T_s - T_a\right) \cdot \alpha_w \cdot \delta x \cdot \delta z \cdot \delta y + h_{fg} \cdot h_D \cdot \left(\omega_{Ts,sat} - \omega_a\right) \cdot \alpha_w \cdot \delta x \cdot \delta z \cdot \delta y \quad (5.8)$$

If we define the Lewis number as

$$Le = \frac{h_C}{h_D \cdot Cp_a \cdot \rho_a} \tag{5.9}$$

and the Number of Transfer Units (NTU) to be

$$NTU = \frac{h_D \cdot L \cdot W \cdot H \cdot \alpha_w \cdot \rho_a}{\dot{M}_a} \tag{5.10}$$

where L = 0.3 m, W = 0.1 m, H = 0.1 m for our experimental set up
then if we combine equations (5.8), (5.9) and (5.10) we arrive at the following equation

$$\Delta h_{a,1\text{-}2} = NTU \cdot Le \cdot \left[\left(h_{Ts,sat} - h_a \right) + h_{fg} \cdot \left(\frac{1}{Le} - 1 \right) \cdot \left(\omega_{Ts,sat} - \omega_a \right) \right] \cdot \frac{\delta y}{W} \tag{5.11}$$

The law of conservation of energy states (since there is no work generation, the potential and kinetic energy changes are zero and assuming there is no heat loss) that the total enthalpy change of air should be equal to the total enthalpy change of the desiccant solution and can be expressed as

$$\dot{m}_a \cdot dh_a = \dot{m}_s \cdot dh_s + d\dot{m}_s \cdot h_s \tag{5.12}$$

by integration we arrive at

$$\dot{m}_a \cdot \Delta h_{a,1\text{-}2} = \dot{m}_s \cdot \Delta h_{s,1\text{-}2} + h_s \cdot \Delta \dot{m}_{s,1\text{-}2} \tag{5.13}$$

The law of conservation of mass between the air and the solution for the control volume is

$$-\dot{m}_a \cdot \Delta \omega_{a,1\text{-}2} = \Delta \dot{m}_{s,1\text{-}2} \tag{5.14}$$

the enthalpy change of the desiccant solution is given by

$$dh_s = Cp_s \cdot dT_s \tag{5.15}$$

which becomes by integration

$$\Delta h_{s,1\text{-}2} = Cp_s \cdot \Delta T_{s,1\text{-}2} \tag{5.16}$$

If we substitute (5.11), (5.14) and (5.15) in (5.13) and if $h_s = Cp_s \cdot T_s$ (T_s at the inlet) then equation (5.13) yields

$$\Delta T_{s,1\text{-}2} = \frac{\dot{m}_a \cdot \left\{ NTU \cdot Le \cdot \left[\left(h_{Ts,sat} - h_a \right) + h_{fg} \cdot \left(\frac{1}{Le} - 1 \right) \cdot \left(\omega_{Ts,sat} - \omega_a \right) \right] \cdot \frac{\delta y}{W} \right\} - Cp_s \cdot T_s \cdot \dot{m}_a \cdot \Delta\omega_{a,1\text{-}2}}{Cp_s \cdot \dot{m}_s} \quad (5.17)$$

The law of conservation of mass for the solution states

$$d\left(\dot{m}_s \cdot X_s\right) = 0 \Rightarrow d\dot{m}_s \cdot X_s + dX_s \cdot \dot{m}_s = 0 \quad (5.18)$$

The change in the water content of the air should be equal to the change in mass of the desiccant solution

$$-\dot{m}_a \cdot d\omega_a = d\dot{m}_s \quad (5.19)$$

if we combine (5.18) and (5.19)

$$-\dot{m}_a \cdot d\omega_a \cdot X_s + dX_s \cdot \dot{m}_s = 0 \quad (5.20)$$

if we separate the variables and integrate from state 1 to state 2 we arrive at the following

$$\dot{m}_s \cdot \int_1^2 \frac{1}{X_s} \cdot dX_s = \dot{m}_a \cdot \int_1^2 d\omega_a \Rightarrow \dot{m}_s \cdot \ln X_s \Big|_1^2 = \dot{m}_a \cdot \omega_a \Big|_1^2$$

which yields $X_{s,2} = X_{s,1} \cdot e^{\frac{\dot{m}_a}{\dot{m}_s}\Delta\omega_{a,1\text{-}2}}$ (5.21)

hence $\Delta X_{s,1\text{-}2} = X_{s,1} \cdot \left(e^{\frac{\dot{m}_a}{\dot{m}_s}\Delta\omega_{a,1\text{-}2}} - 1 \right)$ (5.22)

Equations (5.17) and (5.11) are equivalent to the equations presented by Liu *et al.* (2007b). This physical model describes the process of heat and mass transfer that takes place in the packing material of a cross flow desiccator. The experimental cross flow desiccator constructed in lab utilises CELdek® (7090-15) as packing material. Therefore, suitable predictive formulas of Nusselt and Sherwood numbers are needed in order to be used for calculating the heat and mass transfer coefficients h_c and h_D respectively. The Nusselt and

Sherwood formulas found in the literature were developed based on the special geometrical characteristics of CELdek® in a similar dehumidifying process using LiCl as liquid desiccant (Chung *et al.*, 1996). In this work the Nusselt formula was used as originally presented in reference (Chung *et al.*, 1996) and the Sherwood formula was slightly modified.

$$Nu = 2.78 \cdot 10^{-6} \cdot \mathrm{Pr}^{1/3} \cdot \mathrm{Re}^{1.6} \cdot (1 - X_s)^{1.8} \cdot \left(\frac{\dot{m}_s}{\dot{m}_a} \right)^{0.4} \tag{5.23}$$

$$Sh = 2.25 \cdot 10^{-5} \cdot \mathrm{Sc}^{1/3} \cdot \mathrm{Re} \cdot (1 - X_s)^{-0.75} \cdot \left(\frac{\dot{m}_s}{\dot{m}_a} \right)^{0.1} \tag{5.24}$$

Thus the heat and mass transfer coefficients can be calculated by the following formulas:

$$h_D = \frac{Sh \cdot D_{w\text{-}a}}{L_c} \tag{5.25}$$

where $D_{w\text{-}a}$ is the binary diffusion coefficient of water vapour in air and L_c is the characteristic length

$$h_c = \frac{Nu \cdot k_a}{L_c} \tag{5.26}$$

where k_a is the thermal conductivity of air.

5.3.2 Finite Volume Model for cooling tubes

Besides CELdek® the desiccator has embedded cooling tubes (see Fig.5.3a and 5.3b). The heat and mass transfer occurring at the tubes is more complicated because of the water flow inside the tubes. Therefore a different model was developed assuming that the properties of water change only in the z direction.

Equations (5.3), (5.4), (5.5) and (5.22) are still valid for the following analysis (parameterised accordingly where needed).

The mass transfer coefficient is now expressed (in kg m^{-2} s^{-1}) as

$$h_{\mathrm{D}} = \left(\frac{6 \cdot D_{\mathrm{w-a}} \cdot \dot{m}'_{\mathrm{s}}}{\pi \cdot \rho_{\mathrm{s}} \cdot \delta \cdot l} \right)^{1/2} \cdot \rho_{\mathrm{a}} \tag{5.27}$$

(Treybal, 1980)

where $D_{\mathrm{w-a}}$ is the mass diffusivity of water vapour in air, $\dot{m}'_{\mathrm{s}}$ is the solution mass flow rate per unit width, ρ_{s} is the solution's density, *l* is the length and δ is the solution film thickness given by

$$\delta = \left(\frac{3 \cdot \mu_{\mathrm{s}} \cdot \dot{m}'_{\mathrm{s}}}{\rho_{\mathrm{s}}^2 \cdot g} \right)^{1/3} \tag{5.28}$$

(Treybal, 1980)

where μ_{s} is the dynamic viscosity of the solution and g is the gravitational acceleration.

The energy balance equation of the control volume is now:

$$\dot{m}_{\mathrm{a}} \cdot dh_{\mathrm{a}} + \dot{m}_{\mathrm{s}} \cdot dh_{\mathrm{s}} + d\dot{m}_{\mathrm{s}} \cdot h_{\mathrm{s}} + \dot{m}_{\mathrm{w}} \cdot dh_{\mathrm{w}} = 0 \tag{5.29}$$

where $\dot{m}_{\mathrm{w}}$ is the water mass flow in a tube and h_{w} is the specific enthalpy of water.

If we integrate (5.29) then

$$\dot{m}_{\mathrm{a}} \cdot \Delta h_{\mathrm{a,1\text{-}2}} + \dot{m}_{\mathrm{s}} \cdot \Delta h_{\mathrm{s,1\text{-}2}} + \Delta\dot{m}_{\mathrm{s,1\text{-}2}} \cdot h_{\mathrm{s}} + \dot{m}_{\mathrm{w}} \cdot \Delta h_{\mathrm{w,1\text{-}2}} = 0 \tag{5.30}$$

If we substitute equations (5.7), (5.14), (5.16) and consider that $\Delta h_{\mathrm{w,1\text{-}2}} = Cp_{\mathrm{w}} \cdot \Delta T_{\mathrm{w,1\text{-}2}}$ in equation (5.30) and solve for $\Delta T_{\mathrm{a,1\text{-}2}}$ then it yields

$$\Delta T_{\mathrm{a,1\text{-}2}} = \frac{\dot{m}_{\mathrm{a}} \cdot Cp_{\mathrm{s}} \cdot T_{\mathrm{s}} \cdot \Delta\omega_{\mathrm{a,1\text{-}2}} - \dot{m}_{\mathrm{s}} \cdot Cp_{\mathrm{s}} \cdot \Delta T_{\mathrm{s,1\text{-}2}} - \dot{m}_{\mathrm{a}} \cdot h_{fg} \cdot \Delta\omega_{\mathrm{a,1\text{-}2}} - \dot{m}_{\mathrm{w}} \cdot Cp_{\mathrm{w}} \cdot \Delta T_{\mathrm{w,1\text{-}2}}}{\dot{m}_{\mathrm{a}} \cdot Cp_{\mathrm{a}}} \tag{5.31}$$

$\Delta T_{\mathrm{s,1\text{-}2}}$ and $\Delta T_{\mathrm{w,1\text{-}2}}$ are calculated by an effectiveness-NTU model.

It should be noted that condensation occurring at the dry areas of the tubes (as a result of reducing the water vapour temperature below its saturation temperature) was neglected because calculations carried out based on the Nusselt analysis (Incropera *et al.*, 2007) showed that the effect on the overall mass flux of water absorption was not significant.

Methodology of effectiveness-NTU model

In the experimental model tested, there are embedded cooling tubes and they are connected vertically in groups of ten (see Fig. 5.3a and 5.3b). If we consider each group as a cross flow heat exchanger and assume that the tube is constantly and totally wet by the solution, then heat exchange takes place directly and only between the solution and the surface of each cooling tube.

The water is assumed to be perfectly mixed in each cross sectional area to each element. Following the well known method of the effectiveness-NTU for heat exchangers (Incropera *et al.*, 2007) the effectiveness of a cross flow heat exchanger (single pass) with $C_{\min}$ (mixed) and $C_{\max}$ (unmixed) is given by

$$\varepsilon = 1 - \exp\left[-\frac{1}{Cr} \cdot \left(1 - \exp(-Cr \cdot NTU\right) \right] \tag{5.32}$$

where Cr is the heat capacity ratio defined as

$$Cr = \frac{C_{\mathrm{h}}}{C_{\mathrm{c}}} = \frac{\dot{m}_{\mathrm{s,tube}} \cdot Cp_{\mathrm{s}}}{\dot{m}_{\mathrm{w,tube}} \cdot Cp_{\mathrm{w}}} \tag{5.33}$$

where C_{h} is the heat capacity of the hot fluid, C_{c} is the heat capacity of the cold fluid
NTU is determined from the expression

$$NTU = \frac{U_0 \cdot A}{C_{\min}} \tag{5.34}$$

$$C_{\min} = C_h = \dot{m}_s \cdot Cp_s \tag{5.35}$$

U_0 is the overall heat transfer coefficient computed for local properties and heat transfer coefficients and is given from the following formula (Cengel, 2006, Incropera *et al.*, 2007):

$$U_0 = \left[\left(\frac{1}{h_\theta} \right) + \left(\frac{1}{h_w} \right) + \left(\frac{\ln\left(\frac{r_2}{r_1} \right)}{2 \cdot \pi \cdot \delta l \cdot k_{cop}} \right) + 4 \cdot Rf \right]^{-1} \tag{5.36}$$

where δl is the length of the tube, r_2 is the external diameter of the tube and r_1 is the internal diameter, k_{cop} is the thermal conductivity of copper, h_θ is the heat transfer coefficient for external flow of solution at the tube surface defined as

$$h_\theta = \frac{0.687 \cdot \text{Re}_s^{0.11} \cdot Nu_\theta \cdot k_{sol}}{L_{c,tube}} \tag{5.37}$$

(Kocamustafaogullari and Chen, 1988)

with Reynolds number given by

$$\text{Re}_s = \frac{4 \cdot \dot{m}_{\text{s,tube}}}{\pi \cdot \frac{D}{2} \cdot \mu_{\text{s}}} \tag{5.38}$$

(Jain *et al.*, 2000)

Nu_θ is the Nusselt number for external flow determined from the expression

$$Nu_\theta = (0.35 + 0.34 \cdot \text{Re}_s^{0.5} + 0.15 \cdot \text{Re}_s^{0.58}) \cdot \text{Pr}_{\text{s}}^{0.3} \tag{5.39}$$

(Sanitjai and Goldstein, 2004)

h_{w} is the heat transfer coefficient of the internal flow of water defined as

$$h_{\text{w}} = \frac{Nu_{\text{D}} \cdot k_{\text{w}}}{D} \tag{5.40}$$

Nu_{D} is the Nusselt number which for fully developed internal laminar flow ($\text{Re}_w \prec 2300$) in tubes with uniform heat flux is considered constant

$$Nu_{\mathrm{D}} = 4.36 \tag{5.41}$$

Pr_{s} is the solution Prandtl number defined as

$$\mathrm{Pr}_{\mathrm{s}} = \frac{Cp_{\mathrm{s}} \cdot \mu_{\mathrm{s}}}{k_{\mathrm{s}}} \tag{5.42}$$

The effectiveness ε is by definition the ratio of the actual heat transfer to the maximum possible heat transfer

$$\varepsilon = \frac{Q}{Q_{\max}} \tag{5.43}$$

where Q can be either

$$Q_{\mathrm{s}} = \dot{m}_{\mathrm{s,tube}} \cdot Cp_{\mathrm{s}} \cdot \left(T_{\mathrm{s}}^{\ \mathrm{out}} - T_{\mathrm{s}}^{\ \mathrm{in}}\right) \tag{5.44}$$

or

$$Q_{\mathrm{w}} = \dot{m}_{\mathrm{w,tube}} \cdot Cp_{\mathrm{w}} \cdot \left(T_{\mathrm{w}}^{\ \mathrm{out}} - T_{\mathrm{w}}^{\ \mathrm{in}}\right) \tag{5.45}$$

and

here $Q_{\max} = \dot{m}_{\mathrm{s,tube}} \cdot Cp_{\mathrm{s}} \cdot \left(T_{\mathrm{s}}^{\ \mathrm{in}} - T_{\mathrm{w}}^{\ \mathrm{in}}\right)$ (5.46)

Thus by substituting equation (5.44) in (5.43) yields

$$T_{\mathrm{s}}^{\ \mathrm{out}} = T_{\mathrm{s}}^{\ \mathrm{in}} - \varepsilon \cdot \left(T_{\mathrm{s}}^{\ \mathrm{in}} - T_{\mathrm{w}}^{\ \mathrm{in}}\right) \tag{5.47}$$

and by substituting equation (5.45) in (5.43) yields

$$\varepsilon = \frac{\dot{m}_{\mathrm{w,tube}} \cdot Cp_{\mathrm{w}} \cdot \left(T_{\mathrm{w}}^{\ \mathrm{out}} - T_{\mathrm{w}}^{\ \mathrm{in}}\right)}{\dot{m}_{\mathrm{s,tube}} \cdot Cp_{\mathrm{s}} \cdot \left(T_{\mathrm{s}}^{\ \mathrm{in}} - T_{\mathrm{w}}^{\ \mathrm{in}}\right)} \tag{5.48}$$

solving for $T_{\mathrm{w}}^{\ \mathrm{out}}$ we arrive at

$$T_{\mathrm{w}}^{\ \mathrm{out}} = T_{\mathrm{w}}^{\ \mathrm{in}} + \left[\frac{\varepsilon \cdot \dot{m}_{\mathrm{s,tube}} \cdot Cp_{\mathrm{s}} \cdot \left(T_{\mathrm{s}}^{\ \mathrm{in}} - T_{\mathrm{w}}^{\ \mathrm{in}}\right)}{\dot{m}_{\mathrm{w,tube}} \cdot Cp_{\mathrm{w}}}\right] \tag{5.49}$$

The detail computational procedure is described on the next chapter along with the GPROMs model. The properties of air, water and $MgCl_2$ solution were determined using published formulas or by polynomial equations based on experimental data found in the literature (Cengel, 2006, Incropera *et al.*, 2007, Lobo, 1989, Zaytsev and Aseyev, 1992).

5.4 Experimental equipment and methods

The performance of a packed column type desiccator used in a cross flow configuration is affected by:

c) Ambient conditions such as air temperature and humidity and
d) Design parameters such as the mass flow rate, temperature and concentration of the desiccant solution, the air mass flow rate, the packing material, the wetted surface area and the width of the column.

The aim here is to validate the theoretical model developed in section 5.3, an essential part of the whole system model, and thus investigate how the design parameters should be chosen so as to optimise the performance under the ambient conditions according to the local climate.

In this study we have investigated the performance of the desiccator under lab conditions. The experimental set up enabled us to control the air mass flow, the temperature and relative humidity of the air, the solution mass flow and the solution concentration. The performance of the regenerator was assessed under dry and under humid ambient conditions.

5.4.1 Set up

The experimental desiccator is constructed with four separate cellulose structured pads each one sized 0.1×0.1×0.3m. Each pad consists of specially impregnated and corrugated cellulose paper sheets with different flute angles, one steep (60 deg) and one flat (30 deg) that have been bonded together (CELdek® 7090-15). The packed column is cooled by fifty copper tubes (15mm OD) embedded inside it (tap water is used as the cooling fluid). The strong magnesium chloride solution flows through two manifolds from the top to bottom inside the column, wetting the cellulose structured packing. As the humid air passes

horizontally, in cross-flow configuration through the column, moisture is removed as the water vapour is absorbed by the liquid desiccant. A tank at the bottom is used to collect the weak magnesium chloride solution which freely flows through a tube to the regenerator. The strong solution flowing out of the regenerator is collected in a tank and then the peristaltic pump (see section 4.3.1 for pump specifications) returns the solution at the inlet of the desiccator. Figure 5.3 shows a schematic side view of the desiccator. The desiccator is fitted inside a rectangular PVC tunnel (see Fig. 5.5 and Fig. 5.6).

To minimise heat exchange with the surroundings, the PVC tunnel is insulated with a 6 mm insulation wool blanket (Superwool607 MAX Blanket, RS) and Airtec double insulation material (ScrewFix). Two air sampling tubes for measuring the dry bulb and wet bulb temperatures of the incoming humid air and the out coming dehumidified air are mounted on the tunnel. For this purpose a fan (Micronel panel mount fan, 12Vdc, 60mm dia) is fitted inside each sampling tube that draws air out of the rig and recycles it back to the process air, and two Pt Resistance Temperature Detectors (PT100 ±0.03 °C @ 0 °C, Pico Technology®) are placed at the fan inlet of each tube. One of them is covered with a wick (manufactured for scientific hygrometers) which is kept wet by immersing its end in water. Platinum resistance detectors are also used for measuring the solution temperature and the cooling water temperature at the inlet and the outlet of the desiccator. The readings are scanned and recorded by the PicoLog data logging software every second.

The process air is heated and humidified before entering the tunnel by an existing environmental chamber that allows the digital control of the heat and water vapour supply to the incoming air stream. The process air is drawn out of the tunnel using a 12 Vdc centrifugal blower (ebmpapst, max volumetric flow 220m^3/h). Attached to the outlet of the blower, an orifice plate setup was constructed according to BS EN ISO 5167-1:2003 guidelines in order to measure the air mass flow accurately (± 1.5 percent error). An inclined manometer is used to measure the pressure difference along the orifice plate with a reading error of ±2.5 Pa.

The air flow at the outlet fan is controlled by a DC power regulator. It was calibrated so as to be able to calculate the volumetric flow rate by knowing the voltage only. The calibration graph (Fig. A4.3) can be found in appendix 4.The air flow at the inlet fan is adjusted using a digital control showing the percentage of power output. This fan was also

calibrated so as to calculate the volumetric flow rate by knowing the percentage power output. The calibration graph (Fig. A4.4) can be found in appendix 4.

5.4.2 Experimental procedure

Each experiment comprised the following steps:

1. Mix up the $MgCl_2$ solution by stirring known masses of water with known masses of $MgCl_2$.
2. Decant approximately 8L of the solution in the rectangular plastic tank (see bubble No7 in Fig. 4.7).
3. Put all the temperature probes for measuring solution and ambient air temperature in place (see Fig. 4.7).
4. Switch on the fan of the environmental chamber rig at the desired speed
5. Switch on the fan at the outlet of the desiccator rig at the desired speed
6. Switch on the heating element of the environmental chamber rig at the desired temperature. Wait until thermal balance is achieved by measuring the temperatures of the air before and after the packed column
7. Start the peristaltic pump at the desired speed. Wait until the desiccator is wetted
8. Switch on the humidifier at the desired relative humidity level
9. Switch on the solar simulator
10. Switch on the air sampling fans
11. Turn on the tap water for the cooling tubes
12. Measure the volumetric flow of water at the outlet of the cooling tubes; adjust it to the desired value.
13. Set the computer to log temperature readings
14. Take solution sample from the desiccator outlet (repeat 30 min)
15. Take solution sample from the regenerator outlet (repeat 30 min)
16. Measure RI of samples after the end of the experiment.
17. Remove the temperature probes and wash them with water.

5.5 Results and Discussion

5.5.1 Experimental design and calculations

In order to explore the effect of the various parameters affecting the performance of the desiccator, only one parameter was varied at a time while the others were kept constant. Two series of experiments were conducted. The first series consisted of four experiments

i.e. D1, D2, D3 and D4 that were carried out under dry ambient conditions (RH = 60-63%). The air volumetric flow rate and the desiccant solution flow rate were kept constant in D2, D3 and D4. D1 was conducted with a lower solution mass flow rate. D3 was carried out at higher air flow in order to investigate the effect of the air flow to the performance of the desiccator. Table 5.2 summarizes the conditions under each experiment of the first series was conducted. The second series consisted of five experiments i.e. H1, H2, H3, H4 and H5 that were carried out under humid conditions (RH = 67 – 75%). All of them were carried out using internal cooling and the only variable was the solution mass flow. We focused more on humid conditions since the proposed cooling system is designed for hot and humid climates. Tables 5.2 and 5.3 summarize the conditions under each experiment of the second series were conducted.

Table 5.2: Experimental conditions for Series 1.

Series 1	DRY CONDITIONS (RH=60-62%)			
Experiment	D1	D2	D3	D4
Air flow (%max flow)	60	60	80	60
Solution flow (kg/s)	0.0034	0.004	0.004	0.004
Air Temperature (^{o}C)	30	35	30	35
Internal cooling	no	no	no	yes
Water flow (kg/s)	0	0	0	0.062

Table 5.3: Experimental conditions for Series 2.

Series 2	HUMID CONDITIONS (RH=67-75%)				
Experiment	H1	H2	H3	H4	H5
Air flow (%max flow)	60	60	60	60	60
Solution flow (kg/s)	0.0021	0.0028	0.0036	0.0041	0.0064
Air Temperature (^{o}C)	35	35	35	35	35
Internal cooling	yes	yes	yes	yes	yes
Water flow (kg/s)	0.062	0.062	0.062	0.062	0.062

The initial concentration of the solution varied in a narrow range 0.34-0.36 kg of solute / kg of solution. We chose to conduct all of the experiments with high initial concentrations of $MgCl_2$ that correspond to 39%-32% ERH as our hypothesis is that highly concentrated brines, rich in $MgCl_2$, can be used as liquid desiccants for cooling greenhouses. Besides, if the desiccator is to work even under dry and hot conditions (below 60% RH) efficiently then this would be achieved with a solution of lower than 40% ERH.

The air mass flow rate was calculated using the following formula (BS.EN.ISO.5167-1:2003)

$$\dot{m}_{\text{air}} = \frac{C}{\sqrt{1-\beta^4}} \cdot \varepsilon \cdot \frac{\pi}{4} \cdot d^2 \cdot \sqrt{2\Delta p \cdot \rho_{\text{air}}} \tag{5.50}$$

where C is the orifice coefficient discharge, d is the orifice diameter, D is the upstream internal pipe diameter, β is the diameter ratio (d/D), Δp is the differential pressure (measured by the inclined manometer), ε is the expansibility factor, ρ_{air} is the upstream air density. A section view of the orifice plate can be seen in the appendix 5, Fig. A5.1.

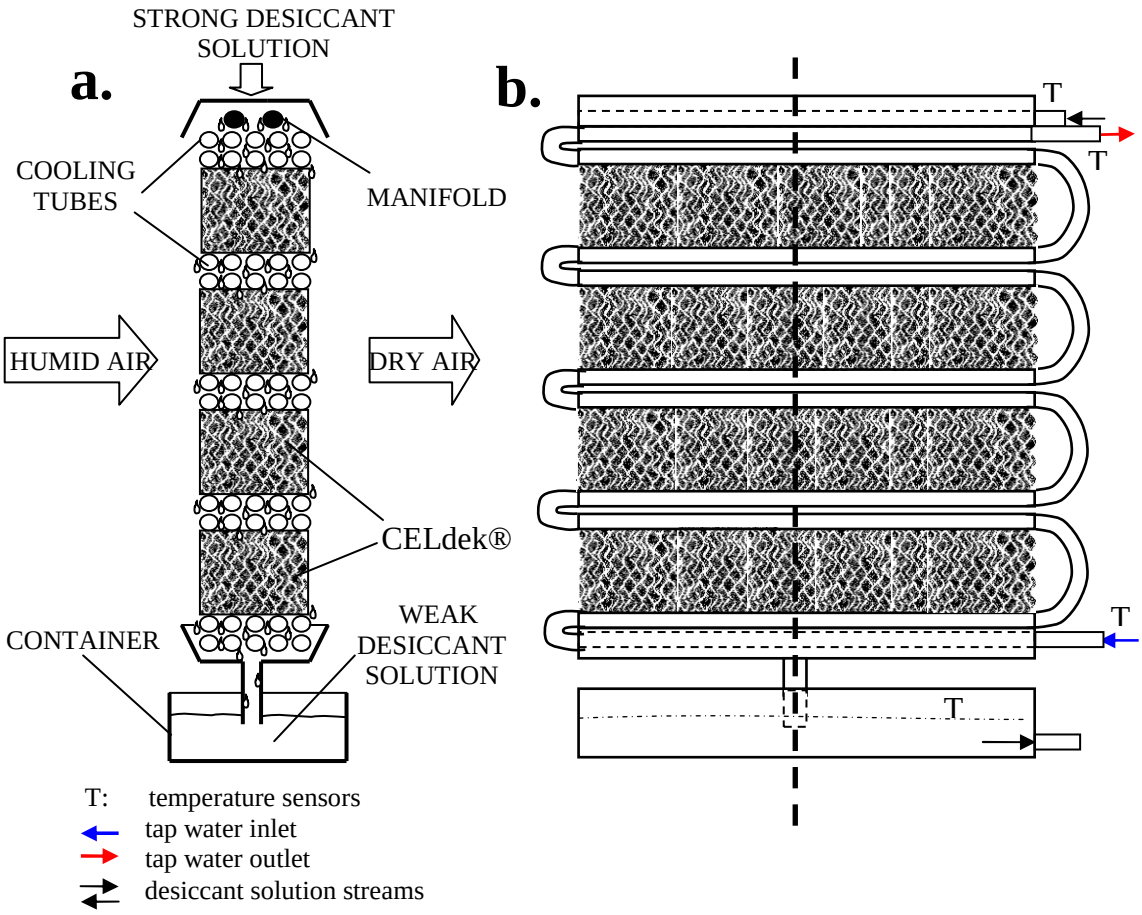

Fig. 5.3: Section view (a) and side view (b) of the desiccator.

Therefore, for a steady-flow open system the inflow energy will be equal to the outflow energy,

$$\dot{E}_{\text{in}}^{\text{tot}} = \dot{E}_{\text{in}}^{\text{tot}} \Rightarrow$$

$$\dot{Q}_{\text{in}} + \dot{W}_{\text{in}} + \sum \dot{H}_{\text{in}} + \sum \dot{K}e_{\text{in}} + \sum \dot{P}e_{\text{in}} = \dot{Q}_{\text{out}} + \dot{W}_{\text{out}} + \sum \dot{H}_{\text{out}} + \sum \dot{K}e_{\text{out}} + \sum \dot{P}e_{\text{out}} \tag{5.51}$$

In particular, if we assume for our system that there is no heat loss (adiabatic), no change in kinetic energy, no change in potential energy and no work generation equation (5.51) becomes

$$\sum \dot{H}_{\text{in}} = \sum \dot{H}_{\text{out}} \Rightarrow \dot{H}_{\text{air}}^{\text{in}} + \dot{H}_{\text{sol}}^{\text{in}} + \dot{H}_{\text{water}}^{\text{in}} = \dot{H}_{\text{air}}^{\text{out}} + \dot{H}_{\text{sol}}^{\text{out}} + \dot{H}_{\text{water}}^{\text{out}} + \dot{H}_{\text{latent}} \tag{5.52}$$

where $\dot{H}$ is the enthalpy rate and can be expressed as

$$\dot{H}_{\text{i}}^{\text{j}} = \dot{m}_{\text{i}} \cdot Cp_{\text{i}} \cdot T_{\text{i}}^{\text{j}} \tag{5.53}$$

$$\dot{H}_{\text{air}}^{\text{j}} = \dot{m}_{\text{air}} \cdot \left(Cp_{\text{air}} \cdot T_{\text{air}}^{\text{j}} + \omega_{\text{j}} \cdot h_{\text{g}} \right) \tag{5.54}$$

for i = water, solution and j = in, out

where h_{g} is the specific enthalpy of saturated water vapour and can be approximately calculated by the following formula

$$h_{\text{g}} \cong 2501.3 + 1.84 \cdot T_{\text{db}} \tag{5.55}$$

(Cengel and Boles, 1998)

The latent heat rate of absorption that is released during the stripping of water vapour from the air stream to the desiccant solution is expressed as

$$\dot{H}_{\text{latent}} = \dot{m}_{\text{abs}} \cdot h_{\text{fg}} \tag{5.56}$$

where h_{fg} is the water latent heat of absorption taken to be constant and equal to 2255.8 kJ kg^{-1}.

The water rate of absorption $\dot{m}_{\text{abs}}$ is calculated by the following formula

$$\dot{m}_{\text{abs}} = \dot{m}_{\text{air}} \cdot \left(\omega_{\text{in}} - \omega_{out} \right) \tag{5.57}$$

where ω_{in} and ω_{out} are the absolute humidities of the incoming and outcoming air respectively.

The enthalpy effectiveness and moisture effectiveness of the dehumidifier describe the combined heat and mass transfer performances and they were calculated by the following equations:

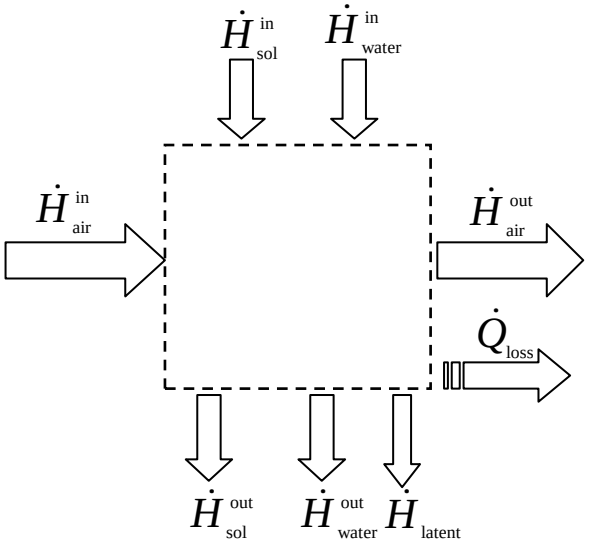

Fig. 5.4: Schematic of the energy flows at the desiccator rig

$$\eta_h = \frac{\dot{H}^{in}_{air} - \dot{H}^{out}_{air}}{\dot{H}^{in}_{air} - \dot{H}_e} \cdot 100\% \tag{5.58}$$

$$\eta_w = \frac{\omega_{in} - \omega_{out}}{\omega_{in} - \omega_e} \cdot 100\% \tag{5.59}$$

where $\dot{H}_e$ is the enthalpy of air in equilibrium with the solution and is calculated by the following formula:

$$\dot{H}_e = \left[1.007 \cdot T_{db} - 0.026 + \omega_e \cdot \left(2501 + 1.84 \cdot T_{db}\right)\right] \cdot \dot{m}_{air} \tag{5.60}$$

and ω_e is the saturated water content of the air at the surface of the solution and can be calculated as

$$\omega_e = \frac{0.622 \cdot ERH \cdot P_s}{P_{amb} - ERH \cdot P_s} \tag{5.61}$$

where P_s is the saturated pressure of water vapour calculated by

$$\log P_s = 30.59051 - 8.2 \cdot \log T'_{db} + 2.4804 \cdot 10^{-3} \cdot T'_{db} - 3142.31 \cdot T'^{-1}_{db} \quad (5.62)$$

(National Engineering Laboratory, 1964)

where $T'_{db} = 273.16 + T_{db}$.

For each experiment equation (5.52) was applied and found that there was a deviation from the energy conservation law. This unbalance is mainly attributed to heat loss from the shell of the rig as it was not perfectly insulated. It was expressed as a percentage of the total incoming enthalpy flow rate:

$$\dot{Q}_{loss} = \frac{\left|\sum \dot{H}_{in} - \sum \dot{H}_{out}\right|}{\sum \dot{H}_{in}} \cdot 100\% \quad (5.63)$$

A summary of the energy balance calculation results and the calculated $\dot{Q}_{loss}$ % are shown in Table 5.4 (see appendix A6 for a more analytical table). It is seen that the heat losses represent only 1-8% of the total incoming enthalpy flow rate which can be considered insignificant.

Table 5.4: Energy balance calculated results

Experiment	$\sum \dot{H}_{in}$ (kJ s^{-1})	$\sum \dot{H}_{out}$ (kJ s^{-1})	$\Delta \sum \dot{H}_{in\text{-}out}$	$\dot{Q}_{loss}$ %
H1	7.31	7.66	-0.35	5
H2	7.46	7.86	-0.41	5
H3	6.62	7.08	-0.46	7
H4	7.62	8.10	-0.47	6
H5	7.19	7.70	-0.50	7
D1	2.21	2.19	0.02	1
D2	2.77	2.71	0.05	2
D3	3.00	3.03	-0.03	1
D4	7.92	8.53	-0.61	8

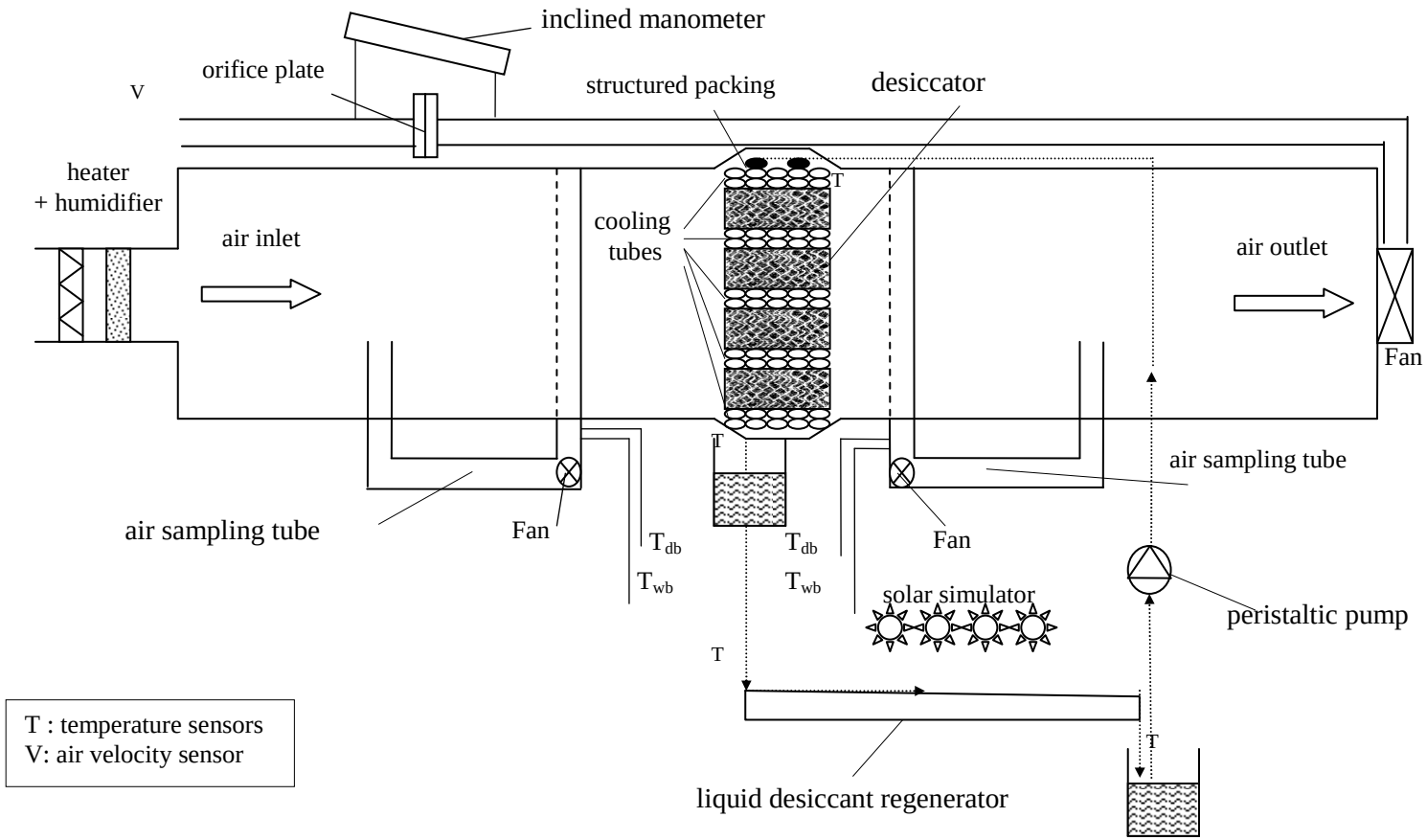

Fig. 5.5: Schematic diagram of the experimental rig

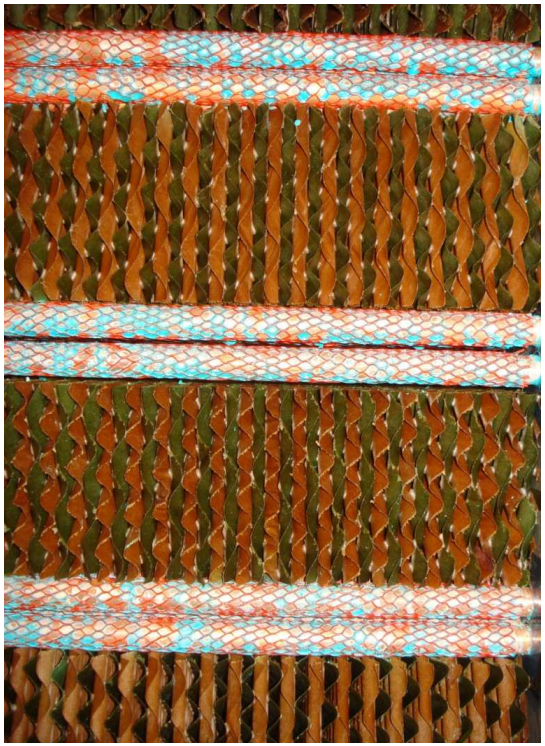

Fig. 5.6: Photos of the experimental rig in the lab (right) and the desiccator (left).

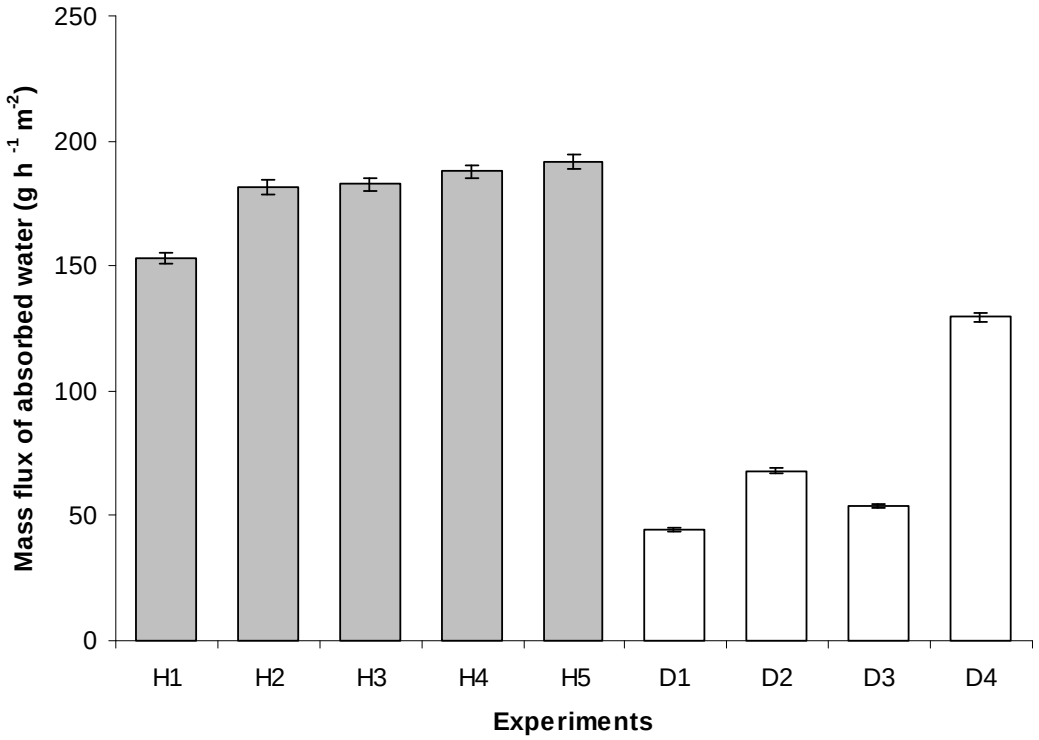

Fig. 5.7: The calculated mass flux of absorbed water under humid (H series) and dry (D series) conditions.

The calculated mass flux of absorbed water for each experiment conducted in the laboratory under humid and dry conditions is illustrated in Figure 5.7. It is seen that when internal cooling is employed (in H1-H5 and in D4) the mass flux is considerably increased. Experiment D4 can be compared to D2 since their only difference is the cooling treatment. In particular, the mass flux of absorbed water in experiment D4 is approximately 47.5% higher than of D2. This significant improvement can be explained by the fact that internal cooling decreases the temperature of the solution. As a result the temperature gradient between the solution film and the process air is increased. Consequently this results in a higher vapour pressure gradient at the interface as the vapour pressure of the solution is decreased. Thus, higher mass transfer rates are induced.

The comparison between D4 and H3 showed that the performance of the desiccator dropped significantly under dry conditions. In fact the mass flux of absorbed water in H3 is 29% higher than the one measured in D4. The H series showed the effect of the solution mass flow on the performance of the regenerator. As it is seen in Figure 5.8 there is an

optimum solution flow value under the current conditions, beyond which there is no significant change in the mass flow of absorbed water for values higher than 3000g h^{-1} m^{-2}.

The calculated experimental moisture and enthalpy effectiveness of the H series of experiments are illustrated in Fig 5.8. The moisture effectiveness ranged between 50% and 65.4% while the enthalpy effectiveness varied approximately from 54.6% to 70%. It is worth noticing that the effectiveness (either way expressed) reaches a plateau for solution mass flow values higher than 3000 g h^{-1} m^{-2}.

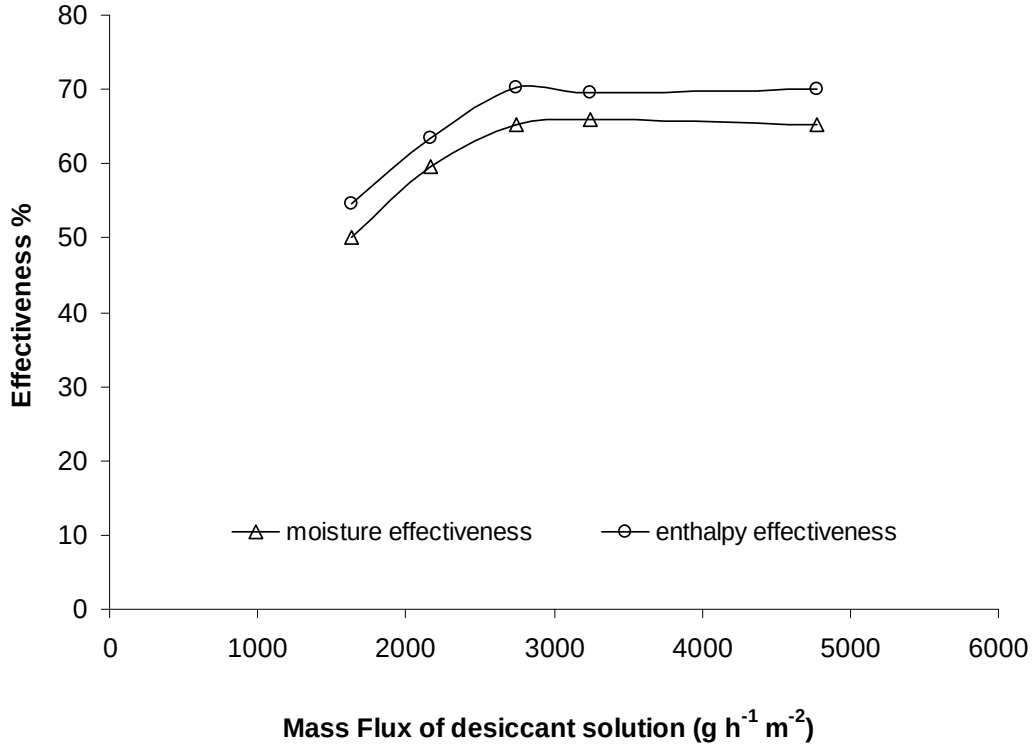

Fig. 5.8: The calculated moisture and enthalpy effectiveness of H series against the mass flux of the $MgCl_2$ solution.

5.5.2 Comparison with theoretical model

The developed desiccator model managed to predict the mass flux of absorbed water, $\dot{m}_{abs}$, with a 11 % average error when compared to the experimental values. It should be noted that the model predicts higher mass fluxes of absorbed water for all the experimental input data because it considers that the whole surface area of the desiccator is wetted and thus effective (ideal). However, this was not the case when conducting the experiments, since areas of the desiccator were not fully wetted and channeling flow patterns were observed.

Therefore, in order to compensate this significant effect a parameter was introduced to the model i.e. the ratio of wetted surface area per volume, α_{abs} (see Section 5.3) which is a constant when all the surface area of CELdek is wetted equal to 1. The results presented here take into account an average $0.8\,\alpha_{abs}$ for all the experiments. The predicted values of the mass flux of absorbed water along with the experimental values against the ratio of air mass flow to solution mass flow are illustrated in Fig 5.9.

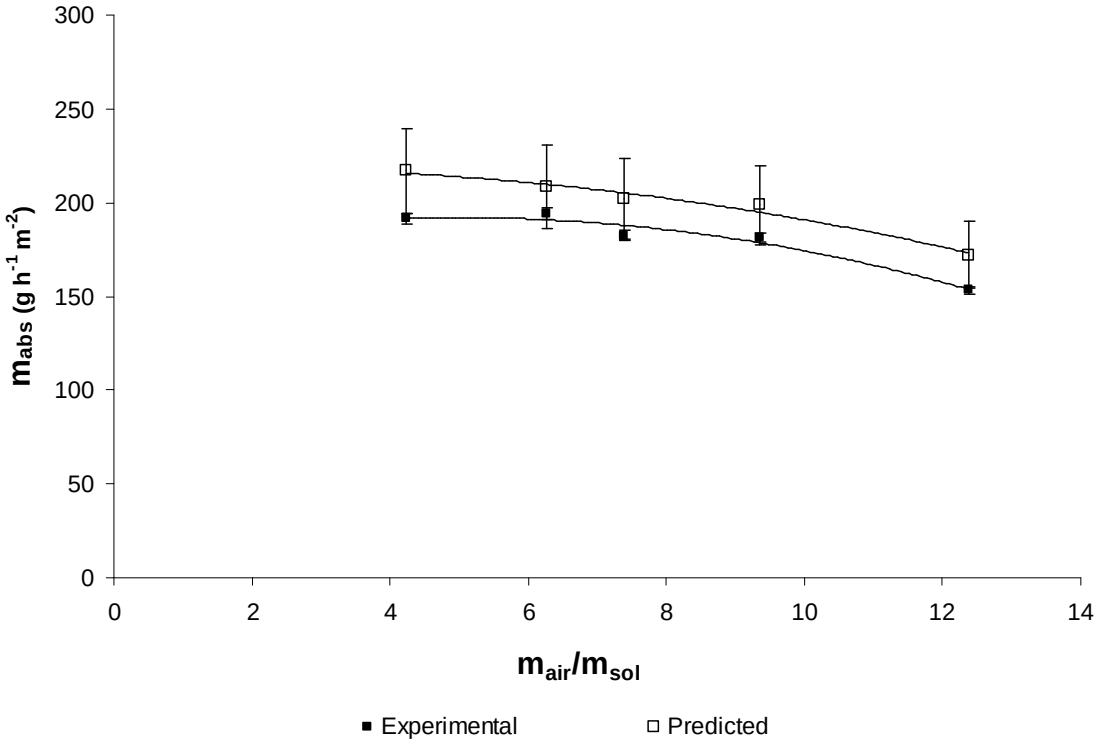

Fig. 5.9: Experimental and predicted values of $\dot{m}_{abs}$ against the ratio of air mass flow to solution mass flow.

The inlet values of temperature (air, solution, water), relative humidity and $MgCl_2$ concentration for each experiment are presented in Table 5.5. These values were fed into the model and the predicted results, along with the percent errors, are presented in Table 5.6.

It is seen that the average relative error for the predicted air temperature, the predicted solution temperature, predicted water temperature, predicted relative humidity, predicted moisture effectiveness and enthalpy effectiveness are 5%, 9%, 5%, 4%, 8% and 8% respectively.

5.6 Conclusion

According to the literature review, finite difference models give more accurate performance predictions but their solution can be cumbersome. In contrast, the effectiveness-NTU methodology is less complex and requires only short iteration procedures. On the choice of the desiccator's type, packed columns with internal cooling are preferred because they provide high surface-volume ratio and thus achieve better dehumidification effectiveness. Therefore, we designed and constructed in lab a cross flow desiccator with structured packing and internal cooling. The experimental findings showed that internal cooling improves the performance of the desiccator significantly. This can be attributed to the fact that bigger vapour pressure gradients are induced at the interface of air-solution as a result of lower solution temperature. The performance of the desiccator drops considerably (by 29%) when it is operating under dry conditions, regardless of whether or not internal cooling is used. The moisture and enthalpy effectiveness of the desiccator varies approximately from 50% to 70% under humid conditions and reaches a plateau at 3000 g h^{-1} m^{-2} of solution mass flux. The presented heat and mass transfer model can predict the mass flux of absorbed water vapour with a relative error of 11 %. This model will be used to predict the mass flux of absorbed water vapour as part of the whole system model, using gPROMS®, presented in Chapter 6.

Table 5.5: The temperature values of air, solution and water at the inlet along with the relative humidity and solution concentration.

Experiment	Tain	Tsin	Twin	RHin	Xin
H1	34.7	29.2	18.3	69.1	0.3568
H2	34.9	33.7	17.9	70.6	0.3481
H3	34.7	30.3	15.3	66.8	0.3414
H4	35.2	31.2	18.4	69.5	0.3446
H5	35.2	31.8	16.8	67.1	0.3439

Table 5.6: The predicted values of temperature (air, solution, water), relative humidity, moisture and enthalpy effectiveness at the outlet in comparison with the experimental ones.

Experiment	Ta_{out} (^oC)			Ts_{out} (^oC)			Tw_{out} (^oC)			RH_{out} (^oC)			Moisture effectiveness %			Enthalpy effectiveness %		
	Pred	Exp	% error	Pred	Exp	% error	Pred	Exp	% error	Pred	Exp	% error	Pred	Exp	% error	Pred	Exp	% error
H1	30.8	31.1	1	25.4	26.5	4	20.7	20.4	2	57.1	56.4	1	57.9	50.1	16	62.2	54.6	14
H2	28.6	31.1	8	29.1	26.5	10	21.8	20.3	7	62.9	55.0	14	61.3	59.5	3	66.8	63.4	5
H3	28.3	29.3	3	26.7	25.8	3	19.5	18.3	7	56.2	56.7	1	71.5	65.3	9	76.0	70.2	8
H4	29.5	31.0	5	28.5	26.0	9	22.1	21.3	4	57.3	59.2	3	67.7	65.6	3	72.1	69.3	4
H5	28.1	29.8	6	29.5	24.9	19	21.7	20.2	7	57.0	56.2	1	70.6	65.3	8	75.4	70.0	8
Average			5			9			5			4			8			8

CHAPTER 6. SYSTEM MODELLING AND DESIGN

6.1 Introduction

The whole system model should combine the models of the regenerator, the desiccator and the greenhouse (see section 6.3). Thus to simulate the performance of the system under various climatic conditions, a modelling software package that can combine these individual models is required. In choosing the most suitable, priority was given to process modelling softwares that have the capability to interact with MSExcel® spreadsheet files. That was a prerequisite since the majority of the governing algebraic equations presented earlier had been already introduced in spreadsheets to check their validity.

The software chosen, gPROMS®, is advanced process modelling software that can interact with MSExcel® spreadsheet files, read from spreadsheets and perform calculations, use them as databases or even perform computational procedures in them. gPROMS® uses an equation-based programming language, designed specifically for the modelling of complex processes, where the relationships of the variables can be written as equations. In the same manner, the streams connecting various process units are written as mathematical statements. Complex processes and operating procedures can be modelled by writing equations that do not differ much from the ones written on paper. Mathematical solution techniques are built in gPROMS®, thus it is not necessary to introduce new ones. Another asset of the chosen software is the graphical representation of many elements of the problem such as stream connectors, basic models, etc. in a flowsheet environment. It is worth noticing the ease to call external softwares using gPROMS® gO:Run function. This allows a simulation of any size to be executed behind MSExcel or any other suitable interface. The reader is referred to the PSE website for a detailed description of the capabalities of gPROMS® (http://www.psenterprise.com/).

In this work, the computational procedure of the whole system model is described using flow diagrams and schematic descriptions whereas needed. The whole system consists of three models i.e. the regenerator, the desiccator and the greenhouse. The proposed cooling system is applied to a 1000m^2 greenhouse which utilizes evaporative cooling pads for

cooling and then a simple heat transfer model published in literature by Kittas *et al.* (2003) is used to predict the temperature at the outlet of the greenhouse.

6.2 Program Flow Analysis

The whole system program developed here assumes that it is a pseudo–steady state process and that the heat and mass balance equations are applied between the nodes. Fig. 6.1 illustrates a schematic of the flow of the computer program with the main output variables which are calculated at concrete procedures.

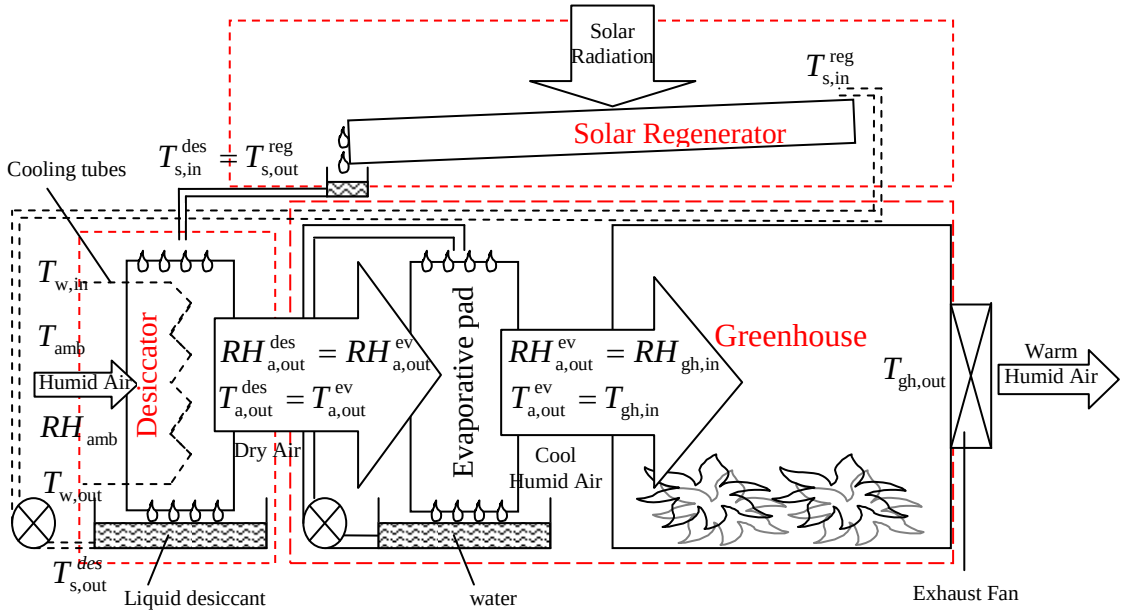

Fig. 6.1: Flow schematic of the computer program showing the basic output variables calculated at a concrete procedure.

The structured packing of the desiccator that consists of Celdek® pad material and cooling tubes is divided into five main sections as shown in Fig.6.2 (the green highlighted volume is one section). Then, each section is further divided into 450 control volumes called finite elements. Hence, each section is a computational domain which is discretized into $I \times J \times K$ meshes and each finite element is identified by a set of three coordinates (*i*, *j*, *k*) that represent the section, the element position along the section and the row, with $i = [1,5]$, $j = [1,30]$ and $k = [1,15]$ respectively. Overall the structured packing of the desiccator was divided into 2250 finite elements.

The governing algebraic equations of section 5.3 are applied to each element separately. The effectiveness-NTU model requires iterations in order to find the water temperature at

the outlet of the cooling tubes. Therefore, a simple iterative scheme is employed to solve the algebraic equations for the first section. When the outlet values of the first section are obtained a second iterative procedure starts for the second section and when a solution is obtained (convergence criterion 0.5%) the program continues to the next section and so on until the last section. It should be noted that local properties, heat and mass transfer coefficients are used for each element.

By averaging the air temperature and absolute humidity of the finite elements at the last slice, the outlet predicted values are obtained correspondingly. By averaging the solution temperatures of the finite elements of the bottom row of each slice, the outlet predicted value is obtained. The predicted outlet water temperature is found by averaging the water temperature of the finite elements where the outlets of the cooling tubes are (see Fig. 6.2).

Figure 6.4 illustrates the computer flow diagram of the whole system. The detailed computer programs of the regenerator, the desiccator, the greenhouse and the combined system written in gPROMS language can be found in appendix 8. A graphical representation of the system as it appears in a gGROMS flowsheet is seen in Figure 6.3. Each icon represents a unit model - process. For each process the following basic entries are required:

1) *Variables*, where all the variables used by the mathematical model are entered with their upper and lower bounds.
2) *Model*, this is the core of the program where the physical problem is described with mathematical relations. Here it is essential to declare the parameters, variables and equations.
3) *Process*, which is a simulation activity and represents an instance of the model. Here the simulation process and the initial conditions are defined.

The model shown in Figure 6.3 is a composite model since it combines three basic models. This is done by using stream connections (subsets of variables) or with equations i.e. by setting the inlet solution concentration at the regenerator to be equal to the outlet solution concentration at the desiccator, etc.

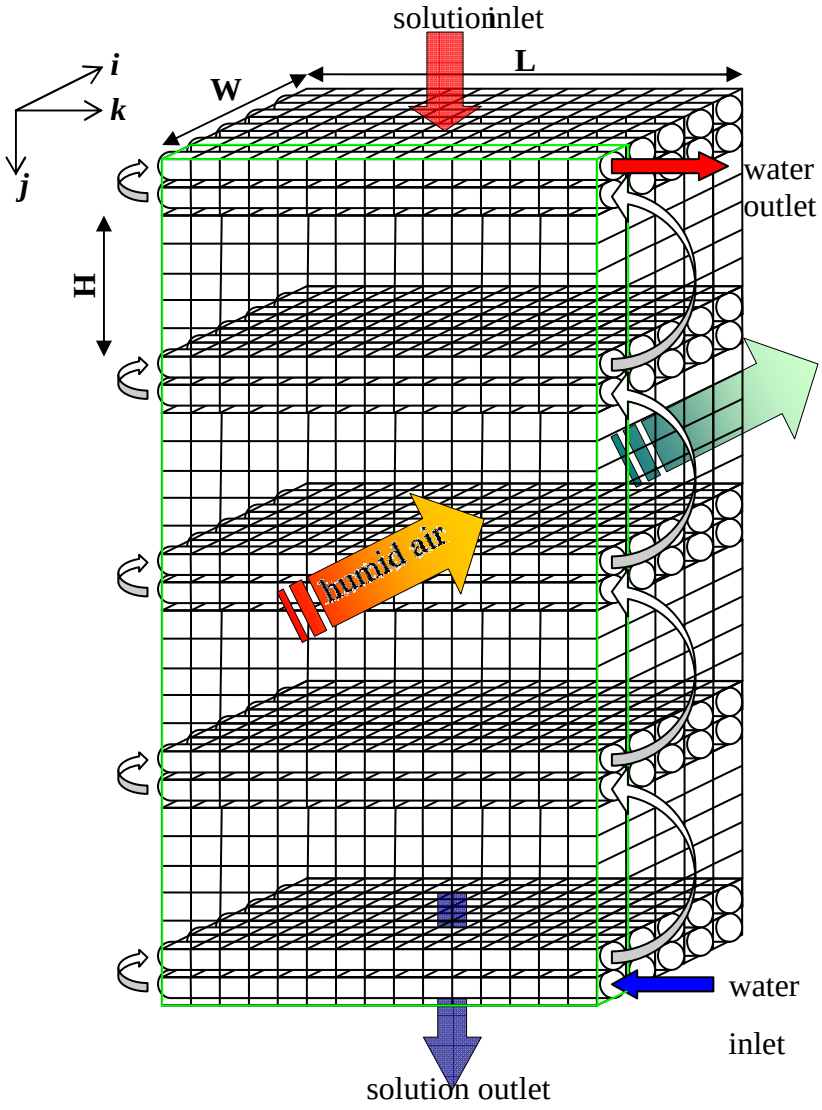

Fig. 6.2: Schematic of the computational domains of the desiccator.

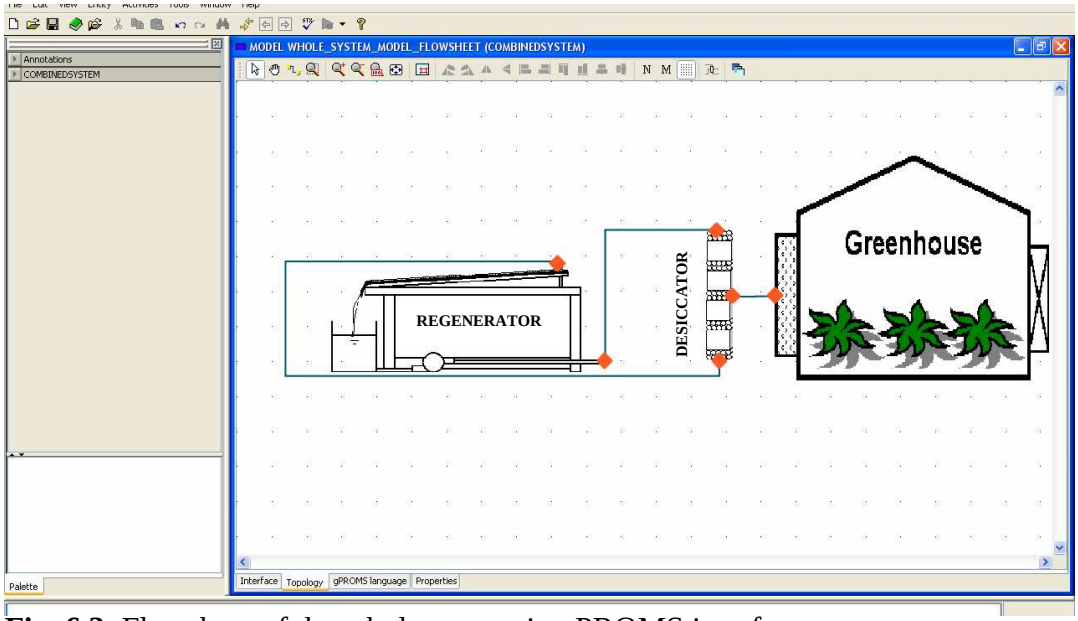

Fig. 6.3: Flowsheet of the whole system in gPROMS interface.

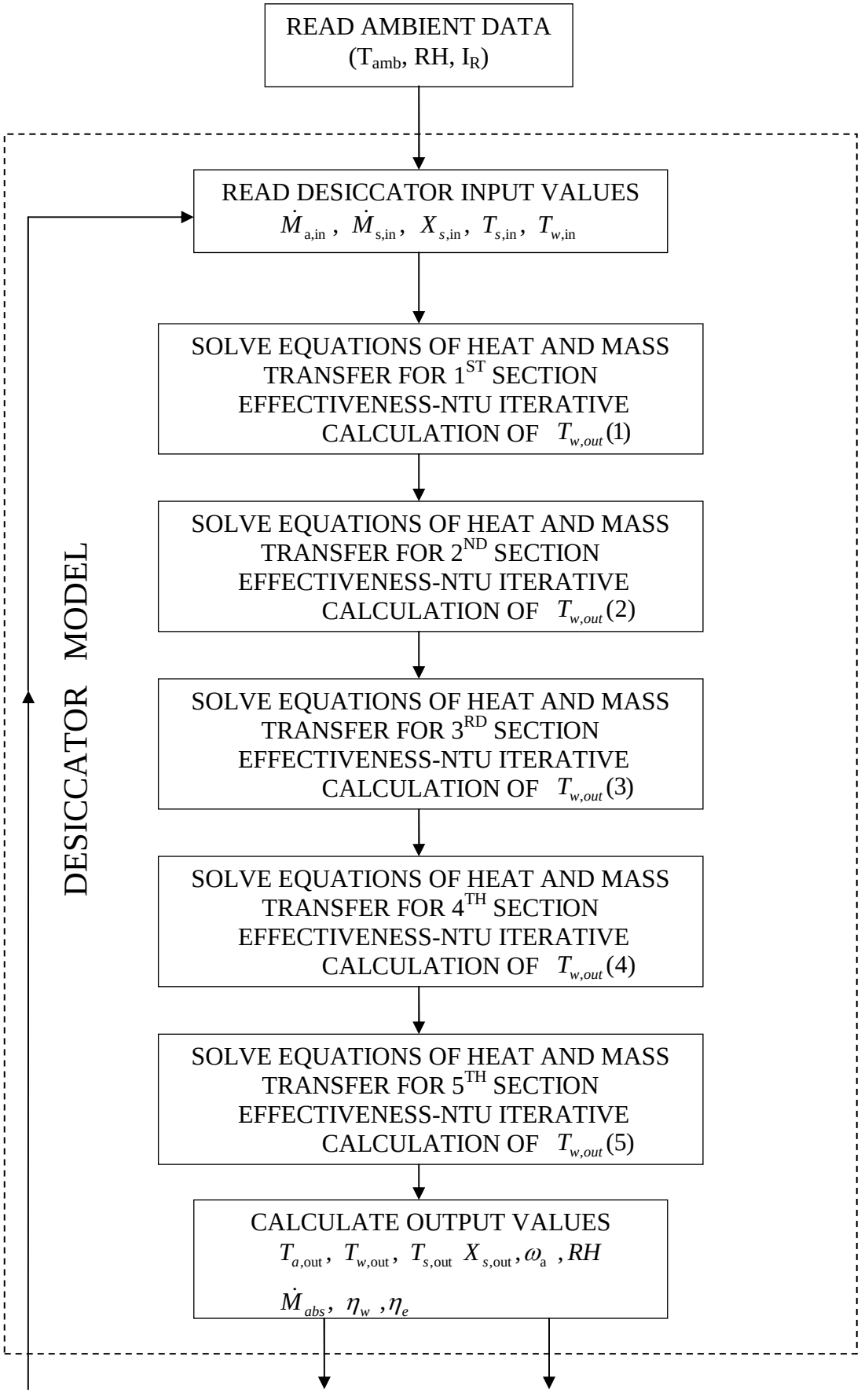
READ AMBIENT DATA
(T_{amb}, RH, I_R)
READ DESICCATOR INPUT VALUES
$\dot{M}_{a,in}$, $\dot{M}_{s,in}$, $X_{s,in}$, $T_{s,in}$, $T_{w,in}$
SOLVE EQUATIONS OF HEAT AND MASS TRANSFER FOR 1ST SECTION EFFECTIVENESS-NTU ITERATIVE CALCULATION OF $T_{w,out}(1)$
SOLVE EQUATIONS OF HEAT AND MASS TRANSFER FOR 2ND SECTION EFFECTIVENESS-NTU ITERATIVE CALCULATION OF $T_{w,out}(2)$
SOLVE EQUATIONS OF HEAT AND MASS TRANSFER FOR 3RD SECTION EFFECTIVENESS-NTU ITERATIVE CALCULATION OF $T_{w,out}(3)$
SOLVE EQUATIONS OF HEAT AND MASS TRANSFER FOR 4TH SECTION EFFECTIVENESS-NTU ITERATIVE CALCULATION OF $T_{w,out}(4)$
SOLVE EQUATIONS OF HEAT AND MASS TRANSFER FOR 5TH SECTION EFFECTIVENESS-NTU ITERATIVE CALCULATION OF $T_{w,out}(5)$
CALCULATE OUTPUT VALUES
$T_{a,out}$, $T_{w,out}$, $T_{s,out}$ $X_{s,out}$, ω_a , RH
$\dot{M}_{abs}$, η_w , η_e
DESICCATOR MODEL

(continued)

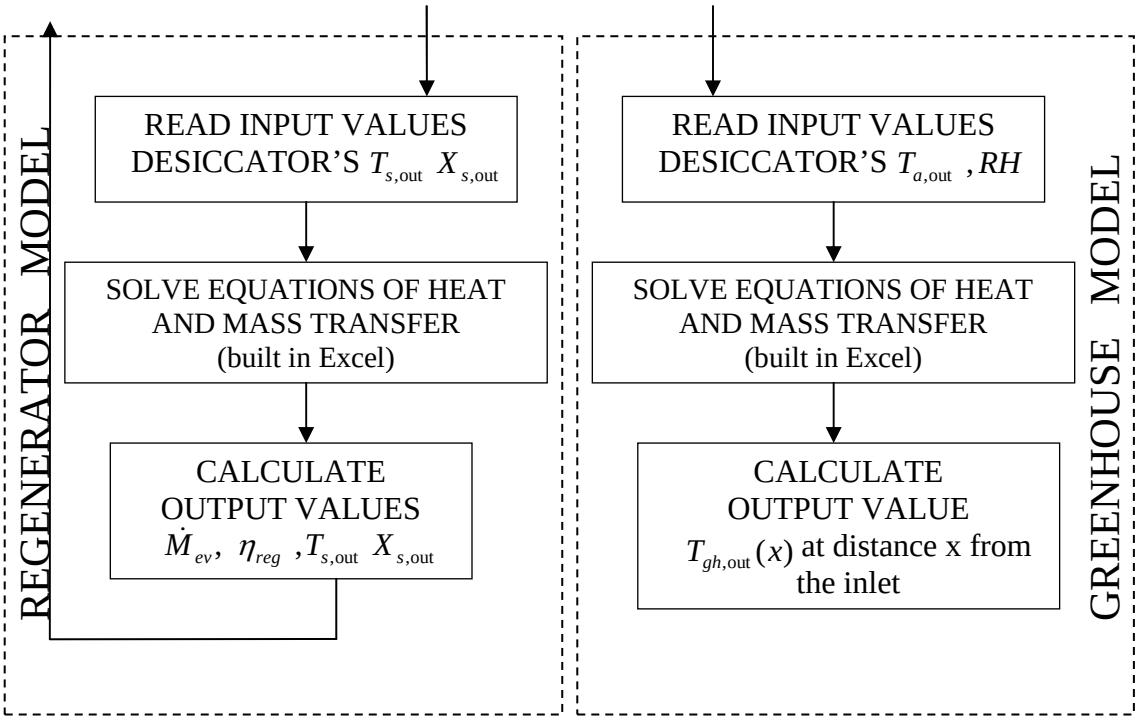

Fig. 6.4: Computer flow diagram.

The results of each simulation are saved to an MSExcel spreadsheet file using the Microsoft Excel output channel. The values of the variables as well the parameters used in the simulation are saved and arranged in worksheets. Fig. 6.5 shows the execution output file of a gPROMS simulation. For each simulation gPROMS solves a system of 80 equations. However, these equations are the ones required by the software in order to communicate with the spreadsheets where most of the heat and mass transfer equations are modelled. Hence in this way the number of the equations modelled in gPROMS is significantly reduced.

The overall system program is designed and written in such a way that makes use of the spreadsheet files where the main equations have been already introduced to check their validity. Thus the simulation results can be verified by the spreadsheets.

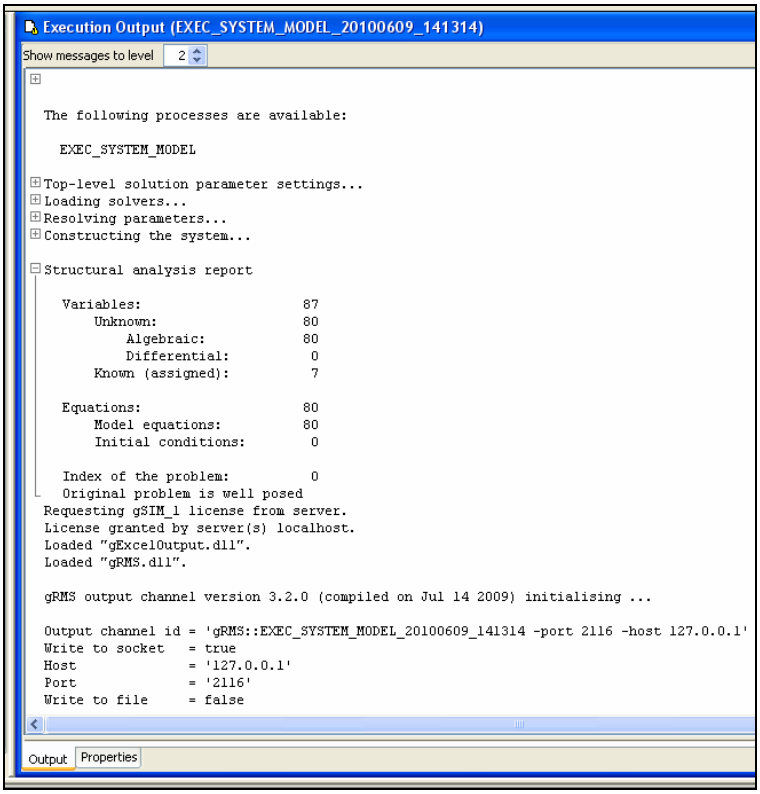

Fig. 6.5: The execution output file of a gPROMS simulation.

6.3 Greenhouse Climate Model

The greenhouse climate model is a simple heat transfer model published in literature (Kittas *et al.*, 2003). Its validity was verified experimentally, the predicted and the experimental values of temperature have a high correlation coefficient R^2 of 91%. It can predict the temperature gradients along a greenhouse cooled with evaporative cooling pads. Here the main equations are presented.

The air temperature along the greenhouse is given by the following equation

$$T_{gh}(x) = T_{amb} + \left[-\eta \cdot \left(T_{amb} - T_{amb,wb} \right) - \frac{A_1}{A_2} \right] \cdot \exp\left(-A_2 \cdot x \right) + \frac{A_1}{A_2} \tag{6.1}$$

where A_1 and A_2 are coefficients determined by

$$A_1 = \frac{\tau \cdot (1-\gamma) \cdot I_R \cdot x}{\dot{V}_a \cdot \rho_a \cdot Cp_a} \tag{6.2}$$

and

$$A_2 = \frac{K_c \cdot x}{\dot{V}_a \cdot \rho_a \cdot Cp_a} \tag{6.3}$$

η is the cooling pad efficiency taken to be 0.8, x is the distance from the inlet of the greenhouse (see Fig. 6.6), τ is the plastic roof transmission equal to 0.60, γ is the plant transpiration coefficient equal to 0.45, $\dot{V}_a$ is the ventilation rate, $T_{\text{amb,wb}}$ is the wet bulb ambient temperature.

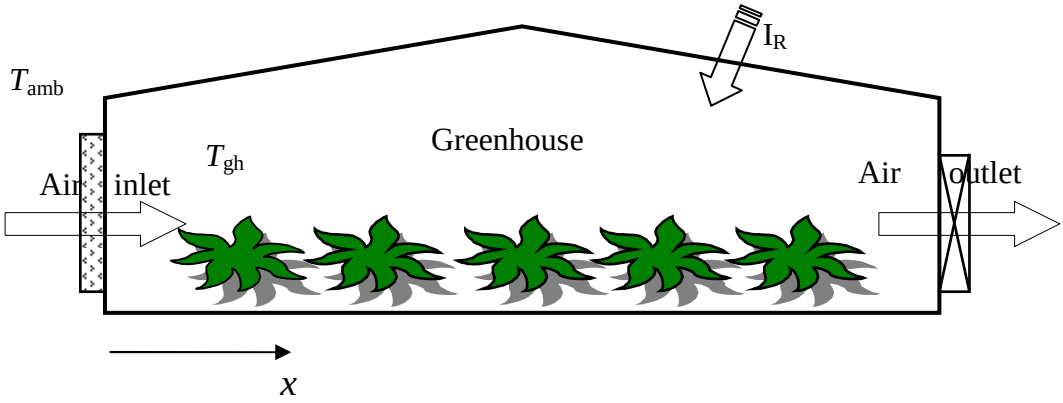

Fig. 6.6: A schematic of the greenhouse.

The calculation of $T_{\text{amb,wb}}$ is done in a spreadsheet with linear interpolation using values from psychometric tables built in Excel with an accuracy of ± 0.4^{o}C.

6.4 Conclusion

The developed computer program of the whole system enables us to combine the essential parts of the proposed cooling system, the regenerator and the desiccator, and investigate its performance when applied to a greenhouse with a fan-to-pad evaporative cooling system. The model can predict the air temperature and RH at the outlet of the desiccator, the air temperature at the inlet/outlet of the greenhouse and the mass fluxes of the evaporated and absorbed water in the regenerator and in the desiccator respectively. The validity of the model was first checked in MSExcel spreadsheets by introducing all the governing equations of heat and mass transfer that define the phenomena of absorption and evaporation in the desiccator and at the regenerator and comparing the predicted values with experimental ones (see chapter 5). Effort was given to finding suitable software that would make use of MSExcel spreadsheets. gPROMS, the software chosen, proved to be a versatile process modelling software that can be used for developing a more complicated system that would incorporate secondary processes such as the fluid circulation pumps and the exhaust fans.

CHAPTER 7. CASE STUDIES

7.1 Introduction

The whole system model developed in gPROMS is used to evaluate the performance of the cooling system when applied to a commercial greenhouse operating under various climatic conditions. Climate is hotter in low latitudes and more humid in coastal areas. Therefore, we emphasized coastal locations in the tropical and subtropical regions where the climate is most likely to be hot and more humid. The proposed cooling system utilises bitterns as liquid desiccants. Another reason for choosing coastal areas is that the greenhouse would be closer to the source of bitterns' production, solar saltworks. The climatic data required for the analysis were obtained by using Meteonorm Version 4.0 software. Cooling systems are usually employed in summer during the hottest hours of the day which are normally between 10:00hrs and 17:00hrs. Therefore, the hottest months (with temperatures exceeding 30^{o}C) were chosen for each location and then the average hourly data over each month of ambient temperature, relative humidity and irradiance were fed into the model.

Fig. 7.1: World map showing the selected countries where the performance of the proposed cooling system was simulated.

Simulations of the system were carried out under the climatic conditions of the following five cities:

- Muscat (Oman)
- Mumbai (India)
- Chittagong (Bangladesh)
- Messina (Italy)
- Havana (Cuba)

The countries for each selected city are illustrated on a world map in Figure 7.1. It is seen that with the exception of Italy all of them are cut by the Tropic of Cancer.

These cities can be categorised according to the Köppen climate classification system. Table 7.1 shows how those cities are classified. A description of the climate symbols and defining criteria are seen on Table A6.2 in appendix 6.

Table 7.1 The cities selected for system simulations and their climate classification.

	City	**Country**	**Climate**	**Köppen classification**
1	Muscat	Oman	Dry	B(wh)
2	Mumbai	India	Tropical	A(w)
3	Chittagong	Bangladesh	Tropical	A(m)
4	Havana	Cuba	Tropical	A(w)
5	Messina	Italy	Temperate	C(sa)

Based on the simulation results the system was optimised for each location and useful conclusions were drawn upon its performance, the design of the desiccator and the size of the regenerator.

7.2 Assumptions and Methodology

The model was parameterized for cooling a 1000m^2 (30mx33.3m) multi arched greenhouse of 4m maximum height covered with double inflated plastic polyethylene-ethylene vinyl acetate films. According to Von Zabeltitz (1999) the pad area of an evaporative cooling system should be about 1m^2 per 20-30m^2 greenhouse area and the maximum fan-to-pad distance should be 30-40m. Hence if the pads are placed over the length of the greenhouse and their height is 1.2m then the total covered area is 40m^2 which satisfies the criterion. In accordance, the dehumidifier should cover the same area.

The evaporative pad and the structured packing of the dehumidifier are made of CELdek® corrugated cellulose paper of 10cm thickness. The efficiency of the fan-pad system is taken to be 0.8. The air velocity inside the greenhouse should be in the range of 0.5-0.7 m s^{-1} since this velocity range is considered optimal for plant growth (ASHRAE, 1985). Thus for an average velocity of 0.5 m s^{-1} inside the greenhouse the ventilation rate was calculated to be 67m^3 h^{-1} by multiplying the velocity with the vertical cross section area of the greenhouse.

The values of cover transmissivity, plant transpiration coefficient and heat loss coefficient required by the greenhouse model are the same as the ones used by Kittas *et al.* (2003). The water mass flow and water temperature inside the cooling tubes were kept constant equal to 0.06 kg s^{-1} and 15^{o}C correspondingly. The solution mass flow is also kept constant equal to 0.0035 kg s^{-1} m^{-2} of regenerator area. The open solar regenerator's performance is highly affected by solar irradiance, ambient temperature, wind and solution mass flow. In this analysis the worst case scenario of no wind was employed. It is to be noted that all the simulations carried out regard steady state analysis.

The total regenerator area A_{tot} required to regenerate the weak desiccant solution at the outlet of the desiccator was calculated from the following formula:

$$A_{tot} = \frac{\dot{M}_{abs}}{\dot{M}_{ev}} \cdot A_{unit} \cdot n \tag{7.1}$$

where A_{unit} is the regenerator area of the regenerator unit taken to be 0.73x3.5 m^2 and *n* is the number of regenerator units required for a 1000 m^2 greenhouse (30 m x 33.3 m) taken to be 222 which is also the number of the experimental structured packing modules required to cover the same size area that the evaporative cooling pads do.

7.3 Simulation Results

7.3.1 Case study 1: Muscat

Oman, like other countries of the Gulf is strongly dependent on food imports almost all year round raising serious concerns about food security. Plant production in open fields is almost infeasible because of the lack of natural water resources and the increased water demand due to the high temperatures. A viable alternative for plant production is cultivation in greenhouses where the environment can be controlled and water

consumption can be minimised. However, temperatures of higher than 30°C inside the greenhouse make plant cultivation impossible. Here we simulate the performance of the cooling system when applied to a greenhouse in Muscat operating during the summer months i.e. in May, June and July. The results of the predicted greenhouse temperature at the outlet of the greenhouse when the liquid desiccant system is used (green dotted line) and when only the evaporative fan-to-pad cooling system is employed (thin brown dotted line) can be seen in Figure 7.2 along with the predicted air temperature at the desiccator

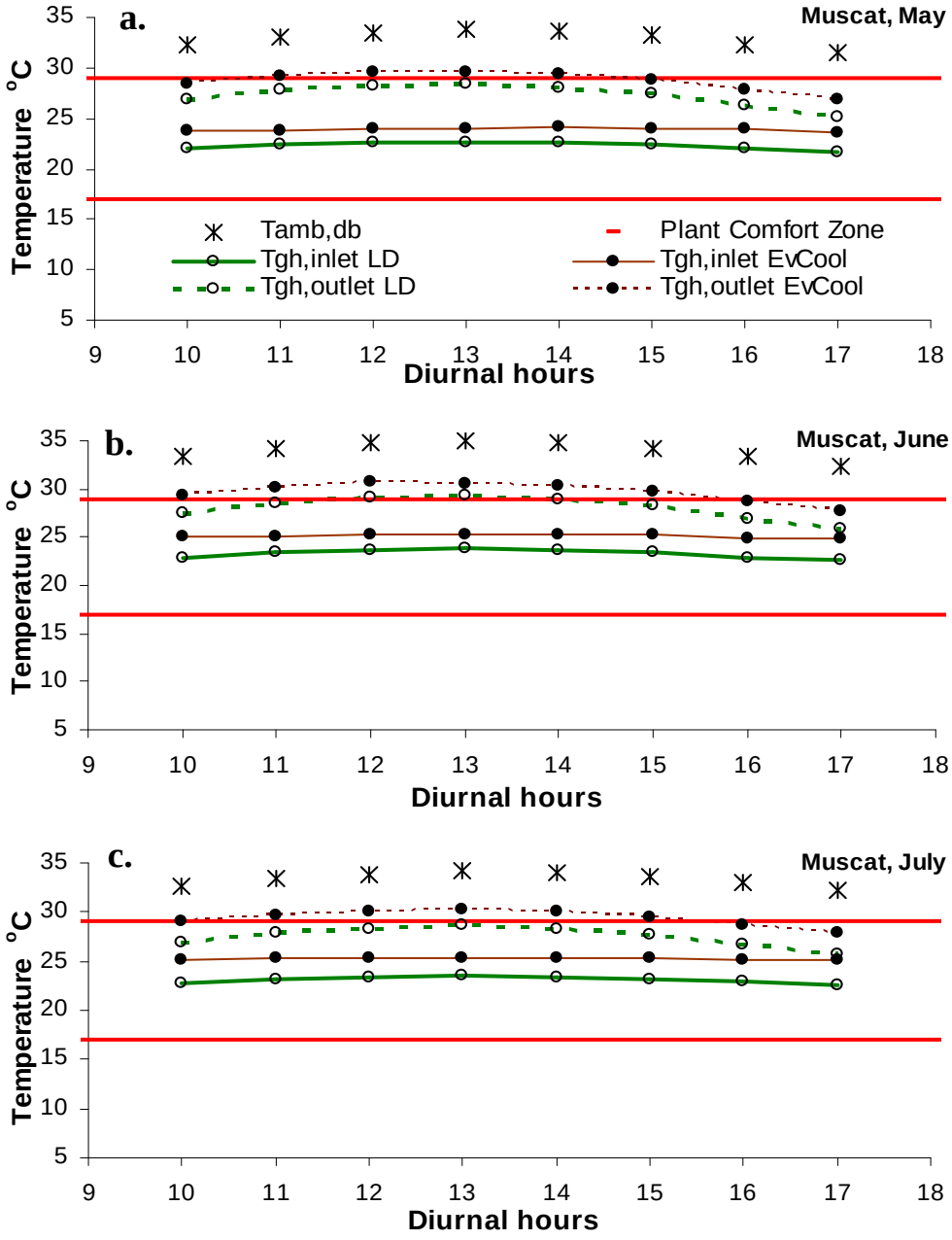

Fig. 7.2: The predicted air temperature at the outlet of the greenhouse with a liquid desiccant cooling system (LD) and without (Evaporative cooling only, EvCool) for a) May, b) June and c) July in Muscat.

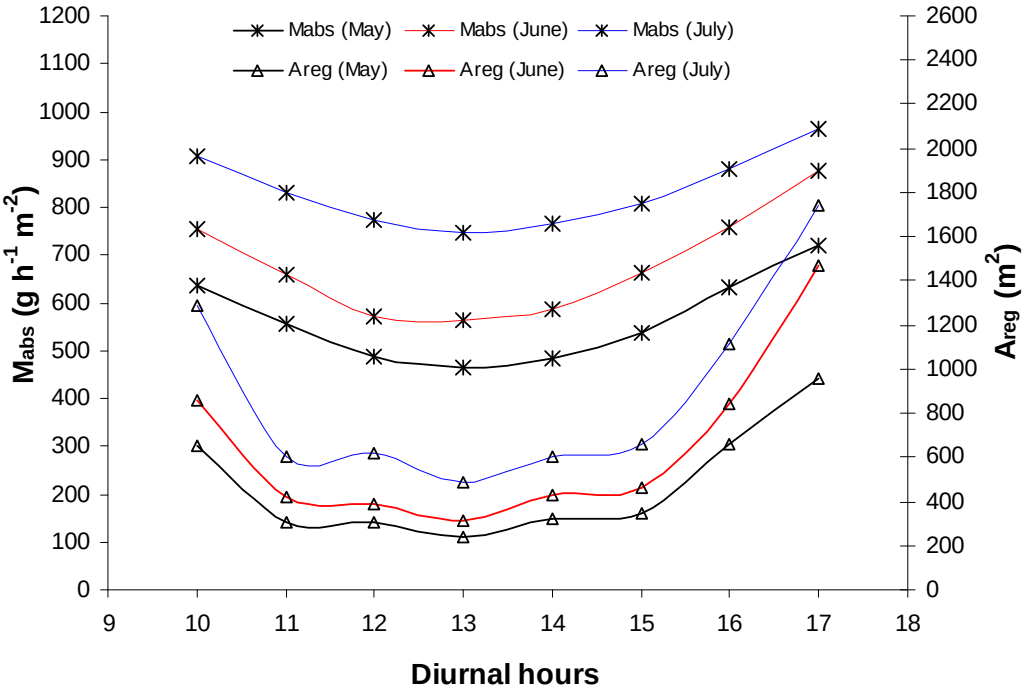

Fig. 7.3: The mass flux of water vapour absorption and the required regenerator area over time for Muscat during May, June and July.

outlet and the ambient dry bulb temperature. The red lines in Fig. 7.2 define the temperature comfort zone of the plants (Zabeltitz, 1999). The mass flux of the absorbed water vapour at the desiccator and the required regenerator area over time for Muscat during May, June and July are illustrated in Figure 7.3.

7.3.2 Case study 2: Mumbai

Food insecurity in India is of different level than of that in the countries of the Gulf. A large part of the total population of approximately 260 million, 22 percent, is undernourished according to FAO (2002) As stated before (see Chapter 1) a key factor in reducing hunger is to increase the agricultural production. Amongst other methods greenhouses can boost the production of crops in existing farmland, thus providing a means to increase agricultural production. In the tropicals the constraints of making feasible the all year crop cultivation inside greenhouses are the excessive heat load and the high humidity during the hot season. High humidity minimises the effect of the evaporative cooling systems.

In this study we simulate the performance of the proposed cooling system when applied to a greenhouse in Mumbai operating during the summer months i.e. in March, April and May. The results of the predicted greenhouse temperature at the outlet of the greenhouse

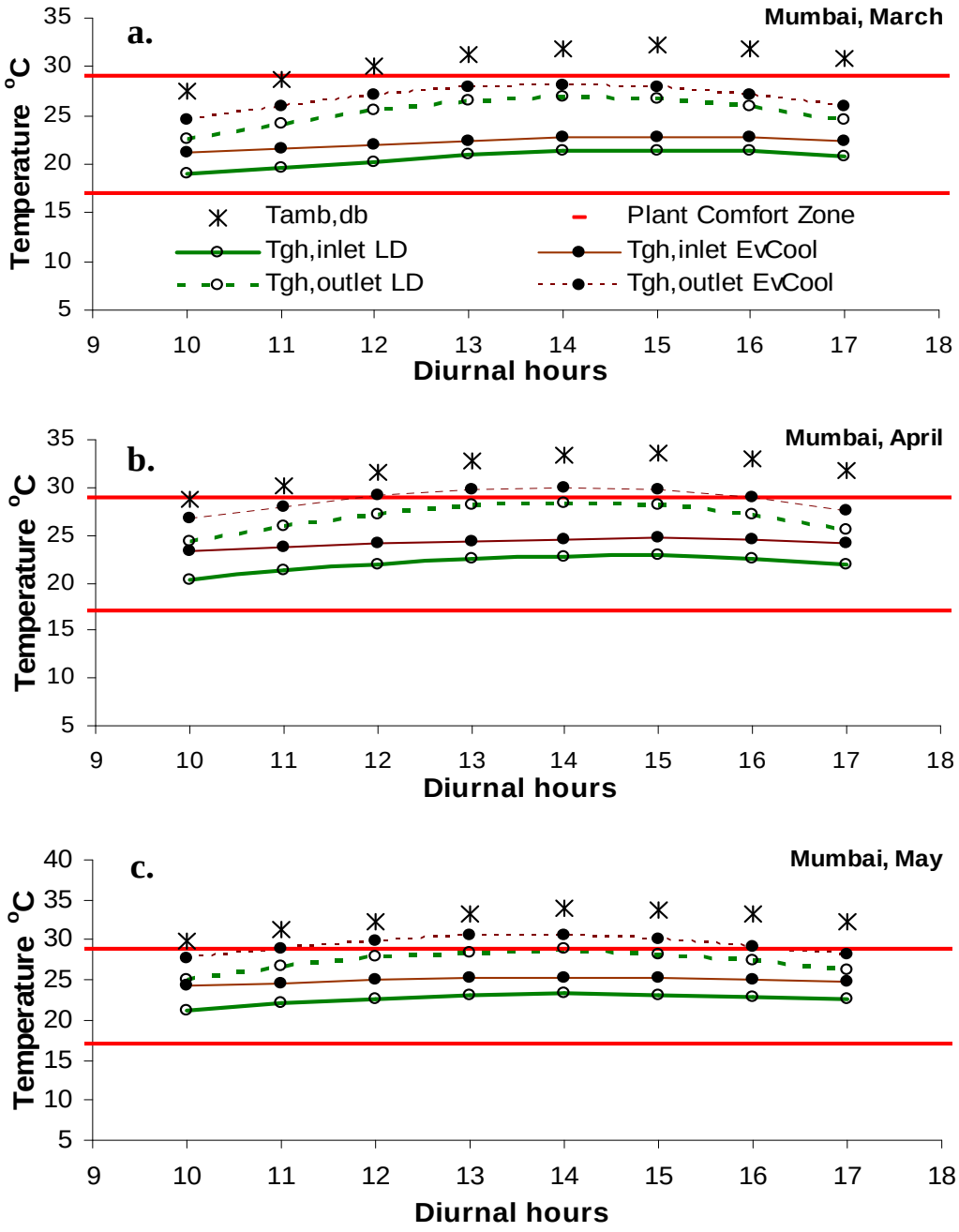

Fig. 7.4: The predicted air temperature at the outlet of the greenhouse with a liquid desiccant cooling system (LD) and without (Evaporative cooling only, EvCool) for a) March, b) April and c) May in Mumbai.

when the liquid desiccant system is used (green dotted line) and when only the evaporative fan-to-pad cooling system is employed (thin brown dotted line) can be seen in Figure 7.4 along with the predicted air temperature at the desiccator outlet and the ambient dry bulb temperature. The mass flux of the absorbed water vapour at the desiccator and the required regenerator area over time for Mumbai during March, April and May are illustrated in Figure 7.5.

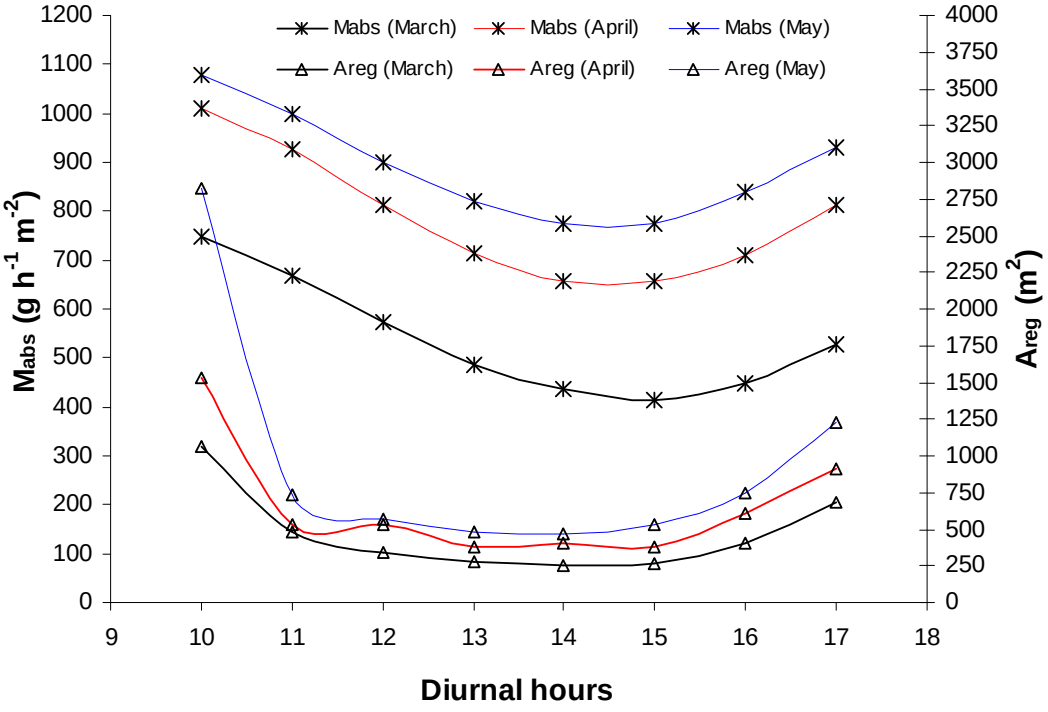

Fig. 7.5: The mass flux of water vapour absorption and the required regenerator area over time for Mumbai during March, April and May.

7.3.3 Case study 3: Chittagong

Food insecurity in Bangladesh is of the same level of that in India. According to FAO a large part of the total population, 26 percent, is undernourished (Food and Agricultural Organization, 2002). Furthermore, Bangladesh is located in the tropical coastal zone and therefore its climate is highly humid and hot during the summer season. If greenhouses are to be used as a means of increasing agricultural production then a cooling system that can maintain the greenhouse air temperature within the plant comfort zone during the hot season is needed. The performance of the proposed cooling system was simulated when applied to a greenhouse in Chittagong, the second largest city of Bangladesh, operating during the summer months i.e. in April, May and June.

The results of the predicted greenhouse temperature at the outlet of the greenhouse when the liquid desiccant system is used (green dotted line) and when only the evaporative fan-to-pad cooling system is employed (thin brown dotted line) can be seen in Figure 7.6 along with the predicted air temperature at the desiccator outlet and the ambient dry bulb temperature. The mass flux of the absorbed water vapour at the desiccator and the required regenerator area over time for Chittagong during March, April and May are illustrated in Figure 7.7.

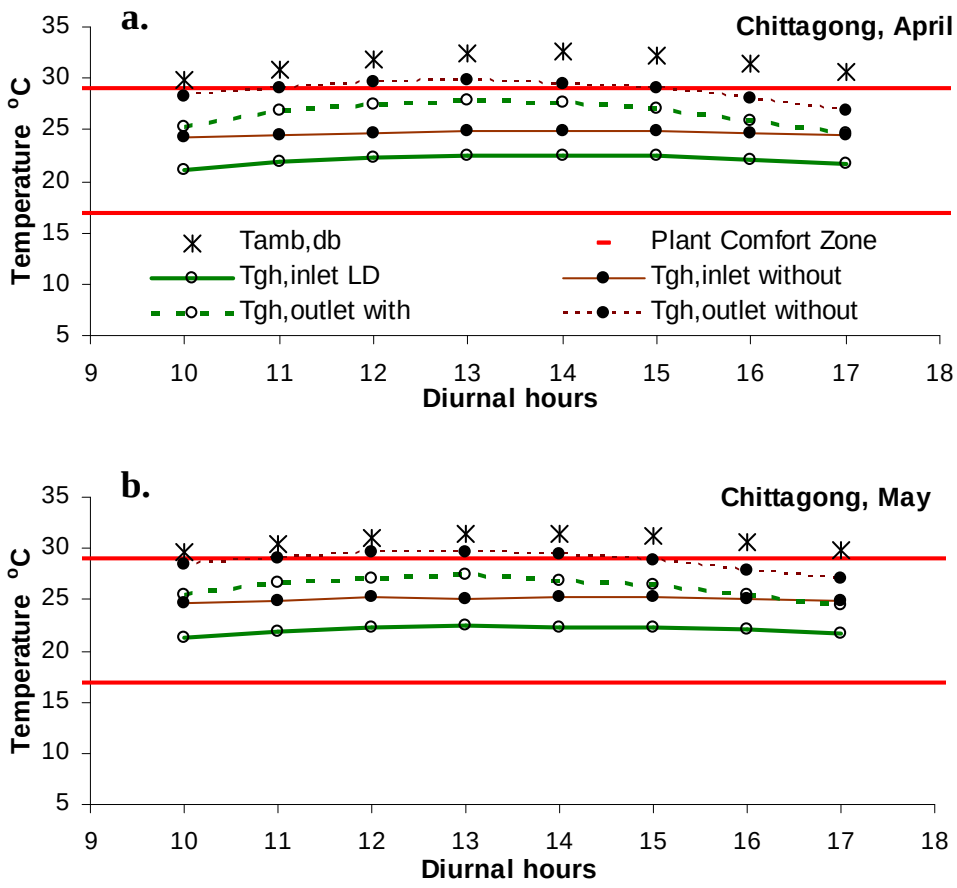

(Fig. 7.6 continued)

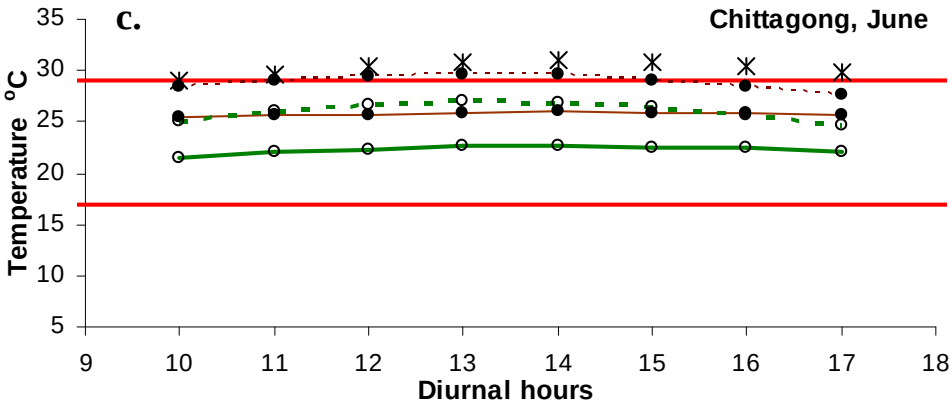

Fig. 7.6: The predicted air temperature at the outlet of the greenhouse with a liquid desiccant cooling system (LD) and without (Evaporative cooling only, EvCool) for a) April, b) May and c) June in Chittagong.

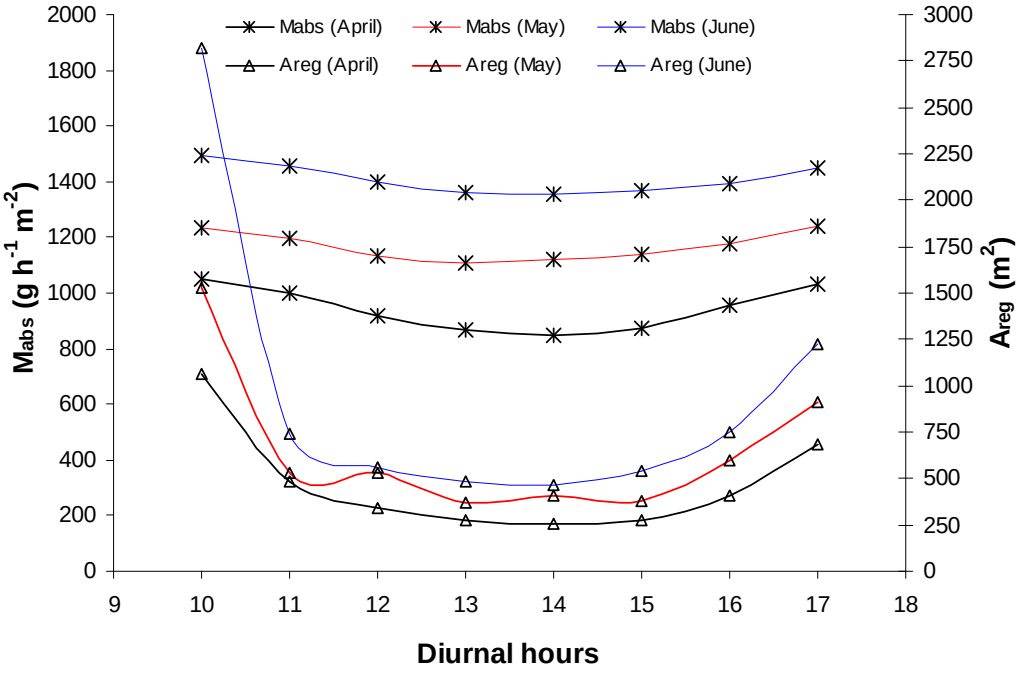

Fig. 7.7: The mass flux of water vapour absorption and the required regenerator area over time for Chittagong during April, May and June.

7.3.4 Case study 4: Havana

Cuba's food security level is similar to that of the Gulf countries due to other reasons though. After the collapse of its sugar sector there was a shift away from large scale agricultural production. Smaller scale systems have been used using sustainable practices

for organic production. These systems may be efficient with regard to energy use and better quality crop production but is of low agricultural production. In Cuba 84 percent of all food consumed is imported (FAS/USDA, 2008). Food security risks can be reduced if agricultural production is increased. Greenhouses can help achieving higher crop yields all year round. However, all year round cultivation can be feasible if during the hot season the greenhouse temperature is maintained within the plant comfort zone. Here, we simulate the performance of the cooling system when applied to a greenhouse in Havana operating during the summer months i.e. in July, August and September.

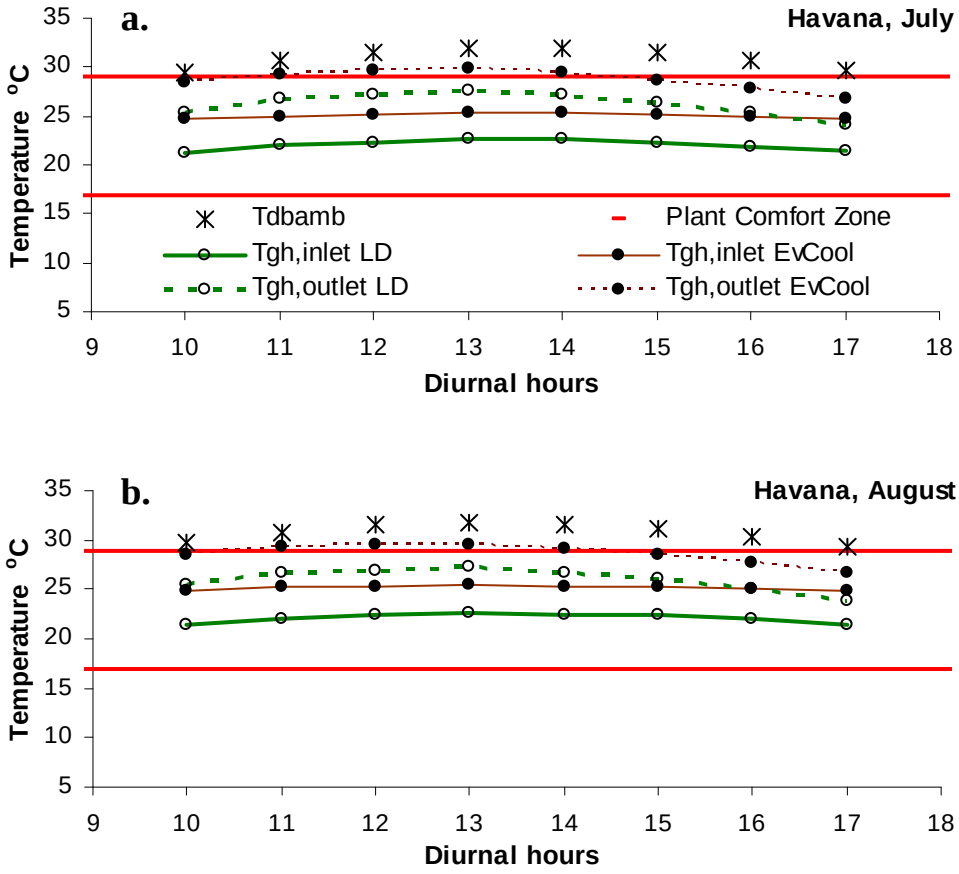

(Fig. 7.8 continued)

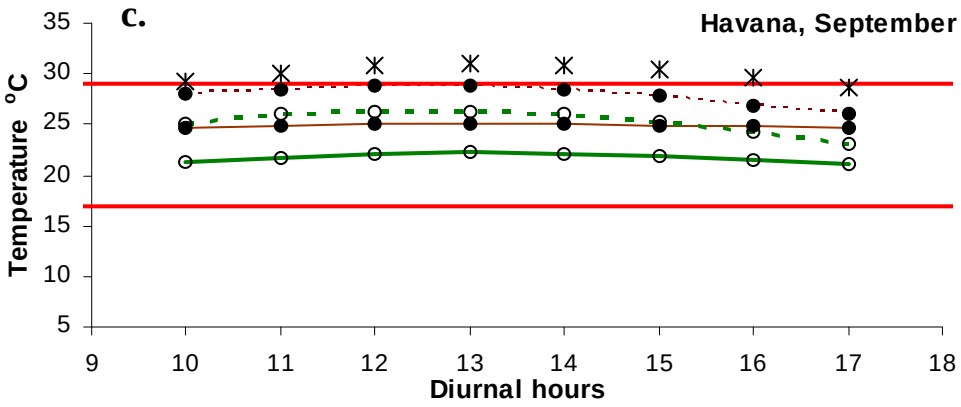

Fig. 7.8: The predicted air temperature at the outlet of the greenhouse with a liquid desiccant cooling system (LD) and without (Evaporative cooling only, EvCool) for a) July, b) August and c) September in Havana.

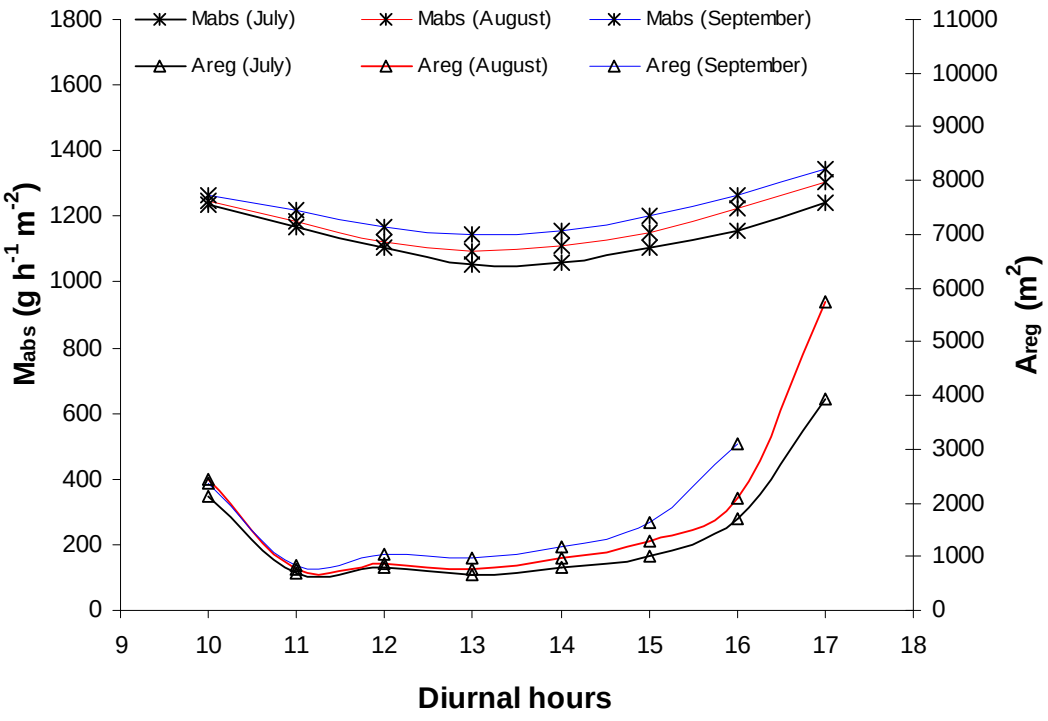

Fig. 7.9: The mass flux of water vapour absorption and the required regenerator area over time for Havana during July, August and September.

The results of the predicted greenhouse temperature at the outlet of the greenhouse when the liquid desiccant system is used (green dotted line) and when only the evaporative fan-to-pad cooling system is employed (thin brown dotted line) can be seen in Figure 7.8 along

with the predicted air temperature at the desiccator outlet and the ambient dry bulb temperature. The mass flux of the absorbed water vapour at the desiccator and the required regenerator area over time for Havana are illustrated in Figure 7.9.

7.3.5 Case study 5: Messina

In the south European countries, such as Italy, Spain, Cyprus and Greece, evaporative cooling normally addresses the problem of summer high temperatures induced inside greenhouses satisfactorily. However, heat waves are often with temperatures exceeding 35^{o}C during summer. The plant response to heat stress varies depending on the cultivar species e.g. leafy vegetables are more sensitive. However, it can cause serious physiological disorders and even plant death. This, in accordance, leads to quality degradation and reduced yields. Many greenhouse growers do not grow crops during summer because of those reasons. Here we investigate the performance of the proposed cooling system in Messina (Italy) as a means of better temperature control inside the greenhouses during the hottest months of the year i.e. July and August.

The results of the predicted greenhouse temperature at the outlet of the greenhouse when the liquid desiccant system is used (green dotted line) and when only the evaporative fan-to-pad cooling system is employed (thin brown dotted line) can be seen in Figure 7.10 along with the predicted air temperature at the desiccator outlet and the ambient dry bulb temperature. The mass flux of the absorbed water vapour at the desiccator and the required regenerator area over time for Messina during July and August are illustrated in Figure 7.11.

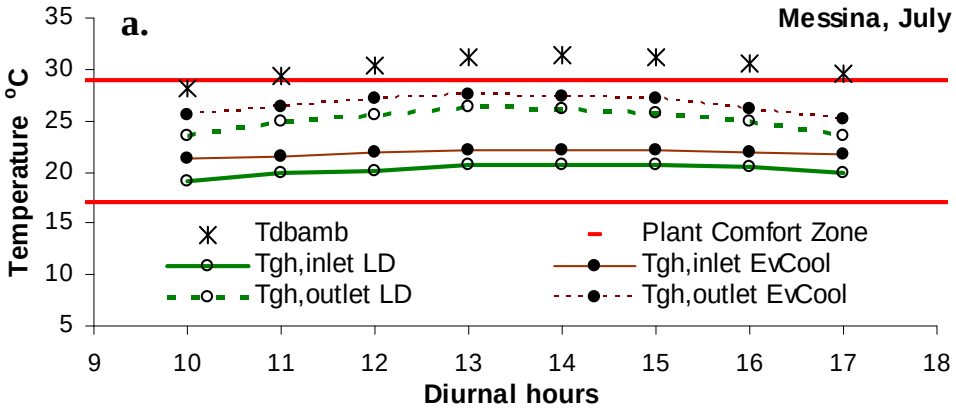

(Fig. 7.10 continued)

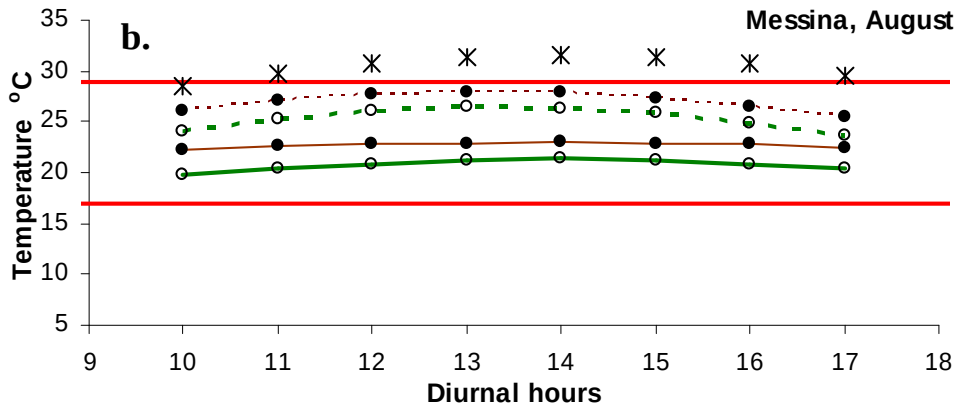

Fig. 7.10: The predicted air temperature at the outlet of the greenhouse with a liquid desiccant cooling system (LD) and without (Evaporative cooling only, EvCool) for a) July and b) August in Messina.

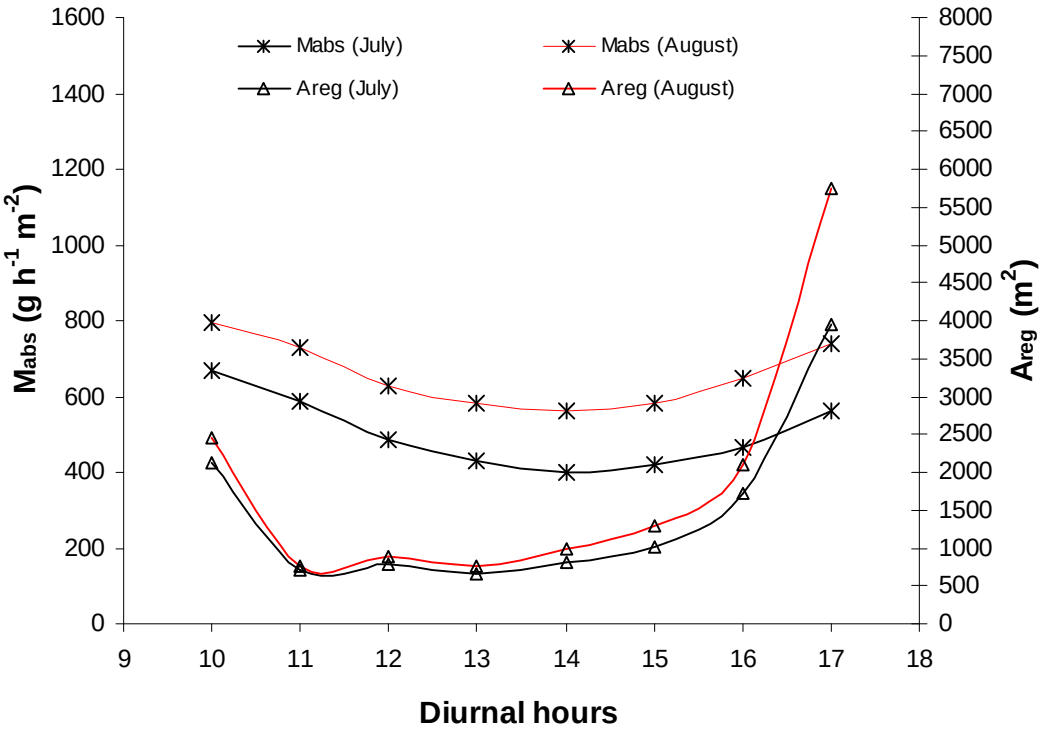

Fig. 7.11: The mass flux of water vapour absorption and the required regenerator area over time for Messina during July and August.

Analytical tables of the predicted temperatures for each case study can be found in appendix 7.

7.4 Optimisation

To find the optimum operational conditions of an open system, such as the one under study, can be cumbersome because it is affected by many parameters and especially by the climate. The performance of the flat plate open regenerator, for example, is strongly dependent on the ambient conditions. Here we mainly look into optimising the performance of the desiccator since it is the core component of the system that produces the cooling effect.

The performance of the desiccator is more easily controlled by changing design parameters such as the thickness of the structured packing material or by adjusting the air mass flow rate and the solution mass flow rate. However there are limitations to the changes that can be made. When increasing the thickness of the structured packing material pressure drop increases, thus resulting in higher energy consumption by the exhaust fans. There are also limitations to the air mass flow rate/ventilation rate since there is an optimum range of average air velocity (0.5 - 0.7 m s^{-1}) for plant cultivation inside greenhouses. High mass flow rates can cause flooding and carry over effects in the process air resulting in the contamination of the soil and the air of the greenhouse.

In this analysis the thickness of the desiccator was increased to 0.2m and consequently the number of cooling tubes was doubled. The model was parameterised accordingly and simulations of the performance of the system were carried out for each location as in section 7.3. It is to be noted though that this time the analysis was carried out for two scenarios. Based on the simulations of section 7.3 the lowest and highest performance (cooling effect) of the system was observed and these were chosen to be the climatic conditions that fed the model. Hence there are two scenarios i.e. the low performance (dry conditions) and the high performance scenario (humid conditions) for each location.

Following the same methodology as before, simulations were also carried out using higher air mass flow (with a 0.1m thickness desiccator pad) or ventilation rate of 93.3 m^3 s^{-1} that corresponds to an average air velocity of 0.7 m s^{-1} inside the greenhouse. In summary the following three set up treatments were investigated:

1. Desiccator thickness = 0.1m and Ventilation rate = 66.7 m^3 s^{-1}
2. Desiccator thickness = 0.2m and Ventilation rate = 66.7 m^3 s^{-1}

3. Desiccator thickness = 0.1m and Ventilation rate = 93.3 $m^3 s^{-1}$

The pressure drop for each set up was calculated based on Celdek® spec. sheet (see appendix 7, Fig. A7.1). Regarding the first and second set up, the Celdek® pad surface velocity was estimated to be 1.66 m s^{-1} that corresponds to approximately 45Pa and 70Pa pressure drop respectively. Regarding the third set up, the Celdek® pad surface velocity was estimated to be 2.33 m s^{-1} that corresponds to a 95Pa pressure drop.

Finally, the liquid desiccant system (LDCS) was compared to a fan-to-pad evaporative cooling system (EvCool). The predicted temperatures at the outlet of the greenhouse along with the ambient conditions in Mumbai, Muscat, Chittagong, Havana and Messina when using the LDCS and with EvCool only can be seen in Tables 2 – 7. The last column of the tables headed $\boldsymbol{T}_{gh}^{out}\Big|_{LDCS}^{EVCool}$ is the temperature difference between the air temperature at the outlet of the greenhouse with LDCS and the air temperature at the outlet of the greenhouse with EvCool only. It represents the additional cooling effect achieved by the proposed liquid cooling system when compared to the fan-to-pad evaporative cooling system. The mass flux of water absorption and the required regenerator area for each location are presented in Table 7.7.

7.5 Discussion

The analysis in section 7.3 showed that the first set up with LDCS improved cooling in Mumbai, Muscat, Chittagong, Havana and Messina by 1.2–2.7^{o}C, 1.1–2.2^{o}C, 1.9–3.3^{o}C, 2.3–3^{o}C and 1.2–2.1^{o}C respectively. In Mumbai the lowest cooling effect is of 1.2^{o}C observed at 32^{o}C ambient temperature and 47%RH while the highest is of 2.7^{o}C observed at 29^{o}C and 65%RH. In Muscat the lowest cooling effect is of 1.1^{o}C observed at 33.8^{o}C ambient temperature and 47%RH while the highest is of 2.2^{o}C observed at 32.6^{o}C and 57%RH. In Chittagong the lowest cooling effect is of 1.9^{o}C observed at 32.4^{o}C ambient temperature and 56%RH while the highest is of 3.3^{o}C observed at 29^{o}C and 78%RH. In Havana the lowest cooling effect is of 2.3^{o}C observed at 31.9^{o}C ambient temperature and 61%RH while the highest is of 3^{o}C observed at 29.7^{o}C and 70%RH. In Messina the lowest cooling effect is of 1.2^{o}C observed at 31.3^{o}C ambient temperature and 47%RH while the highest is of 2.1^{o}C observed at 28.6^{o}C and 60%RH. The predicted required regenerator area in Mumbai, Muscat, Chittagong, Havana and Messina varied from 255 m^2 to 2823 m^2, 242 m^2 to 1291 m^2 , 482 m^2 to 2834 m^2, 648 m^2 to 2451 m^2 and 260 m^2 to 969 m^2

correspondingly. Figures 7.3, 7.5, 7.7, 7.9 and 7.11 can be used for sizing the regenerator. For example in Muscat (see Fig. 7.3) the hottest and more humid month, July, sets the limit for the size of the regenerator which should be no less than 1000 m^2. Similarly for Mumbai this could be 1250 m^2, for Chittagong 1500 m^2, for Havana 3000 m^2 and for Messina 1150 m^2.

The second set up with LDCS (0.2m desiccator) improved cooling in Mumbai, Muscat, Chittagong, Havana and Messina by 2.4–4.9^oC, 2.3–3.7^oC, 3.1–5.6^oC, 4-5.4^oC and 2.2–3.8^oC respectively. In this set up the predicted required regenerator area in Mumbai, Muscat, Chittagong, Havana and Messina varied from 421 m^2 to 4440 m^2, 416 m^2 to 2042 m^2, 760 m^2 to 4152 m^2, 996 m^2 to 3659 m^2 and 480 m^2 to 2488 m^2 respectively.

Regarding the third set up with LDCS, cooling was improved in Mumbai, Muscat, Chittagong, Havana and Messina by 1.2–2.4^oC, 0.9–1.9^oC, 1.7–2.9^oC, 2.1–2.7^oC and 1.1–1.9^oC correspondingly. Furthermore, the predicted required regenerator area in Mumbai, Muscat, Chittagong, Havana and Messina varied from 342 m^2 to 3808 m^2, 369 m^2 to 1570 m^2, 649 m^2 to 3379 m^2, 871 m^2 to 2898 m^2 and 369 m^2 to 1306 m^2 respectively.

The best cooling performance was observed in the second set up. In comparison to the first one there was a 39-52% increase of cooling. This can be explained by the fact that a thicker desiccator provides a larger wetted surface area and thus better dehumidification efficiency. Consequently the air becomes drier and in accordance the cooling effect is increased when passing through the evaporative cooling pad.

The third set up (higher ventilation rate) did not improve the cooling performance. In fact when compared to the first set up there was a 0-15% decrease of cooling. This may partially attributed to the fact that the air leaving the desiccator is less cooled because at this air mass flow rate the internal cooling tubes absorb less sensible heat from the air (the residence time of air in contact with the tubes is lesser than before). In addition the increased predicted mass flow rates of water absorption in the third set up are mainly due to the relatively higher air mass flow rate. In the simulations the mass flow rate of water absorption is calculated by the following formula:

$$M_{\mathrm{abs}} = M_{\mathrm{a}} \cdot \sum_{i=1,n} \Delta\omega_{\mathrm{a}} \tag{7.1}$$

Table 7.2 The optimisation results for Mumbai with LDCS (liquid desiccant cooling system) and evaporative cooling only (EvCool).

Mumbai		**LDCS**				**EvCool**				$T_{gh}^{out}\Big\vert_{LDCS}^{EVCool}$
Set up	*Scenario*	T_{gh}^{out} (°C)	$T_{des,db}^{out}$ (°C)	$RH_{des,db}^{out}$ %	$T_{des,wb}^{out}$ (°C)	T_{gh}^{out} (°C)	$T_{amb,db}$ (°C)	RH_{amb}%	$T_{amb,wb}$ (°C)	
Des. Thickness = 10cm	low	26.9	30.9	44	21.4	28.1	31.9	47	22.8	-1.2
Ven. Rate = 66.7 m^3 s^{-1}	high	25.0	28.2	56	21.2	27.8	29.8	66	24.3	-2.7
Des. Thickness = 20cm	low	25.7	29.9	43	20.2	28.1	31.9	47	22.8	-2.4
Ven. Rate = 66.7 m^3 s^{-1}	high	22.9	26.5	51	18.9	27.8	29.8	66	24.3	-4.9
Des. Thickness = 10cm	low	26.0	31.2	44	21.4	27.1	31.9	47	22.8	-1.2
Ven. Rate = 93.3 m^3 s^{-1}	high	24.7	28.7	55	21.4	27.1	29.8	66	24.3	-2.4

Table 7.3 The optimisation results for Muscat with LDCS (liquid desiccant cooling system) and evaporative cooling only (EvCool).

Muscat		**LDCS**				**EvCool**				$T_{gh}^{out}\Big\vert_{LDCS}^{EVCool}$
Set up	*Scenario*	T_{gh}^{out} (°C)	$T_{des,db}^{out}$ (°C)	$RH_{des,db}^{out}$ %	$T_{des,wb}^{out}$ (°C)	T_{gh}^{out} (°C)	$T_{amb,db}$ (°C)	RH_{amb}%	$T_{amb,wb}$ (°C)	
Des. Thickness = 10cm	low	28.5	32.9	43	22.7	29.6	33.8	47	24	-1.1
Ven. Rate = 66.7 m^3 s^{-1}	high	26.9	31.4	50	22.7	29.1	32.6	57	25.2	-2.2
Des. Thickness = 20cm	low	27.3	31.7	43	21.5	29.6	33.8	47	24	-2.3
Ven. Rate = 66.7 m^3 s^{-1}	high	25.4	30.1	46	21.1	29.1	32.6	57	25.2	-3.7
Des. Thickness = 10cm	low	27.6	33.1	43	22.9	28.6	33.8	47	24	-0.9
Ven. Rate = 93.3 m^3 s^{-1}	high	26.5	31.8	49	23	28.4	32.6	57	25.2	-1.9

Table 7.4 The optimisation results for Chittogong with LDCS (liquid desiccant cooling system) and evaporative cooling only (EvCool).

Chittagong		**LDCS**				**EvCool**				$T_{gh}^{out}\Big\vert_{LDCS}^{EVCool}$
Set up	*Scenario*	T_{gh}^{out} (°C)	$T_{des,db}^{out}$ (°C)	$RH_{des,db}^{out}$ %	$T_{des,wb}^{out}$ (°C)	T_{gh}^{out} (°C)	$T_{amb,db}$ (°C)	RH_{amb}%	$T_{amb,wb}$ (°C)	
Des. Thickness = 10cm	low	27.9	31.5	48	22.6	29.8	32.4	56	24.8	-1.9
Ven. Rate = 66.7 m^3 s^{-1}	high	25.1	27.6	61	21.5	28.4	29.0	78	25.4	-3.3
Des. Thickness = 20cm	low	26.7	30.8	45	21.3	29.8	32.4	56	24.8	-3.1
Ven. Rate = 66.7 m^3 s^{-1}	high	22.8	26.1	53	19.0	28.4	29.0	78	25.4	-5.6
Des. Thickness = 10cm	low	27.2	31.7	48	22.8	28.8	32.4	56	24.8	-1.7
Ven. Rate = 93.3 m^3 s^{-1}	high	24.8	28.0	61	21.9	27.7	29.0	78	25.4	-2.9

Table 7.5 The optimisation results for Havana with LDCS (liquid desiccant cooling system) and evaporative cooling only (EvCool).

Havana		LDCS				EvCool				$T_{gh}^{out}\Big\vert_{LDCS}^{EVCool}$
Set up	*Scenario*	T_{gh}^{out} (°C)	$T_{des,db}^{out}$ (°C)	$RH_{des,db}^{out}$ %	$T_{des,wb}^{out}$ (°C)	T_{gh}^{out} (°C)	$T_{amb,db}$ (°C)	RH_{amb}%	$T_{amb,wb}$ (°C)	
Des. Thickness = 10cm Ven. Rate = 66.7 m^3 s^{-1}	low	27.6	31	51	22.6	29.9	31.9	61	25.4	-2.3
	high	25.6	28	58	21.5	28.6	29.7	70	25	-3
Des. Thickness = 20cm Ven. Rate = 66.7 m^3 s^{-1}	low	25.9	29.9	46	20.8	29.9	31.9	61	25.4	-4
	high	23.2	26.2	52	19	28.6	29.7	70	25	-5.4
Des. Thickness = 10cm Ven. Rate = 93.3 m^3 s^{-1}	low	26.9	31.3	51	22.8	29	31.9	61	25.4	-2.1
	high	25.1	28.5	57	21.8	27.8	29.7	70	25	-2.7

Table 7.6 The optimisation results for Messina with LDCS (liquid desiccant cooling system) and evaporative cooling only (EvCool).

Messina		LDCS				EvCool				$T_{gh}^{out}\Big\vert_{LDCS}^{EVCool}$
Set up	*Scenario*	T_{gh}^{out} (°C)	$T_{des,db}^{out}$ (°C)	$RH_{des,db}^{out}$ %	$T_{des,wb}^{out}$ (°C)	T_{gh}^{out} (°C)	$T_{amb,db}$ (°C)	RH_{amb}%	$T_{amb,wb}$ (°C)	
Des. Thickness = 10cm Ven. Rate = 66.7 m^3 s^{-1}	low	26.2	30.2	44	20.8	27.4	31.3	47	22.1	-1.2
	high	24	27.4	51	19.8	26.2	28.6	60	22.2	-2.1
Des. Thickness = 20cm Ven. Rate = 66.7 m^3 s^{-1}	low	25.2	29.4	42	19.8	27.4	31.3	47	22.1	-2.2
	high	22.4	26	47	18.1	26.2	28.6	60	22.2	-3.8
Des. Thickness = 10cm Ven. Rate = 93.3 m^3 s^{-1}	low	25.3	30.5	44	20.9	26.4	31.3	47	22.1	-1.1
	high	23.5	27.7	51	19.9	25.4	28.6	60	22.2	-1.9

Table 7.7 The mass flux of water absorption for each location and the required regenerator area

		Muscat		Mumbai		Chittagong		Havana		Messina	
Set up	*Scenario*	M_{abs} (g h^{-1} m^{-2})	A_{reg} (m^2)	M_{abs} (g h^{-1} m^{-2})	A_{reg} (m^2)	M_{abs} (g h^{-1} m^{-2})	A_{reg} (m^2)	M_{abs} (g h^{-1} m^{-2})	A_{reg} (m^2)	M_{abs} (g h^{-1} m^{-2})	A_{reg} (m^2)
Des. Thickness = 10cm Ven. Rate = 66.7 m^3 s^{-1}	low	467	242	438	255	865	482	1056	648	402	260
	high	908	1291	1080	2823	1495	2834	1246	2451	795	969
Des. Thickness = 20cm Ven. Rate = 66.7 m^3 s^{-1}	low	772	416	724	421	1363	760	1625	996	680	480
	high	1427	2042	1699	4440	2281	4152	1948	3659	2049	2488
Des. Thickness = 10cm Ven. Rate = 93.3 m^3 s^{-1}	low	627	369	589	342	1164	649	1421	871	539	369
	high	1226	1570	1457	3808	2017	3379	1685	2898	1072	1306

where M_a is the air mass flow rate through a desiccator unit and $\sum_{i=1,n} \Delta\omega_a$ is the sum of the absolute humidity change in all the finite elements of the unit. The ventilation rate and hence the mass flow rate are 10 times higher in magnitude than $\sum_{i=1,n} \Delta\omega_a$. Consequently, even though there is a low water vapour absorption rate in the desiccator this is counterbalanced by the air mass flow rate. In accordance the mass flux of water absorption is higher despite the fact that the RH of the air leaving the desiccator in the third set up is similar to that of the first one.

7.6 Conclusion

The case studies showed the potential of the cooling system when applied to a greenhouse located in Mumbai, Muscat, Chittagong, Havana and Messina. It was found that the proposed cooling system can improve cooling by 2.3–5.6^{o}C. The initial set up managed to maintain the greenhouse air temperature within the plant comfort zone in Mumbai, Chittagong, Havana and Messina during the hot season for each location. In Muscat, it managed to maintain the greenhouse air temperature below 30^{o}C marginally. However, when the system was optimised by increasing the thickness of the desiccator cooling was improved in all cases and thus the greenhouse air temperature was within the desired range. Where the evaporative cooling system failed to produce enough cooling e.g. in Mumbai, Muscat, Chittagong and Havana the proposed cooling system achieved further cooling which was enough to sustain the greenhouse air temperature below 30^{o}C. Furthermore, the simulations pointed out the regenerator's size requirements thus enabling us to set a benchmark for the regenerator size to each location based on the hottest and more humid month. It was also resulted that the system performed better under humid conditions. The more humid the air is the better the cooling performance. Lastly the optimisation simulations showed that the thickness of the desiccator is an important design parameter and that a high ventilation rate does not necessarily improve cooling but can cause an adverse effect.

CHAPTER 8. CONCLUSIONS

This Chapter responds to the aim and objectives set out in Chapter 1. For each objective in turn, it recapitulates the research outcomes and activities that led to them. Following on from this, it responds concisely to the overall aim that was achieved through those objectives. The original contributions to knowledge arising from this work are highlighted throughout. The limitations of the study are also recognised; consequently, the Chapter finishes with recommendations of further work that would be required before realising the solar-powered liquid desiccant cooling system forming the subject matter of this thesis.

The Chapter can also be read as an extended summary of the whole thesis.

8.1 Responses to the Objectives

Objective 1: *To determine the properties of concentrated salt solutions obtainable from seawater, consisting of magnesium chloride and impurities including calcium, sodium and sulphate ions. Properties to be measured include vapour pressure, density and viscosity.*

This objective was achieved in Chapter 3. Measurements were carried out on salt solutions made up in the laboratory by mixing salts (sodium chloride, potassium chloride, magnesium chloride, magnesium sulphate, calcium chloride and lithium chloride) with water to achieve the composition of bitterns (ie. concentrated seawater brines) occurring in solar-salt works as reported in the literature Amdouni (2000). Vapour pressure was measured using an isoteniscope; density using a pyknometer; viscosity using a U tube viscometer.

We also carried out a literature review of the theory of the physical properties of electrolyte solutions that enabled us to find suitable mathematical models for predicting water activity (and thus water vapour pressure), density and dynamic viscosity. Six models that can predict these properties as a function of the composition, concentration and temperature were identified and then verified by the experimental results since their accuracy was previously guaranteed for more dilute solutions (up to 6molal). The outcome of this is a simple mathematical model based on the theory of Zdanovskii–Stokes–Robinson could be used to predict the physical properties of bitterns in the design of the

proposed cooling system to within an accuracy of 96 percent. This study also showed that the properties of bitterns are similar to those of pure magnesium chloride solution. The maximum density measured was 1339 kg/m^3; the dynamic viscosity of the most concentrated brine measured was 13.2 mPa.s. Especially vapour pressure was found to be less affected by the presence of impurities. In fact the lowest measured equilibrium relative humidity in the brines investigated was 34% which is close to that of pure saturated $MgCl_2$ 32.8%. The latter confirmed the predictions of the work of Davies and Knowles (2006) that proposed (based on the literature but without any experimental or detailed theoretical investigation) the possibility of using bitterns as liquid desiccants for greenhouse cooling.

The original contributions to knowledge made by this Chapter are therefore:

- Quantitative knowledge, obtained through experiment and theory, of the properties of concentrated seawater bitterns with regard to liquid desiccant cooling
- Identification of the appropriate theory to represent these properties as a function of chemical composition.

The work of Chapter 3 has been published in *Desalination* (Lychnos *et al.*, 2010a)

Objective 2: *To review the state of the art in greenhouse cooling technology. This will set a benchmark against which any new system must be judged and will define the original contribution of this thesis.*

This objective was achieved in Chapter 2. This review looked into the main greenhouse cooling methods that have been under research for many years and have become commercial such as ventilation, shading and reflection, and evaporative cooling. The physical process of each method was described and thus useful conclusions were drawn about their cooling capacity. It was found that ventilation provides sufficient cooling for greenhouses located in high latitudes of the temperate zone. However, in lower latitudes ventilation does not provide enough cooling. In the subtropics, additional methods to ventilation are used for cooling e.g. shading-reflection. In warmer climates the need for cooling is stronger and thus the combination of ventilation and shading-reflection fails to produce enough cooling. Instead evaporative cooling methods (fan-pad and fog-mist) have proved to be the most effective, especially, in hot and dry climates. However, even this method which is considered the state-of-the-art in greenhouse cooling can only achieve a marginal decrease in greenhouse air temperature by 2^{o}C during 12-14hrs (high irradiance,

high ambient relative humidity ~ 75%) or sustain temperature at the ambient level under hot and humid conditions (Ambient temperature>35^{o}C, RH>65%) thus not being able to maintain the air temperature within the plant comfort zone (17^{o}C – 29^{o}C). Therefore it was concluded that the current greenhouse cooling technology cannot address the problem of the excessive heat load during summer in hot and humid places. The liquid desiccant cooling system emerges from this review as an option that could lower summer temperature by 5°C according to claims made in the literature (Davies, 2005), thus providing the starting point for the detailed work of this thesis.

As a result of the work of Chapter 2, the outcome and contribution to knowledge has been an up-to-date review of the state of the art in greenhouse cooling, in which the various approaches are compared and emphasis is given to emerging technologies that could achieve lower temperatures than in the past.

Objectve 3: To develop the solar regenerator and characterise its performance under a range of conditions.

This objective was met in Chapter 4. We performed an experimental and theoretical study that investigated the performance of an open flat plate solar regenerator in lab under various conditions in order to identify which design parameters affect significantly its performance under ambient conditions. To arrive at this choice of the regenerator type we carried out a literature review that highlighted the advantages and disadvantages of the different types i.e. the open type regenerator performs effectively under hot and dry climatic conditions while the closed type glazed regenerator perform better than the open under hot and humid conditions; the closed type is not affected by windy conditions and thus there is no clogging problem due to dust; solar stills do not perform as well as the other two types. We chose to focus on open flat plate regenerators because they are low cost and simple structures. Further, we looked into the various mathematical models developed for describing the physical processes occurring at the surface of the regenerator and chose an analytical one to predict the water evaporation rate. Consequently, the model was validated against the experimental results obtained from a prototype regenerator that was constructed in laboratory with a 6mm black neoprene foam sheet and a woven black mulch sheet on the top, supported by a steel backing. It was inclined by 2.5 degrees to the horizontal and measured 0.73 m long, in the direction of flow, by 0.84 m wide, giving an

active area of 0.61 m^2. For simulating the ambient conditions a solar simulator was constructed by an array of lamps. It was calibrated and optimised for better distribution of light at the surface of the regenerator using a diffusion paper sheet It should be noted though that the mathematical model chosen was parameterised for use with solutions of $MgCl_2$, new experimental correlations of heat and mass transfer were derived that are expected to be of broader applicability. The performance of the regenerator was investigated under various irradiance levels and solution mass flows and found to range between 40 percent (for concentrated solutions) and 68 percent (for dilute solutions). It was concluded that the higher the irradiance the higher the water evaporation rate is, regardless of the flow. The mathematical model developed for the regenerator was used as a sub model in the whole system model described in Chapter 6.

The original contribution to knowledge of Chapter 4 are the characterisation of a regenerator using magnesium chloride, since no other author has reported work with this compound in this field of liquid desiccant cooling.

Objective 4: *To design and build the desiccator and characterise its performance through experiments.*

The desiccator was developed in Chapter 5. It was designed and constructed after a thorough literature review that looked into the different types of desiccators (e.g. packed columns with random and structured packing, wetted wall columns, spray champers) based on their design characteristics. The review focused on packed towers or columns since they provide high wetted surface area per volume and thus higher water absorption rates. Further we focused on cross flow desiccators with structured packing, and based on the findings a prototype cross flow desiccator internally cooled with embedded tubes was constructed in lab. In accordance its performance was assessed under hot and humid conditions and also under hot and dry conditions utilising $MgCl_2$ as liquid desiccant which again constituted originality. To compare the experimental results a finite element model was developed based on relevant mathematical models found in literature; the effectiveness–NTU methodology was used for modelling the heat exchanger and Liu *et al.* (2007b) approach for modelling the structured packing. However, in order to simplify the complexity of the mathematical problem the differential equations were simplified and

reduced to algebraic form. The developed model used correlations of Nusselt and Sherwood numbers for predicting the heat and mass transfer coefficients in Celdek structured packing material at their original form or slightly modified. It was concluded that internal cooling has a significant positive effect on the performance of the desiccator. In contrast it was found that under dry conditions the desiccator underperforms regardless of using internal cooling. The developed heat and mass transfer model can predict the mass flux of absorbed water vapour with a relative error of 11 %. As for the regenerator, the model of the desiccator became a sub-model in that of the whole system.

The specific contributions to knowledge of Chapter 5 are therefore:

- Characterisation of the performance of a desiccator using magnesium chloride solution (which is representative of seawater bitterns) which contrasts to earlier studies with respect to the desiccant used.
- Characterisation of the configuration using pipes embedded in a Celdek pad, which differs to earlier studies with respect to heat and mass transfer analysis.
- A simplified and therefore more easily applied mathematical model of the cross flow desiccators which is an advance on the models reported in the literature.

Objective 5*: Alongside the above, to develop appropriate mathematical models for scaling, thus providing predictions of performance for the full size system, and to apply these in specific case studies to arrive at overall conclusions about the system compared to alternative approaches.*

This objective was partially met in Chapter 4 and 5 where the mathematical models were developed. However it was fully accomplished in Chapters 6 and 7. In Chapter 6 the mathematical models of the regenerator and the desiccator were combined with a greenhouse climate model published in literature by Kittas *et al.* (2003) into a computer program that can predict the cooling performance of the full size system. The gPROMS software package was chosen as the most suitable for developing the whole system composite model. The capability of this software to communicate with MSExcel files simplified the program since most of the modelling equations had been already introduced in spreadsheets and thus the results could be verified at any time. In Chapter 7, five cities were selected in the tropical and subtropical regions and their climatic conditions were fed

into the model developed in the Chapter 6. The aim here was to simulate the performance of the system under different ambient conditions and thus draw useful conclusions about its cooling capacity. Regarding the choice of the location, we selected on countries with food security problems i.e. Cuba, India, Bangladesh and Oman. The simulations revealed the efficacy of the proposed cooling system; cooling was improved in Havana, Mumbai, Chittagong and Muscat by 4-5.4^{o}C, 2.4–4.9^{o}C, 3.1–5.6^{o}C, and 2.3–3.7^{o}C respectively depending on the climatic conditions of each location. They also confirmed that the system performs better under humid conditions. Lastly it was pointed out that important parameters of the system are the thickness of the desiccator and the size of the regenerator. A 0.2m thickness regenerator is recommended for a better cooling effect; the size of the regenerator could be equal to the size of the greenhouse or larger under dry conditions, while under humid conditions it could be three times larger.

The original contributions arising with respect to this objective are the detailed modelling, using experimental verified assumptions about the performance of the sub-systems, of a greenhouse cooled by liquid desiccant cooling. This part of the work is original in respect of both the application of an open liquid desiccant cooling system to greenhouses, and the choice of specific desiccant chosen (ie. magnesium chloride solution which is representative of seawater bitterns).

Preliminary results from the modelling work were published in (Lychnos and Davies, 2008) and a more complete version has been accepted for publication at the World Renewable Energy Congress XI taking place on September 2010 in Abu Dhabi, UAE (Lychnos *et al.*, 2010b).

8.2 Response to Overall Aim

The aim of the current work is to investigate, at the laboratory scale, the feasibility of a solar-powered liquid desiccant cooling system for greenhouses, using desiccants obtained from concentrated seawater brines.

The overall aim of this work was achieved through the successful accomplishment of the main objectives as described above. In Chapter 2 the benchmark of the cooling

performance was set against which the proposed system was judged. In Chapter 3 we determined the properties of bitterns and investigated further the concept of using them as liquid desiccants; we showed that bitterns are suitable for greenhouse cooling and that they do have similar physical properties with pure $MgCl_2$ solutions (Lychnos *et al*, 2010). In Chapters 4 and 5 the essential components of the proposed cooling system i.e. the regenerator and desiccator were designed and constructed and their performance was critically assessed by conducting a series of experiments. The mathematical models developed in the relevant chapters for the regenerator and the desiccator were used in Chapter 6, along with a greenhouse model, to build the whole system model. This enabled us to investigate the performance of the solar powered liquid desiccant cooling system at different locations around the world and thus assess its cooling capacity (Chapter 7). Where the evaporative cooling system failed to produce enough cooling the solar powered liquid desiccant cooling system achieved further cooling which was enough to sustain the greenhouse air temperature below 30^oC thus suggesting that the cultivation period in greenhouses can be extended all year round. However, the best results were achieved when the thickness of the desiccator was increased from 0.1 to 0.2 m, which would increase the cost. It is worth of remark that under hot and dry conditions such as in Muscat the cooling effect drops. This suggests that under extreme high temperatures the system would not be able to generate enough cooling. Although the predicted cooling effect was not quite as good as previously suggested (Davies, 2005) it showed that the proposed system can be an alternative cooling system that improves cooling especially in hot and humid places such as Havana, Chittagong, etc. This research has successfully investigated a solar liquid cooling system for greenhouses which utilises bitterns as desiccants and based on the findings it is suggested that the problem of high temperatures induced in greenhouses during summer in hot and humid places can be addressed.

8.3 Future Work

Within this work, we have successfully demonstrated that a solar-powered liquid desiccant cooling system for greenhouses can reduce the high temperatures during the hot season in hot and humid places and maintain the temperature within the plant comfort zone. Although the basic components of the system were thoroughly investigated, there are aspects of the system that require further investigation such as the size of pumps and the exhaust fans, the choice of materials for the parts of the system that come in contact with

the bitterns which is very corrosive to most metals. Moreover, through focussing on the key parts of the cooled greenhouse, this thesis has not dealt with the design of structure as a whole and thus a significant amount of detailed architectural design would be needed to integrate the components into a single structure that is suitable for manufacture. In addition it would be interesting to explore the efficacy of the system when combined with passive cooling methods e.g. shading. Furthermore, it is worth performing a case study that would quantify the benefits of using greenhouses for food cultivation all year round in places with food insecurity problems thus showing the impact of this technology. The next step for the development of this system before becoming commercial is the construction and implementation of a pilot system of a real greenhouse where the performance of the system would be assessed under real climate conditions.

This has been a technical rather than a commercial feasibility study. The fact that the system is technically feasible does not guarantee that it is justified. Only by assessment of the costs of the technology can it eventually be assessed whether it will be a viable option compared to the other types of protected cultivation which, as emphasised in Chapter 1, is needed to maintain food security in face of the world's growing population and changing climate.

References

ABRAHAM, M. & ABRAHAM, M. C. (2000) Electrolyte and water activities in very concentrated solutions. *Electrochimica Acta,* 46 (1)**,** 137-142.

ABRAMS, D. S. & PRAUSNITZ, J. M. (1975) Statistical thermodynamics of liquid mixtures: A new expression for the excess Gibbs energy of partly or completely miscible systems. *AIChE Journal,* 21**,** 116-128.

AHMED, M., ARAKEL, A., HOEY, D. & COLEMAN, M. (2001) Integrated power, water and salt generation: a discussion paper. *Desalination,* 134**,** 37-45.

AHMED, M., ARAKEL, A., HOEY, D., THUMARUKUDY, M. R., GOOSEN, M. F. A., AL-HADDABI, M. & AL-BELUSHI, A. (2003) Feasibility of salt production from inland RO desalination plant reject brine: A case study. *Desalination,* 158**,** 109-117.

ALI, A., VAFAI, K. & KHALED, A. R. A. (2004) Analysis of heat and mass transfer between air and falling film in a cross flow configuration. *International Journal of Heat and Mass Transfer,* 47**,** 743-755.

ALIZADEH, S. & SAMAN, W. Y. (2002) Modeling and performance of a forced flow solar collector/regenerator using liquid desiccant. *Solar Energy,* 72**,** 143-154.

ALLY, M. R. & BRAUNSTEIN, J. (1998) Statistical mechanics of multilayer adsorption: electrolyte and water activities in concentrated solutions *The Journal of Chemical Thermodynamics,* 30 (1)**,** 49-58.

AMDOUNI, R. (2000) Chemical Study of free brine in solar salt works of Sfax Saline (E.S of Tunisia). *8th World Salt Symposium.* Arnhem, The Netherlands, Elsevier.

ARBEL, A., BARAK, M. & SHKLYAR, A. (2003) Combination of Forced Ventilation and Fogging Systems for Cooling Greenhouses. *Biosystems Engineering,* 84**,** 45-55.

ARBEL, A., YEKUTIELI, O. & BARAK, M. (1999) Performance of a Fog System for Cooling Greenhouses. *Journal of Agricultural Engineering Research,* 72**,** 129-136.

ASHRAE (1985) *Handbook of Fundamentals,* Atlanta GA, ASHRAE.

ASTM (1997 (Reapproved 2002)) D 2879 - 97 Standard Test Method for Vapor Pressure-Temperature Relationship and Initial Decomposition Temperature of Liquids by Isoteniscope.

BAILLE, A., KITTAS, C. & KATSOULAS, N. (2001) Influence of whitening on greenhouse microclimate and crop energy partitioning. *Agricultural and Forest Meteorology,* 107**,** 293-306.

BATTISTI, D. S. & NAYLOR, R. L. (2009) Historical Warnings of Future Food Insecurity with Unprecedented Seasonal Heat. *Science,* 323**,** 240-244.

BAUM, V. A., KAKABAEV, A. & KHANDURDYEV, A. (1972) Efficiency of a solar cooler with an open flat solution regenerator. *Geliotekhnika,* 8**,** 34-39.

BOULARD, T. & DRAOUI, B. (1995) Natural Ventilation of a Greenhouse with Continuous Roof Vents: Measurements and Data Analysis. *Journal of Agricultural Engineering Research,* 61**,** 27-36.

BOULARD, T., FEUILLOLEY, P. & KITTAS, C. (1997) Natural Ventilation Performance of Six Greenhouse and Tunnel Types. *Journal of Agricultural Engineering Research,* 67**,** 249-266.

BOULARD, T., MENESES, J. F., MERMIER, M. & PAPADAKIS, G. (1996) The mechanisms involved in the natural ventilation of greenhouses. *Agricultural and Forest Meteorology,* 79**,** 61-77.

BRONSTED, J. N. (1922) Calculation of the osmotic and activity functions in solutions of uni-univalent salts. *J. Am. Chem. Soc.,* 44**,** 938-948.

BS188:1977 Methods for determination of the viscosity of liquids.

BS4522:1988 Method for determination of absolute density at 20oDC of liquid chemical products for industrial use.

BS.EN.ISO.5167-1:2003 Measurement of fluid flow by means of pressure differential devices inserted in circular cross-section conduits running full. General principles and requirements

CASTILLA, N. & MONTERO, J. I. (2008) ENVIRONMENTAL CONTROL AND CROP PRODUCTION IN MEDITERRANEAN GREENHOUSES. *Acta Hort. (ISHS),* 797**,** 25-36.

CENGEL, Y. & BOLES, M. (1998) *Thermodynamics, An Engineering Approach,* William C Brown Pub.

CENGEL, Y. A. (2006) *Heat and mass transfer: a practical approach,* Singapore, McGraw-Hill Education.

CHEN, C.-C., BRITT, H. I., BOSTON, J. F. & EVANS, L. B. (1982) Local composition model for excess Gibbs energy of electrolyte systems. Part I: Single solvent, single completely dissociated electrolyte systems. *AIChE Journal,* 28**,** 588-596.

CHEN, C.-C. & EVANS, L. B. (1986) A local composition model for the excess Gibbs energy of aqueous electrolyte systems. *AIChE Journal,* 32**,** 444-454.

CHEN, X. Y., LI, Z., JIANG, Y. & QU, K. Y. (2006) Analytical solution of adiabatic heat and mass transfer process in packed-type liquid desiccant equipment and its application. *Solar Energy,* 80**,** 1509-1516.

CHENGQIN, R., YI, J., GUANGFA, T. & YIANPIN, Z. (2005) A characteristic study of liquid desiccant dehumidification/regeneration processes. *Solar Energy,* 79**,** 483-494.

CHENGQIN, R., YI, J. & YIANPIN, Z. (2006) Simplified analysis of coupled heat and mass transfer processes in packed bed liquid desiccant-air contact system. *Solar Energy,* 80**,** 121-131.

CHUNG, T.-W. (1994) Predictions of moisture removal efficiencies for packed-bed dehumidification systems. *Gas Separation & Purification,* 8**,** 265-268.

CHUNG, T.-W., GHOSH, T. K. & HINES, A. L. (1993) Dehumidification of Air by Aqueous Lithium Chloride in a Packed Column. *Separation Science and Technology,* 28**,** 533 - 550.

CHUNG, T.-W., GHOSH, T. K., HINES, A. L. & NOVOSEL, D. (1995) Dehumidification of Moist Air with Simultaneous Removal of Selected Indoor Pollutants by Triethylene Glycol Solutions in a Packed-Bed Absorber. *Separation Science and Technology,* 30**,** 1807 - 1832.

CHUNG, T. W., GHOSH, T. K. & HINES, A. L. (1996) Comparison between Random and Structured Packings for Dehumidification of Air by Lithium Chloride Solutions in a Packed Column and Their Heat and Mass Transfer Correlations. *Ind. Eng. Chem. Res.,* 35**,** 192-198.

CLEGG, S. L. & SEINFELD, J. H. (2004) Improvement of the Zdanovskii-Stokes-Robinson Model for Mixtures Containing Solutes of Different Charge Types. *J. Phys. Chem. A,* 108 (6)**,** 1008-1017.

CLEGG, S. L., SEINFELD, J. H. & EDNEY, E. O. (2003) Thermodynamic modelling of aqueous aerosols containing electrolytes and dissolved organic compounds. II. An extended Zdanovskii-Stokes-Robinson approach. . *Journal of Aerosol Science,* 34 (6)**,** 667-690.

COELHO, M., BAPTISTA, F., FITAS DA CRUZ, V. & GARCIA, J. L. (2006) COMPARISON OF FOUR NATURAL VENTILATION SYSTEMS IN A MEDITERRANEAN GREENHOUSE. *International Symposium on Greenhouse Cooling* Acta Hort. (ISHS)

COHEN, S. & FUCHS, M. (1999) Measuring and predicting Radiometric Properties of Reflective Shade Nets and Thermal Screens. *Journal of Agricultural Engineering Research,* 73**,** 245-255.

COHEN, Y., STANHILL, G. & FUCHS, M. (1983) An experimental comparison of evaporative cooling in a naturally ventilated glasshouse due to wetting the outer roof and inner crop soil surfaces. *Agricultural Meteorology,* 28**,** 239-251.

COLLIER, R. K. (1979) The analysis and simulation of an open cycle absorption refrigeration system. *Solar Energy,* 23**,** 357-366.

DAI, Y. J., WANG, R. Z., ZHANG, H. F. & YU, J. D. (2001) Use of liquid desiccant cooling to improve the performance of vapor compression air conditioning. *Applied Thermal Engineering,* 21**,** 1185-1202.

DAVIES, P. A. (2005) A solar cooling system for greenhouse food production in hot climates. *Solar Energy,* 79**,** 661-668.

DAVIES, P. A., HARRIS, I. & KNOWLES, P. R. (2006) Cooling of Greenhouses using Seawater:a solar-driven liquid desiccant cycle for greenhouse cooling in hot climates. *International Symposium on Greenhouse Cooling.* Almería.

DAVIES, P. A. & KNOWLES, P. R. (2006) Seawater bitterns as a source of liquid desiccant for use in solar-cooled greenhouses. *Desalination,* 196**,** 266-279.

DEMRATI, H., BOULARD, T., BEKKAOUI, A. & BOUIRDEN, L. (2001) SE--Structures and Environment: Natural Ventilation and Microclimatic Performance of a Large-scale Banana Greenhouse. *Journal of Agricultural Engineering Research,* 80**,** 261-271.

EL GUENDOUZI, M., AZOUGEN, R. & BENBIYI, A. (2005) Thermodynamic properties of the mixed electrolyte systems {y$MgCl_2$+(1-y)NaCl}(aq) and {y$MgCl_2$+(1-y)$CaCl_2$}(aq) at 298.15 K. *Calphad,* 29**,** 114-124.

EL GUENDOUZI, M., BENBIYI, A., DINANE, A. & AZOUGEN, R. (2004) Thermodynamic properties of multicomponent NaCl-LiCl-H_2O aqueous solutions at temperature 298.15 K. *Calphad,* 28**,** 97-103.

FACTOR, H. M. & GROSSMAN, G. (1980) A packed bed dehumidifier/regenerator for solar air conditioning with liquid desiccants. *Solar Energy,* 24**,** 541-550.

FAGBENLE, R. L. & KARAYIANNIS, T. G. (1998) A thermodynamic analysis of a simple open-flow solar regenerator. *Applied Thermal Engineering,* 18**,** 1359-1374.

FAOSTAT (2010), http://www.fao.org/economic/ess/food-security-statistics/fao-hunger-map/en/.

FAS/USDA (2008) Cuba's Food & Agriculture Situation Report. USA.

FERNÁNDEZ, J. E. & BAILEY, B. J. (1992) Measurement and prediction of greenhouse ventilation rates. *Agricultural and Forest Meteorology,* 58**,** 229-245.

FOOD AND AGRICULTURAL ORGANIZATION, U. N. (2008) CLIMATE CHANGE:Implications for Food Safety Rome.

FOOD AND AGRICULTURAL ORGANIZATION, U. N. O. (2002) The state of food insecurity in the world. Rome.

FOOD AND AGRICULTURAL ORGANIZATION, U. N. O. (2009) Food Security and Agricultural Mitigation in Developing Countries: Options for Capturing Synergies

FUCHS, M., DAYAN, E. & PRESNOV, E. (2006) Evaporative cooling of a ventilated greenhouse rose crop. *Agricultural and Forest Meteorology,* 138**,** 203-215.

FUCHS, M., DAYAN, E., SHMUEL, D. & ZIPORI, I. (1997) Effects of ventilation on the energy balance of a greenhouse with bare soil. *Agricultural and Forest Meteorology,* 86**,** 273-282.

GANDHIDASAN, P. (1982) Simple analysis of a forced flow solar regeneration system. *Journal of Energy* 6**,** 436-437

GANDHIDASAN, P. (1983a) A simple analysis of an open regeneration system. *Solar Energy,* 31**,** 343-345.

GANDHIDASAN, P. (1983b) Theoretical study of tilted solar still as a regenerator for liquid desiccants. *Energy Conversion and Management,* 23**,** 97-101.

GANDHIDASAN, P. (1983c) Thermal Performance Predictions and Sensitivity Analysis for a Parallel Flow Solar Regenerator. *Journal of Solar Energy Engineering,* 105**,** 224-228.

GANDHIDASAN, P. (1984) Comparative study of two types of solar regenerators for liquid absorption dehumidification system. *ASHRAE transactions,* 90**,** 78-84

GANDHIDASAN, P. (2004) A simplified model for air dehumidification with liquid desiccant. *Solar Energy,* 76**,** 409-416.

GANDHIDASAN, P., SRIRAMULU, V. & GUPTA, M. C. (1981) Heat and mass transfer in a solar regenerator. *The Chemical Engineering Journal,* 21**,** 59-63.

GANGULY, A. & GHOSH, S. (2007) Modeling and analysis of a fan-pad ventilated floricultural greenhouse. *Energy and Buildings,* 39**,** 1092-1097.

GARCIA-ALONSO, Y., ESPI, E., SALMERON, A., FONTECHA, A., GONZALEZ, A. & LOPEZ, J. C. (2006) NEW COOL PLASTIC FILMS FOR GREENHOUSE COVERING IN TROPICAL AND SUBTROPICAL AREAS. *Acta Hort. (ISHS),* 719**,** 131-138.

GARZOLI, K. V. (1989) COOLING OF GREENHOUSES IN TROPICAL AND SUB-TROPICAL CLIMATES. *Acta Hort. (ISHS)* 257**,** 93-100.

GAZQUEZ, J. C., LOPEZ, J. C., BAEZA, E., SAEZ, M., SANCHEZ-GUERRERO, M. C., MEDRANO, E. & LORENZO, P. (2006) YIELD RESPONSE OF A SWEET PEPPER CROP TO DIFFERENT METHODS OF GREENHOUSE COOLING. *Acta Hort. (ISHS)* 719**,** 507-514.

GHOSAL, M. K. & TIWARI, G. N. (2006) Modeling and parametric studies for thermal performance of an earth to air heat exchanger integrated with a greenhouse. *Energy Conversion and Management,* 47**,** 1779-1798.

GHOSAL, M. K., TIWARI, G. N. & SRIVASTAVA, N. S. L. (2003) Modeling and experimental validation of a greenhouse with evaporative cooling by moving water film over external shade cloth. *Energy and Buildings,* 35**,** 843-850.

GHOSAL, M. K., TIWARI, G. N. & SRIVASTAVA, N. S. L. (2004) Thermal modeling of a greenhouse with an integrated earth to air heat exchanger: an experimental validation. *Energy and Buildings,* 36**,** 219-227.

GIACOMELLI, G. & ROBERTS, W. (1989) TRY ALTERNATE METHODS OF EVAPORATIVE COOLING. *Acta Hort. (ISHS),* 257**,** 29-30.

GOMMED, K. & GROSSMAN, G. (2004) A Liquid Desiccant System for Solar Cooling and Dehumidification. *Journal of Solar Energy Engineering,* 126**,** 879-885.

GOMMED, K. & GROSSMAN, G. (2007) Experimental investigation of a liquid desiccant system for solar cooling and dehumidification. *Solar Energy,* 81**,** 131-138.

GROSSMAN, G. (2002) Solar-powered systems for cooling, dehumidification and air-conditioning. *Solar Energy,* 72**,** 53-62.

GUGGENHEIM, E., A. (1935) The specific thermodynamic properties of aqueous solutions of strong electrolytes. *Philosophical Magazine,* 19**,** 588-643.

HA, Z. & CHAN, C. K. (1999) The Water Activities of $MgCl_2$, $Mg(NO_3)_2$, $MgSO_4$, and Their Mixtures. *Aerosol Science and Technology,* 31**,** 154-169.

HAIM, I., GROSSMAN, G. & SHAVIT, A. (1992) Simulation and analysis of open cycle absorption systems for solar cooling. *Solar Energy,* 49**,** 515-534.

HAMER, P. J. C., BAILEY, B. J., FORD, M. G. & VIRK, G. S. (2006) NOVEL METHODS OF HEATING AND COOLING GREENHOUSES: A FEASIBILITY STUDY. *Acta Hort. (ISHS)*, 719**,** 223-230.

HANAN, J. J. (1998) *Greenhouses : Advanced Technology for Protected Horticulture*, Boca Raton, Florida, CRC Press.

HAWLADER, M. N. A., STACK, A. P. & WOOD, B. D. (1992) Performance Evaluation of Glazed and Unglazed Collectors/Regenerators in a Liquid Absorbent Open-Cycle Absorption Cooling System. *International Journal of Sustainable Energy*, 11**,** 135 - 164.

HEFTER, G., MAY, P. M., SIPOS, P. & STANLEY, A. (2003) Viscosities of concentrated electrolyte solutions. *Journal of Molecular Liquids*, 103-104**,** 261-273.

HEMMING, S., KEMPKES, F., VAN DER BRAAK, N., DUECK, T. & MARISSEN, N. (2006) GREENHOUSE COOLING BY NIR-REFLECTION. *Acta Hort. (ISHS)* 719**,** 97-106.

HICKMAN, G. W. (2010) Greenhouse Vegetable Production Statistics. IN CONSULTANTS, C. R. G. (Ed.).

HOWE, P. & DEVEREUX, S. (2004) Famine Intensity and Magnitude Scales: A Proposal for an Instrumental Definition of Famine. *Disasters*, 28**,** 353-372.

HU, Y. Y.-F. (2000) A new equation for predicting the density of multicomponent aqueous solutions conforming to the linear isopiestic relation. *Physical chemistry chemical physics*, 2**,** 2379-2382.

INCROPERA, F. P., DEWITT, D. P., BERGMAN, T. L. & LAVINE, A. S. (2007) *Fundamentals of heat and mass transfer*, USA, John Wiley & Sons, Inc.

IPCC (Ed.) (2007) *Climate Change 2007: Synthesis Report. Contribution of Working Groups I, II and III to the Fourth Assessment Report of the Intergovernmental Panel on Climate Change* Geneva, Switzerland, IPCC

IVAN DMITRIEVICH ASEYEV & GEORGIEVICH, G. (1992) *Properties of aqueous solutions of electrolytes*, Boca Raton ; London, CRC.

JAIN, S. & BANSAL, P. K. (2007) Performance analysis of liquid desiccant dehumidification systems. *International Journal of Refrigeration*, 30**,** 861-872.

JAIN, S., DHAR, P. L. & KAUSHIK, S. C. (2000) Experimental studies on the dehumidifier and regenerator of a liquid desiccant cooling system. *Applied Thermal Engineering*, 20**,** 253-267.

JARETUN, A. & ALY, G. (2000) New local composition model for electrolyte solutions: multicomponent systems. *Fluid Phase Equilibria*, 175**,** 213-228.

JENSEN, M. H. (2010) Plasticulture in the Global Community - View of the past and the future. University of Arizona,Tucson, Arizona, USA, www.plasticulture.org.

JIANG, W., QU, D. & MU, D. (2003) Protected Cultivation of Horticultural Crops in China. *Horticultural Reviews*, 30**,** 115-162.

JIRKA, V., KUCERAVÝ, V., MALÝ, M., PECH, F. & POKORNÝ, J. Energy flow in a greenhouse equipped with glass raster lenses. *Renewable Energy*, 16**,** 660-664.

KABEEL, A. E. (2005) Augmentation of the performance of solar regenerator of open absorption cooling system. *Renewable Energy*, 30**,** 327-338.

KAKABAEV, A. & KHANDURDYEV, A. (1969) Absorption solar refigeration unit with open regeneration of solution. *Geliotekhnika*, 5**,** 28-32.

KAUDINYA, J. V. & KAUSHIK, S. C. (1986) Experimental validation of theoretical studies on open and forced flow solar regenerator. *International Journal of Solar Energy*, 4**,** 13-23.

KAUSHIK, S. C., KAUDINYA, J. V. & YADAV, Y. K. (1992) Studies on some solar collector/regenerator systems for open cycle absorption air conditioning/liquid desiccant cooling systems. *Heat Recovery Systems and CHP*, 12**,** 357-363.

KHAN, A. Y. (1998) Cooling and dehumidification performance analysis of internally-cooled liquid desiccant absorbers. *Applied Thermal Engineering,* 18**,** 265-281.

KHAN, A. Y. & BALL, H. D. (1992) Development of a generalized model for performance evaluation of packed-type liquid sorbent dehumidifiers and regenerators. *ASHRAE transactions,* 98**,** 525-533.

KIM, D. S. & INFANTE FERREIRA, C. A. (2008) Solar refrigeration options - a state-of-the-art review. *International Journal of Refrigeration,* 31**,** 3-15.

KITTAS, C., BAILLE, A. & GIAGLARAS, P. (1999) Influence of Covering Material and Shading on the Spectral Distribution of Light in Greenhouses. *Journal of Agricultural Engineering Research,* 73**,** 341-351.

KITTAS, C., BARTZANAS, T. & JAFFRIN, A. (2003) Temperature Gradients in a Partially Shaded Large Greenhouse equipped with Evaporative Cooling Pads. *Biosystems Engineering,* 85**,** 87-94.

KITTAS, C., DRAOUI, B. & BOULARD, T. (1995) Quantification du taux d'aération d'une serre à ouvrant continu en toiture. *Agricultural and Forest Meteorology,* 77**,** 95-111.

KITTAS, C., KARAMANIS, M. & KATSOULAS, N. (2005) Air temperature regime in a forced ventilated greenhouse with rose crop. *Energy and Buildings,* 37**,** 807-812.

KITTAS, C., KATSOULAS, N. & BAILLE, A. (2001) SE--Structures and Environment: Influence of Greenhouse Ventilation Regime on the Microclimate and Energy Partitioning of a Rose Canopy during Summer Conditions. *Journal of Agricultural Engineering Research,* 79**,** 349-360.

KOCAMUSTAFAOGULLARI, G. & CHEN, I. Y. (1988) Falling film heat transfer analysis on a bank of horizontal tube evaporator. *A.I.Ch.E.,* 34**,** 1539-1549.

KOLKER, A. & DE PABLO, J. (1996) Thermodynamic Modeling of the Solubility of Salts in Mixed Aqueous-Organic Solvents. *Ind. Eng. Chem. Res.,* 35**,** 228-233.

KOLKER, A. & DE PABLO, J. J. (1995) Thermodynamic modeling of concentrated multicomponent aqueous electrolyte and non-electrolyte solutions. *Chemical Engineering Science,* 50**,** 1953-1959.

KOZAI, T., SASE, S. & NARA, M. (1980) A modelling approach to greenhouse ventilation control. *Acta Hort.,* 106**,** 125-136.

KUMAR, D. S. (2003) *Heat And Mass Transfer,* S. K. Kataria & Sons.

KUMAR, K. S., TIWARI, K. N. & JHA, M. K. (2009) Design and technology for greenhouse cooling in tropical and subtropical regions: A review. *Energy and Buildings,* 41**,** 1269-1275.

KUMAR, P. & DEVOTTA, S. (1989) Modelling of the thermal behaviour of a solar regenerator for open-cycle cooling systems. *Applied Energy,* 33**,** 287-295.

KUMAR, P., DEVOTTA, S. & HOLLAND, F. A. (1985) EXPERIMENTAL HEAT AND MASS TRANSFER STUDIES ON THE SOLAR GENERATOR OF AN OPEN CYCLE ABSORPTION COOLER. *Chemical Engineering Research and Design,* 63a 139 - 148

KURAMOCHI, H., OSAKO, M., KIDA, A., NISHIMURA, K., KAWAMOTO, K., ASAKUMA, Y., FUKUI, K. & MAEDA, K. (2005) Determination of Ion-Specific NRTL Parameters for Predicting Phase Equilibria in Aqueous Multielectrolyte Solutions. *Ind. Eng. Chem. Res.,* 44**,** 3289-3297.

KUSIK, C. L. & MEISSNER, H. P. (1978) Electrolyte activity coefficients in inorganic processing. *AIChE Symp. Ser.,* 173, 14.

LIETZKE, M. H. & STOUGHTON, R. W. (1972) A simple empirical equation for the prediction of the activity-coefficient value of each component in aqueous electrolyte mixtures containing a common ion. . *Journal of Solution Chemistry,* V1 (4)**,** 299-308.

LIETZKE, M. H. & STOUGHTON, R. W. (1975) Extension of a two-structure model for electrolyte solutions to aqueous mixed electrolyte systems. *Journal of Inorganic and Nuclear Chemistry,* 37**,** 2503-2506.

LIMA, M. C. P. & PITZER, K. S. (1983a) Thermodynamics of saturated aqueous solutions including mixtures of NaCl, KCl, and CsCl. *Journal of Solution Chemistry,* 12**,** 171-185.

LIMA, M. C. P. & PITZER, K. S. (1983b) Thermodynamics of saturated electrolyte mixtures of NaCl with Na2SO4 and with MgCl2. *Journal of Solution Chemistry,* 12**,** 187-199.

LIU, X., JIANG, Y., XIA, J. & CHANG, X. (2007a) Analytical solutions of coupled heat and mass transfer processes in liquid desiccant air dehumidifier/regenerator. *Energy Conversion and Management,* 48**,** 2221-2232.

LIU, X. H., JIANG, Y. & QU, K. Y. (2007b) Heat and mass transfer model of cross flow liquid desiccant air dehumidifier/regenerator. *Energy Conversion and Management,* 48**,** 546-554.

LIU, X. H., QU, K. Y. & JIANG, Y. (2006a) Empirical correlations to predict the performance of the dehumidifier using liquid desiccant in heat and mass transfer. *Renewable Energy,* 31**,** 1627-1639.

LIU, X. H., ZHANG, Y., QU, K. Y. & JIANG, Y. (2006b) Experimental study on mass transfer performances of cross flow dehumidifier using liquid desiccant. *Energy Conversion and Management,* 47**,** 2682-2692.

LOBO, V. M. M. (1989) *Handbook of electrolyte solutions. Parts A & B,* Elsevier.

LOEHE, J. R. & DONOHUE, M. D. (1997) Recent advances in modeling thermodynamic properties of aqueous strong electrolyte systems. *AIChE Journal,* 43**,** 180-195.

LONGO, G. A. & GASPARELLA, A. (2005) Experimental and theoretical analysis of heat and mass transfer in a packed column dehumidifier/regenerator with liquid desiccant. *International Journal of Heat and Mass Transfer,* 48**,** 5240-5254.

LYCHNOS, G. & DAVIES, P. A. (2008) A SOLAR POWERED LIQUID-DESICCANT COOLING SYSTEM FOR GREENHOUSES. *Acta Hort. (ISHS)* 797**,** 95-109.

LYCHNOS, G., FLETCHER, J. P. & DAVIES, P. A. (2010a) Properties of seawater bitterns with regard to liquid-desiccant cooling. *Desalination,* 250**,** 172-178.

LYCHNOS, G., HOSSAIN, A. K. & DAVIES, P. A. (2010b) A solar-powered liquid desiccant cooling system (LDCS) to adapt crop production to climate change. *World Renewable Energy Congress XI.* Abu Dhabi, UAE.

MCALLAN, J. V. (1965) Oil manometer for the range 0-100 torr. *Journal of Scientific Instruments* 42**,** 290-291

MEI, L. & DAI, Y. J. (2008) A technical review on use of liquid-desiccant dehumidification for air-conditioning application. *Renewable and Sustainable Energy Reviews,* 12**,** 662-689.

MONTERO, J. I., ANTON, A., BIEL, C. & FRANQUET, A. (1990) COOLING OF GREENHOUSES WITH COMPRESSED AIR FOGGING NOZZLES. *Acta Hort. (ISHS),* 281**,** 199-210.

MONTERO, J. I., STANGHELLINI, C. & CASTILLA, N. (2009) GREENHOUSE TECHNOLOGY FOR SUSTAINABLE PRODUCTION IN MILD WINTER CLIMATE AREAS: TRENDS AND NEEDS. *Acta Hort. (ISHS)* 807**,** 33-44.

MOON, C. G., BANSAL, P. K. & JAIN, S. (2009) New mass transfer performance data of a cross-flow liquid desiccant dehumidification system. *International Journal of Refrigeration,* 32**,** 524-533.

MULLICK, S. C. & GUPTA, M. C. (1974) Solar desorption of absorbent solutions. *Solar Energy,* 16**,** 19-24.

NASA (2010), http://data.giss.nasa.gov/gistemp/.

NATIONAL ENGINEERING LABORATORY, B., R. W. (1964) *Steam tables 1964 : physical properties of water and steam, 0-800 degrees C / 0-1000 bars. Prep. by R.W.Bain,* Edinb. :, H.M.S.O.

NELSON, D. J. & WOOD, B. D. (1990) Evaporation Rate Model for a Natural Convection Glazed Collector/Regenerator. *Journal of Solar Energy Engineering,* 112**,** 51-57.

NIELSEN, O. F. (2002) SE--Structures and Environment: Natural Ventilation of a Greenhouse With Top Screen. *Biosystems Engineering,* 81**,** 443-451.

NOVAK, K. S. & WOOD, B. D. (1985) Solar Collector/Regenerator performance based on experimental heat and mass transfer correlations. *lNTERSOL 85.* Montreal, Canada.

NOVAK, K. S., WOOD, B. D. & NELSON, D. J. (1985) Experimentally determined correlations for solar collector/regenerator heat and mass transfer. *ASME,* No 85-WA/SOL-7.

OIML (1996) The scale of relative humidity of air certified against saturated salt solutions. Paris, Bureau Internationale de Mètrologie Lègale.

OLANDER, D. (1961) Design of Direct Contact Cooler-Condensers. *Industrial & Engineering Chemistry,* 53**,** 121-126.

OLANDER, D. R. (1960) Simultaneous mass transfer and equilibrium chemical reaction. *A.I.Ch.E.,* 6**,** 233-239.

OLIVEIRA, A. C., AFONSO, C. F., RIFFAT, S. B. & DOHERTY, P. S. (2000) Thermal performance of a novel air conditioning system using a liquid desiccant. *Applied Thermal Engineering,* 20**,** 1213-1223.

ÖZTÜRK, H. H. (2003) Evaporative Cooling Efficiency of a Fogging System for Greenhouses. *Turk. J. Agric. For.,* 27**,** 49-57.

PAPADAKIS, G., FRANGOUDAKIS, A. & KYRITSIS, S. (1992) Mixed, forced and free convection heat transfer at the greenhouse cover. *Journal of Agricultural Engineering Research,* 51**,** 191-205.

PAPADAKIS, G., MERMIER, M., MENESES, J. F. & BOULARD, T. (1996) Measurement and Analysis of Air Exchange Rates in a Greenhouse with Continuous Roof and Side Openings. *Journal of Agricultural Engineering Research,* 63**,** 219-227.

PARDOSSI, A., TOGNONI, F. & INCROCCI, L. (2004) Mediterranean greenhouse technology. *Chronica Horticulturae,* 44**,** 28-34.

PEEL, M. C., FINLAYSON, B. L. & MCMAHON, T. A. (2007) Updated world map of the Köppen-Geiger climate classification. *Hydrol. Earth Syst. Sci.,* 11**,** 1633-1644

PENG, C. P. & HOWELL, J. R. (1982) Analysis of open inclined surface solar regenerators for absorption cooling applications--Comparison between numerical and analytical models. *Solar Energy,* 28**,** 265-268.

PENG, C. S. P. & HOWELL, J. R. (1984) The Performance of Various Types of Regenerators for Liquid Desiccants. *Journal of Solar Energy Engineering,* 106**,** 133-141.

PEREZ-VILLASENOR, F., IGLESIAS-SILVA, G. A. & HALL, K. R. (2002) Osmotic and Activity Coefficients Using a Modified Pitzer Equation for Strong Electrolytes 1:1 and 1:2 at 298.15 K. *Ind. Eng. Chem. Res.,* 41**,** 1031-1037.

PÉREZ PARRA, J., BAEZA, E., MONTERO, J. I. & BAILEY, B. J. (2004) Natural Ventilation of Parral Greenhouses. *Biosystems Engineering,* 87**,** 355-366.

PERRY, R. H., GREEN, D. W. & MALONEY, J. O. (1984) *Perry's Chemical engineers' handbook,* New York, McGraw-Hill.

PITZER, K. S. (1973) Thermodynamics of electrolytes. I. Theoretical basis and general equations. *J. Phys. Chem* 77**,** 268 - 277.

PITZER, K. S. (1975) Thermodynamics of electrolytes. V. effects of higher-order electrostatic terms. *Journal of Solution Chemistry,* V4**,** 249-265.

PITZER, K. S. (1981) Characteristics of very concentrated aqueous solutions. *Physics and Chemistry of The Earth,* 13-14**,** 249-272.

PITZER, K. S. (1991) *Activity coefficients in electrolyte solutions,* Boca Raton, FL, CRC Press.

PITZER, K. S. & GUILLERMO, M. (1974) Thermodynamics of electrolytes. III. Activity and osmotic coefficients for 2-2 electrolytes. *Journal of Solution Chemistry,* 3**,** 539-546.

PITZER, K. S. & KIM, J. J. (1974) Thermodynamics of electrolytes. IV. Activity and osmotic coefficients for mixed electrolytes. *J. Am. Chem. Soc.,* 96 (18)**,** 5701-5707.

PITZER, K. S. & MAYORGA, G. (1973) Thermodynamics of electrolytes. II. Activity and osmotic coefficients for strong electrolytes with one or both ions univalent. *J. Phys. Chem.,* 77**,** 2300-2308.

PITZER, K. S., OLSEN, J., SIMONSON, J. M., ROY, R. N., GIBBONS, J. J. & ROWE, L. (1985) Thermodynamics of aqueous magnesium and calcium bicarbonates and mixtures with chloride. *J. Chem. Eng. Data,* 30 (1)**,** 14-17.

PITZER, K. S., PEIMING, W., JOSEPH, A. R. & SIMON, L. C. (1999) Thermodynamics of Electrolytes. 13. Ionic Strength Dependence of Higher-Order Terms; Equations for CaCl2 and MgCl2. *Journal of Solution Chemistry,* V28**,** 265-282.

POPULATION.ACTION.INTERNATIONAL (2007), http://www.populationaction.org/Publications/Interactive_Databases/climate_map.shtml.

POTNIS, S. V. & LENZ, T. G. (1996) Dimensionless Mass-Transfer Correlations for Packed-Bed Liquid-Desiccant Contactors. *Ind. Eng. Chem. Res.,* 35**,** 4185-4193.

RAHAMAH, A., ELSAYED, M. M. & AL-NAJEM, N. M. (1998) A numerical solution for cooling and dehumidification of air by a falling desiccant film in parallel flow. *Renewable Energy,* 13**,** 305-322.

REILLY, P. J., WOOD, R. H. & ROBINSON, R. A. (1971) Prediction of osmotic and activity coefficients in mixed-electrolyte solutions. *J. Phys. Chem.,* 75 (9)**,** 1305-1315.

REN, C. Q. (2008) Effectiveness-NTU relation for packed bed liquid desiccant-air contact systems with a double film model for heat and mass transfer. *International Journal of Heat and Mass Transfer,* 51**,** 1793-1803.

RENON, H. & PRAUSNITZ, J. M. (1968) Local compositions in thermodynamic excess functions for liquid mixtures. *AIChE Journal,* 14 135-144.

ROBINSON, R. A. & STOKES, R. H. (1959) *Electrolyte Solutions,* London, Butterworths Publications LTD.

ROBINSON, R. A. & STOKES, R. H. (1970) *Electrolyte solutions : the measurement and interpretation of conductance, chemical potential and diffusion in solutions of simple electrolytes,* London, Butterworths.

ROGERS, G. F. C. & MAYHEW, Y. R. (1995) *Thermodynamic and Transport Properties of Fluids,* Oxford, Blackwell Publishers Ltd.

ROMERO, P., GIACOMELLI, G. A., CHOI, C. Y. & LOPEZ-CRUZ, I. (2006) VENTILATION RATES FOR A NATURALLY-VENTILATED GREENHOUSE IN CENTRAL MEXICO Acta Hort. (ISHS)

SABEH, N. C., GIACOMELLI, G. A. & KUBOTA, C. (2006) WATER USE FOR PAD AND FAN EVAPORATIVE COOLING OF A GREENHOUSE IN A SEMI-ARID CLIMATE. *Acta Hort. (ISHS)* 719**,** 409-416.

SAMAN, W. Y. & ALIZADEH, S. (2001) Modelling and performance analysis of a cross-flow type plate heat exchanger for dehumidification/cooling. *Solar Energy,* 70**,** 361-372.

SAMAN, W. Y. & ALIZADEH, S. (2002) An experimental study of a cross-flow type plate heat exchanger for dehumidification/cooling. *Solar Energy,* 73**,** 59-71.

SANGSTER, J. & LENZI, F. (1974) On the choice of methods for the prediction of the Water-activity and Activity coefficient for multicomponent aqueous solutions. *The Canadian Journal of Chemical Engineering,* 52**,** 392-396.

SANITJAI, S. & GOLDSTEIN, R. J. (2004) Forced convection heat transfer from a circular cylinder in crossflow to air and liquids. *International Journal of Heat and Mass Transfer,* 47**,** 4795-4805.

SANTAMOURIS, M., MIHALAKAKOU, G., BALARAS, C. A., ARGIRIOU, A., ASIMAKOPOULOS, D. & VALLINDRAS, M. (1995) Use of buried pipes for energy conservation in cooling of agricultural greenhouses. *Solar Energy,* 55**,** 111-124.

SASE, S., TAKAKURA, T. & NARA, M. (1984) Wind tunnel testing on airflow and temperature distribution of a naturally ventilated greenhouse. *Acta Hortic.*, 148 329.

SETHI, V. P. & SHARMA, S. K. (2007) Survey of cooling technologies for worldwide agricultural greenhouse applications. *Solar Energy,* 81**,** 1447-1459.

SETHI, V. P. & SIDHU, G. S. (2004) Journal of Agricultural Engineering, ISAE. 41**,** 1-4.

SHAMIM, T. & MCDONALD, T. W. (1995) Experimental study of heat transfer through liquid foam. *Proceedings of ASHRAE***,** 150–157.

SONI, P., SALOKHE, V. M. & TANTAU, H. J. (2005) Effect of Screen Mesh Size on Vertical Temperature Distribution in Naturally Ventilated Tropical Greenhouses. *Biosystems Engineering,* 92**,** 469-482.

SONNEVELD, P. J., SWINKELS, G. L. A. M., KEMPKES, F., CAMPEN, J. B. & BOT, G. P. A. (2006) GREENHOUSE WITH AN INTEGRATED NIR FILTER AND A SOLAR COOLING SYSTEM. *Acta Hort. (ISHS)* 719**,** 123-130.

SOULIOTIS, M., TRIPANAGNOSTOPOULOS, Y. & KAVGA, A. (2006) THE USE OF FRESNEL LENSES TO REDUCE THE VENTILATION NEEDS OF GREENHOUSES. *Acta Hort. (ISHS),* 719**,** 107-114.

STOKES, R. H. & ROBINSON, R. A. (1966) Interactions in Aqueous Nonelectrolyte Solutions. I. Solute-Solvent Equilibria. *J. Phys. Chem.*, 70 (7).

SUTAR, R. F. & TIWARI, G. N. (1995) Analytical and numerical study of a controlled-environment agricultural system for hot and dry climatic conditions. *Energy and Buildings,* 23**,** 9-18.

TANG, I. N., TRIDICO, A.C., FUNG, K.H. (1997) Thermodynamic and optical properties of sea salt aerosols. *Journal of Geophysical Research,* 102**,** 23,269-23,275.

TEITEL, M., BARAK, M. & ZHAO, Y. (2006) VENTILATION OF A GREENHOUSE WITH CONTINUOUS ROOF AND SIDE VENTS. *International Symposium on Greenhouse Cooling* Acta Hort. (ISHS).

TOIDA, H., KOZAI, T., OHYAMA, K. & HANDARTO (2006) Enhancing Fog Evaporation Rate using an Upward Air Stream to improve Greenhouse Cooling Performance. *Biosystems Engineering,* 93**,** 205-211.

TREYBAL, R. E. (1980) *Mass transfer operations,* USA, McGraw-Hill.

TRIPANAGNOSTOPOULOS, Y., SOULIOTIS, M., TONUI, J. K. & KAVGA, A. (2005) IRRADIATION ASPECTS FOR ENERGY BALANCE IN GREENHOUSES. *Acta Hort. (ISHS),* 691**,** 733-740.

ULLAH, M. R., KETTLEBOROUGH, C. F. & GANDHIDASAN, P. (1988) Effectiveness of Moisture Removal for an Adiabatic Counterflow Packed Tower Absorber

Operating with CaCl2-Air Contact System. *Journal of Solar Energy Engineering,* 110**,** 98-101.

UNITED NATIONS, D. E. S. A., POPULATION DIVISION (2009) World Population Prospects: The 2008 Revision, Highlights, Working Paper No. ESA/P/WP.210.

WANG, P., ANDERKO, A. & YOUNG, R. D. (2002) A speciation-based model for mixed-solvent electrolyte systems. *Fluid Phase Equilibria,* 203**,** 141-176.

WANG, P., SPRINGER, R. D., ANDERKO, A. & YOUNG, R. D. (2004) Modeling phase equilibria and speciation in mixed-solvent electrolyte systems. *Fluid Phase Equilibria,* 222-223**,** 11-17.

WILLITS, D. H. (2003) Cooling Fan-ventilated Greenhouses: a Modelling Study. *Biosystems Engineering,* 84**,** 315-329.

WILSON, G. M. (1964) Vapor-Liquid Equilibrium. XI. A New Expression for the Excess Free Energy of Mixing. *J. Am. Chem. Soc.,* 86**,** 127-130.

WITTWER, S. H. & CASTILLA, N. (1995) Protected cultivation of horticultural crops worldwide. *HortTechnology (USA),* 5**,** 6-23.

YILDIZ, I. & STOMBAUGH, D. P. (2006) SIMULATED PERFORMANCES OF A HEAT PUMP SYSTEM FOR ENERGY AND WATER CONSERVATION IN OPEN AND CONFINED GREENHOUSE SYSTEMS. *Acta Hort. (ISHS),* 718**,** 341-350.

YIN, Y. & ZHANG, X. (2008) A new method for determining coupled heat and mass transfer coefficients between air and liquid desiccant. *International Journal of Heat and Mass Transfer,* In Press, Corrected Proof.

YOON, J.-I., PHAN, T.-T., MOON, C.-G. & BANSAL, P. (2005) Numerical study on heat and mass transfer characteristic of plate absorber. *Applied Thermal Engineering,* 25**,** 2219-2235.

ZABELTITZ, V. (1999) Greenhouse structures. IN STANHILL, G. & ENOCH, H. Z. (Eds.) *Ecosystems of the world.* Elsevier science.

ZAYTSEV, I. D. & ASEYEV, G. G. (1992) *Properties of aqueous solutions of electrolytes,* Boca Raton ; London, CRC.

APPENDICES

APPENDIX 1. Pitzer's model equations

APPENDIX 2. Solar simulator calibration

APPENDIX 3. Analytical measurements of water evaporation flux and solution concentration

APPENDIX 4. Calibration graphs

APPENDIX 5. Orifice plate

APPENDIX 6. Analytical table of heat loss

APPENDIX 7. Analytical tables of simulation results

APPENDIX 8. gPROMS computer codes

APPENDIX 1.

Pitzer's model:

$$\phi - 1 = 2\left(\sum_i m_i\right)^{-1}\left\{\frac{-A^{\phi} I^{3/2}}{\left(1+1.2I^{1/2}\right)} + \sum_c \sum_a m_c m_a \left[B_{ca}^{\phi} + ZC_{ca}\right] + \right.$$

$$\left. \sum_c \sum_{c'} m_c m_{c'} \left[\Phi_{cc'}^{\phi} + \sum_a m_a \psi_{cc'a}\right] + \sum_a \sum_{a'} m_a m_{a'} \left[\Phi_{aa'}^{\phi} + \sum_c m_c \psi_{aa'c}\right]\right\} \quad (1)$$

(applicable to ≥ 1 salt, ≥ 2 cations, ≥ 2 anions)

where $z = \sum_i m_i |z_i|$,

$B_{ca}^{\phi} = \beta_{ca}^{(o)} + \beta_{ca}^{(1)} \exp(-a_1 I^{1/2}) + \beta_{ca}^{(2)} \exp(-a_2 I^{1/2})$ for 2-2 or higher valence

with a_1 =1.4 and a_2 =12,

$B_{ca}^{\phi} = \beta_{ca}^{(o)} + \beta_{ca}^{(1)} \exp(-a_1 I^{1/2})$ for lower valence with a_1 =2.

$C_{ca} = C_{ca}^{\phi} / 2|z_c z_a|^{1/2}$

$$\ln \gamma_{MX} = |z_M z_X| f^{\gamma} + (2\nu_M/\nu)\sum_a m_a \left[B_{Ma} + (\sum mz) C_{cX} + (\nu_X/\nu_M)\theta_{Xa}\right] + (2\nu_X/\nu)\sum_c m_c \left[B_{cX} + (\sum mz) C_{cX} + (\nu_M/\nu_X)\theta_{Mc}\right] +$$

$$\sum_c \sum_a m_c m_a \left\{|z_M z_X| B'_{ca} + \nu^{-1}\left[2\nu_M z_M C_{ca} + \nu_M \psi_{Mca} + \nu_X \psi_{caX}\right]\right\} + \frac{1}{2}\sum_c \sum_{c'} m_c m_{c'} \left[(\nu_X/\nu)\psi_{cc'X} + |z_M z_X| \theta'_{cc'}\right] +$$

$$\frac{1}{2}\sum_a \sum_{a'} m_a m_{a'} \left[(\nu_M/\nu)\psi_{Maa'} + |z_M z_X| \theta'_{aa'}\right]$$

APPENDIX 2.

Solar Simulator Calibration

Introduction

An array of 90 bulbs (4.5kW power supply) arranged in a triangular pattern as shown in Fig. A2.1 was made up to be the solar simulator. It is constructed to simulate a range of altitude and sun ray inclination combinations. Each bulb was an EIKO Q50MR16 Solux bulb, 50W, 4700 K (daylight simulation bulb), 36 deg. Dichroic spot. They were arranged with a pitch of 109mm between them. Before using the solar simulator the uniformity of the irradiance E (W/m^{-2}) on the horizontal surface was investigated.

Procedure

The array of lamps was set at the horizontal plane (altitude 90^{o}, zero inclination). A 10cmX10cm grid was drawn on the horizontal surface where the measurements were taken as shown in sketch Fig. A2.2. A pyranometer CMP 11 (Kipp & Zonen, Delft, The Netherlands) was used to measure the irradiance. Measurements were taken by placing the instrument at the nodes of the grid and at the centre of each grid square. A working area was defined based on the dimensions of the regenerator rig (shaded area showed in sketch 2). Thus the measurements were taken only at the area of interest. The irradiance was measured at four different heights (the vertical distance measured from the horizontal surface where the pyranometer was placed up to the face of the lamps) by ascending the array of lamps at: a) 23cm, b) 33cm, c) 52.5cm, and d) 61.5cm, e) 67.5cm, f) 73.5cm.

Results

The measurements were averaged for each height; the standard deviation was calculated along with the coefficient of variance (SD/AVG %) in a spreadsheet.

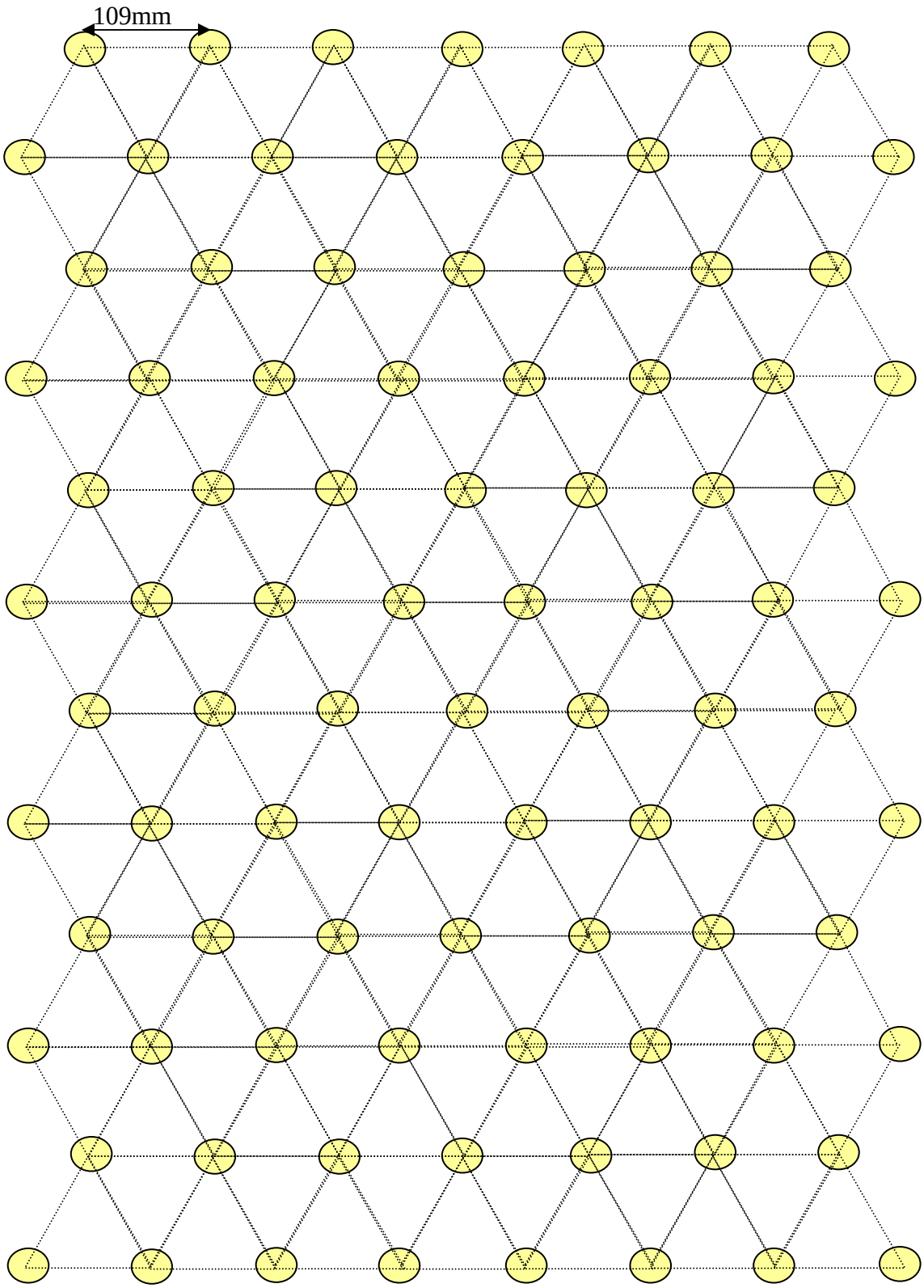

Fig. A2.1: Sketch of the pattern of bulbs.

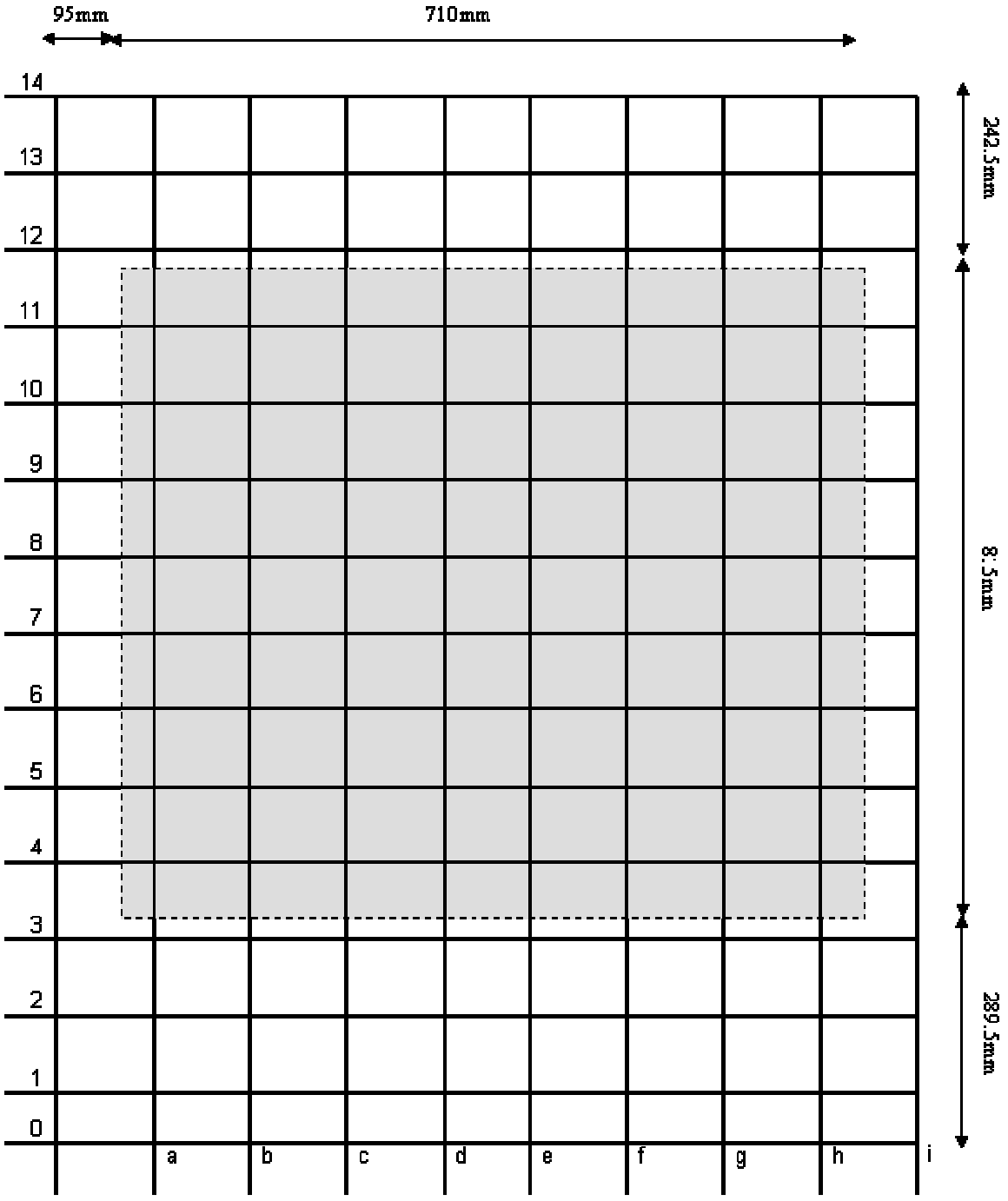

Fig. A2.2: Sketch of the grid.

APPENDIX 3.

Analytical Tables of measured mass flux of evaporation and concentration at 760, 400, 600 and 970 W m-2 irradiance and three solution mass fluxes.

Table A3.1

760 W m-2, 0.0031 kg s-1 m-2		
TIME (h)	**Mass flux of Evaporation** g h^{-1} m^{-2}	**Concentration** kg kg^{-1}
0.25	178.1	0.3276
0.5	267.1	0.3290
0.75	356.2	0.3310
1	445.2	0.3334
1.25	498.6	0.3357
1.5	534.2	0.3383
1.75	508.8	0.3411
2	534.2	0.3432
2.25	554.0	0.3449
2.5	534.2	0.3471
2.75	518.1	0.3489
3	504.6	0.3505

Table A3.2

760 W m-2, 0.0101 kg s-1 m-2		
TIME (h)	**Mass flux of Evaporation** g h^{-1} m^{-2}	**Concentration** kg kg^{-1}
0.25	178.1	0.3200
0.5	178.1	0.3209
0.75	237.4	0.3222
1	267.1	0.3243
1.25	320.5	0.3262
1.5	356.2	0.3282
1.75	381.6	0.3312
2	400.7	0.3335
2.25	415.5	0.3350
2.5	409.6	0.3372
2.75	420.9	0.3380
3	430.4	0.3401
3.25	424.7	0.3425
3.5	419.8	0.3443
3.75	427.4	0.3466
4	434.1	0.3503

(Table A3.2 continued)

4.25	429.5	0.3517
4.5	425.4	0.3546
4.75	421.8	0.3567
5	418.5	0.3586

Table A3.3

760 W m-2, 0.0062 kg s-1 m-2		
TIME (h)	**Mass flux of Evaporation** g h^{-1} m^{-2}	**Concentration** kg kg^{-1}
0.25	178.1	0.2943
0.5	356.2	0.2971
0.75	415.5	0.2976
1	445.2	0.2986
1.25	463.0	0.3022
1.5	474.9	0.3051
1.75	483.4	0.3062
2	489.7	0.3074
2.25	494.7	0.3110
2.5	498.6	0.3129
2.75	501.9	0.3141
3	504.6	0.3153
3.25	506.8	0.3170
3.5	496.1	0.3194
3.75	510.5	0.3221
4	500.9	0.3249
4.25	513.3	0.3269
4.5	504.6	0.3293
4.75	515.5	0.3305
5	507.5	0.3329
5.25	508.8	0.3351
5.5	510.0	0.3375
5.75	503.3	0.3389
6	497.1	0.3412
6.25	491.5	0.3438

Table A3.4

400 W m-2, 0.0034 kg s-1 m-2		
TIME (h)	**Mass flux of Evaporation** g h^{-1} m^{-2}	**Concentration** kg kg^{-1}
0.5	89.0	0.3308
1	178.1	0.3327
1.5	207.8	0.3354
2	222.6	0.3379
2.5	231.5	0.3404
3	237.4	0.3429
3.5	241.7	0.3454
4	233.7	0.3481
4.5	237.4	0.3506
5	231.5	0.3525
5.5	226.7	0.3544
6	215.2	0.3566
6.5	205.5	0.3581

Table A3.5

400 W m-2, 0.0060 kg s-1 m-2		
TIME (h)	**Mass flux of Evaporation** g h^{-1} m^{-2}	**Concentration** kg kg^{-1}
0.5	89.0	0.3279
1	133.6	0.3297
1.5	178.1	0.3326
2	200.3	0.3346
2.5	213.7	0.3368
3	222.6	0.3388
3.5	229.0	0.3411
4	233.7	0.3458
4.5	237.4	0.3479
5	240.4	0.3497
5.5	242.8	0.3520
6	244.9	0.3546
6.5	239.7	0.3559
7	241.7	0.3576
7.5	237.4	0.3598
8	233.7	0.3600

Table A3.6

400 W m-2, 0.0106 kg s-1 m-2		
TIME (h)	**Mass flux of Evaporation** g h^{-1} m^{-2}	**Concentration** kg kg^{-1}
0.5	89.0	0.3349
1	133.6	0.3365
1.5	178.1	0.3378
2	200.3	0.3397
2.5	213.7	0.3416
3	222.6	0.3435
3.5	229.0	0.3458
4	222.6	0.3482
4.5	227.5	0.3497
5	231.5	0.3519
5.5	234.7	0.3540
6	230.0	0.3559
6.5	232.9	0.3574
7	229.0	0.3596
7.5	231.5	0.3596
8	233.7	0.3600
8.5	230.5	0.3589
8.75	229.0	0.3589

Table A3.7

600 W m-2, 0.0033 kg s-1 m-2		
TIME (h)	**Mass flux of Evaporation** g h^{-1} m^{-2}	**Concentration** kg kg^{-1}
0.5	178.1	0.3321
1	267.1	0.3356
1.5	356.2	0.3400
2	400.7	0.3435
2.5	409.6	0.3479
3	415.5	0.3513
3.5	432.5	0.3557
4	434.1	0.3600
4.5	435.3	0.3600
5	427.4	0.3581

Table A3.8

600 W m-2, 0.0067 kg s-1 m-2		
TIME (h)	**Mass flux of Evaporation** g h^{-1} m^{-2}	**Concentration** kg kg^{-1}
0.5	89.0	0.3317
1	267.1	0.3351
1.5	326.5	0.3385
2	356.2	0.3427
2.5	374.0	0.3463
3	385.8	0.3500
3.5	394.3	0.3544
4	400.7	0.3579
4.5	405.6	0.3591
5	400.7	0.3596
5.5	388.5	0.3587

Table A3.9

600 W m-2, 0.0104 kg s-1 m-2		
TIME (h)	**Mass flux of Evaporation** g h^{-1} m^{-2}	**Concentration** kg kg^{-1}
0.5	89.0	0.3328
1	267.1	0.3370
1.5	326.5	0.3403
2	356.2	0.3440
2.5	374.0	0.3478
3	385.8	0.3520
3.5	394.3	0.3558
4	400.7	0.3600
4.5	395.7	0.3587
5	391.8	0.3587
5.5	388.5	0.3587

Table A3.10

970 W m-2, 0.0033 kg s-1 m-2		
TIME (h)	**Mass flux of Evaporation** g h^{-1} m^{-2}	**Concentration** kg kg^{-1}
0.25	178.1	0.3267
0.5	267.1	0.3294
0.75	415.5	0.3327
1	489.7	0.3344
1.25	534.2	0.3375
1.5	563.9	0.3405
1.75	595.3	0.3436
2	623.3	0.3468
2.25	633.2	0.3497
2.5	641.1	0.3527
2.75	647.6	0.3560
3	653.0	0.3585
3.25	643.8	0.3600
3.5	636.0	0.3593
3.75	617.4	0.3593

Table A3.11

970 W m-2, 0.0067 kg s-1 m-2		
TIME (h)	**Mass flux of Evaporation** g h^{-1} m^{-2}	**Concentration** kg kg^{-1}
0.25	178.1	0.3288
0.5	267.1	0.3308
0.75	415.5	0.3332
1	534.2	0.3368
1.25	605.5	0.3411
1.5	623.3	0.3446
1.75	636.0	0.3477
2	645.5	0.3504
2.25	672.8	0.3540
2.5	676.7	0.3572
2.75	680.0	0.3599
3	697.5	0.3600
3.25	684.9	0.3600
3.5	674.2	0.3584

Table A3.12

600 W m-2, 0.0104 kg s-1 m-2		
TIME (h)	**Mass flux of Evaporation** g h^{-1} m^{-2}	**Concentration** kg kg^{-1}
0.25	178.1	0.3310
0.5	267.1	0.3344
0.75	415.5	0.3359
1	489.7	0.3385
1.25	534.2	0.3413
1.5	563.9	0.3445
1.75	585.1	0.3473
2	601.0	0.3505
2.25	613.4	0.3540
2.5	623.3	0.3573
2.75	631.4	0.3600
3	638.1	0.3600
3.25	643.8	0.3600
3.5	636.0	0.3592
3.75	629.2	0.3592

APPENDIX 4

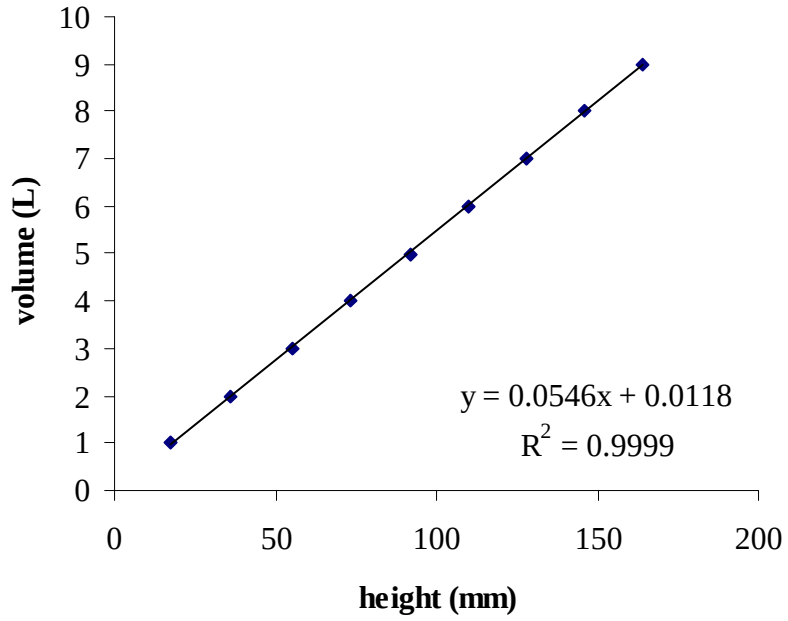

Fig. A4.1 Calibration graph for tank used in the regenerator experiments

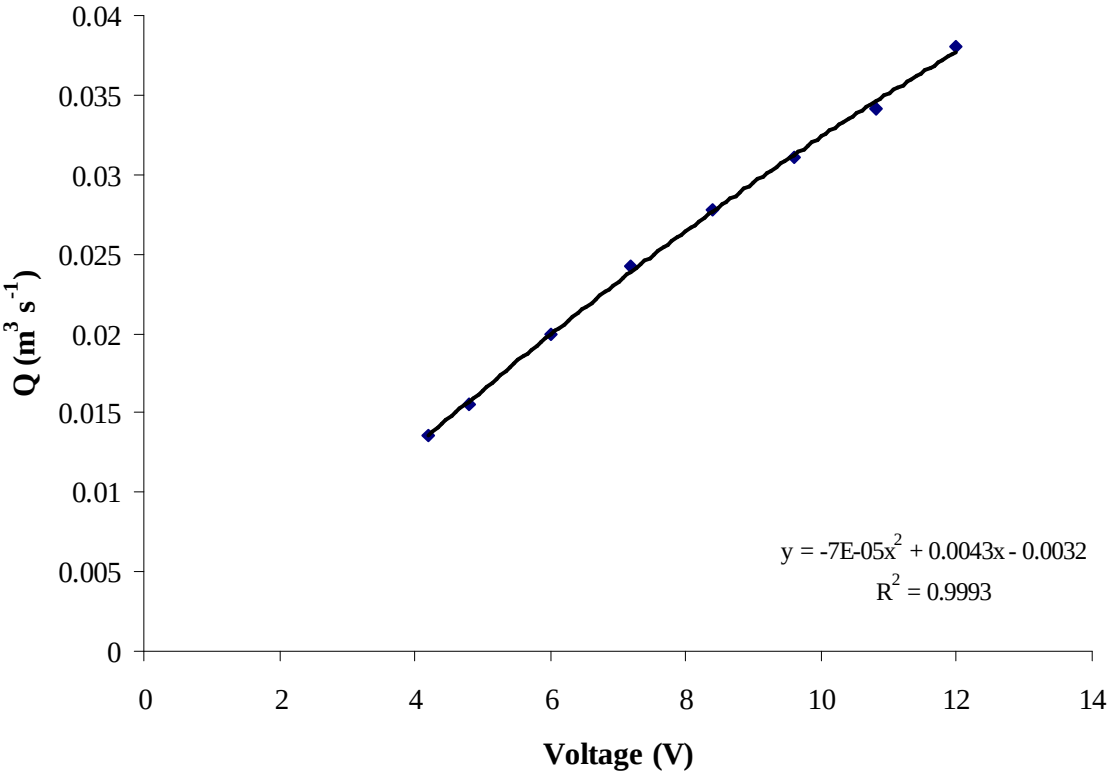

Fig. A4.2: Calibration graph for the outlet fan.

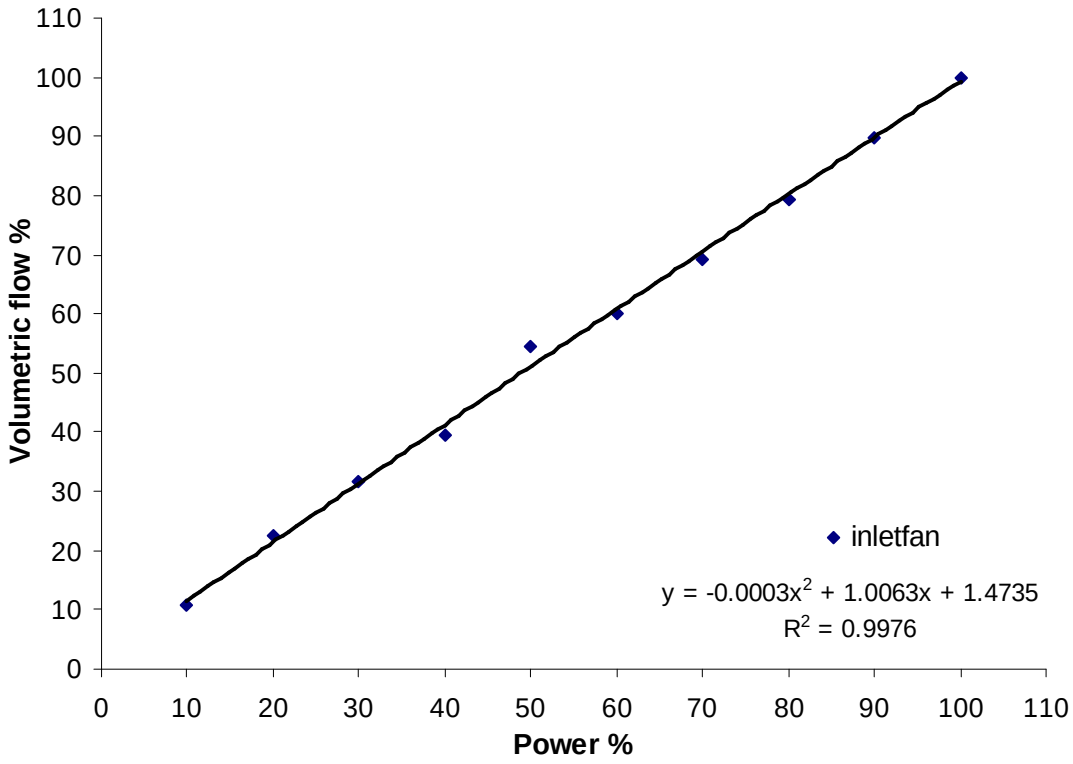

Fig. A4.3: Calibration graph for the inlet fan

APPENDIX 5

Orifice plate

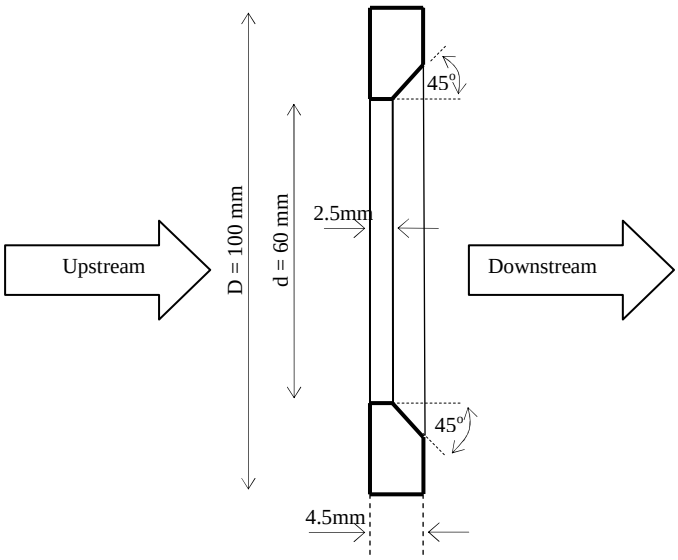

Fig.A5.1:. Section view of the orifice plate.

APPENDIX 6

Energy balance calculation results

Table A6.1

	$Q_{a,in}$	$Q_{a,out}$	Q_{sin}	Q_{sout}	Q_{win}	Q_{wout}	H_{in}	H_{out}
H1	2.57	1.96	0.16	0.14	4.59	5.11	2.57	1.96
H2	2.63	1.92	0.24	0.19	4.59	5.22	2.63	1.92
H3	2.51	1.75	0.28	0.22	3.83	4.57	2.51	1.75
H4	2.61	1.85	0.34	0.28	4.68	5.40	2.61	1.85
H5	2.57	1.78	0.51	0.40	4.12	4.96	2.57	1.78
D1	1.92	1.80	0.29	0.27	–	–	1.92	1.80
D2	2.45	2.18	0.31	0.33	–	–	2.45	2.18
D3	3.00	2.61	0.32	0.37	–	–	2.67	2.56
D4	2.45	1.91	0.36	0.31	5.11	5.73	2.45	1.91

Table A6.2 Description of Köppen climate symbols and defining criteria (reproduced from Peel *et al.*(2007)).

APPENDIX 7

Setup 1
Case study: Muscat

Table A7.1

MAY	$T_{amb\ dry}$	$Tair_{\ Des\ out}$	$Tair_{\ in\ with}$	$Tair_{\ in\ without}$	$T_{airout\ with}$	$T_{airout\ without}$
10.00	32.20	30.94	21.97	23.76	26.78	28.41
11.00	33.04	32.20	22.37	23.85	27.83	29.11
12.00	33.50	32.20	22.58	24.02	28.26	29.61
13.00	33.76	32.89	22.70	24.01	28.47	29.62
14.00	33.60	32.40	22.52	24.09	28.00	29.43
15.00	33.20	32.38	22.51	23.98	27.54	28.81
16.00	32.34	31.29	22.05	23.87	26.28	27.89
17.00	31.55	30.71	21.60	23.61	25.13	26.84

Table A7.2

JUNE	$T_{amb\ dry}$	$Tair_{\ Des\ out}$	$Tair_{\ in\ with}$	$Tair_{\ in\ without}$	$T_{airout\ with}$	$T_{airout\ without}$
10.00	33.31	32.11	22.90	25.06	27.52	29.42
11.00	34.15	33.24	23.40	25.15	28.57	30.07
12.00	34.89	33.60	23.68	25.34	29.17	30.68
13.00	34.98	34.07	23.84	25.20	29.40	30.59
14.00	34.78	33.53	23.62	25.25	28.92	30.40
15.00	34.23	33.36	23.49	25.22	28.35	29.83
16.00	33.38	32.34	22.88	24.92	26.97	28.75
17.00	32.36	31.47	22.59	24.85	25.88	27.80

Table A7.3

JULY	$T_{amb\ dry}$	$Tair_{\ Des\ out}$	$Tair_{\ in\ with}$	$Tair_{\ in\ without}$	$T_{airout\ with}$	$T_{airout\ without}$
10.00	32.60	31.39	22.71	25.23	26.92	29.09
11.00	33.39	32.50	23.21	25.32	27.92	29.70
12.00	33.86	32.65	23.33	25.32	28.22	29.98
13.00	34.15	33.23	23.59	25.35	28.66	30.17
14.00	33.98	32.80	23.45	25.42	28.31	30.04
15.00	33.61	32.73	23.19	25.31	27.71	29.50
16.00	33.00	31.95	22.97	25.19	26.80	28.71
17.00	32.18	31.28	22.62	25.06	25.81	27.86

Case study: Havana

Table A7.4

JULY	$T_{amb\ dry}$	$Tair_{\ Des\ out}$	$Tair_{\ in\ with}$	$Tair_{\ in\ without}$	$T_{airout\ with}$	$T_{airout\ without}$
10.00	29.52	27.94	21.30	24.79	25.33	28.37
11.00	30.69	29.83	22.00	25.01	26.74	29.21
12.00	31.42	30.23	22.33	25.13	27.18	29.57
13.00	31.91	30.97	22.57	25.37	27.61	29.93
14.00	31.92	30.80	22.62	25.38	27.18	29.53
15.00	31.41	30.43	22.31	25.11	26.34	28.69
16.00	30.69	29.74	21.93	25.01	25.27	27.84
17.00	29.63	28.74	21.46	24.73	24.01	26.71

Table A7.5

AUGUST	$T_{amb\ dry}$	$Tair_{\ Des\ out}$	$Tair_{\ in\ with}$	$Tair_{\ in\ without}$	$T_{airout\ with}$	$T_{airout\ without}$
10.00	29.71	28.00	21.52	24.96	25.57	28.60
11.00	30.71	29.85	22.02	25.19	26.64	29.24
12.00	31.46	30.29	22.39	25.34	26.97	29.47
13.00	31.76	30.84	22.64	25.42	27.31	29.61
14.00	31.63	30.54	22.40	25.30	26.65	29.10
15.00	31.20	30.23	22.33	25.28	26.00	28.46
16.00	30.32	29.37	21.98	25.02	25.08	27.61
17.00	29.41	28.52	21.45	24.85	23.81	26.61

Table A7.6

SEPTEMBER	$T_{amb\ dry}$	$Tair_{\ Des\ out}$	$Tair_{\ in\ with}$	$Tair_{\ in\ without}$	$T_{airout\ with}$	$T_{airout\ without}$
10.00	29.29	27.85	21.23	24.74	25.01	28.04
11.00	30.07	29.24	21.70	24.80	25.99	28.54
12.00	30.74	29.61	22.00	25.05	26.25	28.83
13.00	31.06	30.08	22.21	25.16	26.31	28.77
14.00	30.92	29.90	22.06	25.04	26.01	28.50
15.00	30.38	29.43	21.85	24.90	25.22	27.76
16.00	29.54	28.63	21.54	24.81	24.24	26.94
17.00	28.59	27.73	21.12	24.58	23.17	26.01

Case study: Mumbai

Table A7.7

MARCH	$T_{amb\ dry}$	$Tair_{\ Des\ out}$	$Tair_{\ in\ with}$	$Tair_{\ in\ without}$	$T_{airout\ with}$	$T_{airout\ without}$
10.00	27.43	26.50	18.94	21.19	22.66	24.60
11.00	28.70	27.78	19.63	21.60	24.17	25.90
12.00	30.04	29.07	20.30	21.99	25.55	27.06
13.00	31.29	30.26	21.04	22.44	26.58	27.86
14.00	31.93	30.95	21.39	22.76	26.88	28.12
15.00	32.26	31.27	21.44	22.82	26.66	27.92
16.00	31.81	30.84	21.30	22.67	25.86	27.11
17.00	30.80	29.95	20.80	22.43	24.54	25.98

Table A7.8

APRIL	$T_{amb\ dry}$	$Tair_{\ Des\ out}$	$Tair_{\ in\ with}$	$Tair_{\ in\ without}$	$T_{airout\ with}$	$T_{airout\ without}$
10.00	28.70	27.44	20.38	23.26	24.24	26.75
11.00	30.14	29.33	21.24	23.67	25.98	28.02
12.00	31.52	30.30	21.83	24.13	27.08	29.10
13.00	32.77	31.85	22.50	24.42	28.16	29.80
14.00	33.45	32.25	22.82	24.58	28.34	29.93
15.00	33.56	32.67	22.94	24.68	28.19	29.68
16.00	32.90	31.81	22.47	24.53	27.08	28.87
17.00	31.69	30.80	21.86	24.09	25.63	27.53

Table A7.9

MAY	$T_{amb\ dry}$	$Tair_{\ Des\ out}$	$Tair_{\ in\ with}$	$Tair_{\ in\ without}$	$T_{airout\ with}$	$T_{airout\ without}$
10.00	29.84	28.19	21.18	24.26	25.02	27.77
11.00	31.21	30.14	22.08	24.59	26.78	28.93
12.00	32.36	31.28	22.62	25.03	27.84	29.90
13.00	33.35	32.24	23.00	25.29	28.52	30.47
14.00	33.85	32.75	23.42	25.31	28.86	30.52
15.00	33.77	32.71	23.18	25.24	28.24	30.03
16.00	33.19	32.17	22.95	25.15	27.36	29.25
17.00	32.16	31.21	22.57	24.86	26.19	28.14

Case study: Chittagong

Table A7.10

APRIL	$T_{amb\ dry}$	$Tair_{\ Des\ out}$	$Tair_{\ in\ with}$	$Tair_{\ in\ without}$	$T_{airout\ with}$	$T_{airout\ without}$
10.00	29.92	28.01	21.19	24.33	25.33	28.16
11.00	30.90	30.06	21.82	24.50	26.77	28.97
12.00	31.75	30.53	22.21	24.70	27.41	29.54
13.00	32.37	31.46	22.58	24.85	27.92	29.81
14.00	32.53	31.38	22.51	24.79	27.57	29.53
15.00	32.29	31.32	22.47	24.78	27.02	28.97
16.00	31.51	30.54	22.03	24.67	25.83	28.04
17.00	30.61	29.73	21.74	24.43	24.68	26.92

Table A7.11

MAY	$T_{amb\ dry}$	$Tair_{\ Des\ out}$	$Tair_{\ in\ with}$	$Tair_{\ in\ without}$	$T_{airout\ with}$	$T_{airout\ without}$
10.00	29.66	28.00	21.35	24.75	25.40	28.37
11.00	30.40	29.54	21.94	24.92	26.63	29.07
12.00	31.13	29.94	22.27	25.22	27.12	29.60
13.00	31.46	30.53	22.39	25.16	27.38	29.67
14.00	31.33	30.21	22.32	25.22	26.91	29.35
15.00	31.14	30.15	22.27	25.23	26.42	28.88
16.00	30.65	29.69	22.07	24.98	25.50	27.92
17.00	29.93	29.02	21.69	24.83	24.45	27.05

Table A7.12

JUNE	$T_{amb\ dry}$	$Tair_{\ Des\ out}$	$Tair_{\ in\ with}$	$Tair_{\ in\ without}$	$T_{airout\ with}$	$T_{airout\ without}$
10.00	28.99	27.59	21.49	25.40	25.08	28.38
11.00	29.69	28.81	22.04	25.58	26.10	28.98
12.00	30.40	29.23	22.21	25.74	26.57	29.50
13.00	30.87	29.91	22.61	25.83	27.07	29.72
14.00	31.03	29.92	22.61	25.97	26.76	29.55
15.00	30.89	29.87	22.57	25.85	26.36	29.08
16.00	30.45	29.44	22.39	25.78	25.71	28.51
17.00	29.81	28.86	22.08	25.69	24.72	27.69

Case study: Messina

Table A7.13

JULY	$T_{amb\ dry}$	$Tair_{\ Des\ out}$	$Tair_{\ in\ with}$	$Tair_{\ in\ without}$	$T_{airout\ with}$	$T_{airout\ without}$
10.00	28.14	26.95	19.13	21.30	23.62	25.58
11.00	29.28	28.55	19.88	21.55	24.99	26.44
12.00	30.36	29.19	20.20	21.88	25.63	27.19
13.00	31.09	30.31	20.70	22.09	26.32	27.55
14.00	31.32	30.18	20.79	22.07	26.19	27.42
15.00	31.19	30.35	20.73	22.17	25.76	27.05
16.00	30.63	29.72	20.43	21.91	24.84	26.18
17.00	29.61	28.82	19.91	21.64	23.61	25.12

Table A7.14

AUGUST	$T_{amb\ dry}$	$Tair_{\ Des\ out}$	$Tair_{\ in\ with}$	$Tair_{\ in\ without}$	$T_{airout\ with}$	$T_{airout\ without}$
10.00	28.60	27.35	19.80	22.19	24.03	26.15
11.00	29.70	28.96	20.39	22.61	25.25	27.10
12.00	30.73	29.55	20.86	22.74	26.02	27.71
13.00	31.31	30.51	21.24	22.84	26.52	27.90
14.00	31.48	30.37	21.32	22.98	26.37	27.86
15.00	31.34	30.47	21.21	22.87	25.83	27.27
16.00	30.65	29.74	20.82	22.86	24.84	26.58
17.00	29.59	28.78	20.43	22.52	23.69	25.47

Fig. A7.1 Pressure drop vs. air surface velocity in Celdek®.

APPENDIX 8

gPROMS codes

```
MODEL TESTO (COMBINEDSYSTEMwithstreams)
PARAMETER
CLIMDATA                    as  FOREIGN_OBJECT "ExcelFO"

PORT
   inlet AS MATERIAL_CONDITIONS
   outlet1 AS MATERIAL_CONDITIONS
   outlet2 AS MATERIAL_CONDITIONS

 VARIABLE
nentheff    asdimensionless
nabseff    asdimensionless
RHinas dimensionless
RHout   as dimensionless
msolout as massrate
msolin as massrate
mairin as massrate
mairout as massrate
Mabs     as  massrate
Tairinas temperature
Tairoutas temperature
Twatoutas temperature
Xinas dimensionless
Xoutas dimensionless
XoutREAL as dimensionless
TsoloutAS TEMPERATURE
TsoloutREALAS TEMPERATURE
TsolinAS TEMPERATURE
TWo     AS      TEMPERATURE
TWIN1    AS      TEMPERATURE
TWOUT1     AS      TEMPERATURE
DT1      AS      TEMPERATURE
TWIN2    AS      TEMPERATURE
TWOUT2     AS      TEMPERATURE
DT2     AS      TEMPERATURE
TWIN3    AS      TEMPERATURE
TWOUT3     AS      TEMPERATURE
DT3     AS      TEMPERATURE
TWIN4    AS      TEMPERATURE
TWOUT4     AS      TEMPERATURE
DT4     AS      TEMPERATURE
TWIN5    AS      TEMPERATURE
TWOUT5     AS      TEMPERATURE
DT5     AS      TEMPERATURE
AVTWOUTASTEMPERATURE

SET
CLIMDATA    := "C:\Documents and Settings\toshiba_\Desktop\files for gproms\final des
model\TESTOoptimisation.xls";

 EQUATION
nentheff        =climdata.nentheff;
nabseff         =climdata.nabseff;
RHin            =climdata.RHin;
RHout           =climdata.RHout;
mairin           = CLIMDATA.mairin;
mairout          = CLIMDATA.mairout;
 TWo             = CLIMDATA.TWo;
Tairout          =CLIMDATA.Tairout;
TsoloutREAL      =CLIMDATA.TsoloutREAL;
Mabs                =CLIMDATA.Mabs;
DT1              = CLIMDATA.DT1;
```

```
 TWIN1           = CLIMDATA.TWIN1(TWOUT1);
DT2               = CLIMDATA.DT2;
 TWIN2           = CLIMDATA.TWIN2(TWOUT2);
DT3               = CLIMDATA.DT3;
 TWIN3           = CLIMDATA.TWIN3(TWOUT3);
DT4               = CLIMDATA.DT4;
 TWIN4           = CLIMDATA.TWIN4(TWOUT4);
DT5               = CLIMDATA.DT5;
 TWIN5           = CLIMDATA.TWIN5(TWOUT5);
Twatout         =   (TWIN1+TWIN2+TWIN3+TWIN4+TWIN5)/5   ;
XoutREAL        =   CLIMDATA.XoutREAL   ;
AVTWOUT         =   CLIMDATA.AVTWOUT    ;
```

(continued)

MODEL SYSTEM_MODEL (COMBINEDSYSTEMwithstreams)

```
 UNIT
 REGENERATOR    AS  REGENERATORFINAL
 DESICCATOR     AS  TESTO
 GREENHOUSE     AS  GREENHOUSE_EVAPCOOLING

 VARIABLE
 DM         AS  MASSRATE
regenAREA   asarea

 EQUATION
REGENERATOR.Xsolin  = DESICCATOR.Xout;
REGENERATOR.msolin  =   DESICCATOR.msolout;
REGENERATOR.Tin     =  DESICCATOR.Tsolout;
REGENERATOR.msolout =   DESICCATOR.msolin;
REGENERATOR.Tamb    =   DESICCATOR.Tairin;
REGENERATOR.Tout    =   DESICCATOR.Tsolin;
REGENERATOR.Xsolout  =   DESICCATOR.Xin;
DESICCATOR.Tairout  =   GREENHOUSE.TAirin;
DESICCATOR.RHout    =   GREENHOUSE.RHin;
DESICCATOR.mairin   =   GREENHOUSE.Mair;

DM =    REGENERATOR.mev + DESICCATOR.Mabs;
regenAREA   = 2.555*ABS(DESICCATOR.Mabs*222.2)/ABS(REGENERATOR.mev);
```

```
MODEL GREENHOUSE_EVAPCOOLING (COMBINEDSYSTEMwithstreams)
 PARAMETER
COVERTRANS  AS REAL    #t cover tranmissivity
PSRTRAN     AS  REAL   #parameter characterising the influence of solar radiation on
transpiration
Cp          AS  REAL   #SPECIFIC HEAT OF AIR
Ug          AS  REAL   #HEAT LOSS COEFFICIENT OF GREENHOUSE COVER
Lg           AS  REAL   #TOTAL LENGTH OF GREENHOUSE
Wg           AS  real   #total width of greenhouse
nEVAP        AS     REAL #COOLING PAD EFFICIENCY
NoHo        AS  integer
GFO                    as  FOREIGN_OBJECT "ExcelFO"

PORT
    INPUTDATA AS MATERIAL_CONDITIONS

 VARIABLE
 Xg             AS    LENGTH  #DISTANCE OF GREENHOUSE FROM INLET
 RHin             AS  ARRAY(NoHo) OF    DIMENSIONLESS
 TAirin           AS  ARRAY(NoHo) OF    TEMPERATURE
 Tinx           as  ARRAY(NoHo) OF    TEMPERATURE
 TAMBWET        AS  ARRAY(NoHo) OF    TEMPERATURE
 Ia             AS  ARRAY(NoHo) OF    IRRADIANCE
 dair           as  ARRAY(NoHo) OF    density #airdensity
 Vair           as  ARRAY(NoHo) OF    volumetricflowrate
 A1             AS  ARRAY(NoHo) OF     DIMENSIONLESS

 A2             AS  ARRAY(NoHo) OF     DIMENSIONLESS
 Mair           as  array(noho) of     massrate

 SET
 GFO             := "C:\Documents and Settings\toshiba_\Desktop\files for
gproms\Greenhouse_copyOptimisation.xls";
COVERTRANS       := 0.6;
PSRTRAN          := 0.45;
Cp               := 1.005;
Ug               := 4.2;
Lg               := 30;
Wg               := 1000/30;
NoHo             := 0;
nEVAP            := 0.8;

 EQUATION
Tinx=   TAirin + ((-nEVAP*(TAirin-TAMBWET) - (A1/A2))*EXP(-A2*XG))+(A1/A2);
    A1 = (COVERTRANS*(1-PSRTRAN)*Ia*Lg)/(dair*Vair*Cp*1000);
    A2 = (Ug*Lg)/(dair*Vair*Cp*1000);
Xg            =GFO.Xg;
 RHin             =GFO.RH;
 TAirin           =GFO.TAMB;
 TAMBWET        =GFO.TAMBWET;
 Ia             =GFO.Ia;
 dair           =GFO.dair ;
 Vair           =GFO.Vair;
 Mair           =GFO.Mair;
```

```
MODEL regeneratorfinal (COMBINEDSYSTEMwithstreams)
 PARAMETER
yas integer
FO                      as  FOREIGN_OBJECT "ExcelFO"
 Ia                      as  real
 Pa                      as  REAL
  fi                     AS real

PORT
    inlet AS MATERIAL_CONDITIONS
    outlet AS MATERIAL_CONDITIONS

 VARIABLE
nefficiency              as dimensionless
msolin                   as  MASSRATE
msolout                     as massrate
 Xsolin                   as  DIMENSIONLESS
 Xsolout                 as    Dimensionless
Tin                     as temperature
RHamb                   as  dimensionless
 Tamb                    as  temperature


 UL                 as heatlosscoefficient
 hm                 as pressuremasstransfercoefficient
 hD                 as concentrationmasstransfercoefficient
 Cpsol              as specificheatcapacity
 hfg                as specificenthalpy #latent heat#
 Pamb               as pressure
 Psol               as pressure

 Tout               as temperature
 mev                as massrate
 Psatamb            as pressure
 Psatinter            as pressure
 a                  as dimensionless
 b                  as dimensionless
 c                  as dimensionless

Ir                  as specificenthalpy
 Tfilm              as temperature
 Dwa                as diffusivity
 L                  as length #characteristic#
 Sch    as dimensionless
 Sh             as dimensionless
 Nu                 as dimensionless
 da                 as density
 va                 as kinviscosity
 mia                 as dynviscosity
 thexp              as thermalexpansion
 Grcon              as dimensionless
 Grheat             as dimensionless
 Grtotal            as dimensionless
 wa                 as watercontent
 winter             as watercontent
 Aeq1               as dimensionless
 Aeq2               as dimensionless
 Aeq3               as dimensionless
 K1                 as dimensionless
 K2                 as dimensionless
 ERH                as dimensionless
 hr                 as heatransfercoefficient
```

```
 hc                as heatransfercoefficient
 slopeadjustment   as dimensionless
 x                    as  length
 w                    as  length

 SET
 FO            := "C:\Documents and Settings\toshiba_\Desktop\files for
gproms\RegeneratorFinalModelOptimisation.xls";
 Ia            := FO.Ia;
 Pa            := FO.Pa;
 fi            := FO.fi;
 y:=1;

 EQUATION
 Tin           = FO.Tin;
msolin   = FO.msol;
 Xsolin = FO.Xsol;
RHamb   = FO.RHamb;
 Tamb   = FO.Tamb;
msolout   = FO.msolout;
 Xsolout = FO.Xsolout;
  UL= FO.UL(x, w);
Ir = FO.Ir ;
   hD= FO.hD;
    hm= FO.hm;
  Cpsol= FO.Cpsol;
 hfg= FO.hfg;
 Pamb= FO.Pamb;
 Psol= FO.Psol(a,b,c);
 Dwa=  FO.Dwa;
 Sh=   FO.Sh;
 Grtotal=  FO.Grtotal;
 Grcon=    FO.Grcon;
 Grheat=    FO.Grheat;
 va=        FO.va;
 da=    FO.da;
 wa=        FO.wa;
 winter=    FO.winter;
 Psatinter= FO.Psatinter;
 Psatamb=   FO.Psatamb;
 L=    FO.L;
 Aeq1=      FO.Aeq1;
 Aeq2=      FO.Aeq2;
 Aeq3=      FO.Aeq3;
 K1=        FO.K1;
 K2=        FO.K2;
 Tout= FO.Tout;
 mev= FO.mev;
 slopeadjustment=   FO.slopeadjustment;
 Tfilm= FO.Tfilm;
 hr=    FO.hr;
 hc=    FO.hc;
 Sch=   FO.Sch;
 Nu=    FO.Nu;
 mia=   FO.mia;
 thexp= FO.thexp;
    ERH = FO.ERH;
    nefficiency = FO.nefficiency;

if Tin >= 20 and Tin < 25 then  a=75.925334;

else
```

(continued)

```
        if Tin >= 25 and Tin < 30 then a=99.076739;

else
        if Tin >= 30 and Tin< 40 then a=134.90955;
else    if Tin >= 40 and Tin< 45 then a=140.5607387;
else    if Tin >= 45 and Tin< 50 then a=141.775612;
else a = 0 ;
end
    end
        END
            end
                end

if Tin>= 20 and Tin< 25 then  b=792.7006;
else
        if Tin>= 25 and Tin< 30 then b=1083.514;
else
        if Tin>= 30 and Tin< 40 then b=1493.499;
else    if Tin >= 40 and Tin< 45 then b=2200.015371;
else    if Tin >= 45 and Tin< 50 then b=2200.024366;
else b = 0 ;
end
    end
        END
            end
                end
if Tin>= 20 and Tin< 25 then
 c=-23709.98;
else
        if Tin>= 25 and Tin< 30 then
 c=-31600;
else
        if Tin>= 30 and Tin < 40 then c=-43684.56;
else    if Tin >= 40 and Tin< 45 then c=-47500.0015;
else    if Tin >= 45 and Tin< 50 then c=-47499.99761;
else c = 0 ;
end
    end
        END
            end
                end
```

```
PROCESS EXEC_SYSTEM_MODEL (COMBINEDSYSTEMwithstreams)
UNIT
EXEC AS SYSTEM_MODEL

 ASSIGN
 EXEC.REGENERATOR.x :=3.5;
 EXEC.REGENERATOR.w :=0.73;
EXEC.DESICCATOR.TWOUT1:=21;
EXEC.DESICCATOR.TWOUT2:=21;
EXEC.DESICCATOR.TWOUT3:=21;
EXEC.DESICCATOR.TWOUT4:=19;
EXEC.DESICCATOR.TWOUT5:=19;

 SOLUTIONPARAMETERS
IdentityElimination := OFF
FPI:="ExcelFP::C:\Documents and Settings\toshiba_\Desktop\files for gproms\final des
model\TESTOoptimisation.xls" ;
gexceloutput    := "<steady-state>C:\Documents and Settings\toshiba_\Desktop\files for
gproms\RESULTS.xls"   ;

 SCHEDULE
SEQUENCE

while EXEC.DESICCATOR.DT1 > 0.001  DO

                    PARALLEL
                    GET
                      EXEC.DESICCATOR.TWIN1:= "TWIN1" ;
                      EXEC.DESICCATOR.TWOUT1:=   "TWOUT1" ;
                      EXEC.DESICCATOR.DT1:= "DT1";
                    END
    if EXEC.DESICCATOR.DT1 > 0.001 then
REPLACE EXEC.DESICCATOR.TWOUT1
WITH
EXEC.DESICCATOR.TWOUT1 := OLD(EXEC.DESICCATOR.TWOUT1) + 0.02;
END
    else
reset
EXEC.DESICCATOR.TWOUT1 := OLD(EXEC.DESICCATOR.TWOUT1);
end

    end

    if EXEC.DESICCATOR.DT1< 0.001 then

SEQUENCE
PARALLEL
                    GET
                      EXEC.DESICCATOR.TWIN2:= "TWIN2" ;
                      EXEC.DESICCATOR.TWOUT2:=   "TWOUT2" ;
                      EXEC.DESICCATOR.DT2:= "DT2";
                    END
    if EXEC.DESICCATOR.DT2 > 0.001 then
REPLACE EXEC.DESICCATOR.TWOUT2
WITH
EXEC.DESICCATOR.TWOUT2 := OLD(EXEC.DESICCATOR.TWOUT2) + 0.02;
END
    else
reset
EXEC.DESICCATOR.TWOUT2 := OLD(EXEC.DESICCATOR.TWOUT2);
end
    end
```

```
    if EXEC.DESICCATOR.DT2< 0.001 then
SEQUENCE
PARALLEL
                    GET
                      EXEC.DESICCATOR.TWIN3:= "TWIN3" ;
                      EXEC.DESICCATOR.TWOUT3:=   "TWOUT3" ;
                      EXEC.DESICCATOR.DT3:= "DT3";
                    END
    if EXEC.DESICCATOR.DT3 > 0.001 then
REPLACE EXEC.DESICCATOR.TWOUT3
WITH
EXEC.DESICCATOR.TWOUT3 := OLD(EXEC.DESICCATOR.TWOUT3) + 0.02;
END
    else
reset
EXEC.DESICCATOR.TWOUT3 := OLD(EXEC.DESICCATOR.TWOUT3);
end
    end

    if EXEC.DESICCATOR.DT3< 0.001 then
SEQUENCE
PARALLEL
                    GET
                      EXEC.DESICCATOR.TWIN4:= "TWIN4" ;
                      EXEC.DESICCATOR.TWOUT4:=   "TWOUT4" ;
                      EXEC.DESICCATOR.DT4:= "DT4";
                    END
    if EXEC.DESICCATOR.DT4 > 0.001 then
REPLACE EXEC.DESICCATOR.TWOUT4
WITH
EXEC.DESICCATOR.TWOUT4 := OLD(EXEC.DESICCATOR.TWOUT4) + 0.02;
END
    else
reset
EXEC.DESICCATOR.TWOUT4 := OLD(EXEC.DESICCATOR.TWOUT4);
end
    end

    if EXEC.DESICCATOR.DT4< 0.001 then
SEQUENCE
PARALLEL
                    GET
                      EXEC.DESICCATOR.TWIN5:= "TWIN5" ;
                      EXEC.DESICCATOR.TWOUT5:=   "TWOUT5" ;
                      EXEC.DESICCATOR.DT5:= "DT5";
                    END
    if EXEC.DESICCATOR.DT5 > 0.001 then
REPLACE EXEC.DESICCATOR.TWOUT5
WITH
EXEC.DESICCATOR.TWOUT5 := OLD(EXEC.DESICCATOR.TWOUT5) + 0.02;
END
    else
reset
EXEC.DESICCATOR.TWOUT5 := OLD(EXEC.DESICCATOR.TWOUT5);
end
    end

 if EXEC.DESICCATOR.DT5< 0.001 then
stop
end
```

(continued)

```
end
end
end
end
end
end
end
END
end
end
end
end
end
end
end
```